Keele University

Novel stem cell and PHBHHx approaches to tendon repair

William Richard Webb

School of Postgraduate Medicine

Institute for Science and Technology in Medicine

Keele University

Thesis Submitted to Keele University for the degree of

Doctor of Philosophy

July 2014

SUBMISSION OF THESIS FOR A RESEARCH DEGREE

Part I. DECLARATION by the candidate for a research degree. To be bound in the thesis

Degree for which thesis being submitted Doctor of Philosophy

Title of thesis Novel stem cell and PHBHHx approaches to tendon repair

This thesis contains confidential information and is subject to the protocol set down for the submission and examination of such a thesis.

NO

Date of submission 02-06-2014 Original registration date 11-01-2010

(Date of submission must comply with Regulation 2D)

Name of candidate Mr William Richard Webb

Research Institute ISTM Name of Lead Supervisor Dr Nicholas R Forsyth

I certify that:

(a) The thesis being submitted for examination is my own account of my own research
(b) My research has been conducted ethically. Where relevant a letter from the approving body confirming that ethical approval has been given has been bound in the thesis as an Annex
(c) The data and results presented are the genuine data and results actually obtained by me during the conduct of the research
(d) Where I have drawn on the work, ideas and results of others this has been appropriately acknowledged in the thesis
(e) Where any collaboration has taken place with one or more other researchers, I have included within an 'Acknowledgments' section in the thesis a clear statement of their contributions, in line with the relevant statement in the Code of Practice (see Note overleaf).
(f) The greater portion of the work described in the thesis has been undertaken subsequent to my registration for the higher degree for which I am submitting for examination
(g) Where part of the work described in the thesis has previously been incorporated in another thesis submitted by me for a higher degree (if any), this has been identified and acknowledged in the thesis
(h) The thesis submitted is within the required word limit as specified in the Regulations

Total words in submitted thesis (including text and footnotes, but excluding references and appendices) 53,014 words.

Signature of candidate …… Date 23-06-2014

Declaration Part 1. To be bound in the thesis

Note

Extract from Code of Practice: If the research degree is set within a broader programme of work involving a group of investigators – particularly if this programme of work predates the candidate's registration – the candidate should provide an explicit statement (in an 'Acknowledgments' section) of the respective roles of the candidate and these other individuals in relevant aspects of the work reported in the thesis. For example, it should make clear, where relevant, the candidate's role in designing the study, developing data collection instruments, collecting primary data, analysing such data, and formulating conclusions from the analysis. Others involved in these aspects of the research should be named, and their contributions relative to that of the candidate should be specified (*this does not apply to the ordinary supervision, only if the supervisor or supervisory team has had greater than usual involvement*).

Abstract

Tendon injuries continue to be a financial burden on the health care system of many western countries, whilst also remaining common and a significant challenge within the orthopaedic discipline with no consensus of opinion on the best therapeutic regime to be employed.

Many polymers have been investigated for use in tendon repair. A range of polymers have shown good integration with limited immune response. However, to date no implant has been capable of delivering the physical properties observed in native undamaged tendon. Many of the polymers implanted have resulted in re-rupture or reduced mechanical function. Therefore, improvements are required in the choice of polymer and mechanical properties of the polymer are required. One means of achieving such improvements is to utilise co-polymers such as PHBHHx, which have shown favourable elastic properties when the ratio of HHx to PHB has been increased.

Therefore, a PHBHHx polymer based scaffold was investigated as a potential scaffold for tendon repair. Whilst, also investigating the potential of FGF-4, FGF-6 and FGF-8 to differentiate both human embryonic and mesenchymal stem cells towards a tenocyte-like lineage. Finally, an investigation into whether a controlled production of PHBHHx based nanoparticles could produce different nanoparticles sizes that can be predicted and result in differing release profiles. This may allow for the synthesis of size controlled nanoparticles capable of delivering differing drug concentrations and sustained release properties.

Results have shown that PHBHHx in conjunction with collagen and tenocytes can be used as a scaffold material for the treatment of damaged tendon tissue *in vivo.* The implanted scaffold was capable of returning function and did not elucidate an immune response when *in situ*.

In Vitro studies demonstrated that the combination of FGF-4, 6 & 8 supplementation of differentiation media containing Vitamin C, as being capable of maintaining tendon specific genes TNMD and THBS-4 in both embryonic stem cells and mesenchymal stem cell when cultured at 2% O_2.

Design of experiment methodology studies have shown that we can accurately predict PHBHHx nanoparticle size ranging from 95 – 200nm in size. This function will enable accurate size production of nanoparticles for a controlled and sustained release of growth factors for tendon regeneration.

In conclusion, the combination of studies have shown the effectiveness of PHBHHx as both a tendon scaffold and potential use in nanoparticle delivery for drug and growth factors, such as FGF-4, FGF-6 and FGF-8 which are potentially capable of cellular priming of stem cells to differentiate towards a tenocyte “like” lineage. The findings of these studies provide a pathway for future innovations in regenerative medicine and wider scientific community.

Contents

List of Figures

List of Tables

List of Equations

List of Standard Curves

Acknowledgements

This thesis I dedicate to my family and friends. Especially Alice Brown, who as my partner has had to tolerate my being away and abroad for the duration of the undertaking of this study.

I would like to mention the support of Dr. Nick Forsyth as without his guidance and understanding the endurance of such an undertaking would not have been possible.

To all the students who have frequented the Skills Lab and a special mention is afforded to: Khondoker Akram, Deepak Kumar, Tina Dale, Hari, Sammy, Vaz and the Irish contingent.

A special mention and big thanks to Alex Lomas for his friendship and support while we endured a 6 month study in Tsinghua University, Beijing, China. To the staff and students of the school of life sciences, Tsinghua University especially: Riang Wang, Professor George Chen, Meng Meng (and family) and Gao Dong Zheng.

I would also like to thank Thomas Heathman for his friendship whilst on 6 month exchange at the West China School of Pharmacy, Sichuan University, Chengdu, China. I would like to thank those who I would also think of as life friends: Professor Xun Sun for her infectious laugh when I mentioned PQ for giving a visiting professor a bike ride to the school. Also, Professor Zhirong Zhang, Jainfeng for his pole dancing (I still have the pictures) and all the students who Tom and I shared many hotpots with.

Publications

Lomas, A. J., **Webb, W. R.**, Han, J., Chen, G. Q., Sun, X., Zhang, Z., El Haj, A. J., Forsyth, N. (2013) Poly (3-hydroxybutyrate-co-3-hydroxyhexanoate)/collagen hybrid scaffolds for tissue engineering applications. Tissue Eng Part C Methods.

Webb, W. R., Dale, T. P., Lomas, A. J., Zeng, G., Wimpenny, I., El Haj, A. J., Forsyth, N. R., Chen, G. Q. (2013). The application of poly (3-hydroxybutyrate-co-3-hydroxyhexanoate) scaffolds for tendon repair in the rat model. Biomaterials.

DONG C-L, **WEBB W. R.**, PENG Q, TANG J Z, FORSYTH N R, CHEN G-Q; EL HAJ A J. The effect of controlled release platelet derived growth factor-BB (PDGF-BB) from phospholipid complex loaded PHBHHx nanoparticles on human mesenchymal stem cell proliferation in collagen hydrogels. *Journal of Biomaterial Research Part A*

HEATHMAN T. R. J*., **WEBB W. R.***, DANB Z., CHENC G Q, FORSYTH N. R., EL HAJ A. J., ZHANG Z. R. & SUN X. Controlled production of poly (3-hydroxybutyrate- co-3-hydroxyhexanoate) (PHBHHx) nanoparticles for targeted and sustained drug delivery. *Journal of Pharmaceutical Research* (* Joint first Authors, Accepted for Publication 07/05/2014)

Manuscript Preperation

Webb WR, Damani I., Lal S., Forsyth NR, FGF-4, 6 & 8 induced Tenogenic differentiation of both hESC and hMSC.

Webb WR, Dale TP, Zhou J., Damani I., Maffulli N., Chen GQ., El Haj AJ. & Forsyth NR, BMP 12/13 induced Tenogenic differentiation of hESC.

Lomas AJ, Britchford ER, **Webb WR**, Lal S, Forsyth NR, El Haj AJ, The Effect of Cyclical Mechanical Stress and Growth Factor Addition on Human Stem Cell Seeded PHBHHX/Collagen Hybrid Scaffolds

International Conferences and Symposia Published in full proceedings

WR Webb, Lomas AJ, Zeng G, Chen GQ, El Haj AJ, Forsyth NR. Poly(3-hydroxybutyrate- co-3-hydroxyhexanoate)(PHBHHx) Scaffolds for Tendon Repair in the Rat Model. European Cells and Materials 2011 Vol. 22 Suppl. 3 (page 34)

Lomas AJ, **Webb WR**, Zeng G, Forsyth NR, El Haj AJ, Chen GQ. Poly(3-hydroxybutyrate- co-3-hydroxyhexanoate)(PHBHHx) Scaffolds for Tendon Repair in the Rat Model. Histology and Histopathology: 2011, Vol. 26. Suppl. 1 (page 60)

Chapter 1: Literature Review

1.1 Introduction

Tissue engineering is an emerging interdisciplinary field that utilises the areas of material sciences, stem cell biology and clinical sciences to deliver a fresh approach to the development of therapies and treatments to patients. To date, tissue engineering has produced fresh approaches to orthopaedics in the development of articular cartilage implant [1] and in general medicine with the recent highly publicised development of the synthetic larynx implantation [2].

The musculoskeletal system consists of three major components: skeletal tissue, which provides structural support and defines the mechanical units; muscular tissue, which generates force; tendon and ligament, which transmit force generated during muscle contraction of the skeleton and contribute to joint stability [3]. Therefore, tendon and ligament play a significant role in the modulation of force transmission between bone-bone, bone and skeletal muscle and consequently protect muscle fibres from contraction or high strain induced injuries [3-6]. Tendon injury is a financial burden on the health care system of many western countries, with in excess of 4.83 incidents per 100,000 hand tendon injuries, 12 incidents per 100,000 Achilles tendon injuries and 3.73 per 100,000 rota cuff tendon injuries per year [7]. Tendon injuries remain common and a significant challenge within the orthopaedic discipline with no consensus of opinion on the best therapeutic regime to be employed.

One of the major problems with surgical tendon repair is the incidence of re-injury and possibility of complete tendon rupture leading to further incapacitation which negatively impacts on both healthcare economics (in the cost of treatment) and patient economics (in relation to loss of income). Failure rates for tendon repair range from 2-13% (4-13%

due to suture overloading, 2-4% for Achilles tendon re-rupture, 4.3% percutaneous repair and non-surgical bracing 12.2%) [7].

Due to the failure rates new strategies have been developed for tendon repair, the three most promising approaches include:

1) Biopolymer based scaffold repair
2) Stem cell based therapy
3) Stem cell/biopolymer therapy

To date many polymers have been investigated as a possible scaffold for tendon repair with varying degrees of success. However, the translation of the animal, studies have yet to be explored within the human subject. The use of stem cell based therapies remains under researched in the area of tendon repair. One possible approach that could lead to a more positive outcome could be the combination therapy. The combination of both stem cell and biopolymer-based approaches utilising a polymer based nanoparticle delivery method for growth factors to induce stem cell differentiation towards a tenocyte lineage. The utilisation of such an approach would:-

1. Enable the body to be utilised as a bioreactor
2. Localised growth factor induced differentiation
3. Force transmission to the implant via the body to induce mechanotransduction and subsequent differentiation.

1.2 Embryonic Development

During early embryonic development the precise mechanisms of embryonic polarisation and spatial patterning have yet to be understood. Embryonic polarisation is the initiator of the primary plan for the formation of the body axis. The symmetry of the embryo is established after oogenesis. Mammalian development has been best observed within the mouse. The mouse oocyte has no clear polarity with no specific molecules responsible for lineage specification yet identified [8]. Most embryos develop with bilateral symmetry and become polarized along anterior-posterior, dorsal-ventral and left-right axes [9]. One of the major milestones in embryonic development is the initiation and generation of the asymmetrical architecture which underpins the orientation and polarity of the three-axes, Rostral (Head) – caudal (Tail), Dorso (Back) – Ventral (Front), and Left – Right (Figure 1.1), which will become the basic body plan along which embryonic development will follow [9].

One, well documented feature of mammalian development is the maintenance of a population of pluripotent stem cells which will give rise to the mature organism [10]. The inner cell mass (ICM) is made up of 10 – 20 cells, which appear to be developmentally identical, which is located at one end of the 3.5 days post coitum (d.p.c) blastocyst [10]. Mammalian development requires the regulated proliferation of these cells and allocation of descendants to specific cell lineages post differentiation [11-13].

At d.p.c 4.0 the ICM cells that line blastocoelic cavity start to differentiate and become extraembryonic primitive endoderm. The cells that remain within the ICM retain pluripotency and this is now referred to as the “epiblast” which is surrounded by extraembryonic endoderm and trophectoderm, it is at this point the embryo implants

into the uterine wall [10]. After implantation into the uterine wall the pluripotent cells begin to rapidly proliferate and primitive endoderm cells migrate along the pluripotent cell surface and differentiate into one of two cell types (visceral endoderm and parietal endoderm), the mechanism and control of this migration/differentiation has yet to be elucidated [10].

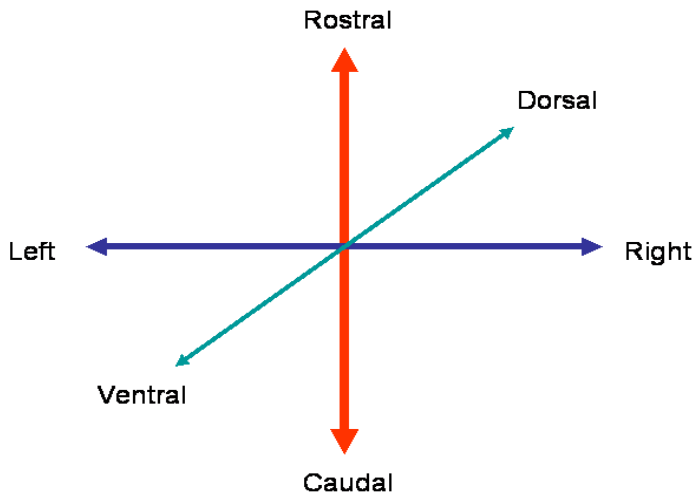

Figure 0.1 Orientation and Polarity of the three axises.

The Red arrow indicates the Rostral – Caudal axis, the green arrow indicates Dorso – Ventral axis and blue arrow indicates the Left – Right axis [10].

1.2.1 Limb Development

The primitive endoderm cells that remain in contact with the pluripotent cells then differentiate into visceral endoderm (possibly by means of juxtacrine or cell-cell signalling in conjunction with yet to be identified growth hormones and growth factors, while the primitive endoderm cells that migrate onto the blastocoelic surface of the trophectoderm now differentiate into parietal endoderm [10]. The formation of the primitive endoderm provides the substrate for gastrulation and initiates at 6.5 d.p.c. and it is this process that transforms the pluripotent monolayer into a multi-layered embryo consisting of the 3

primary germ layers namely the mesoderm, ectoderm and endoderm from which all the tissues required for adult life give rise [10].

Research conducted using Quail-chick chimeras has shown that tendon and cartilage cells differentiate from the same mesodermic compartment and this is distinct from the area that gives rise to muscle cells [14]. Axial tendon, develop from the sclerotomal compartment form along the axis of the body. The limb-tendon(s) develop from the lateral plate and the limb and axial muscles originate from the dermomyotomes [14]. Although, these have different origins, tendon and muscle development/morphogenesis happens with close spatial and temporal association [14].

Ros *et al*. established that tenocyte differentiation starts at Embryonic day (E) 7 in Quail-chick chimeras, this was observed by the increase in deposition of ECM [15]. The increase in synthesis of ECM leads to the formation of early collagen fibrils and the overall architecture of the tendon is apparent by E14 [14]. At E17 proliferation of tendon cells appears to have stopped, however there is an increase in the rate of synthesis of collagen and associated matrix glycoproteins (as E17 is just prior to birth), this results in an increase in length and diameter of the collagen fibrils which results in the provision of the required mechanical properties of mature tendon [14].

However, Quail-chick based research studies are still unable to address major questions such as; 1) Is tendon development initiated by growth factors such as FGF-8?, 2) Micro-movement induced mechanical stimuli?, 3) A combination of growth factor/micro mechano-stimuli?, or 4) Is there a transitional relationship between growth factor induced differentiation, which then leads to mechano-stimuli driven differentiation?

1.2.2 Limb Abnormalities

Polydactyly is the most frequent congenital hand malformation observed in humans and has a prevalence of 5-19 in 10,000 live births [16, 17]. Research conducted by Bouldin *et al,* which employed the use of Dorking's chickens suggests the ectopic post-axial digit is due to the deregulated-expression of FGF's in the AER, especially anterior expression of FGF-4 within the AER [18].

However, deregulated- FGF expression is not limited to polydactyly. Bose *et al* proposed that changes in FGF expression by the AER has a role to play in syndactyly and that limb patterning is independent to each limb [19] (Figure 1.2).

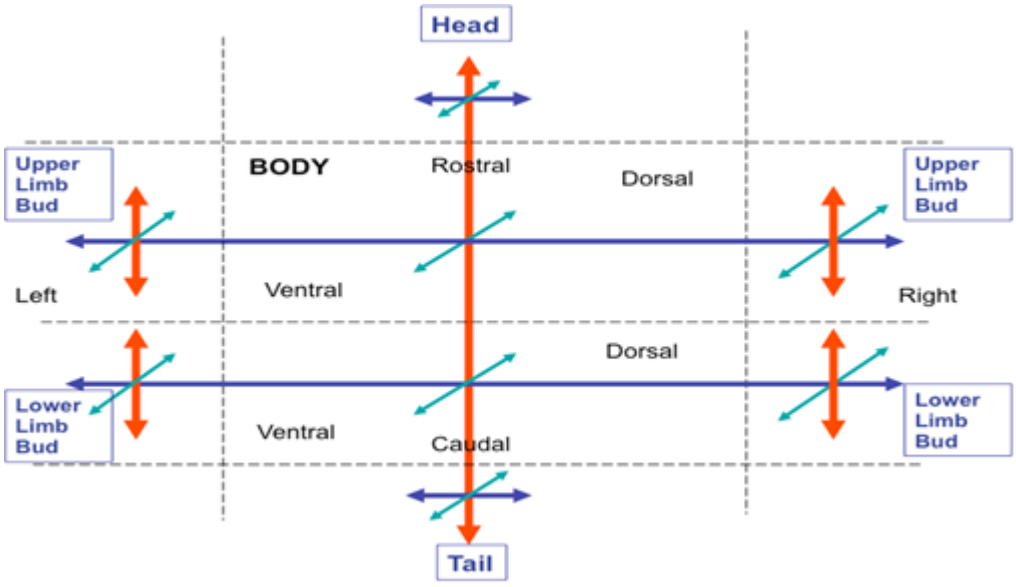

Figure 0.2 Independent Limb Development

The above image depicts independent limb development. Each limb develops independently in relation to proximo-distal patterning, with each limb bud developing its own polarity axises. The red arrows indicates the rostral- caudal axises, the light blue arrows indicate the dorsal-ventral axises and the blue arrows indicate the left-right axises.

Yu *et al* showed a vital role of FGF-4, FGF-8 and FGF-10 in limb formation. The lack of FGF-4, FGF-8 and FGF-10 resulted in agenesis (absence of limb formation) in mouse models.

This further highlighted the importance of the development and maintenance of AER-FGF signalling during limb formation [20]. The research found that FGF-4 and FGF-8 are required for normal limb bud development and complete inactivation of FGF-4 and FGF-8 resulted in SOX-9 expressing cells not being able to commit to osteochondral progenitors and failure to form any chondrogenic primordial [20]. Owing to distal mesenchymal defects, the AER or AER functions are not maintained at later stages and distal mesenchymal proliferation is inevitably reduced, which further reduces limb bud size [20].

By understanding the signals and the sequence of signals involved in the patterning and developmental process of limbs the use of stem cells as a therapeutical regime for limb injuries and disease can become more realistic and a possible future option. Embryonic development holds many a key to the patterning of limbs and subsequent development of specific components of the musculo-skeletal system.

1.2.3 Tendon Development

The molecular signalling and subsequent control of tendon synthesis has yet to be completely elucidated. Cell signal, cellular positioning and/or cellular polarity may play a role in the initial development of tendon with a transition from signal induced tendon development towards micro-movement maintenance of tendon development. To date, very little documentation in respect of the control and maintenance of tendon formation is available. Due to the close proximity of tendon to bone and muscle it is likely that the signalling patterns involved in bone and muscle formation may play a role in tendon formation. However, the role of collagen synthesis, secretion and subsequent extra cellular matrix formation plays a major role in tendon formation. The formation of the extra cellular matrix which contains collagen is vital in the provision of the mechanical properties observed in tendon [21]. Tendon development has been shown as early as E14.5 in the murine model and between days 6-9 in the chick embryo [22]. At this point the extra cellular matrix becomes populated with narrow-diameter collagen fibrils [22]. The majority of early embryonic tendon formation studies have been performed using chicks and between the days 6-9 in embryonic tendon, the tendon mass is mainly made up from cells and very little extra cellular matrix (ECM) [15]. Early tendon formation is as a result of the tendon fibroblast synthesising and secreting ECM [23].

The majority of early tendon research has been conducted using animal models. However research conducted by Shaw *et al.*[24] described early foetal human samples ranging from 51 days old through to 138 days old [24].

However, pre 45 days gestation there is little documentation of Achilles tendon initiation/differentiation and early formation. During foetal development (45-57mm) the

Achilles tendon is highly cellular with little sign of fibril genesis [24]. The Achilles tendon is indirectly attached to the cartilaginous anlagen of the calcaneus by a thick perichondrium [24]. It was also noted that the fat cells that are present in both the Kager's triangle and the plantar fascia had yet to develop and were only visible post 110mm (98 -100 days gestation). The formation of the fat pad within the Kager's triangle conveys a mechanical advantage in that the fat pad increases the lever arm of the tendon which leads to mechano stimuli of the developing tendon [24].

More recently the role of mechanical stimuli during embryonic Achilles tendon development is gaining attention. A delicate and essential relationship between development progression and mechanical stimuli is gaining favour. Research conducted by Vogel and Koob [25] and Gao *et al.* [26] showed mechanical loading induced metaplasia of tendon fibroblasts into fibrocartilage cells. The importance of mechanical loading was then further highlighted by Thomopoulos *et al*. [27] who showed that paralysis of the supraspinatus muscle in a murine model resulted in delayed development of the Achilles tendon and enthesis fibrocartilage. The relationship between tendon development and adjacent musculosketal components which transfer mechanical forces to the tendon were highlighted in 1949 by Wood Jones [28] and more recently by Benjamin *et al.* [29].

The development of a fully functional tendon structure requires not only chemical cues but also mechano-stimulation. However, to date the relationship between chemical cues and mechano-stimulation has yet to be elucidated in embryonic human development.

1.3 Tendon Structure

Healthy tendons are bright white in colour with a fibroblastic appearance. Tendons demonstrate a marked variation in form; they can be rounded chords, strap-like bands, or flattened ribbons. Within the extracellular matrix of the tendon, tenocytes and tenoblasts constitute 90% - 95% of the cellular element of the tendon [6]. The remaining 5% - 10% of the cellular element of tendons consists of chondrocytes at the region of bone attachment/insertion sites, synovial and vascular cells, including capillary endothelial cells and smooth muscle of the arterioles [6]. Tenoblasts are immature tendon cells, and are spindled-shaped with numerous cytoplasmic organelles, which reflect their high metabolic activity [6, 30]. Tenoblasts have a spindle morphology with an ovoid nucleus and size ranges from 20-70µm in length and 8-20 µm in width [31]. They contain large numbers of organelles like Golgi bodies, endoplasmic reticulum (ER) and also contain myosin and actin filaments [31]. As the tenoblast matures, they become elongated and transform into tenocytes. Tenocytes have a lower nucleus/cytoplasmic ratio than tenoblasts[5]. They are thin and long with reduced metabolism [5].

Tenocytes are metabolically adaptive and can generate energy via the aerobic Krebs cycle, anaerobic glycolysis, and the pentose phosphate shunt [32, 33]. As, tenocytes age the metabolic pathway choice shifts from an aerobic to an anaerobic preference [32, 33]. The oxygen consumption of tendons is approximately 7.5 times lower than that of skeletal muscle [33]. This lower metabolic rate and well-developed anaerobic energy generation capacity are essential to carry loads and maintain tension for long periods. This reduces the risk of ischemia and subsequent necrosis. However, the lower metabolic rate results in increase in time required for healing after injury [33].

Another factor resulting in the metabolic shift from aerobic to anaerobic energy generation by the tenocytes is how tendon is supplied by nutrients, namely the perfusion of tendon. Mayer *et al* [34] , Ahmed *et al.* [35] and Theobald *et al* [36] who collectively demonstrated that the majority of tendon perfusion was delivered by vessels contained within the anterior paratenon, derived from the posterior tibial artery in rabbits. The consensus opinion is that the human tendon is primarily perfused by the paratenon which decreases with age especially the mid-tendon region [36].

The tendon is composed of a collagen-tenocyte network and extracellular matrix, which contains proteoglycans, glycosaminoglycan, glycoproteins and other small molecules [5]. Adhesive glycoproteins such as fibronectin, tenomodulin and thrombospondin, participate in the repair and regeneration process in tendon [32, 37, 38]. The dry mass of human tendon is approximately 30% of the total tendon mass, with water accounting for the remaining 70%. Collagen type I is predominant (65% - 80%) but collagen Types III, IV, V and VI and proteoglycans, glycosaminoglycan, glycoproteins and other small molecules make up the remainder of tendon extracellular matrix (ECM) [31].

The collagen found within tendon is arranged in levels of increasing hierarchical complexity. This begins with tropocollagen, which is a triple-helix polypeptide chain, which unites into fibrils (primary bundles); fascicles (secondary bundles); tertiary bundles; and the tendon itself (Figure 1.3). The soluble tropocollagen molecules secreted by the tenoblast cross-link to create insoluble collagen molecules, which aggregate to form collagen fibrils. The collagen fibre is the smallest tendon unit that can be tested mechanically. Although collagen fibres are mainly orientated longitudinally, fibres also run transversely and horizontally, forming spirals and plaits [33].

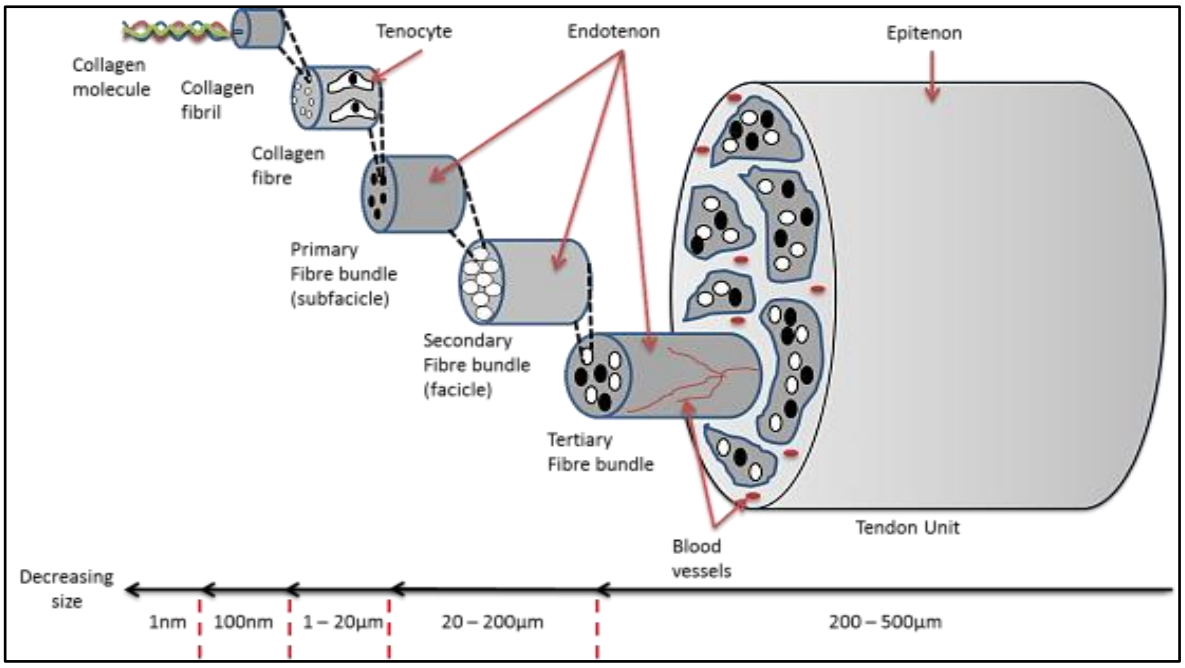

Figure 0.3 Normal Structure of Tendon

Tendon tissue has a multi-unit structure composed essentially of the fibril-forming type I collagen molecules, which are organised into individual sub-fascicles and fascicles separated by the ECM of the epitenon. Groups of fascicles form the body of the functional tendon, within which is a rich, vascularised and innervated ECM that is synthesized and maintained by the tendon fibroblasts, which typically align longitudinally in rows along the collagen fibres. Numerical diameter values taken from Richardson *et al* 2007 [39].

The other structural zones of the tendon are the epitenon and the endotenon which all contribute to the unique tendon properties. The epitenon, a fine, loose connective-tissue sheath containing vascular, lymphatic and nerve supply to the tendon, covers the whole tendon and extends deep within it between the tertiary bundles as the endotenon. The endotenon is a thin reticular network of connective tissue investing each tendon fibre [37]. The epitenon is surrounded by paratenon, a loose areolar connective tissue consisting of collagen fibrils Type I and Type III, some elastic fibrils and an inner lining of synovial cells [38]. Synovial tendon sheaths are found in areas subjected to increased mechanical stress, such as tendons of the hand and feet, where efficient lubrication is

required. Synovial sheaths consist of an outer fibrotic sheath and an inner synovial sheath, which consists of thin visceral and parietal sheets [3, 40, 41]. The inner synovial sheath invests the tendon body and functions as an ultra-filtration membrane to produce synovial fluid [42]. The fibrous sheath forms condensations, the pulleys, which function as fulcrums to aid the tendon function[43].

Tendons are linked to both bone and muscle through osteotendinous and myotendinous junctions, respectively. The osteotendinous junction is composed of four zones: a dense tendon zone, fibrocartilage, mineralised fibrocartilage, and bone [42]. The specialised structure of the osteotendinous junction prevents collagen or fibril bending, fraying, shearing and failure [43]. At the myotendinous junctions, tendinous collagen fibrils are inserted into deep recesses formed by myocyte processes, allowing the tension generated by intracellular contractile proteins of muscle fibres to be transmitted to the collagen fibrils [38]. This complex architecture reduces the tensile stress exerted on the tendon during muscle contraction and the complex interactions and arrangement of the collagen molecules and proteoglycans that convey the mechanical properties such as Young's modulus to tendon tissue [38, 43]. The fine structure and interactions between collagen-cellular and proteoglycan components of the tissue structure are what give tendon its unique mechanical properties such as Young's modulus However, the myotendinous junctions still remain the weakest point of the muscle-tendon unit and point of increased injury susceptibility.

1.3.1 Biochemical Components of Tendon Extra Cellular Matrix

The complex arrangements and interactions of the collagen fibres, elastin fibrils and proteoglycans deliver the unique mechanical properties of tendon [44]. Tendons are

composed of approximately 55 – 70% water of which a substantial part can be attributed to the association with the proteoglycans (PG) [45]. The most abundant collagen present in tendon is collagen I, and is organised into a helical arrangement along the largest axis of the tendon [46-49]. The micro structure of tendon is based around the helical structure of type 1 collagen with a typical helical protein of 270nm in length which is undergoes extracellular assembly resulting in a larger supra molecule of around 300nm diameter, which can eventually result in a helical collagen structure of up to several centimetres in length (Figure 1.2) [50]. Between 60 – 85% of the ECM component of tendons being made up of collagen [51]. This can then be further broken down to the exact types of collagen such as: ~60% Collagen type I [51], Collagen type II [52, 53],0 – 10% collagen III [54], ~2% Collagen type IV [55, 56], collagen type V and VI [45, 57-60], up to 1% Proteoglycans [61], ~ 2% elastin [62] and up to 1% cartilage oligomeric matrix protein (COMP) [63, 64].

1.3.1.1 Tenomodulin

The tenomodulin gene is located on the X-chromosome loci q21.33-q23. Tenomodulin is highly expressed in ligaments, tendon and eyes and some expression was also seen in liver, thymus, lungs, cartilage [65]. In tenomodulin deficient mice it was apparent that tenomodulin is involved in accelerating division of tenocytes and increasing the number of cells but that it did not affect synthesis of collagen type I and formation of blood vessels. It was also observed that in tenomodulin deficient mice the tendon's surface was rough as compared to smooth in case of normal mice. Tenomodulin also affects the collagen VI network by causing changes in its epitopes [66]. During tenocyte culture when scleraxis was expressed expression of the tenomodulin also increased [67]. This shows that tenomodulin expression depends on expression of scleraxis [68]

1.3.1.2 Tenascin –C

The tenascin-C gene can be found on chromosome 9q33.1. Tenascin C is expressed in the blastema, differentiated primordial and proximal tendons [69]. Tenascin-C has been used to mark primordial tendons. However, as it is also expressed in cartilage and nerves (glial) Tenascin-C cannot be used as a single tendon specific genetic marker[70].

1.3.1.3 Thrombospondin-4

The thrombospondins are a family of extracellular proteins that bind calcium and modulate cellular phenotype during tissue genesis and remodelling [71]. All of the thrombospondin proteins have been reported to bind not only calcium, but also heparin [71]. The thrombospondin-4 (THBS-4) gene loci is 5q.13 [71] and the subsequent pentamer protein product has been shown to also bind to fibrinogen, fibronectin, laminin and type V collagen [68]. However, the exact function of THBS-4 has yet to be discovered [68]. Research conducted by Baumeister *et al* has shown THBS-4 to be present in tendon mesenchyme. Both TNMD and THBS-4 have been detected in tendon tissue. A recent study by Jelinsky *et al* [68] has shown THBS-4 in conjunction with TNMD to be very specific to tendon tissue.

1.3.1.4 Collagen 1A2

The collagen 1A2 gene can be found on Chromosome 7 loci q22.1. The COL1A2 gene provides instructions for making part of a large molecule called type I collagen. Collagens are a family of proteins that strengthen and support many tissues in the body, including cartilage, bone, tendon, skin, and the white part of the eye (the sclera). Type I collagen is the most abundant form of collagen in the human body [72].

The COL1A2 gene produces a component of type I collagen called the pro-α2 (I) chain. Collagens begin as procollagen molecules, which must be processed by the enzymes outside the cell to remove extra protein segments from their ends (procollagen peptidase) and collagen cross-linking (lysyl oxidase). Each rope-like procollagen molecule is made up of three chains: two pro-α1(I) chains, which are produced from the COL1A1 gene, and one pro-α2(I) chain, which is produced from the COL1A2 gene [72]. After procollagens are processed, the resulting mature collagen molecules arrange themselves into long, thin fibrils. Individual collagen molecules are cross-linked to one another within these fibrils. The formation of cross-links results in very strong type I collagen fibrils, which are found in the spaces around cells.

1.3.1.5 Collagen 3A1

The collagen 3A1 gene can be found on Chromosome 2 loci q31. Type III collagen is found in tissues such as the skin, lungs, intestinal walls, and the walls of blood vessels [73]. The COL3A1 gene produces the components of type III collagen, called pro-alpha1 (III) chains. Three copies of this chain combine to make a molecule of type III pro-collagen. These triple-stranded, rope-like procollagen molecules are then processed by the enzymes outside (procollagen peptidase) the cell to remove extra protein segments from their ends. Once these molecules are processed, the collagen molecules arrange themselves into long, thin fibrils. Within these fibrils, the individual collagen molecules are cross-linked to one another by the enzyme lysyl oxidase. These cross-links result in the formation of very strong mature type III collagen fibrils, which are found in the spaces around cells [73].

1.3.1.6Decorin

Decorin (DCN) is a proteoglycan gene which can be found on chromosome 12 loci q21.33 and decorin belongs to the small leucine-rich proteoglycan family with an average size between 90 – 140 kDa [74]. Decorin consists of a protein core which contains leucine repeats and a glycosaminoglycan chain which may contain either chondroitin sulphate or dermatan sulphate [75]. Decorin has a structure similar to biglycan and can be either cellular or pericellular [74]. Decorin plays two major roles in tendon tissue: 1) matrix organisation and 2) fastening adjoining collagen fibrils together and the possible mechanical coupling of fibrils [76, 77]. Furthermore, decorin has also been shown to regulate the assembly of collagen fibrils and is a major contributor to the biomechanical properties of developing tendon [78].

1.3.1.7Fibromodulin

The gene coding for the fibromodulin protein is FMOD and has the gene loci of 1q32. Fibromodulin is a member of the small interstitial proteoglycan family and has a molecular weight of 67 – 110 kDa [79]. Lack of fibromodulin in developing tendon has been shown to result in alterations in collagen fibrils resulting in joint instability and abnormal gait [80]. Further investigation using double knockout mouse models have shown thinner collagen fibrils resulting in abnormal fibres in tendon [81]. Also an increased deposition of lumican was observed in the fibromodulin knockout mouse model leading to subtle changes in collagen architecture and mechanical properties in the collagen matrix which would account for the observations in gait change made by Ameye *et al*. [80, 81].

1.3.1.8Scleraxis

The Scleraxis gene (SCX) can be found on chromosome 8q24.3 and codes for a 60-100 amino acid protein which functions as a DNA-binding protein/transcription factor. SCX has been shown to be expressed from early stages of tendon development in limb bud tendon progenitors and in the syndetome somatic compartment that contains tendon progenitor cells during mouse embryogenesis [69]. Its expression in the buds of the limb was observed in four different phases. In the first phase (stage 21) both ventral and dorsal parts of limb showed scleraxis expression, in the second phase (25-27) the scleraxis expression was highly complex, in the third phase (28) formation of fibres occurred followed by their elongation and in the fourth phase (31) all the tendons of the limb were expressing scleraxis. It was also found that in order to maintain the expression of the scleraxis in the tendons, presence of FGF-4 was essential [70]. It was observed that in absence of (Fibroblast Growth Factor) FGF-4, tenascin and scleraxis expression was decreased in the limb of chick but on application of FGF-4 both these transcription factors showed an increment in their expression in the normal limbs and limbs of the chick that did not contain muscles [82]. Along with FGF4, FGF8 was also involved in increasing the expression of scleraxis but only at the last phase of development of the tendon. These factors (FGF-4 and 8) were released by the myogenic cells [4]. The expression of this protein can be stopped by BMPs but at the same time noggin can antagonize this effect [83]. It was also found that more collagen was produced by the activation of a promoter (COL1α1) due to attachment of SCX/E47 to the E box of the TSE2 so for the activation of COL1α1, TSE1 and 2 are essential. In fibroblast of the tendons, NFATc and SCX induce activation of the COL1α1 [84]. In mouse that were lacking this protein, the organization of the cells and matrix showed distorted geometry [85]

1.4 Mechanical Properties of Tendon

Tendons are designed for the transmission of forces with minimal deformation and energy loss [86]. The two primary features of tendon are stress-relaxation (decreased stress over time with constant deformation) and creep (increased length over time with a constant load). These two properties give rise to load-deformation relationship of tendon that is dependent on the activities prior to assessment [86].

1.4.1 Young's Modulus of Tendon

The primary role of tendon is the transmission of force from the muscle to the bone to enable joint movement [87, 88]. Unlike bone, tendon does not behave as a rigid body but instead exhibits viscoelastic behaviour [87, 88]. The most vital characteristic of tendon is observed in its Young's modulus when compared to other skeletal tissues. Young's modulus describes the elastic properties of a solid undergoing compression or tension in only one direction, and can be summarised as the normal stress divided by the linear strain (Figure 1.4). The mechanical properties of tendon depend largely on its location within the body. A typical small adult human tendon (from the forearm) has a Young's modulus of 1-2 GPa, an ultimate stress of around 100 MPa and an ultimate strain of 4-10% [89]. Similarly, the estimated Young's modulus for adult Achilles tendon has been reported to be 2 GPa , an ultimate stress of 80 MPa and an ultimate strain of 3.6-8.8% [90] and conversely for the human patella tendon an estimated Young's modulus of 1.5-1.7 GPa, an ultimate stress of 34-43MPa and an ultimate strain of 5.3-5.8% dependant on age [91]

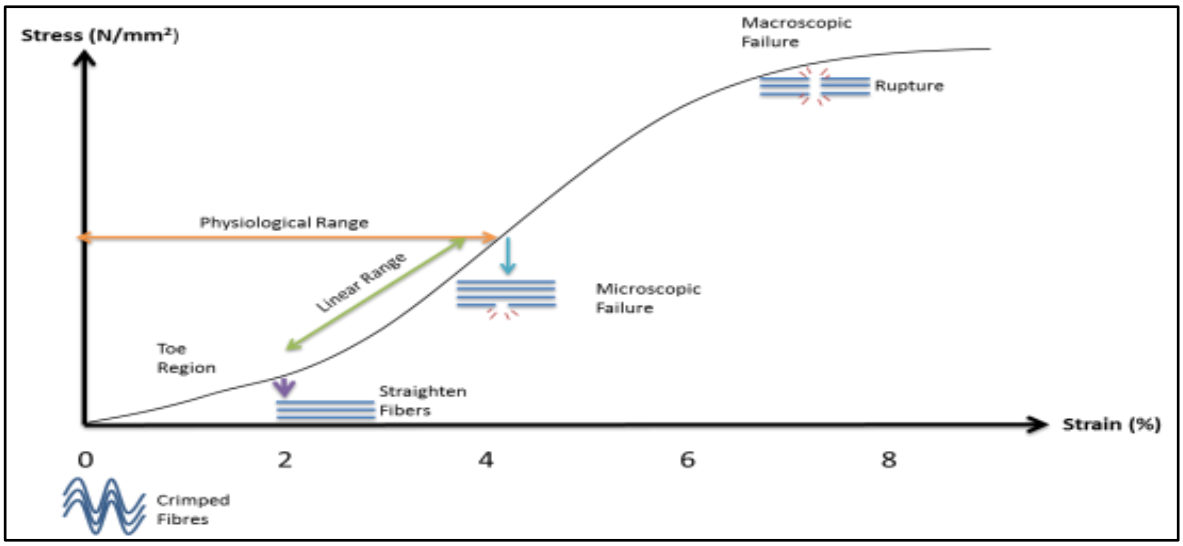

Figure 0.4 Graph to Illustrate the Young's Modulus for Tendon

The load-deformation curve of tendon has four distinct features in relation to the anatomic microstructure. The initial "toe" region corresponds to the arrangement of the fibres with the direction of stress. The linear region of the curve is as a result of the helical structure. The end linear region is where unpredictable failure begins, leading to eventual rupture and the recoil of tendon at the ruptured end [92].

1.5 Tendon Injury

As previously mentioned tendon injuries place a strain on the health care of many countries. Tendon injuries can be acute or chronic: the aetiology of tendon injuries can be classified as intrinsic or extrinsic factors. The intrinsic factors include: any anatomical predisposition, inability of the body's biomechanics to absorb forces. Extrinsic factors can include environmental factors and poor training techniques [30, 93].

Chronic tendon disorders have a high level interaction between intrinsic and extrinsic factors [30]. The main pathological stimulus for tendon degeneration has been shown to be excessive loading during high level physical training [30] . The formation of micro-trauma within the tendon structure over time and repeat excessive loading eventually

results in increased non-uniform stress and an increase in frictional forces resulting in partial or complete tendon rupture requiring medical intervention [30].

1.6 Tendon Healing

The major studies into tendon healing have predominantly been performed on animal models. Therefore, the relevance to the healing of tendinopathic human tendon still remains unclear [30]. Tendon healing has been classified into two modes namely intrinsic and extrinsic healing [94]. Intrinsic healing includes the migration and proliferation of cells from both the endotenon and epitenon to the injury site. The migrated cells lay-down and establish an extracellular matrix and an internalised neo-vasculature. Extrinsic t healing consists of the migration and infiltration of cells from the tendon periphery and external tissue source [94] . Once the cells have invaded the injury site they further initiate and promote repair and regeneration[94].

The combination of extrinsic and intrinsic tendon healing has been described as a three-phase process with each process having overlaps: -

- *First Phase*: (inflammatory phase) erythrocytes and inflammatory cells (neutrophils) infiltrate the site of injury. During the first 24 hours necrotic tissue is phagocytosed by macrophage and monocyte cells. Around the site of injury vasoactive chemicals such as nitric oxide and chemotactic factors such as cytokines are released and result in an increase in vascular permeability, angiogenesis initiation and an increase in tenocyte proliferation and migration of tenocytes to the wound where type III collagen synthesis starts.
- *Second Phase*: (Proliferative Phase) 2-4 days post injury the proliferative phase commences where synthesis of Collagen 3 is at highest and will last up to 2-3 weeks. Also, the concentration of water and glycosaminoglycans are elevated during this time.

- *Third Phase:* (Remodelling Phase) Approximately 6 weeks post injury remodelling commences. A decrease in cell numbers and reduced collagen and glycosaminoglycan synthesis. The remodelling phase can be sub-divided into two stages of consolidation and maturation stage. The consolidation stage starts approximately 6 weeks post injury and can last up to 10 weeks in this time the repair tissue shifts from cellular to fibrous. Also tenocyte metabolism remains elevated and the alignment of collagen fibres and tenocytes occurs also a shift to type I collagen synthesis occurs. After 10 weeks, the maturation phase occurs, where there is a shift from fibrous tissue to scar-like tendon, which can take up to 1 year.

Further to the cellular response in both intrinsic and extrinsic healing the application of exercise in the form of physiotherapy has been shown to improve tendon repair in numerous biomechanical studies [95]. The regime of exercise requires strict monitoring and will differ between patients [95]. Immobilised tendons have been shown to have a higher risk of adhesion formation [95]. Forces such as friction have been calculated for tendon and can be used to calculate the amount of force required (such as tension) to induce tendon gliding and can be applied to healing tendon as to prevent complications such as adhesion formation [95].

1.6.1 Current Treatments for Tendon Repair

Two major approaches are followed for the treatment of tendon injuries; conservative and surgical. However, both of these treatments regimes do not return tendon integrity or function to levels prior to injury [96].

With the *conservative route,* relief from pain is achieved by rest, analgesia, anti-inflammatory medication and physiotherapy (Table 1.1 that gives explanations for various conservative treatment regime/methods).

Treatment	Putative Target or Mode of Action
Rest or modification of activity	Removal of precipitating factors and prevention of re-injury
Orthotics (e.g. Heal inserts)	As above
Cryotherapy (e.g. Ice pack or baths)	Reduction of acute inflammation and decrease in cell metabolism
Heat Treatment	Stimulation of cell activity and a localised increase in blood flow
Physiotherapy (including massage and controlled motion)	As above
Electrical stimulation	Reduction of pain perception, stimulation of blood flow and increase in cellular activity
Laser treatment (pulsed or continued)	Possible analgesic effects and unspecified (unknown) effects on cell activity
Pulsed electromagnetic fields	As above
Ultrasound (0.75 - 3.0MHz, pulsed or continued)	Thermal effects on tissue, stimulation of cell activity and increased blood flow
Extracorporea; shock-wave therapy	As above, with possible stimulatory effects on neovascularisation and inhibition of nociception
NSAIDs	Reduction of inflammation through inhibition of prostaglandin synthesis
Corticosteroid injection (peritendinous)	Reduction of inflammation and other unknown effects (generally inhibitory to protein synthesis)
Low-Dose Heparin	Effects on tendon blood flow, possibly results in improved healing
Actovegin (deproteinised extract of calf's blood)	Unknown (suggested to promote glucose uptake and other effects on tendon cell metabolism that promotes repair and resolution)
Glycoaminoglycan polysulphate	Inhibition of inflammation, possibly also acting to inhibit metalloproteinase enzyme activity
Eccentric exercise therapy	Thought to promote restoration of normal tissue structure, possibly through an effect on cell activity and matrix remodelling
Sclerosant injection (ultrasound - guided)	Blocks tendon blood flow(targets neovascularisation and associated nerve in-growth)
Platelet-rich plasma injection	Contains growth factors (e.g. Transforming growth factor -β and platelet-derived growth factor that promote matrix synthesis and tissue repair

Table 0.1 Conservative methods for treating tendinopathy

Conservative treatment regime and putative target or mode of action for tendon injuries. Table replicated and adapted from Riley (2008) [37].

The conservative treatment of tendon injuries still requires a long period of time. This is due to the poor vasculisation and subsequent low rate of metabolism of the tendon cells, which results in a reduced healing capacity of tendon tissue [97].

To enhance the healing of the tendon, mechanical conditioning can be delivered by mechanical stimulus which is in turn converted into biochemical signalling via a process known as mechanotransduction [98]. Tendons can alter their composition and structure to adapt to load (mechanical) changes by up-regulating expression of those genes that code for growth factors which promote healing, such as platelet-derived growth factor (PDGF), vascular endothelial growth factor (VEGF), basic fibroblast growth factor (bFGF/FGF-2) and transforming growth factor beta (TGF-β) [92].

Other than the conservative route for tendon injuries the use of surgery is applied. The open technique may utilise suture or grafts [99]. If the injury is large, then grafts are utilised, but they have some drawbacks such as implants do not have a long practical life *in situ*. Also, poor biocompatibility which leads to an immune response which may lead to further or re-injury [100]. Allograft and autologous grafts may be used but both have some drawbacks such as the danger of immune rejection (allograft) due to immunological reactions [101], which may cause problems during remodelling [101, 102]. Further complications due to immune responses may occur. Such as adhesions that limit joint flexion, fibrosis and paucity of tendon differentiation signals during remodelling [103, 104]. Also, the lack of adequate donors limits the use of allografts. The use of autografts is restricted by surgical induced morbidity of the donor site [98]. The damage induced at the point at of harvest may cause further tendonitis and pain, leading to long time periods of rehabilitation [105]. However, since the development of cell culture and bio-scaffolds, the use of autograft can be re-evaluated when using scaffold along with autologous cell harvest and expansion techniques. Rather than harvesting whole tissue for implantation

the harvest of cells to be expanded or differentiated and then re-implanted as part of a scaffold that can induce cellular attachment.

1.6.2 Synthetic Tendon Implants

A more recent strategy which employs a synthetic scaffold to bridge the tendon defect, have been employed by many research group. This strategy which uses scaffold only and has utilised materials such as: nylon, carbon fibres and dacron for tendon injuries repair, but the success is very much limited, with high rates of failure [96]. Therefore, another strategy is highly desired to provide a functional alternative. More recently, research has been focused on the use of synthetic and biological scaffolds that are capable of withstanding the physical properties endured by tendon. Once the physical requirements of the scaffold have been addressed the incorporation of a cellular component to the scaffold. The addition of a cellular component that can be incorporated to the scaffold and either induce cellular regeneration or actually become "new" tendon is highly desired. Cells such as tenocytes or mesenchymal stem cells could be introduced with the scaffold and mechanically stimulated. Mechanical stimulation has been shown to enhance development of matrix, improve structural properties and drive the differentiation process. Another component could be added to the tendon scaffold such as a growth factor delivery system which could further enhance differentiation and ultimately scaffold integration. However, to date such a scaffold system does not exist and limited success in tenocytes-scaffold fusion to the proposed scaffold [106].

Synthetic Scaffolds require specific properties as they are exposed to various mechanical and biological factors after their implantation into the patient's body. These properties should include as a prerequisite:

- Immunologically inert
- The ability to withstand the mechanical properties endured by native tissue
- Biodegradable or bioresorbable

Ideally the synthetic scaffold should be metabolised by enzymes that are "natural" to the metabolic pathways of the specific tissue at point of implantation within the body. Furthermore, the rate of formation of new tissue and scaffold degradation should show an inverse relationship (as the tissue formation increases the mass of implant decreases until the new tissue completely replaces the implant/scaffold).

1.6.3 Acellular tendon implants

Acellular tissue grafts have been used in the repair of neglected tendon ruptures [107, 108], graftjacket® being used in both the augmentation of mid-substance peroneal tendon defects [109] and the repair of lacerated anterior tibial tendon [110]. Graftjacket® has been shown to reduce pain and has also been shown to be tolerated well by recipients with the implant showing integration to the recipient tissue after 20 -30 months [110]. Barber *et al*. showed graftjacket® to have favourable mechanical properties when implanted to augment rotator cuff repair [111, 112]. However, when repairing Achilles tendon defects the graftjacket® had an ultimate load failure of 50% of native tendon and a 33% stiffness when compared to native tendon [111, 112]. Due to the failure rates in mechanical properties the requirement for a tissue engineered approach especially for Achilles tendon is highly desired and may include the use of synthetic polymers.

1.6.4 Synthetic Polymers Currently Being Researched as Tendon Implants

Many polymers have been investigated for their potential use in tendon repair. Examples of such polymers are shown below in Table 1.2.

Polymer	Repair Type	Outcome	Reference
Polyglycolic Acid (PGA)	Canine Rotator cuff	Slight improvement in mechanical properties compared to the control group.	Derwin *et al.*[113]
Polylactic Acid (PLA)	Rabbit Rotator cuff	Fibroblast alignment and tissue pattering in compared to control.	Yokoya *et al.*[114]
Poly (lactic-co-glycolic) Acid (PLGA)	Rabbit Achilles Tendon	Cellular infiltration and polymer integration at point of attachment.	Ouyang *et al.*[115]

Table 0.2 Polymers implanted in a tendon repair model.

Previous studies using implants to repair tendon injuries have employed polymers such as polyglycolic acid (PGA) and polylactic acid (PLA) [113]. Varying degrees of success have emerged ranging from histological indications of fibroblast alignment and patterning in PLA models when compared to the PLA control and slight improvement in mechanical properties of the repaired tendon in Japanese white rabbits with the PGA scaffold [114]. However, to date there are no commercially available polymer based scaffold available for the treatment of tendon injury. PLGA implanted to repair a tendon defect in the rabbit model showed cellular infiltration and integration at the point of attachment [115]. Although the implants researched have shown tissue integration, cellular alignment and

minimal immune response and improved mechanical function compared to control groups. PLA, PLGA and PGA implants have failed to return the mechanical properties observed in native tendon.

One promising polymer group that has a potential use in tendon repair is the polyhydroxyalkanoates (PHAs). PHAs are a group of natural polyesters that can be biologically synthesised by a wide range of micro-organisms [116]. PHAs are synthesised via biosynthesis pathway (Figure 1.5) and form granules within the cytoplasm, Therefore, the PHA serves as an energy store much like lipids/glycogen in mammalian cells. PHAs can contribute up to 80% (w/w) of the cell dry weight matter of cell or even more. Due to the high percentage w/w ratio up scaling of the production of the PHAs is being highly researched. Large-scale production of PHA is based upon the industrial fermentation employed by pharmaceutical industry in the production of antibiotics in the early 1920s [117]

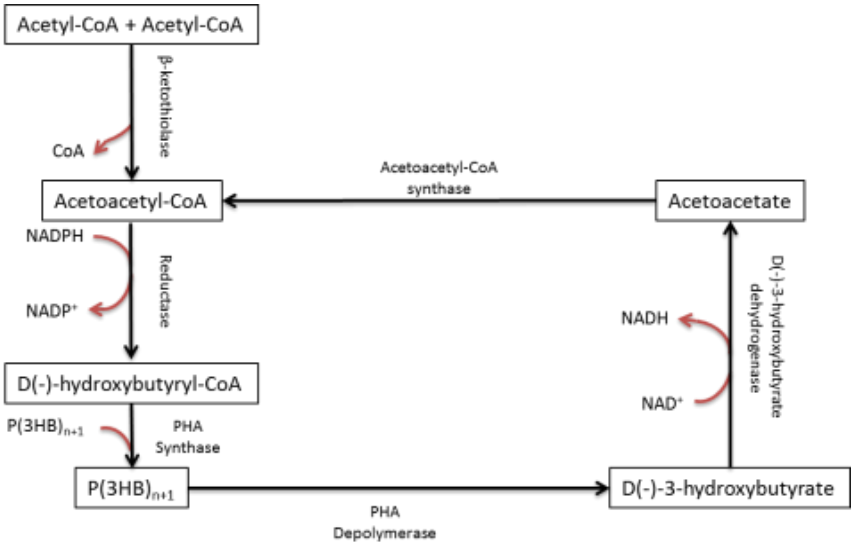

Figure 0.5 Metabolic pathway involved in the synthesis and breakdown of PHB in Eutropha

When carbon source is plenty and the organism is stressed the PHB metabolic pathway for *Europha* is activated and Acetyl-CoA is channelled to towards P(3HB) synthesis which in turn is channelled towards D(-)-3-hydroxybutyrate [118]**.**

Depending on the nutrient stress placed on to the organism can results in different PHA molecules being synthesised (Figure 1.6). This can allow manipulation of the growth environment to produce a range of polymers.

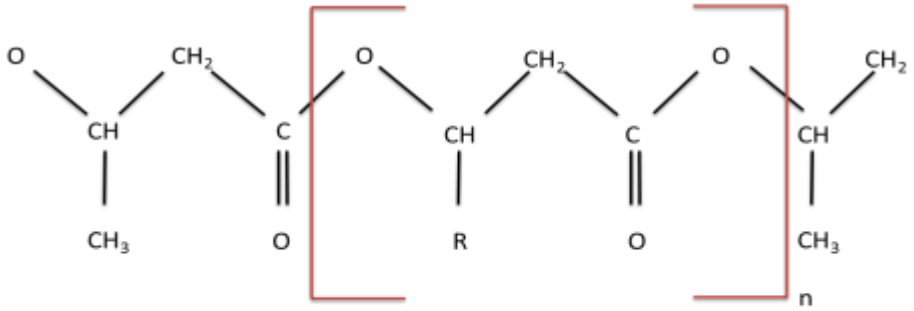

R = Functional group

(n varies from 600 to 35000)

R= Hydrogen	Poly(3-Hydroxypropionate)
R= Methyl	Poly(3-Hydroxybutyrate)
R= Ethyl	Poly(3-Hydroxyvalerate)
R= Propyl	Poly(3-hydroxyhexanoate)
R= Pentyl	Poly(3-Hydroxyoctanoate)
R= Nonyl	Poly(3-hydroxydodecanoate)

Figure 0.6 Structure of polyhydroxylalkanoates

Basic carbon backbone structure of PHBHHx, with R indicating the position of the functional group with the polyhydroxyalkanoate polymer. The blending of a polyhydroxyalkanoate can be achieved by varying the functional group. The percentage ratio of different functional groups can convey different mechanical properties [118]**.**

1.6.5 Poly -3- hydroxybutyrate-co-3-hydroxyhexanoate

Polyhydroxybutyrate (PHB) was the first Polyhydroxyalkanoate (PHA) to be discovered and is the most extensively studied [118]. Poly-3-hydroxybutyrate-co-3-hydroxyhexanoate (PHBHHx) is a co-polymer, which consists of 3-hydroxybutyrate and 3-hydroxyhexanoate [119]. Both polymers are members of the PHA family and are produced by microorganisms when stressed due to unbalanced growth conditions with the presence of excess carbon source and are stored within the cytoplasm of the organism as insoluble inclusions [119, 120].

PHBHHx has also been made in to fibres (Figure 1.7) and electro-spun microfibers making this material very pliable and adaptable for control of degradation rates dependant on surface area/volume ratio and molecular weight [119]. Furthermore, improvements in

some of the physical properties of the PHBHHx polymer have been achieved by adjusting the ratio of HB to HHx. The adjustments in the ratio of HB to HHx results in an alteration in both Young's modulus and strength of the PHBHHx polymer, allowing the polymer to be used in a possible array of applications [119].

Recent research into the biocompatibility of PHBHHx and its blends, have been evaluated *in-vitro* by the use of murine fibroblast cell line L929. Results from this study showed PHB and PLA films to have poor biocompatibility ,whilst PHB - PHBHHx and PHBHHx showed a vast improvement in biocompatibility and the level of improvement was dependant on the amount of PHBHHx present in the blend [119].

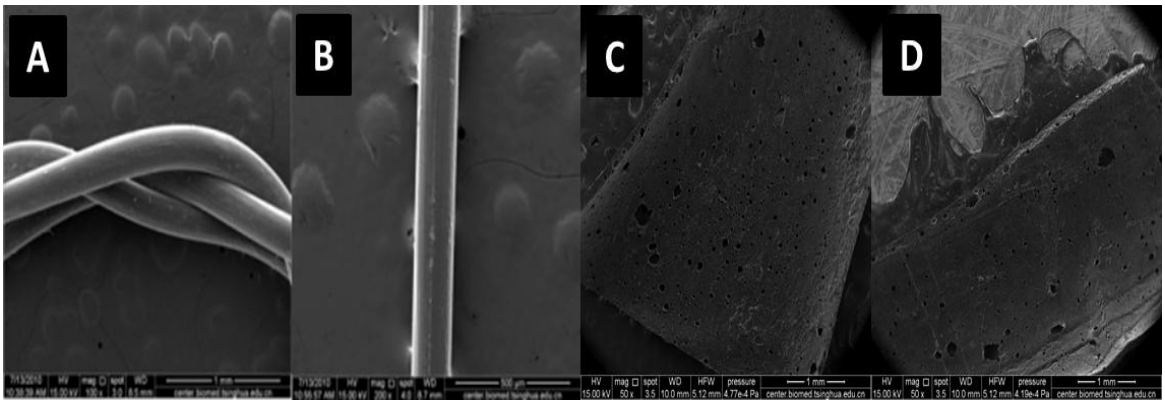

Figure 0.7 Scanning electron micrograph of PHBHHx fibres

A) PHBHHx weave of 3 strands of 217um in width and B) Shows a single strand of PHBHHx used in A, C & D) show cross-section samples of PHBHHx porous filmsAll images were taken at the Department of Microscopy using Scanning Electron Microscopy, Tsinghua University, China.

Also, by mixing blends alterations in young's modulus and strength have been reported [119]. Therefore, PHBHHx is a good choice for investigation into its potential use as a biodegradable implant in the treatment and repair of tendon using cell based therapies and developmental biology.

1.7 Vitamin C

Vitamin C (ascorbic acid) has been shown to be vital in many biological processes. Early research into collagen synthesis has shown Vitamin C to be vital in the synthesis of healthy collagen [121, 122]. Research performed by Elster showed that collagen did not require ascorbic acid [123]. Whereas, Robertson and Schwatrz showed that precollagen increased when guinea pigs were nutritionally supplemented with ascorbic acid in a wound healing model [121].

The requirement for ascorbic acid for collagen synthesis is vital in connective tissue development as ascorbic acid is required for enzyme activity in the synthesis of both hydroxyproline and hydroxylysine [124, 125]. The major function of hydroxyproline is to serve as a molecular stabiliser in that hydroxyproline stabilises the collagen triple helix and the absence of this molecule leads to unstable collagen [125]. Hydroxylysine is required for not only the intercellular crosslinking of collagen but also the glycosylation of collagen which is thought to be important in the crosslinking of collagen and further adding to the mechanical properties of collagen [125].

The major modulation of collagen synthesis is achieved by ascorbic acid through its effects on prolyl hydroxylation via prolyl hydroxylase (Figure 1.8) [125]. Murad *et al* also noted and increase in lysyl hydroxylase activity when human fibroblast cells were supplemented with ascorbate [125]. Lysyl hydroxylase is vital in the cross link formation of collagen and ascorbic acid has been shown to increase intracellular hydroxylation and inhibit extracellular oxidation of collagen residues [126]. Furthermore, Murad *et al* postulated that due to collagen levels continuing to rise even after optimum levels of ascorbate had been achieved that the influence of ascorbate on collagen synthesis could

not be only attributed to hydroxylation. However, ascorbic acid is a key component for collagen synthesis [125]

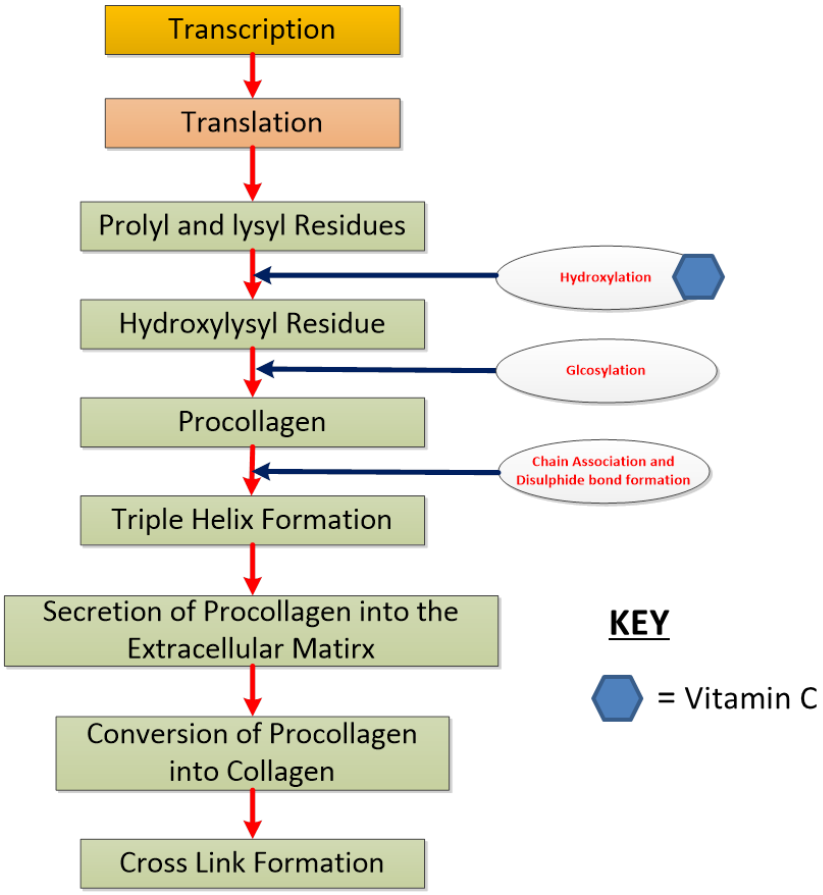

Figure 0.8 Effects of Vitamin C on the biosynthesis of collagen flowchart.

Biosynthetic pathway for collagen indicating the point of cofactor interaction by Vitamin C adapted from Sharma et al [124].

1.8 Oxygen Tension

The most critical component for aerobic cell survival is the presence of oxygen [127]. A reduction in oxygen availability can lead to not only loss of cellular functionality, but also cell death [127]. 21% Oxygen culture environment is widely considered to be the normoxic condition, however, physiological normoxia is actually within the range of 2% - 9% for the majority of cell types within the adult mammalian system [128].Due to the requirement of oxygen over the course of animal evolution, both special and sensitive mechanisms have developed to minimise the possible disastrous effects of low oxygen, such as transcriptional profile alteration [129].

The importance of oxygen gradients within the stem cell niche can be traced to early research conducted on endometrial and trophoblastic tissues in early pregnancy [130]. Prior to the formation of a circulatory system, the delivery of oxygen to the developing embryo is subject to the limitations of diffusion, with the estimated diffusion distance for oxygen being 150µm [131, 132]. Therefore, early mammalian development actually occurs in a relatively low oxygen environment.

Hypoxic culture environments have been shown to maintain the undifferentiated state of stem cells such as hematopoietic stem cells [133], mesenchymal stem cells [134], neural stem cells [135] and human embryonic stem cells [136]. Furthermore, hypoxic conditions have also been shown to influence quiescence, proliferation, differentiation leading to cell fate commitment [127]. Stem cells are primarily defined by their ability to self-renew and maintain a production of mature cells, which has been found to reside predominantly within a hypoxic niche [137, 138].

The hypoxia inducible factor (HIF) group of gene products play a major role in the maintenance of stem cell potency [129]. Currently, there are six known HIF genes which code for six transcription factors (Table 1.3).

Recent observations in the hypoxic cultivation of hMSCs not only prevents their differentiation, but also increases their proliferation potential [139]. Further research by Grayson *et al* (2007) showed that cultivation in hypoxic conditions leads to an increase in the expression levels of the *HIF-2α* protein and the *Oct4* protein which is associated with not only undifferentiated phenotype but also the self-renewal of stem cells [140].

Member	Protein	Gene
HIF-1α	Hypoxia-inducible factor 1, alpha subunit	*HIF1A*
HIF-1β	Aryl hydrocarbon receptor nuclear translocator	*ARNT*
HIF-2α	Endothelial PAS domain protein 1	*EPAS1*
HIF-2β	Aryl hydrocarbon receptor nuclear translocator 2	*ARNT2*
HIF-3α	Hypoxia-inducible factor 3, alpha subunit	*HIF3A*
HIF-3β	Aryl hydrocarbon receptor nuclear translocator 3	*ARNT3*

Table 0.3 Members of the HIF transcription factors and genes.

HIF are sub divided into 3 groups of 2 members namely α and β. The table above shows the HIF member and associated protein along with gene name [129]**.**

An array of studies have been undertaken to investigate the effects of low oxygen environments on ESCs which employed the use of ESCs derived from many species (e.g. human, and ovine), where an increase in the inner cell mass size has been observed in ovine research [141]. Low oxygen tension has also shown an enhancement in hESC clonal recovery and a reduction in chromosomal abnormalities [142]. HIF-2α has also been shown to be up-regulated in hESC which results in the suppression of p53 and ultimately

enhances the stemness and regenerative potential when cultured under hypoxic conditions [143].

Therefore, the differentiation of both mesenchymal and embryonic stem cells towards a tenocyte lineage should be investigated at both 21% and 2% oxygen environments due to the effects of HIF proteins on differentiation.

1.9 Stem Cell Therapy

Since the discovery and subsequent isolation for embryonic stem cells, which Nobel Prize was awarded to Sir Martin Edwards, Mario R. Capeechi and Oliver Smithies. Stem cells and their potential application have held hope for those afflicted with incurable and degenerative disease. To date, the treatments and/or therapies that employ embryonic stem cells that have been translated from the laboratory to the clinical application have been very few.

Stem cells were first studied by Becker *et al.* in 1963 with the injection of bone marrow cells into irradiated mice and subsequent nodule development in the spleens of the mice in proportion to the number of bone marrow cells injected. From this research, they concluded that each nodule arose from a single marrow cell. Subsequently, they determined that these cells were capable of infinite self-renewal, a central characteristic of stem cells [144]. Thus, stem cells by definition have two essential properties, i.e. the capacity of self-renewal, giving rise to more stem cells, and the capacity to differentiate into different cell lineages under appropriate conditions. Broadly speaking, there are two main types of stem cells, embryonic and non-embryonic. Embryonic stem cells (ESCs) are pluripotent and, accordingly, they can differentiate into all three embryonic germ layers [145]. Non-embryonic stem cells (non-ESCs) derived from marrow, fat or cord-blood are

multipotent; their potential to differentiate into different cell types seems to be more limited [146].

1.9.1 Human Embryonic Stem cells

Alexis Carrel was a Nobel laureate and an innovative surgeon, his experiments with the transplantation and repair of body organs led to advances in the field of surgery and tissue culture. In January 1912, he placed part of a chicken's embryo heart in a culture containing fresh nutrient medium. He found that every 48hrs the tissue doubled in size. This continued for 34 years, outliving Carrel himself. Even though these cells were unlikely to be embryonic stem cells but more likely related to chord-derived or foetal cells, this experiment showed the future potential of embryonic/foetal cells and tissue culture [147, 148].

Murine Embryonic Stem (ES) cells were first described in 1981 [145, 149]. The development of ES cells evolved from the work on murine teratocarcinomas, which are tumours that arise in the gonads and consist of an array of somatic tissue arranged in a disorganised fashion [150]. In 1995 primate ES cells were derived from rhesus monkey pre-implantation blastocysts and later from the marmoset [151, 152]. It was not until 1998 when expanding the previous primate studies that Thompson and co-workers derived human ES cells from surplus blastocysts donated by couples undergoing fertility treatment and it was at this point at which embryonic stem cell research evolved [150, 153].

Many of the advances in stem cell science are based on developmental studies of mouse embryogenesis. The first stage of life, the fertilized egg, has the potential to generate an entire organism. This capacity is defined as totipotency and is retained by the early

progeny of the zygote up to the eight-cell morula. Subsequently, cell differentiation results in the formation of a blastocyst composed of the outer trophoblast cells and undifferentiated inner cells, commonly referred to as the inner cell mass (ICM) (Figure 1.9 differential pathway from zygote to blastocyst).

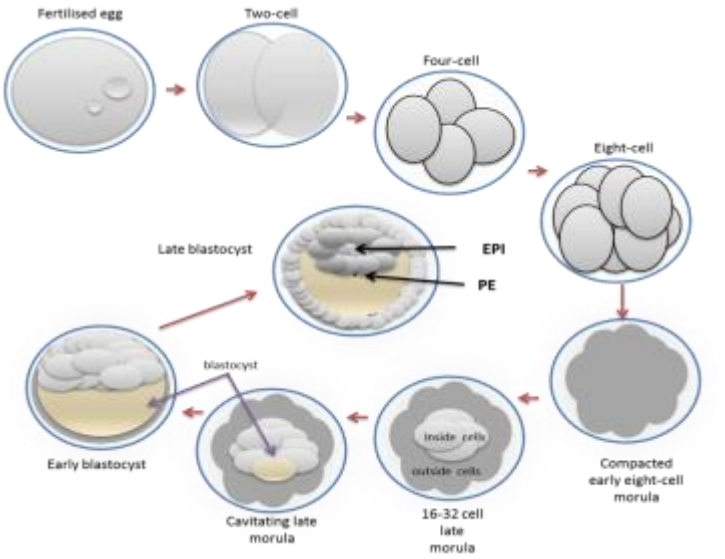

Figure 0.9 Post fertilisation blastocyst development prior to embryonic stem cell extraction.

The fertilised egg from 2 cells to 4 to 8 cells to become the early morula. When the morula reaches 16 to 32 cells there are distinctive inner and outer cells, as the morula continues to develop a distinct late cavitation. The morula can be observed until the early blastocyst has developed. The early balstocycst continues to develop through to the late blastocyst were the PE-Primitive endoderm and EPI-Pluripotent epiblast are found [150].

Cells of the ICM are no longer totipotent but do retain the ability to develop into all cell three germ layers and subsequently the specific tissue types (Figure 1.10). The cells within the blastocyst then become the one of three germ layers (Ectoderm, Endoderm and Mesoderm) that will eventually give rise to all the cellular components and tissue of a fully developed foetus.

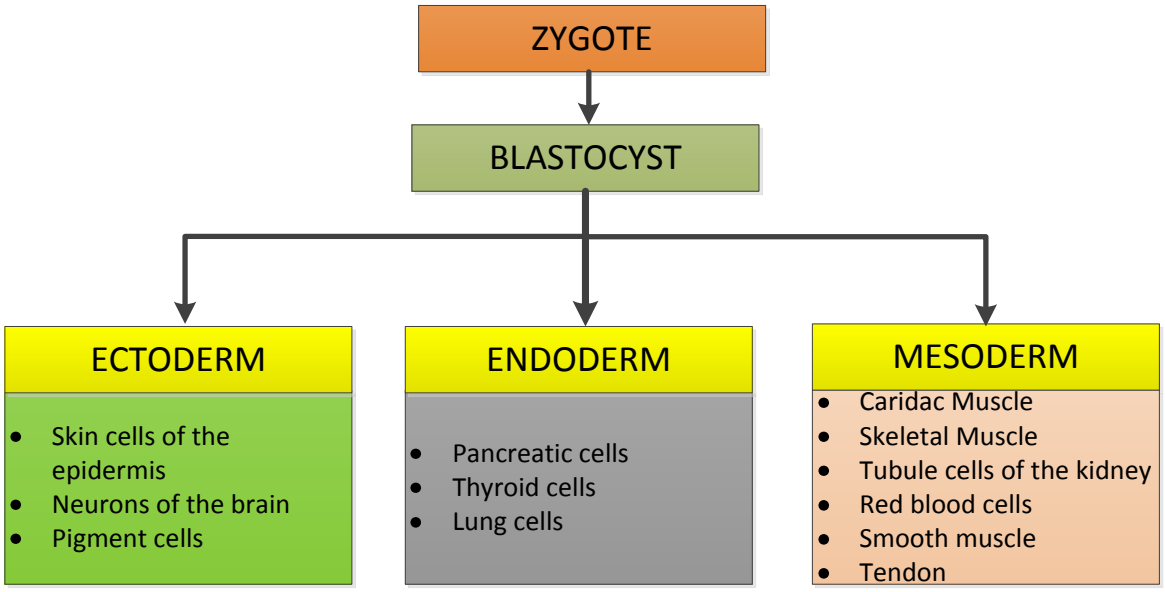

Figure 0.10 ESC differential potential of embryonic stem cells

The early zygote develops into the blastocyst from which all three germ layers will arise and eventually develop in to a fully developed foetus [150]**.**

1.9.2 Human Mesenchymal Stem Cells

The concept of mesenchymal stem cells (MSCs) is a term first coined by Arnold Caplain (1991) and can be traced to experiments demonstrating that the transplantation of bone marrow (BM) to heterotrophic anatomical sites resulted in *de novo* generation of ectopic bone and marrow [154]. Further examples of such studies date back to the 19th century by Goujon, and also the work of Tavassoli and Crosby (1968), which clearly established proof of an inherent osteogenic potential associated with BM. The Tavassoli and Crosby experiments were conducted with entire fragments of bone-free BM, the precise identity of any cell functioning as a progenitor of differentiated bone cells and therefore of non-haemopoietic, mesenchymal cells could not be delineated.

It was not until a series of seminal studies conducted by Friedenstein and co-workers in the 1960s and 1970s, who demonstrated that the osteogenic potential, as revealed by

heterotrophic transplantation of BM cells, was associated with a minor subpopulation of BM cells [154, 155]. These cells were distinguishable from the majority of haemopoietic cells by their rapid adherence to tissue culture vessels and also by the fibroblastic-like morphology of their progeny in culture, which indicated their origin from the stromal compartment of BM [155]. Further work by Friedenstein and co-workers provided a second major breakthrough by showing that seeding of BM cells suspensions at clonal density resulted in the establishment of discrete colonies initiated by single cells (known as the colony-forming unit fibroblastic, CFU-Fs) [155]. *In vivo* transplantation led to the recognition that multiple skeletal tissues (bone, cartilage, adipose tissue, and fibrous tissue) could be experimentally generated, *in vivo*, by the progeny of a single BM stromal cell [155]. Friedenstein and Owen called this cell an "Osteogenic stem cell", and later in 1988 called the cell a "Stromal stem cell". The implications of these discoveries were initially only appreciated by experimental haematologists, only later was the relevance to tissue biology and disease appreciated.

In 1978 Schofield conceptualised the "Stem cell niche hypothesis" with the notion that haemopoietic stem cells (HSCs) are regulated by their physical association with discrete cellular microenvironment within the BM. This hypothesis was substantiated by further experimental observations by Dexter *et al*., 1977; Allen, 1978; Dexter and Testa, 1976 [155].

The pioneering works by Tevassoli, Friedenstein, and Owen revealed that a second type of stem cell could be present in the BM and, specifically, in the haematopoiesis-supporting stroma [155]. The concept of non-haemopoietic stem cells in BM did not resonate worldwide until the additional work of Pitttenger in 1999. Combined with the

timing of the isolation of ES cells, the term mesenchymal stem cells (MSCs) gained wide popularity and in the minds of many, MSCs became one kind of postnatal human stem cell with a differential properties broader than originally envisioned and possibly as broad as ES cells (Figures 1.11).

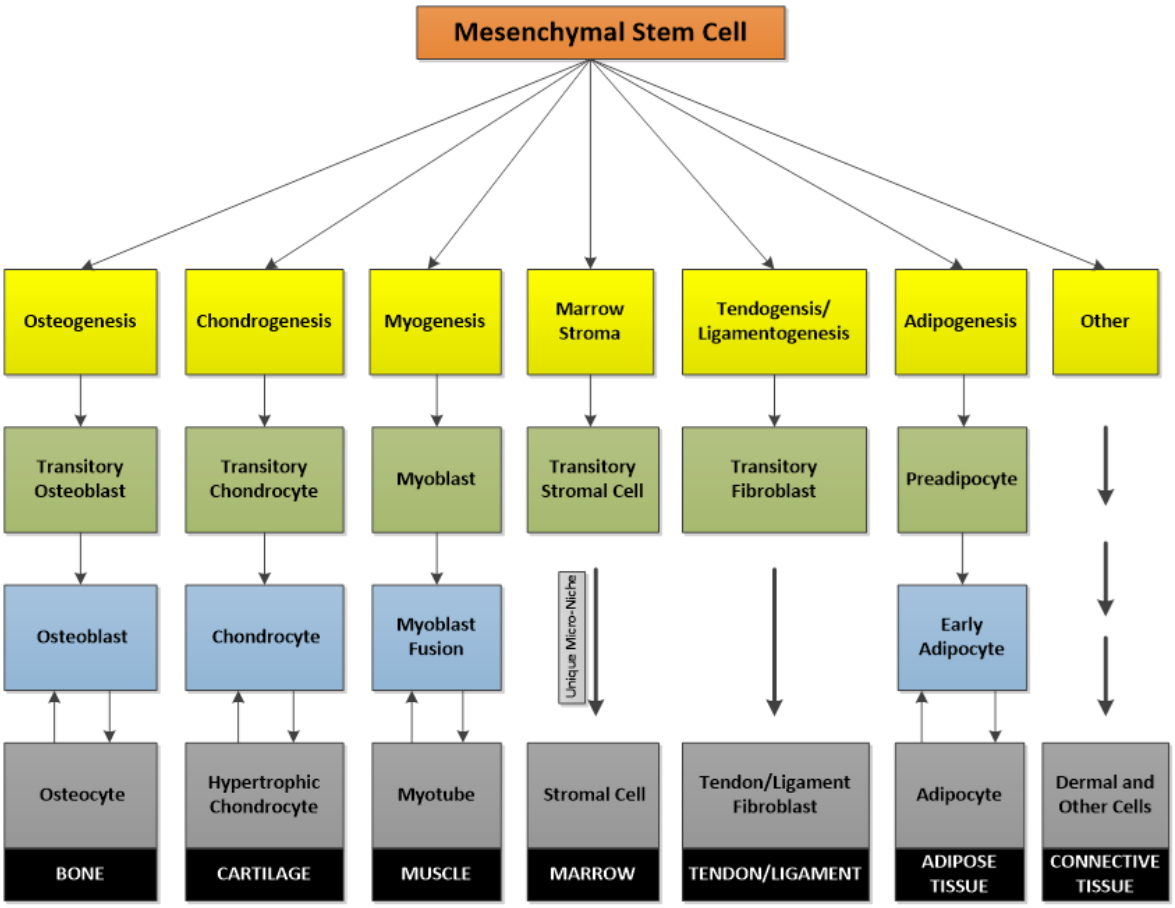

Figure 0.11 Mesenchymal stem cell differentiation potential

Differentiation properties and cell lineage arising from MSCs which include: bone, cartilage, muscle, stromal, tendon/ligament, fat and dermal tissues [155-157].

Currently BM derived MSCs are being used in an array of research topics in tissue engineering including tendon repair [156], tendon and ligament engineering [157], myocyte generation [158] and neuronal differentiation [159] to mention a few.

1.9.3 Tendon Progenitor Cells

Present in the extracellular matrix of the tendons are tendon stem progenitor cells (TSPC) [160]. Comparison of TSPC with cells of the human bone marrow demonstrated that the TSPC showed increased expression of tenomodulin, scleraxis and collagen type I, which are all markers of tendon cells in comparison to bone marrow cells and type II collagen (expressed in case of cartilage and bone) was not expressed by either of these cells. The extracellular matrix was responsible for regulating the renewal and differentiation capacity of TSPC and it was subsequently found that fibromodulin (Fmod) and biglycan (Bgn) was present in the matrix and were highly expressed in TSPC and were responsible for converting TSPC into tendon tissue [160]. These findings have been supported by the fact that when these two proteins were not expressed in the matrix or when their expression was inhibited then bone tissue was formed. This evidence highlighted that the two proteins were playing a very important role in the extracellular matrix (Niche) by regulating the signalling pathway of the BMP in order to give rise to tendons by differentiating TSPC and this conversion of TSPC into tendons often got disturbed in the absence of Bgn and Fmod, leading to the disruption of collagen fibre organisation which lead to big gaps in the tendon followed by an increment in the collagen type II and aggrecan (marker for chondrocyte) and a marked decrease in the expression of collagen (Type I) and scleraxis, ultimately leading to formation of bones [160]. However, the key limitation to the use of TSPC is that tendon contains a reduced number of cells than other tissue meaning a vastly lower number of TSPC within the tendon. Also the process of harvesting the cells would induce further trauma to the tendon [160].

1.10 Growth Factor Induced Tendon Regeneration

Growth factors can engage in autocrine, juxtacrine, paracrine and endocrine stimulation. If the receptor resides on the same cell where the ligand is expressed, the resulting cellular stimulation is autocrine; when the growth factor diffuses from cell to neighbouring cells in the same organ/tissue, stimulation is paracrine, and juxtacrine stimulation is a mode of signalling reserved for those membrane-anchored growth factors, which interact with receptors located on the neighbouring cells. When a factor is transported through the bloodstream from the place of synthesis to other tissues equipped with a receptor that can recognise the factor, stimulation is endocrine, as in the case of hormones such as insulin and human growth hormone (hGH) [161]

Recently many papers have been published in regards the use of growth factor induced tendon regeneration. An array of growth factors and combination of growth factor cocktails have been investigated and include members of the Transforming growth factor super family (TGF), Platelet derived growth factor (PDGF), Bone morphogenic proteins (BMP) and vascular endothelial growth factor (VEGF) with varying degrees of success (Table 1.4).

Growth Factor	Type of treatment and species	Results and References
bFGF	ACL in Canine [162] MCL in Rabbit [163] PT in Rat [164] Flexor tendon in Canine[165]	Enhanced tendon healing was observed in ACL canine[162] . Early formation of tissue repair was observed in MCL in rabbits [163]. Increased expression of Collagen 3 in PT repair in the rat model [164]. No improvement was observed in flexor tendon canine model with increased scar tissue formation was observed [165].
GDF-5	Flexor tendon in Rabbit	All repairs failed. Increased early maximum load observed in GDF-5 treated samples compared to control [166] .
GDF-6	Achilles tendon in Rat	Increase in tendon strength compared to control [167].
IGF-1	Achilles tendon in Rat	Reduction in immune response resulting in increased rate of repair [168].
PDGF-ββ	Achilles tendon in Rat	Increased healing observed [169].
SDF-1	Achilles tendon in Rats	Larger collagen fibrils compared to control and physiological structures [170].
TGF-β1	ACL in Rabbits	Rapid and continuous proliferation of fibroblasts with elevated collagen 1 and 3 [171].
TGF-β2	MCL in Rabbit	Elevated Collagen 1 expression with rapid proliferation [172].

Table 0.4 Growth Factors used in Tendon Repair

The Above table shows growth factors investigated in tendon repair table is adapted from Lui *et al* [173]**.**

1.10.1.1 Transforming Growth Factor-β

The transforming growth factor β (TGF-β) superfamily consists of over 30 members and many subgroups such as Bone Morphogenic Proteins (BMPs), Growth and Differentiation factors (GDFs), Activins and Nodals, all of which have a major function is the development of the foetus [174, 175]. The TGF-β superfamily and the downstream pathway components are a well conserved in vertebrates [174]. The TGF-β superfamily have been shown to have an array of diverse cellular responses which include: growth, adhesion, migration, apoptosis and differentiation [174].

The sub-group of proteins within the TGF-β superfamily, BMPs have been shown to be highly involved in bone and skeletal tissue development. BMP-4 has been shown to be involved in the regulation of bone formation [175], whilst BMP-12 has been shown to be involved in tendon generation [176].

1.10.1.2 Bone Morphogenic Proteins

Bone morphogenic proteins (BMPs) are a sub group of the TGF-β growth factors with 20% – 30% amino acid homology to other members of the TGF-β superfamily [177]. BMPs are considered to be pleiotropic, affecting many different tissues in subtly different ways [177]. BMPs have also been shown to play a role in tissue healing and embryonic development [178]. Currently over 30 BMPs have been identified with some also falling under the growth and differentiation factors group (GDF7 also being known as BMP-12).

Recently, BMP-12 has been researched as having a role to play in tendon differentiation by means of gene transfection [176, 179, 180]. Also, BMP-13 has also been implicated in tenogenic differentiation [181]. However, tenogenic differentiation is not limited to just

BMP-12 and 13, as both BMP-2 and BMP-7 have also been shown to have a role in tendon repair [182].

To date the use of gene transfection has been employed to induce increased repair of damaged tissue and the differentiation of mesenchymal stem cells towards a tendon-like tissue [176, 180]. A study by Fu *et al* showed that BMP-12 was expressed in healthy human patellar tendons and located in clusters of tenoblasts in active remodelling sites and also perivascular mesenchymal cells [183]. However, expression of BMP-12 was not apparent in tenocytes found sitting on intact collagen [183]. This research showed that BMP-12 does actively play a role in certain physiological processes in healthy adult tendon and may be related to tissue regeneration due to the up-regulation of matrix proteins such as procollagen I and II [183]. The data obtained from the study by Fu *et al* lead to the hypothesis that BMP-12 is involved in the remodelling of tendon tissue that has micro-injuries induced by normal activities due to hyper-cellular areas correlating to increased BMP-12 expression. Further findings included the culture of human tendon fibroblasts in the presence of rhBMP-12 showed a marked increase in procollagen types I and III [183].

1.10.1.3 Fibroblast Growth Factor

Fibroblastic growth factor-4 (HST-1, FGF-4) was originally identified as fibroblastic-specific growth factors [184]. Fibroblastic growth factors (FGFs) are a large family of signalling polypeptide growth factors that are evolutionary conserved between species. Currently, there have been 23 members identified within this large family within vertebrates, with a molecular mass ranging from 17 – 34kDa, with a 13 – 71% conservation of amino acid identity [185, 186].

From the 22 genes responsible for the coding of the FGF proteins, the function of FGF-16 still remains unknown [185, 187]. Several of the FGF genes have been shown to be located in clusters, FGF-3, FGF-4 and FGF-19 being a good example of such clustering which can be found on chromosome 11q13 and these individual genes have been shown to be separated by as little as 10 – 40kb [185]. The apparent clustering of FGF genes and the work undertaken by Kelley *et al.* 1992 which showed that a transcriptionally active portion of FGF-7 could be amplified to 16 copies which were dispersed throughout the human genome along with sequence conservation, could be due to chromosomal duplication and truncation during evolution [185, 187, 188].

Fibroblast growth factor -4 (FGF-4) was originally identified by Sakamoto *et al*., 1986 and Deili-Bovi *et al.*, 1987 as HST-1 gene from human stomach cancer and Kaposi's sarcoma by a NIH3T3 transforming assay. The deduced amino acid sequence for FGF-4 has been shown to have 43%, 38% and 40% homologous sequences to fibroblastic growth factor -2 (FGF-2), fibroblastic growth factor -1 (FGF-1) and fibroblastic growth factor -3 (FGF-3), respectively [186]. The gene loci for FGF-4, was located on chromosome 11q13 along with FGF-3 and FGF-19 as a clustered region of FGFs [189-191]. After protein synthesis FGF-4 is cleaved and glycosylated to produce a mature protein of 176 amino acids, which excludes the cleaved 30 amino acids of the signal peptide [192, 193].

Delli-Bovi *et al.* 1988 investigated the effects of inhibition of glycosylation and impaired secretion of FGF-4; it was also found that the stability of FGF-4 was increased by the presence of heparin in the culture media. It was also found that FGF-4 in the un-glycosylated form was cleaved into two NH2-terminally truncated peptides, which were 13 and 15 kDa [194]. These two peptides were investigated and found to be more active

than the wild-type protein and also showed increased affinity for heparin-binding [195, 196]. Kosaka *et al.* 2009 proposed, “That these two proteins could represent a novel mechanism for regulation of FGF-4 mediated biological activity”. FGF-4 is expressed in pre-implantation murine blastocysts and is also present in the inner cell mass (ICM) [197, 198].

The FGF-6 gene is located on chromosome 12p13.32 and encodes for 18.7kDa protein, which consists of 206 amino acids and has been shown to bind to the FGFR-1c, 2c and 4.The FGF-6 gene was first cloned by low stringency hybridization to an FGF-4 probe in 1989 by Marcias and co-workers [199]. De Lapeyriere *et al.* reported in 1990 that FGF-6 transcripts were present in adult muscles and during embryogenesis. Further investigations into the action of FGF-6 by Zhao & Hoffman (2004) in regards embryonic myogenesis revealed FGF-6 was the likely ligand for FGFR-4 and positional cues that dictate the cell determination, proliferation and differentiation into adult muscle[200]. Furthermore, antagonists of Wnt signalling, sFRP1, SFRP2 and sFRP4 (secreted frizzled-related proteins) were significantly up-regulated, which suggested active inhibition of not only the Wnt pathway (Wnt1, 3a, 7a and 11), but also shh (sonic hedgehog) pathway and BMP pathway were not induced in muscle regeneration [200]. Recently, in-situ hybridization studies conducted by Amand *et al.* had shown FGF-6 expression to be restricted to developing skeletal muscle [201, 202]. Studies conducted using the murine model has shown FGF-6 presence at E9.5 and to be exclusively present in the myotomal compartment of the somite [201, 202]. Due to the interaction between muscle and tendon is the transmission of forces between muscle and bone it is also feasible that FGF-

6 could play an integral role in the development of tendon and muscular-tendon junctions.

The FGF-8 gene is located on chromosome 10q25-q26 and encodes for 22.4 kDa protein consisting of 193 amino acids. Early investigation into the role of FGF-8 in limb development was conducted by Moon and Capecchi in 2000 where they undertook experimental work to assess the role of FGF-8 during mouse limb development [203]. As with FGF-4 and FGF-6 the AER provided the signals to maintain mesenchymal cells in the proliferative state in the PZ during limb development.

The research showed that exogenous FGF-8 was capable of inducing ectopic limb development and also used to replace the AER to support continued limb development. The limb patterning along the anterior/posterior axis was also shown to require interactions between the zone of polarising activity (ZPA) and the AER, where *Shh* (sonic hedgehog protein) was the proposed mediator of polarisation [203]. Moon & Capecchi went further in the research to say BMP-2 may be responsible for FGF levels in the AER rather than *Shh* due to asymmetrical expression of downstream genes such as *Hoxd* genes and *BMP-2* [203]. Further research conducted by Park *et al.* showed that FGF-8 as with other FGF family members has a role to play in not only limb development but also organogenesis in this case the heart [204]. This would indicate the combined effect of cellular positioning due to polarisation (local polarisation) and FGF signalling may be the key in development specification. Meaning cell positioning is the primary determining factor in the fate of tissue to develop when FGF signalling initiates and maintains proliferation and differentiation.

Reciprocal interaction between muscle and tendon has been reported in numerous studies, which is vital for their respective tissue development [14, 205-208]. Experimentally generated muscle-less limb models in both the chick and mouse models have shown initial tendon development to be independent from muscle. However, continued tendon development requires the presence of muscle. This requirement was shown by the failure of tendon segregation and differentiation in the absence of muscle [82, 205, 209].

1.10.1.4 Bone Morphogenic Protein Receptor

The BMP12/13 molecule binds first to a type II receptor. The receptor-ligand complex then combines with a type I receptor, forming an oligomeric signalling receptor complex. Both the type I and type II receptors have cytoplasmic serine/threonine kinase domains. With TGF-β (which BMPs are a member) signalling is transmitted via SMADs, which are a family of signal transducers and transcriptional activators [161]. TGF-β receptor activation is a good example of the mutual dependency of dimerization and trans-phosphorylation. Type I receptors have a highly conserved, 30 amino acid long region which precedes the kinase domain. This region is the GS (glycine-serine) domain because it contains the protein sequence GSGS. On interaction with the liganded type II receptor, the GSGS sequence in receptor I is *trans*-phosphorylated by the type II receptor. Phosphorylation of ser165 in the GSGS sequence is crucial and determines the intensity of signalling [161].

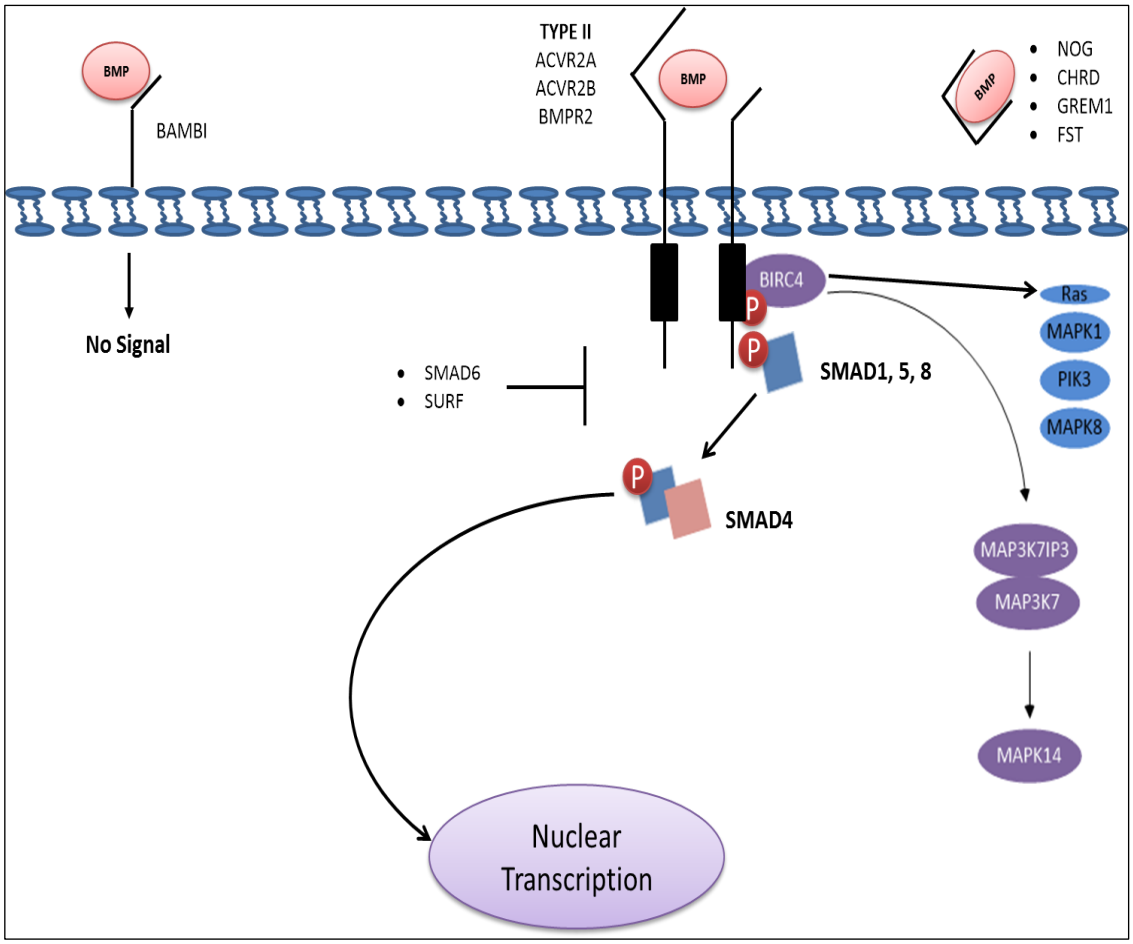

Figure 0.12 BMP-BMPR signal cascade

BMP binds to either BMPR I or BMPR II dependant on ligand specificity. Both BMPR I and II result in the phosphorylation of SMAD-1, 5 and 8 combinations which bind with SMAD-4. Post binding with SMAD 4 the newly formed SMAD complex translocates to within the nucleus and activating co-factors that result in target gene transcription. Activation of both BMPRs can also result in activation of Ras and MAP3K7IP3 and result in further signal transduction with results still to be elucidated [178, 181]**.**

1.10.1.5 Fibroblast Growth Factor Receptors

All FGFs have been shown to contain an internal core with 28 highly conserved amino acids and 6 invariant amino acid residues [187]. Plotnikov *et al* [210], where ten of these conserved amino acids are responsible for the interaction between FGF and its receptor (FGFR). Structural studies by Zhu *et al.* [211] and Eriksson *et al.* [212] both showed that FGF1 and FGF2 contained 12 anti-parallel β strands which were located in the highly conserved protein core region. Faham *et al* [213] went on to show that FGF1 and FGF2 both have a β trefoil structure, which has the presence of 4-stranded β sheets, which were arranged in a triangular array. Furthermore, the 2 β strands (strands β10 and β11) were shown to contain several amino acid residues that formed the primary FGF2 heparin-binding site [210-213].

The four known Fibroblast growth factor receptors (FGFR) FGFR1 through FGFR4 sharing between 55% and 72% homology at the protein level [214, 215] and are a vital component of signalling cascades, which have been shown to control embryonic pattern formation in animals [216]. The general structure of the FGFR family are characterised by a modular structure with seven domains [214]:-

- N – terminal signal sequence
- The presence of usually 3 extracellular Ig-like loops (Ig I to Ig III)
- An acidic domain IgI and IgII
- Single transmembrane domain
- Split tyrosine kinase domain

During FGF and heparin sulphate proteoglycan binding it has been shown that of the 3 Ig-like loops, only the juxtamembrane IgII and IgIII domains are required. Olsen *et al.* 2003

[217] showed the IgI domain is neither essential for FGF binding or receptor activation, but does exert a modulatory, auto-inhibitory function by the folding back to IgII and IgIII [217-219].

The FGF receptors show a high level of conservation in homology between each receptor type (Table 1.5) [220]. Although there are many types of FGFs and they convey a diverse range of effects on target cells, this is achieved by the high level of variance in the receptor[220]. This level of diversity is best demonstrated with FGF-7, which has a mitogenic effect on keratinocytes, however, this effect is not observed with fibroblast or endothelial cell lines [221]. This observation in regards FGF-7 implies that different cell lines will react differently to the same FGF signal and this reaction is dependent upon the cellular expression of receptor and which variant of the receptor the cell expresses [220].

Name	Synonym(s)	Receptors	Reference
FGF-1	Acidic FGF, aFGF	FGFR-1, IIIb & IIIc; FGFR-2, IIIb & IIIc; FGFR-3, IIIb & IIIc; FGFR-4	Ornitz *et al* [222]
FGF-2	Basic FGF, bFGF	FGFR-1, IIIb & IIIc; FGFR-2, IIIc; FGFR-3, IIIc, FGFR-4	Ornitz *et al* [222]
FGF-3	Int-2	FGFR-1. IIIb; FGFR-2, IIIb	Ornitz *et al* [222]
FGF-4	kFGF, Kaposi FGF, hst-1	FGFR-1, IIIc; FGFR-2, IIIc; FGFR-3, IIIc; FGFR-4	Ornitz *et al* [222]
FGF-5		FGFR-1, IIIc; FGFR-2, IIIc	Ornitz *et al* [222]
FGF-6	hst-2	FGFR-1, IIc; FGFR-2, IIIc, FGFR-4	Ornitz *et al* [222]
FGF-7	KGF	FGFR-2, IIIb	Ornitz *et al* [222]
FGF-8	AIGF	FGFR-1, FGFR-2, IIIc, FGFR-3, IIIc, FGFR-4	Ornitz *et al* [222] ,Koga *et al* [223]
FGF-9	GAF	FGFR-2, IIIc; FGFR-3, IIIb & IIIc, FGFR-4	Ornitz *et al* [222]
FGF-10	KGF-10	FGFR-1, IIIb; FGFR-2, IIIb	Ornitz *et al* [222], Miralles *et al.* [224]
FGFs 11 – 14	FGFs	UNKNOWN	Ornitz *et al* [222]
FGF-15		UNKNOWN	Ornitz *et al* [222]
FGFs 16 – 19		FGF-17; FGFR-1, IIIc; FGFR-2, IIIc	Ornitz *et al* [222], Xu *et al.[225]*
FGF-20	XFGF-20	UNKNOWN	Ornitz *et al* [222]

Table 0.5 FGF groups and Associated Receptors

The above table was adapted and reproduced from Powers *et al* [220] **and shows each FGF molecule and its associated receptors** [222-225]**.**

There are possible mechanisms of expression of different forms of FGFR:

1. FGFR gene splice variants

2. Expression of different FGFR genes.

With the employment of splice variants it becomes possible for the same FGFR gene to encode for a variety of different receptor protein isoforms [220] and this kind of diversity is due to the structure of the respective FGFR genes [220]. Genetic analysis of the FGFR-1, FGFR-2 and FGFR-3 genes has shown a remarkably high level of conservation in the arrangement of the intro/exon boundaries [185, 220, 222, 226].

1.10.2 Heparin and FGF

Heparin and HS are heterogeneously linear sulphated polymers consisting of repeating sub-units of the disaccharide hexuronic acid and D-glucosamine [227]. Heparin sulphate (HS) can be found in the interstitial spaces within the extracellular matrix of most tissues and on the surface membrane of most cells

A large volume of evidence implies that the FGF pathways are required for vertebrate and invertebrate development [228-230]. Interactions between FGF and heparin have been shown to stabilise both FGF1 and FGF2 to terminal denaturing and protects FGF2 from proteolysis [187, 231]. The affinity of FGFs for Heparin sulphate (HS) proteoglycans severely limits their diffusion and release into interstitial spaces; therefore FGFs function in a paracrine fashion when bound to heparin [232-234].

The binding of FGFs to heparin or heparin sulphate results in the formations or stabilisation of dimers and higher order oligomers along the proteoglycan chain [221, 231,

235]. It has also been shown that FGFs can form "*Trans*" dimers with a heparin molecule bound between two FGF molecules [236]. The concept of heparin/HS-FGF dimer being an essential component/step in the transduction of FGF/FGFR signalling complex still remains controversial [237]. Although, it is well established that heparin is essential for high affinity binding of FGF to FGFR when cells are unable to synthesis cell-surface HS, cells pre-treated with heparin degrading enzymes or cells exposed to sulphation inhibiting agents [238, 239]. Also studies by Szebenyi *et al (1999)* [240] and Ornitz (2000) [187] showed that heparin/HS complex increased not only FGF/FGFR affinity but also the half-life (T½) of the FGF-FGFR complex.

1.10.3 FGF-FGFR Signal Transduction

FGF binding to the cell surface induces the dimerisation of the FGFR, this then results in the activation of tyrosine kinase and the auto phosphorylation of the cytoplasmic domain of the cognate receptor [241]. The phosphorylated tyrosine's are subsequently recognised by the SH2 domain, which contains signal transducers such as phosphotyrosine phosphatase (SHP-2) which is vital in the downstream activation of target proteins [242]. With FGF-2 signal transduction SHP-2 has been shown to associate with FRS2 were the SH2 domain in the N-terminal has been shown to be important for Ras signalling pathway [243]. Rho GTPase is a member of the Ras super family and plays an opposite role to general Ras proteins and may be involved in JNK/SAPK pathway [243]. Rasp21 is an important intermediate in the FGF-2 induced activation of the Ras/MAPK signalling pathway [243]. Grb2 has been shown to activate Rasp21 which can activate MAPK via the activation of MAPKKK which then activates the level of transcription factor Elk-1 [244-250]. Phospholipase C-gamma (PLC-γ) is phosphorylated by FGFR-1 at position

Y766. Tyrosine phosphorylation of PLC-γ results in activation and subsequent hydrolysis of phosphatidylinositol 4, 5 bisphosphate to inositol 1, 4, 5 triphosphate and diacylglycerol. The generation of two inositol 1, 4, 5 triphosphate, leads to the release of Ca^{2+} from intracellular stores, whereas diacylglycerl accumulation leads to activation of member of the protein kinase C family [251, 252].

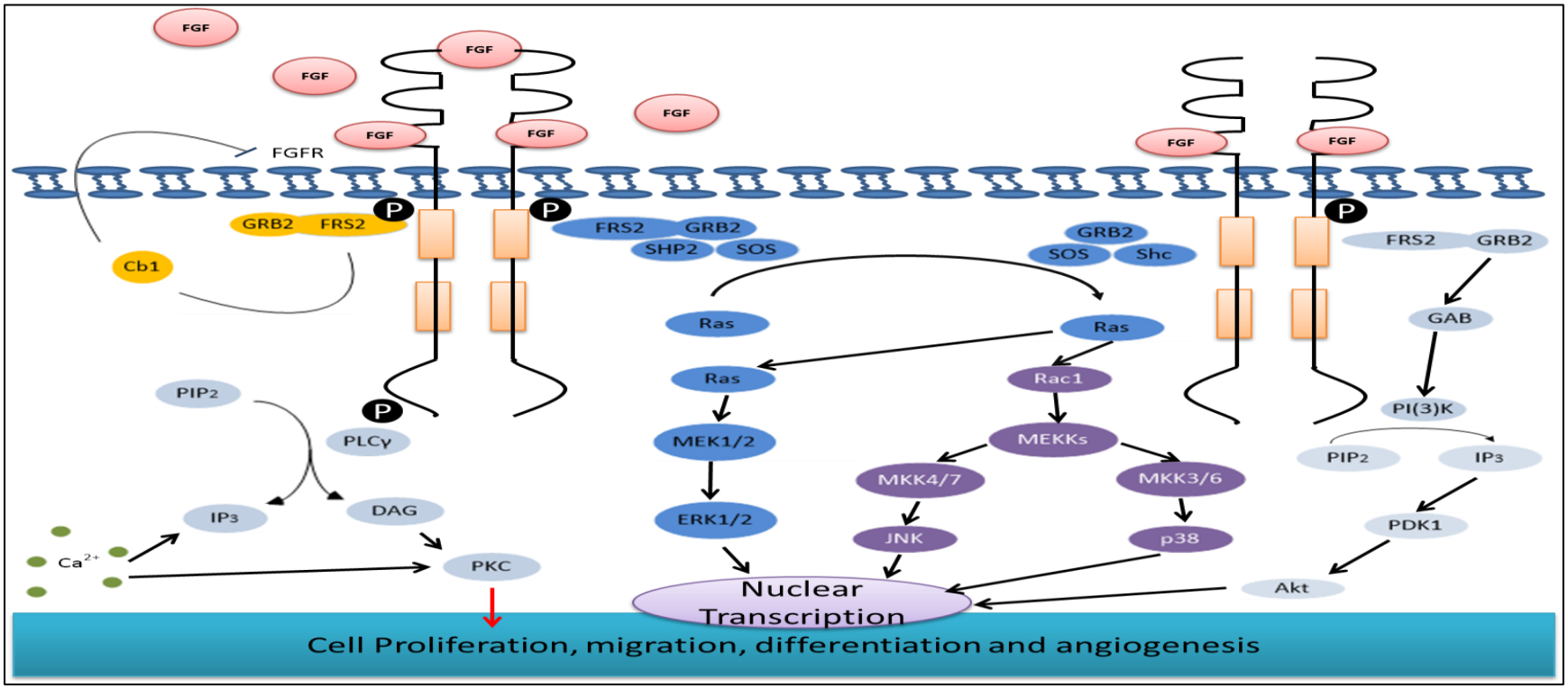

Figure 0.13 FGF-FGFR signalling Cascade

Post FGF-FGFR binding results in an array of signal transduction pathways which can result in transcription factor activation which in turn can result in mitogenic responses via ERK1/2 activation, FGF inhibition (negative feedback) via ERK1/2 activation, stress response via JNK and p38 activation, anti-apoptosis response via Akt activation, cytoskeleton reorganisation and proliferation via phospho kinase C (PKC) activation [241-243, 251-253].

1.11 Drug Delivery Systems

The use of drug delivery systems as a means of delivering a controlled and sustained release of drugs or growth factors has received much attention in recent years [254]. However, tailoring the size and properties of the particle to deliver the growth factor to the desired cell/tissue type has yet to be fully documented. To date the majority of research groups focus upon the encapsulation efficiency of a desired drug/growth factor or hormone without fully exploring the full spectrum of nanoparticle production variables that can control the nanoparticle properties such as size and possibly polydispersity index and charge?

Many polymers have been investigated and are currently being employed for their potential use as a vehicle to deliver drug or growth factors such as lysosomes, synthetic polymers (Table 1.6) and natural polymers (Table 1.7) [255-258]. However, the control of nanoparticle size as a key factor in drug/growth factor delivery has yet to be investigated.

Synthetic Polymer	Main Application	Reference
Poly (glycolic acid); Poly (Lactic acid) and their copolymers	Used in Sutures, drug delivery systems and tissue engineering. Co-polymerized to regulate degradation rate	Mooney *et al. [259]*
Polyhydroxybutyrate	Biodegradable, used as a matrix for drugs.	Holland *et al.* [260]
Poly (carpolactone) and copolymers	Delivery system, Cell microencapsulation	Lee *et al*. [261]
Poly (alkylene succinate)	Properties that can be tuned by chemical modification, copolymerization and blending	Bikiaris *et al*. [262]
Polyanhydrides	Biodegradable, used in tissue engineering for the release of bioactive molecules	Gunatillake & Ahikari [263]
Polyacrylonitrile	Dialysis Membranes	Stoilova *et al.* [264]
Polyamides	Used for sutures and hemofiltration membranes. Inhibitors of DNA transcription	
Poly (ortho esters)	Surface-eroding polymers. Applications in sustained drug delivery, ophthalmology.	Kellomaki *et al.[265]*
Polyphosphazenes	Can be tailored with versatile side-chain functionality. Applications in drug delivery	Peach *et al.* [266]

Table 0.6 Synthetic polymers and application in drug delivery systems

The table above shows the synthetic polymers used for drug delivery along with their main application and references [259-266].

Natural Polymer	Main Application	References
Collagen	Sutures, Drug release	Friess [267]
Gelatin	Used in the preparation of gels and in drug release	DiTizio *et al.* [268]
Albumin	Drug stabilizer and drug release	Elzoghby *et al.*[269]
Carboxymethylcellulose	Drug release, dialysis membranes.	Barbucci *et al*. [270]
Starch	Drug delivery	Tuovinen *et al*. [271]
Agarose	Used in clinical analysis and as a matrix	Wang & Wu [272]
Alginate	Used in the release of bioactive molecules	Tonnesen & Karlsen [273]
Heparin and glycosaminoglycan	Used in ionotropic gelation and in capsules preparation	Liu *et al.* [274]
Dextran and derivatives	Used in drug delivery	Miyazaki *et al*. [275]
Chitosan and derivatives	Used in film preparation and applied in drug delivery	Prabaharan & Mano [276]

Table 0.7 Natural Polymers and application in drug delivery systems

The table above shows the natural polymers used for drug delivery along with their main application and references [267-276].

1.11.1 Polymer Drug delivery systems

Polymer (Polymeric) based drug delivery systems are a versatile class of materials and have the potential to have a vast effect on pharmacological based therapies. Over recent years the two major classes of polymers namely synthetic and natural have been both investigated and utilised as carriers for controlling drug release [258]. Originally the polymer based drug delivery system (DDS) was based on non-degradable polymer matrix. However, the major disadvantage of such a system was that the release kinetics were uncontrollable and dependant on the diffusive properties (behaviour) of the loaded drug through the polymer matrix [258]. As the design of DDS developed combinations of natural and synthetic biodegradable polymers allowed for the controlled release of encapsulated agents. Therefore, allowing for the possibility to address the targeting of the active agent to the target site (cell/tissue) [258].

The primary concern for DDS is the choice of polymer to be employed in the controlled release delivery system, as controlled release depends on the physical, chemical and biological properties of polymer and the DDS constituents (active agent and encapsulation agent) [277]. The most recent generation of DDS are currently under investigation. These systems are designed using multi-component materials which are specifically engineered to avoid biological barriers and stimulate cellular responses such as direct cell proliferation and differentiation [278]

Controlled drug delivery devices can be classified based on the nature of the carriers and can be divided into two major categories: diffusion controlled release systems and degradable delivery systems. With diffusion controlled release systems, the active agent is released from an aqueous solution and is inhibited by the insoluble polymer matrix. The

active agent is released either by passing through pores or between polymer chains and it is these processes that controls the release rate of the active agent [258, 277, 278]. Diffusion controlled systems are divided into two types: reservoir (membrane systems) and matrix systems (Figure 1.14) [258, 277, 278].

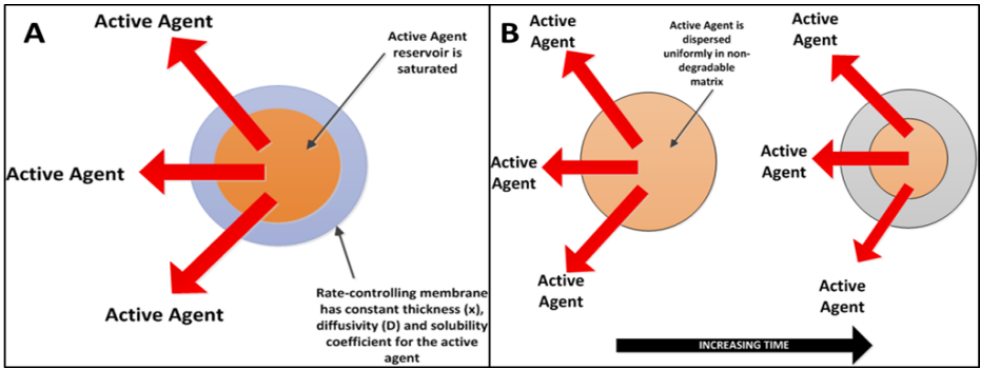

Figure 0.14 (A) Schematic of reservoir drug delivery system and (B) matrix based drug delivery system.

In membrane DDS, the drug is contained in a core, which is surrounded by a polymer membrane, and it is released by diffusion through this rate-controlling membrane. Reservoir DDS have a coating that controls the release rate [258].

- A reservoir based DDS is generally cylindrical, disk-like or spherical in shape and constitutes an agent core in either liquid or powdered form and is contained within a polymeric film. The polymeric layer which is non-biodegradable represents the only barrier through which the agent slowly diffuses. The diffusion rate of the agent is dependent upon the properties of both the agent and the polymer. The reservoir can be either microporous or macroporous polymer film. The composition of which changes from one component to a mixture of polymers, or a heterogeneous matrix in which hydrophilic polymer particles are dispersed in a hydrophobic polymer matrix [279].

- With matrix based diffusion control systems, the agent is uniformly distributed throughout the polymer matrix and is subsequently released from the matrix at a uniform rate as the agent particles disassociate from the polymer network. The agent can be physically embedded into the polymer at large enough concentrations as to create interconnecting pores throughout the matrix which allow for the agent to slowly diffuse out of. The use of such systems allows for hydrophobic and/or viscous hydrophilic polymers to incorporate solid agent dispersal. The release rate is based on the diffusion of the agent molecule to the device surface where they are delivered. This process takes place as long as the higher concentration of the agent in the system core affords a constant flow of agent molecules through the matrix. With this dissolution-diffusion process, the interface between agent reservoir and the release moiety progressively contracts and moves towards the core of the device [280].

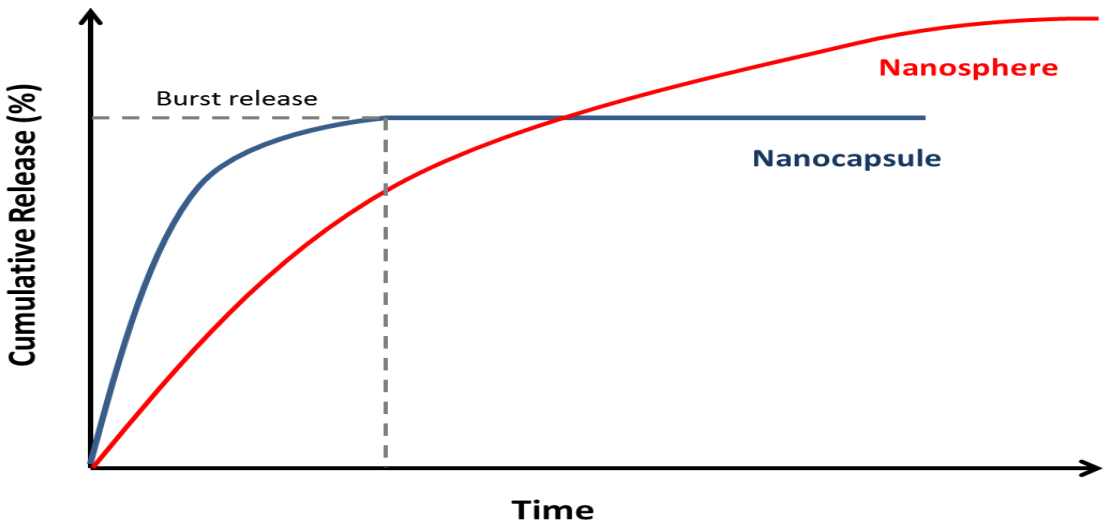

Figure 0.15 Schematic Drug Release Profile for Nanosphere and Nanocapsules

The nanocapsule has an initial burst release followed by continuous release, whilst the nanosphere has a reduced burst release followed by prolonged increased release.

In degradable DDS the agent molecules are initially dispersed in the polymer and are released as the polymer undergoes eroding or degradation. Similar to the reservoir system, the degradable reservoir system has an agent-loaded core which is surrounded (encapsulated) by a polymer coating which undergoes erosion or degradation. These systems combine the advantages of the long-term constant rate of agent release with bio-erodabilty or biodegradability. With a surface-degrading polymer, degradation is confined to the outer surface of the device. With a bulk-degrading polymer, degradation occurs homogeneously throughout the material. With most polymers hydrolysis is a major factor and therefore water intrusion into the device is of significant importance for the study if degradation kinetics as well as agent release kinetics [281].

1.11.2 Polymeric Nanoparticles

Polymeric nanoparticles (NPs) have drawn much attention within the pharmaceutical field as a potential delivery method for pharmaceutical agents. NPs have been defined as solid, colloidal particles within a size range of 10 – 1000nm with a capability to carry an agent to the target site or to release an agent in a controlled manner [282]. The original particulate DDS was primarily based on liposomes and polymer-drug conjugates. Liposomes were originally discovered in the 1960's and can be defined as a spherical vesicle with a lipid bilayer membrane structure, which can encapsulate both hydrophobic and hydrophilic agents [283]. Polymer-drug conjugates have been extensively investigated after first appeared in the 1970's where the drug or bioactive agent is covalently linked to the macromolecular backbone [284]. Today, both liposomes and polymer-drug conjugates provide the foundation for the field of advanced drug delivery systems based on nanotechnologies. However, these systems have many disadvantages and are

characterised accordingly, such as poor encapsulation efficiency and bioavailability of the agents, difficulty in targeting a desired target site and relatively high production costs.

Polymeric NPs offer the capability to achieve controlled release of bioactive agents, improvements in the stability of the active agents (the polymeric shell acts as a protective shield against factors such as pH, enzymes and light) and their relatively small size can allow for the manufacture of a size of NP that may provide a higher cellular uptake than other particulate systems. Another advantage of NP as active agent carriers can include higher encapsulation efficiency, lower polymer content when compared to other DDS and the possibility of utilising polymers with a greater degree of biocompatibility and biodegradability [285]. NPs can be classified as nanocapsules and nanospheres. Polymeric nanospheres may be defined as a matrix based particle with the entire mass is solid and molecules may be adsorbed at the sphere surface or encapsulated within the particulate. Polymeric nanocapsules are a vesicular system, which may act as a reservoir, in which the entrapped agent are confined to a cavity made from a liquid core (which can be oil or water) surrounded by a polymer shell [286].

The design of polymeric NPs depends on the therapeutic application, target site (organs, tissues, cellular or subcellular organelles) and the route of administration. Although injection (subcutaneous or intravenous) is the most common route of administration, these nanocarriers can be also delivered through dermal and oral routes to name a few [287]. For every administration route of drug delivery that the use of a NP delivery vehicle is to be utilised many physical barriers need to be breached. The NPs have to be able to deliver beyond the biological barriers, such as skin, mucus, blood, extracellular matrix and cellular or subcellular barriers. With respect to these factors, the correct selection of the

polymer can affect the NPs intracellular fate, safety, biocompatibility, release kinetics and the capability to overcome biological barriers [288]. Biocompatibility and biodegradability of NPs are essential concerns for the safety of the patients and should be vigorously tested both *in vivo* and *in vitro*.

The use of biodegradable polymers would avoid the concerns in relation to physiological excretion or mechanical removal of the delivery device after agent depletion. The application of biodegradable matrix (Figure 1.16) could provide a further mechanism for release rate control, by combining typical diffusive mechanisms with tuneable polymer degradation [289].

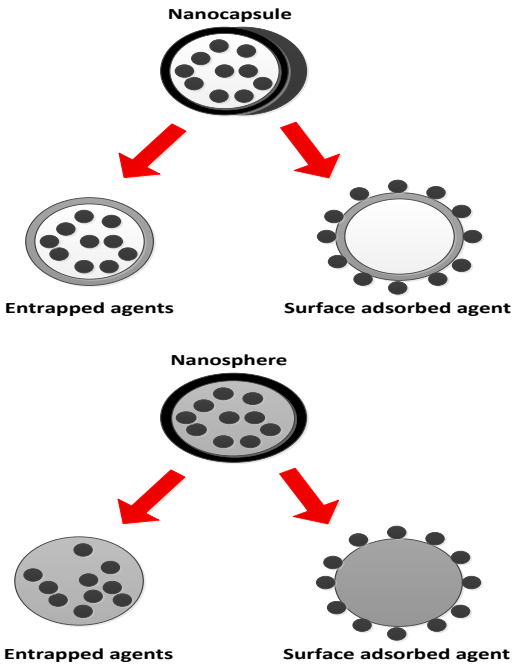

Figure 0.16 Structure of Nanocapsule and Nanosphere.

Shows nanocapsule with the matrix found between the polymer shell and core. The nanosphere with the matrix as a component of the core [290].

The most commonly used biodegradable polymers being utilised for NP production are poly (lactic acid) (PLA), poly (glycolic acid) (PGA), poly (ε-caprolactone) (PCL) and the co-

polymer poly (lactic-*co*-glycolic acid) (PLGA) of PLA and PGA. Along with the natural hydrophilic polymers, such as chitosan, sodium alginate and gelatin have also been utilised to produce drug loaded NPs. However, the aliphatic polyesters based on lactic and glycolic acids are the most widely employed polymers and have been approved for use in humans by the FDA [291]. Furthermore, lactide/glycolide polymer chains are cleaved by hydrolysis to form natural metabolites (lactic and glycolic acids), which are metabolised, utilised and subsequently eliminated from the body via the Krebs cycle [292].

1.11.3 Nanoparticle Preparation Techniques

The properties of NPs have to be optimised according to the particular application. In order to achieve this, the properties of interest, the method of preparation play a key role. Therefore, it is highly advantageous to have several preparation techniques to obtain the NPs with the desired properties. There are several methods for NP production which are outlined briefly below:-

- Emulsion solvent: is the most employed method of NP production. The preparation utilised in this method follows the general protocol of dissolving the polymer in a water immiscible, volatile organic solvent which is then emulsified with an aqueous phase to stabilise the system. The organic solvent is then evaporated which induces the formation of polymer particles from the organic phase droplets [282, 286, 288].
- Salting out: this is an emulsion based approach, with the advantage that this method avoids surfactants and chlorinated solvents. Briefly, a saturated salt solution containing a stabilising agent such as polivinilalcool (PVA) is added under

stirring to an acetone to diffuse into the external aqueous solution of the polymer. An organic/water (o/w) emulsion forms as the salt prevents the water and acetone mixing. Sufficient water is then added to allow the acetone to diffuse into the external aqueous phase and induce nanoparticle formation [282, 286, 288].

- Dialysis: The dialysis method is a simple and effective preparation method for small and narrow size distributed NPs. In this method, the polymer is dissolved in an organic solvent and placed within a dialysis tube with a specific molecular weight cut-off. Dialysis is performed against a non-solvent miscible with the former miscible solvent. The displacement of the solvent inside the membrane is followed by the progressive aggregation of polymer due to the decrease in solubility which leads to formation of homogenous suspension of NPs. The solvent used in such a preparation of the solvent solution has a direct effect on the morphology and particle size of the NPs [282, 286, 288].

Therefore, the choice of NP production method is highly dependent upon the agent being encapsulated and the chemical properties such as solubility of the agent to be encapsulated. By employing a design of experiment approach to nanoparticle production the variables of the procedure can be identified to control nanoparticle size and subsequently the concentration of drug delivered.

1.12 Design of Experiment

Design of experiments (DOE) utilises applied statistics which are capable of dealing with conducting, planning, along with the analysis and interpretation of controlled tests. The primary purpose is to evaluate the factors that control the value of a parameter or group of parameters.

A well-executed DOE can reveal a high volume of data in regards an effect on a response variable due to one or multiple factors, along with their subsequent interactions. Many experiments currently employ the holding of one factor constant whilst varying levels of another factor, basically a one-factor-at-a-time (OFAT). However, this process is inefficient and more costly (in regards time), when compared to changing factor levels simultaneously [293].

By utilising a DOE can reveal:

- Key factors in a process
- Optimum settings (Full factorial 2^3)
- Key and main interactions within a process

1.13 Thesis Aims

The three primary aims of this thesis are:

1. To investigate whether PHBHHx can be used as a scaffold in tendon repair (Undertaken at Tsinghua University, Beijing, China).
2. To Investigate the potential of FGF-4, FGF-6 and FGF-8 and subsequent combinations are capable of initiating human stem cell differentiation towards a tenocyte lineage (Undertaken at Keele University, U.K.)
3. Investigate the controlled manufacture of PHBHHx nanoparticles and whether controlled manufacture results in control of nanoparticles properties utilising a DOE (Undertaken at West China School of Pharmacy, Sichuan University, Chengdu, China & Keele University, U.K.).

The three primary aims of this thesis are to bring together three topic areas of Scaffold design for use in tendon repair, growth factor induced differentiation of both hESC's and hMSC's and finally the controlled production of PHBHHx nanoparticles for use in the delivery of growth factors at a range of concentrations The findings of the topic areas may lead to a self-contained implant that will comprise of three major components: a cellular component (stem cells) with the capability of differentiating towards a tenocyte cell lineage, polymer scaffold to provide structural support and integrity for tissue replacement/cellular delivery and a nanoparticle growth factor delivery vehicle capable of delivering a growth factor cocktail capable of inducing stem cell differentiation.

Chapter 2: Poly 3-hydroxybutyrate- co-3-hydroxyhexanoate Scaffolds for Tendon Repair in the Rat Model

2.1 Introduction

This Chapter is an expansion on the publication in Biomaterials Webb *et al.* 2013 [294]

Tendon injury is an increasing problem in medicine, with over 300,000 tendon procedures performed annually in the United States alone [295]. Tendon is characterised by poor repair following injury or disease, is relatively acellular and has poor blood supply [6]. Treatment can involve many different types of surgical intervention, such as xenograft or allograft to treat large tendon defects, however potential problems with this method (such as foreign body reaction) can occur [296]. A lack of adequate strategies for tendon repair has led to the development of engineered replacement tendon tissue for use in surgical implantation[297]. Tissue engineering could be used to develop a regenerative medicine solution to tendon tissue repair [156].

A range of different materials have been investigated as possible scaffolds for tendon tissue engineering. These include natural materials such as collagen [298] and silks [299] or manufactured materials such as polymers [300]. One current approach is to blend natural and manufactured materials to form a hybrid design which would encourage cellular in-growth and provide mechanical support during the remodelling stage of tendon recovery [3].

An appropriate tendon tissue engineered scaffold would mimic the structure and mechanical properties of the natural tissue. The mechanical properties of tendon depend largely on its location within the body and can vary. For instance a typical small adult human tendon (from the forearm) has a Young's modulus of 1-2 GPa, an ultimate stress of around 100 MPa and an ultimate strain of 4-10% [89] whereas the human patella tendon an estimated Young's modulus of 1.5-1.7 GPa, an ultimate stress of 34-43 MPa and an ultimate strain of 5.3-5.8% ,the estimated Young's modulus for adult Achilles

tendon is 2 GPa with an ultimate stress of 80 MPa and an ultimate strain of 3.6-8.8% [90],[91]. The tendon extracellular matrix is composed mainly of collagen type I arranged in hierarchical levels of increasing complexity, beginning with the triple-helix polypeptide tropocollagen which forms primary bundles (fibrils); secondary bundles (fascicles); tertiary bundles; and the complete tendon itself, which is surrounded by several layers of loose connective tissue sheaths [3, 30, 92, 301-303]. This complexity presents substantial difficulties to the generation of artificially produced structures which mimic tendon anatomical structure.

Polyhydroxyalkanoates (PHA) are a family of biopolymers consisting of polyesters of many different hydroxycarboxylic acid molecules produced by microorganisms as energy and carbon storages in response to unbalanced culture conditions [304]. PHBHHx is the designation of molecules consisting of random copolymers of 3-hydroxybutyrate and 3-hydroxyhexanoate [305] and is one of the few PHA molecules that can currently be produced on a sufficiently large scale for use in both scientific research and medical device construction [306]. PHBHHx has substantial potential as a material for tissue engineering owing to its adaptable mechanical properties, biodegradability and apparent compatibility with many different mesenchyme derived cell types [307-311].

Previous studies using implants to repair tendon injuries have employed polymers such as polyglycolic acid (PGA) and polylactic acid (PLA) [113]. Varying degrees of success have emerged ranging from histological indications of fibroblast alignment and patterning in PLA models when compared to the PLA control and slight improvement in mechanical properties of the repaired tendon in Japanese white rabbits with the PGA scaffold [114].

However, to date there are no commercially available polymer based scaffold available for the treatment of tendon injury.

The aim of this study was to explore the use of PHBHHx, PHBHHx-collagen and PHBHHx-collagen-tenocyte hybrid scaffolds for the *in vivo* treatment of damaged tendon. Here we have demonstrated that the use of PHBHHX and collagen/tenocyte combinations resulted in the absence of any adverse immunological response, return of load bearing and function (as evaluated through the Achilles Functional Index (AFI)), and cell alignment within the scaffold along with scaffold degradation without compromising functionality.

2.2 Materials and Methods

2.2.1 Animals

20 male Sprague-Dawley (SD) rats weighing between 180-200g were obtained from the Centre for Biomedical analysis, Tsinghua University, Beijing, China. Animals were treated kept in authorised, licensed facilities and under local ethical and handling guidelines throughout the experiment.

2.2.2 PHBHHx Fibre Construct

PHBHHx fibres were prepared by melt-spinning using a laboratory-size extruder (Ruojiang Chemical Fibre Machinery Co. Ltd., Beijing, China) with a single nozzle with an inner diameter of 300 µm. Briefly, PHBHHx powder (87.9% HB, 12.1%HHx) was melted, extruded, isothermally crystallized, drawn and annealed under tension (Chinese patent application No. 200810052461).

2.2.3 Porous Tube fabrication

PHBHHx tubes were prepared by dissolving 10% $^{w}/_{v}$ PHBHHx powder (87.9% HB, 12.1% HHx) in 20 mL chloroform (Beijing Chemical Works, 20100303). Following polymer dissolution, 0.04 g NaCl crystals (<100 µm diameter) were suspended in the solution and homogenised by shaking/stirring. To fabricate the tube, a 2.5 mm diameter stainless steel mandrel was dipped into the homogenised solution, then removed and the solvent evaporated in a flow hood for 2 minutes. This process was repeated 5 times after which the mandrel was placed vertically and left for a further 20 minutes to allow the solvent to fully evaporate and the polymer to become rigid. The polymer tube formed around the steel was then removed by hand. The tube was then immersed in deionised H_2O overnight to dissolve the NaCl crystals present in the structure prior to use.

2.2.4 Collagen Gel

Briefly, collagen gels were formed by first neutralising type I rat tail collagen (Sigma Aldrich, C3867-1VL) with 1 M NaOH, and combining 9 parts collagen solution with 1 part 10x DMEM to produce a final collagen concentration of 3mg/mL with the samples placed in an ice bath until required [312, 313].

2.2.5 Scanning Electron Micrograph Analysis of PHBHHx Fibres

Scanning electron microscopy was undertaken at the School of Medicine, Tsinghua University, China. Using a range of magnification (x200 – x2000), Samples were pre-coated with gold particles in a vacuum unit for 10 minutes prior to visualisation.

2.2.6 Mechanical Testing

Maximum force testing was undertaken at the School of Chemical Engineering, Tsinghua University, China. Prior to testing the MTS tension/compression tester was calibrated by staff at Tsinghua University as per manufactures guidelines using 20kip and 50 kip load cells. Post calibration, Samples were placed onto a MTS tension/compression load cell tester (MTS, Canada) (Figure 2.1A) and elongated at a rate of 10mm per second until failure, were the maximum load is recorded under dry conditions, using factory fitted sample clamps (Figure 2.1B).

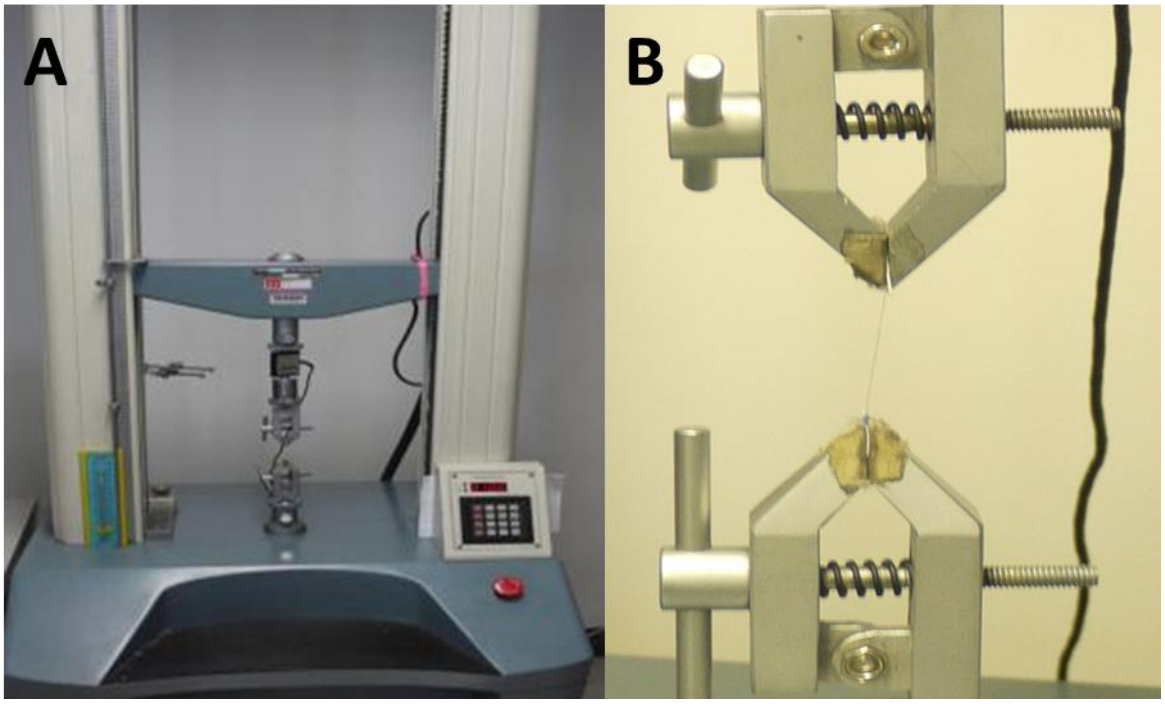

Figure 0.1 MTS Tension Compression load cell tester (NTS, Canada)

A) shows MTS compression load unit, B) Factory fitted sample clamps.

2.2.7 Rat Tendon Harvest

Fresh rat tendon was harvested from 8 weeks old, adult Sprague-Dawley (SD). The rat was sacrificed and the Achilles tendons harvested 24hrs prior to mechanical testing and stored at 4^{o}C in DMEM supplemented with 10% FBS, 5% NEAA, 5% L-Glutamine and 5% streptomycin/penicillin (Lonza) to prevent infection that could affect the outcome of mechanical testing.

2.2.7.1Rat Tenocyte isolation

Fresh rat tendon was harvested from 8 week old, adult Sprague-Dawley (SD) which were sacrificed in accordance with University policy (Tsinghua University, Sichuan University and Keele University). The rat Achilles tendons were then surgically removed from both hind legs. The tendons were then placed in a universal bijou bottle containing a solution

of PBS supplemented with 1000 IU/ml penicillin, 1000µg/ml streptomycin and transported to the laboratory. The tendon was then removed from the transport solution in a Biological Safety Cabinet and placed into a sterile petri dish were the tendon was then subsequently dissected into smaller sections and minced using a scalpel. The petri dishes containing the tendon samples were then placed into an incubator for one hour, allowing the tendon samples to loosely adhere to the petri dish surface. DMEM media supplemented with 1% L-glutamine, 1% NEAA, 10% FBS was then carefully added drop wise to the petri dish until the tendon samples were immersed. After, approximately five days, cells were observed to migrate out of the tendon onto the surface of the petri dish.

The cells in the petri dish were then removed by trypsinisation (1% trypsin/PBS solution) for five minutes, pelleted by centrifugation (three minutes, 200g), then re-seeded into two T-25 tissue culture flasks. One flask was then cultured at 2% O_2 and one flask in 21% O_2 (Keele University). All flasks were cultured at 21% O_2 at Tsinghua and Sichuan Universities.

2.2.7.2 Rat Tenocyte Expansion

Rat tenocytes (rt-tenocytes) were cultured in T-75 culture flasks in Dulbecco's Modified Eagle's Medium High glucose (Invitrogen) supplemented with 10% foetal bovine serum (FBS), 1% Non-essential amino acids (NEAA) (Gibco), 1% L-glutamine (10mM) (Gibco) until confluent. When confluent the cells were passaged with a brief PBS wash before adding 3 ml of 1% Trypsin/PBS solution and standing until detached. The cell suspension was then pipetted into a centrifuge tube, centrifuged (200g, 2 minutes), media aspirated and cell pellet re-suspended and distributed across 5 x T-75 flasks and cultured until 80% - 90% confluent.

2.2.7.3 Rat Tenocyte Cryo preservation

After isolation of rt-tenocytes a substantial number rt-tenocytes cultured at 21% O_2 at passage 1 were cryopreserved for future use. Confluent T-75 flasks of rt-tenocytes were harvested by aspirating the culture media from the T-75 and washing twice with 10ml PBS. Once the PBS was aspirated from the T-75, 3ml of 1% trypsin/PBS solution was added to disassociate the cells from the culture plastic. Once the cells had disassociated from the T-75 flask, 3ml of rt-tenocytes culture media (differentiation media) was added to the trypsin-cell suspension to quench the effects of trypsin. The media-cell-trypsin suspension was then placed into a 15ml centrifuge tube and centrifuged for 3 minutes at 200g. After 3 minutes had elapsed the media- trypsin solution was aspirated from the centrifuge tube to leave a cell pellet. The cell pellet was then re-suspended in 1ml of 90% FBS and 10% DMSO at room temperature. The DMSO-FBS-cell suspension was then placed into a 1.5ml cryovial and placed in a 'Mr Frosty' (C1562 Sigma Aldrich, UK) and placed into a -80^{o}C freezer for 24hrs.. After 24hrs had elapsed the cryovial was then transferred into liquid nitrogen.

2.2.8 Surgical Implantation of PHBHHx Tendon Scaffold

15 male Sprague-Dawley (SD) rats 180-200 g were obtained from the Centre for Biomedical Analysis, Tsinghua University, China. Animals were returned to the centre post operation and held there for the duration of the experiment. The animals were sacrificed at 40 days post operation, with the Achilles tendons from both hind legs being removed for analysis. This study was conducted following the guidelines and requirements of the local ethical committee at Tsinghua University, Beijing, China and in collaboration with Peking Number 1 Hospital, Beijing, China.

Surgical procedures were carried out by experienced (consultant) orthopaedic surgeons at the Surgical Training Centre, Peking University Hospital Number 1, Beijing, China. Animals were anesthetised using 50 mg/Kg sodium pentobarbital. Once anesthetised, a lateral incision was made parallel to the Achilles tendon on the distal side of the right hind leg (Fig. 2.5B) and the tendon exposed (Fig. 2.5C). In the control group, a 5 mm section was removed from the centre of the tendon (Fig. 2.5D), then the incision closed using 3 cross stitches using dissolvable sutures (Fig. 2.5I). Experimental groups had a 5 mm section removed from the tendon, which was then bridged using the scaffold. This was done by first knotting together the 3 fibres and passing each individually through one end of the damaged tendon (Fig. 2.5E). The tube was then passed along the open end of the fibres, and manoeuvred into position (Fig. 2.5F). The remaining open ends of fibre were then passed through the other damaged end of tendon, and the ends bought together to leave a 5 mm gap between the tendon ends. The fibres were then knotted together as previously, fixing the scaffold in place and the leg at the correct anatomical position (Fig. 2.5G). In one experimental group, collagen gel was injected into the scaffold after it had been fixed in place using a syringe (Fig. 2.5H). The surgery was again then closed using 3 cross stitches using dissolvable sutures. Animals were separated until all had recovered from anaesthesia, and then divided according to experimental group.

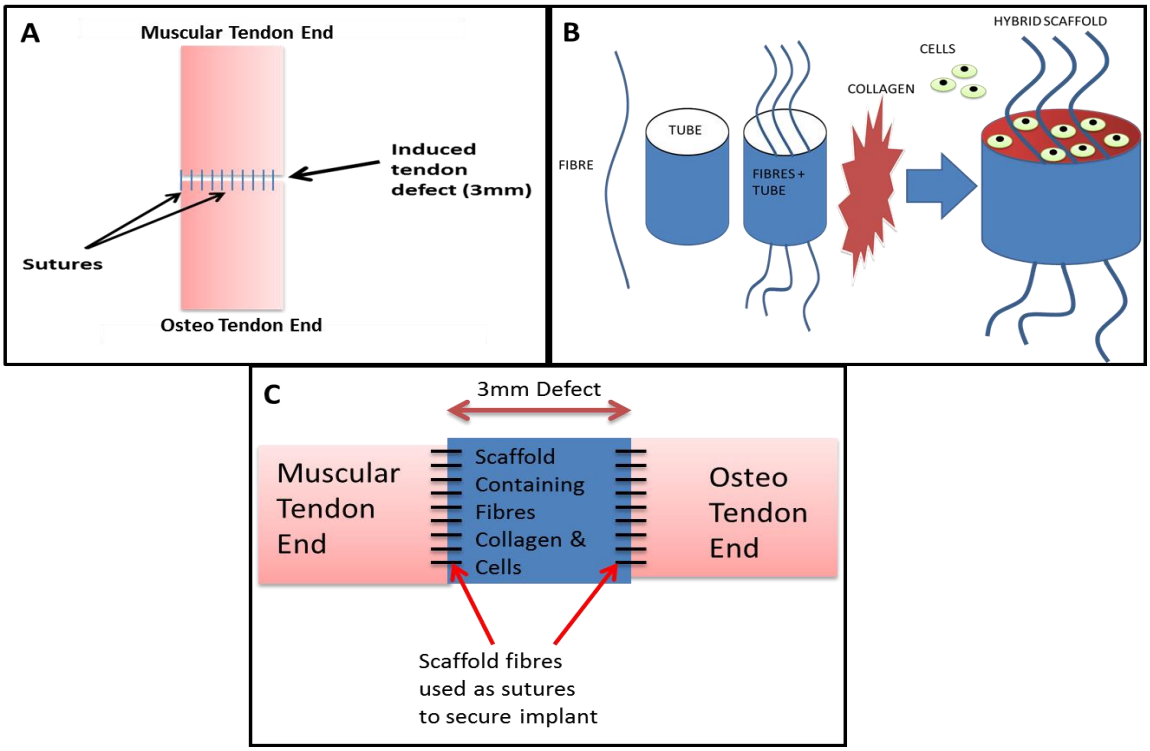

Figure 0.2 Implant Schematic

A) shows the anastomosis where normal silk sutures were used to join the osteo-tendon and muscular tendon ends to repair the induced defect in the control group. B) Shows the components of the PHBHHx scaffold (PHBHHx fibres, PHBHHx porous tube, collagen gel with/without cells. C) shows how the PHBHHX scaffold was used to bridge the 3mm induced defect and the PHBHHx fibres replacing sutures to anchor the implant to both the muscular tendon and osteo tendon ends.

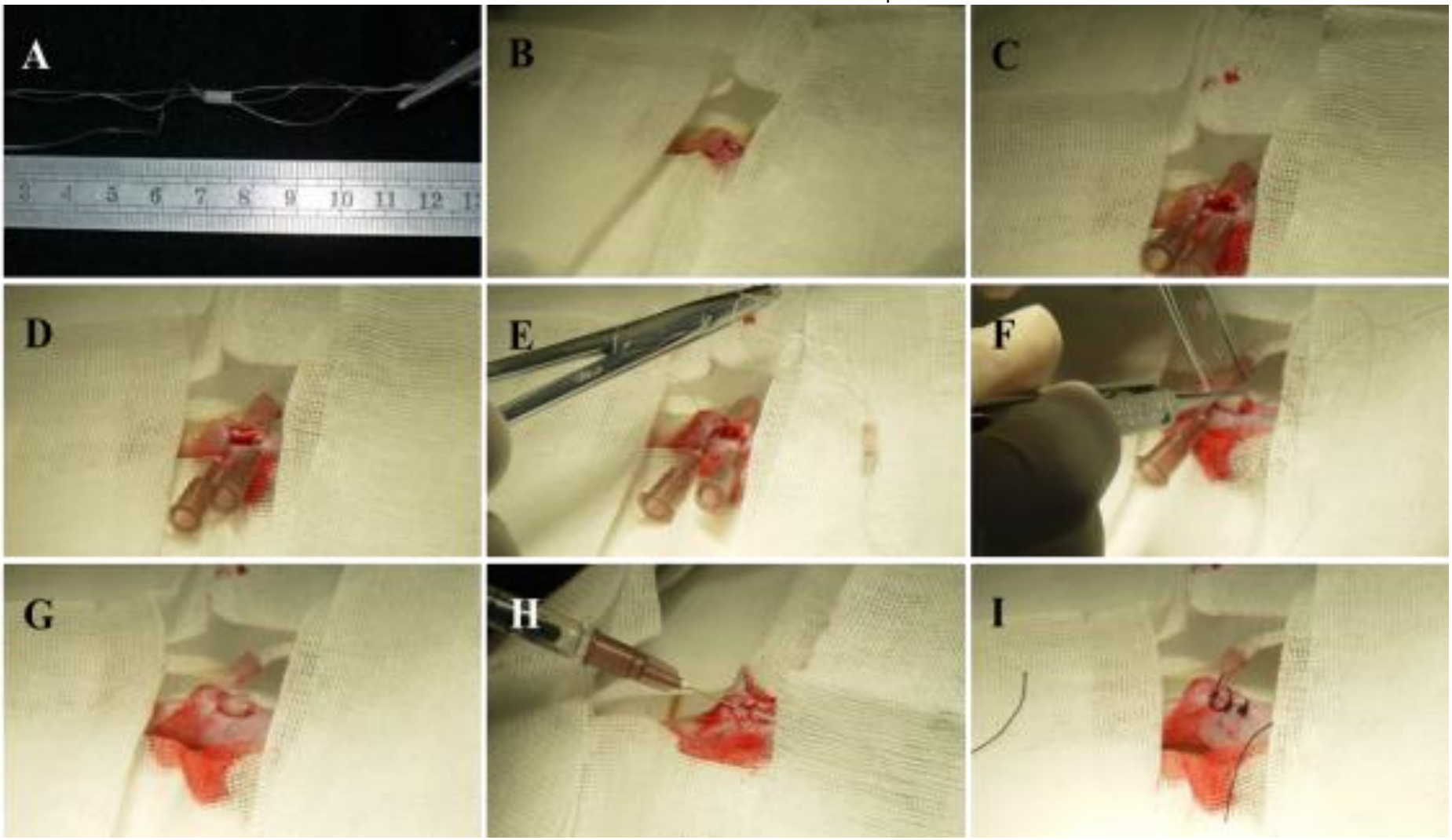

Figure 0.3 Implantation Procedure for Rat Tendon Repair

2.2.9 Immune Response Analysis using C-Reactive Protein

Immune response was monitored by measuring C-Reactive Protein (CRP) levels in the rat serum from day 0 – day 40. Blood was taken from the tail vein of rats on days -2, 2, 5, 10, 20 and 40. Day 0 blood samples were not possible due to blood loss during surgery. Once collected samples were centrifuged at 1500 rpm for 15 minutes and the serum (clear liquid level at the top) collected and stored at -80^{o}C. CRP was measured using a Rabbit anti Rat CRP ELISA kit (BD Bioscience, 557825) according to the manufacture's protocol and read using a Molecular Devices' VersaMax' Micro plate Reader.

2.2.10 Achilles Functional Index

Achilles tendon functional recovery was quantitatively assessed using a modification of Murrell's AFI method [314], similar to Kurtz *et al* [168]. A walkway approximately 80 cm long by 20 cm wide was lined with white paper (Figure 2.4A). A rat's hind paws were then coated with water based ink and the rat placed at the start and allowed to proceed down the walkway. Footprints were scanned and print length, print width (distance from first to fifth toe) and intermediate toe width (distance from second to fourth toe) measured using Image J [315] analysis software. The AFI was then determined using Murrell's formula: AFI = 74(PLF) + 161(TSF) + 48(ITF) -[314] where PLF (print length factor), TSF (toe spread factor) and ITF (intermediate toe factor) represent the difference between the experimental and contralateral print measurements. Prints were obtained pre-operatively at day -2 and for post-operative days 2, 5, 10, 20 and 40 for n=3 rats from each experimental group (Figure 2.4B).

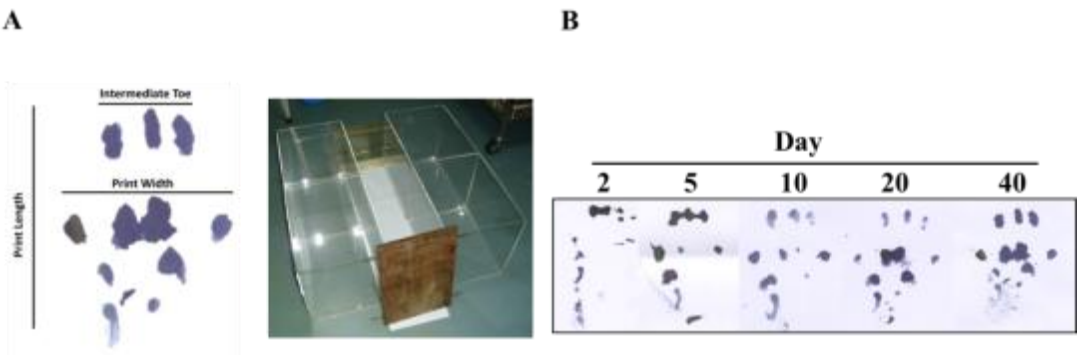

Figure 0.4 AFI Setup

A) Paw pad print required for AFI calculations and Walk Way for acquiring paw pad print, B) Complete experimental Paw pad print during experimental time course excluding day 0.

2.2.11 Explanted Scaffold Mechanical Testing

Stretch to break testing was carried out on 3 separate extracted scaffolds from each experimental group after 40 days. Non-operated tendons were used as control. Following removal, tendons and scaffolds were loaded into the servo controlled system universal testing machine (AI-7000S, GOTECH, Taiwan) where tendon ends were secured by clamps, and stretched at a rate of 10 mm/min until complete failure was observed.

2.2.12 Gel Permeation Chromatography

PHBHHx scaffolds were separated from remaining hind leg tissue by suspending the tissue/tube explant in 3 ml of Trypsin/EDTA (0.01g/l, 0.004g/l) (Lonza (02-007E)) for 24 hrs. After 24hrs the separated tube was washed twice using PBS (Lonza (17-516F)) and allowed to air dry at room temperature. Once dry the PHBHHx tube was dissolved in chromatography grade Chloroform (J.T. Baker, USA) at a ratio of 20% w/v PHBHHx chloroform solution and filtered using 0.22µm organic solution filters (Membrana, Germany) prior to GPC injection.

Molecular weights were studied using GPC (RID-10A, Shimadzu, Japan). Measurements were performed at 40^{o}C using a GPC-804C column (Shimadz, Japan) where all samples were referenced against 10% w/v chloroform solutions of high molecular weight polystyrene standard (Mw 300,000 Da and 150,000 Da) (Fluka, Sigma-Aldrich, Germany) and low molecular weight polystyrene standard (Mw 50000 Da, 30000 Da, 9000 Da and 4000 Da) (Shimadzu, Japan).

2.2.13 Haematoxylin and Eosin

Structural analysis of two samples from each group was performed using Haematoxylin and Eosin (H & E) (Gene Research Lab. Co. PS003) according to standard procedures. Prior to staining the sample was first fixed using 70% methanol for 24 hrs, then embedded in paraffin wax before sectioning into 8 µm sections and placing onto a glass slide. Sections from the injury site and healthy areas of tendon were analysed. Images were taken using a Nikon Eclipse 90i

2.2.14 Experimental Plan

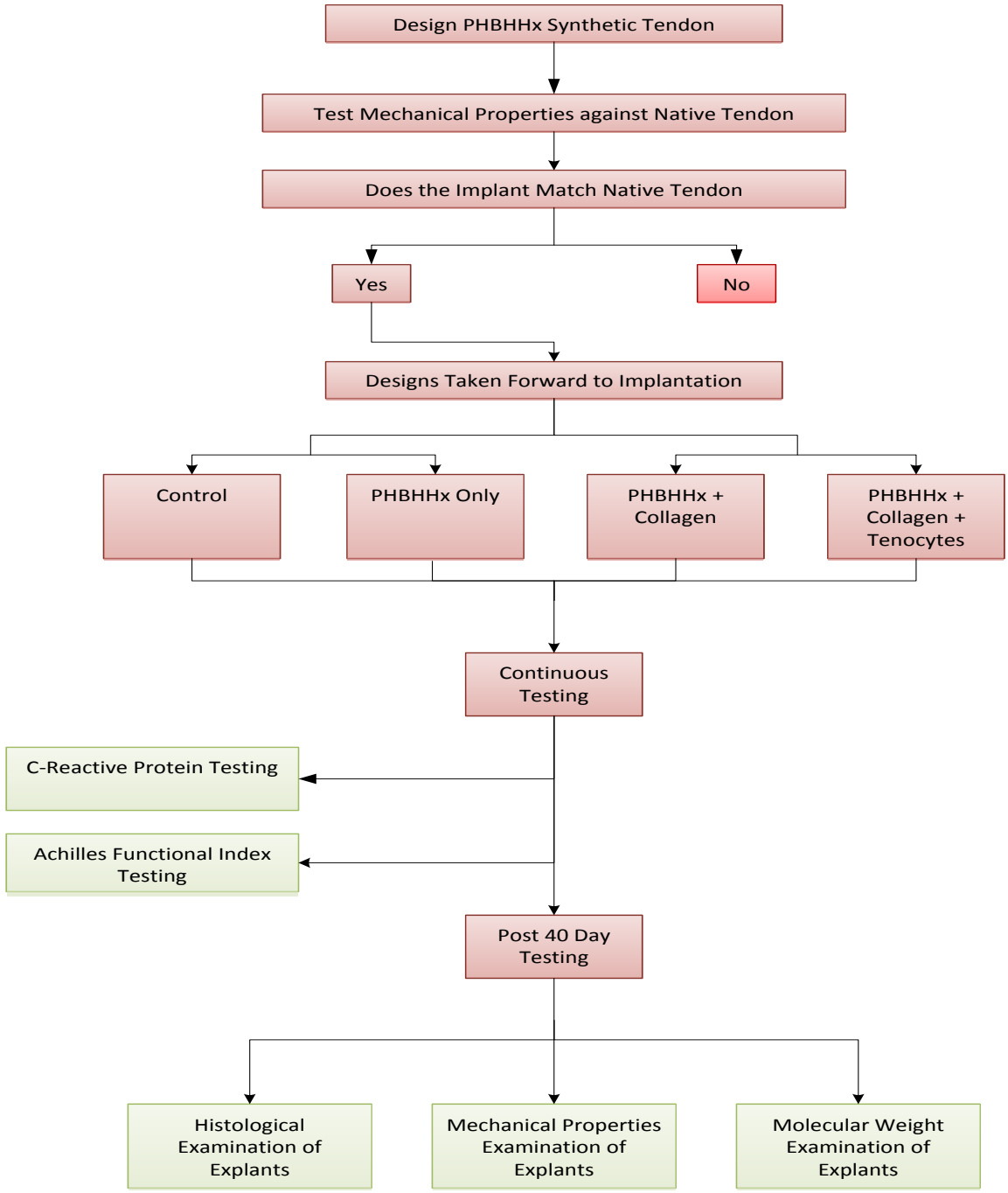

Figure 0.5 Experimental Plan

Experimental work plan showing scaffold selection and continuous monitoring of implant performance and immunological response. Post re-sectioning of scaffold for histological, mechanical and molecular weight analysis post re-sectioning.

2.3 Results

2.3.1 Scaffold Design

PHBHHx Scaffold components were characterised utilising SEM and mechanical force testing. The individual PHBHHx components namely: PHBHHx fibre and PHBHHx tubes were tested individually and in combination along with the addition of collagen to the scaffold core.

2.3.1.1SEM PHBHHx Fibre Examination

SEM analysis of the PHBHHx tubes and fibres was undertaken to measure the tube pore size and diameter of the fibres. From the SEM images and measurements taken average pore size and fibre width were calculated to be: 175.4µm ± 2.4 µm for fibre diameter (Figure 2.6) and 46.01 µm ± 19.21 µm for pore size (Figure 2.7).

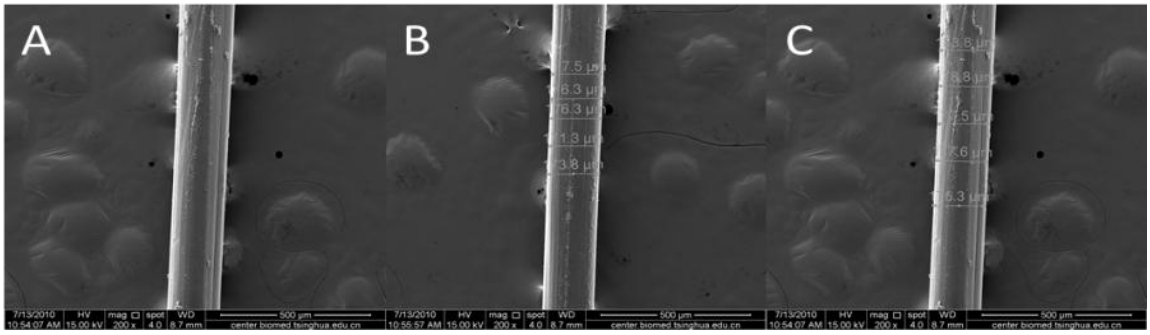

Figure 0.6 Scanning Electron Micrographs (SEM) of the PHBHHx Fibres.

A) Shows PHBHHx fibre prior to measurement, B & C) Show PHBHHx fibre measurements.

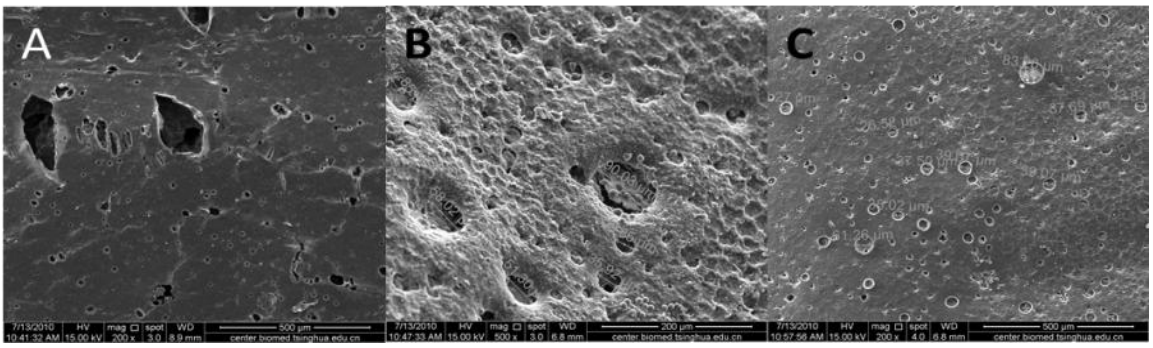

Figure 0.7 Scanning Electron Micrographs (SEM) of Porous PHBHHx Tubes.

A) PHBHHx tube section prior to measurement (sample 1), B) PHBHHx tube section prior to measurement (sample 2) and C) PHBHHx tube section prior to measurement (sample 3).

2.3.1.2Mechanical Force Testing

After SEM analysis comparisons between native tendon and complete scaffold constructs and scaffold components was undertaken utilising MTS tension/compression load cell tester (MTS, Canada) and elongated at a rate of 10mm per second until failure

Rat Achilles tendon has an average breaking load of 17.35 ± 1.76 N (Figure. 2.8). A porous PHBHHX scaffold with varying number of fibres was evaluated to determine which had an approximate mechanical performance to natural tendon (Figure. 2.8). From this it was apparent that: 3 fibres running through the centre of a PHBHHx porous tube had comparable breaking loads with (23.46 ± 4.81 N) and without a collagen core (26.70 ± 1.05 N), were both were significantly stronger than the native rat tendon ($p<0.006$), whilst both the single fibre and tube were significantly weaker than native tendon ($p<0.004$) (Figure 2.8). The 3 fibre construct without a porous tube had a comparable, though weaker value when compared to rat Achilles tendon (13.53 ± 5.37), and displayed wide standard deviations. This design was therefore ruled out for implantation due to the unacceptable degree of variation. From the data described above the scaffold featuring 3

fibres, a porous PHBHHx tube and 3 fibres in a collagen lumen design was applied in the Achilles tendon wound model described in Section 2.2.8.

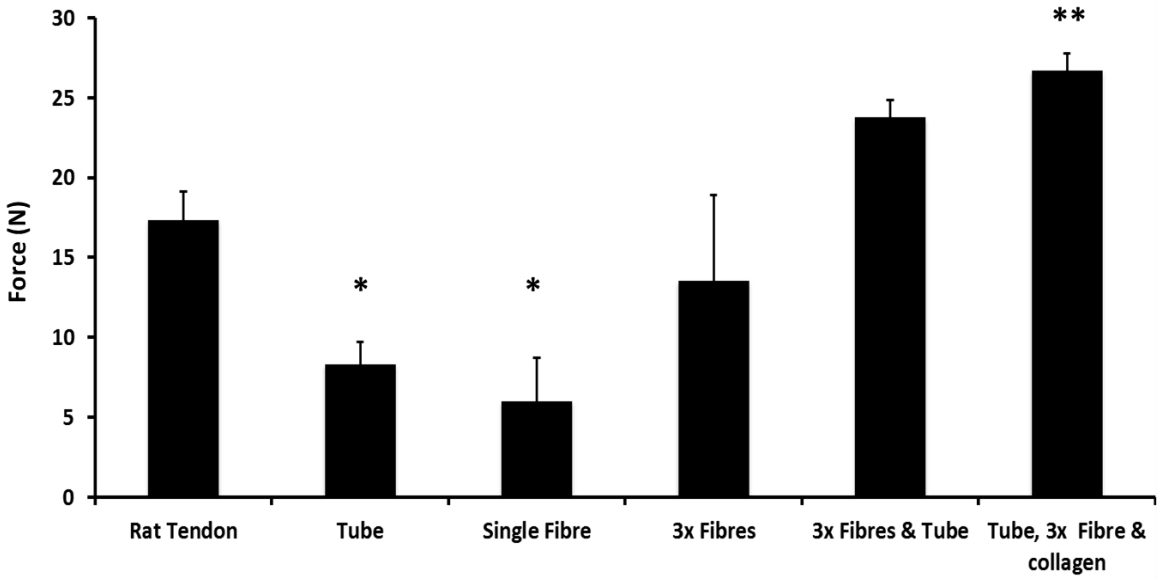

Figure 0.8 Mechanical Testing of Scaffold Designs

Native rat tendon was measured and used as a minimal properties required for scaffold implantation. Scaffold components: PHBHHx tube, Single Fibre, 3 x fibres, 3 x fibres and tube and hybrid scaffold (3x fibres, tube and collagen core) were compared to the native tendon.

From the data obtained in mechanical testing of the scaffold designs and the constituent parts, the hybrid scaffold was selected for implantation. 20 SD rats were subdivided into 4 experimental groups. These groups were: Control (induced tendon defect with no repair), Group SO (Scaffold Only), Group Hybrid Scaffold (Scaffold with collagen core) and the final Group Hybrid scaffold containing Collagen core and the addition of rat tenocytes.

Prior to implantation all 20 rats were treated as a single group so a baseline for C-reactive protein and Achilles Functional Index were obtained for comparison of data collected post implantation.

2.3.2 Immunological Response

Prior to implantation the 20 rats were treated as one group. 300µl of blood was taken from each rat for base line CRP values. Post implantation each experimental group contained five animals (n=5). At time points 2, 5, 10, 20 and 40 days post implantation 300µl of blood was taken from each rat in all experimental groups for CRP comparison prior to implantation. We were then able to monitor immune response to the implanted PHBHHx scaffold and also possible infection during implantation.

The immune response was quantified by measuring C-reactive protein (CRP) concentration in blood serum. Samples were taken at time-points pre and post-surgery. Prior to surgery all rats were considered as one group (n=20) where an initial CRP concentration at day -2 of 1251.48 ± 31.42 µg/L (Figure. 2.9) was noted. Surgery was performed on day 0 and blood samples were not taken to minimize discomfort. CRP had increased significantly in all groups at day +2 after surgery, ranging in level from the scaffold only group (1502.25 ± 45.46 µg/L), the tenocyte-PHBHHx-collagen group (1437.38 ± 44.11 µg/L) to the control group (1357.58 ± 82.91 µg/L) ($p<0.02$). CRP levels were significantly elevated in all groups in comparison to Day -2 ($p<0.04$). By day +5, CRP levels ranged from 1244.39 ± 136.09 µg/L (PHBHHx-Collagen), 1160 ± 57.00 µg/L (PHBHHx), 1132.58 ± 23.21 µg/L (Control) to the tenocyte-PHBHHx-collagen group (985.46 ± 20.75 µg/L ($p<0.05$ vs. day-2; $p<0.0007$ vs. all other groups). All groups displayed reduced CRP levels at day +5 in comparison to Day +2 with a significantly lower value for CRP being observed in the PHBHHx only group ($p<0.03$) and in the tenocyte-PHBHHx-collagen group ($p<4.05E-08$) when compared to pre-surgery CRP levels. CRP levels continued to fall further at day +10 where all groups had lower concentrations than

pre-implantation values. The tenocyte-PHBHHx-collagen only group recorded the lowest level at 960.89 ± 20.07 µg/L and all groups were lower than pre-implantation CRP levels ($p<0.02$) and post implantation day +2 ($p<0.04$). CRP levels in the control group stabilised at Day+10 levels while CRP levels for all other groups continued to decrease. CRP levels stabilised from Day+20 onwards through to Day +40 when final analysis was performed. All CRP levels for all groups remained significantly below the pre-implant values and post implantation levels (Day -2) ($p<0.05$).

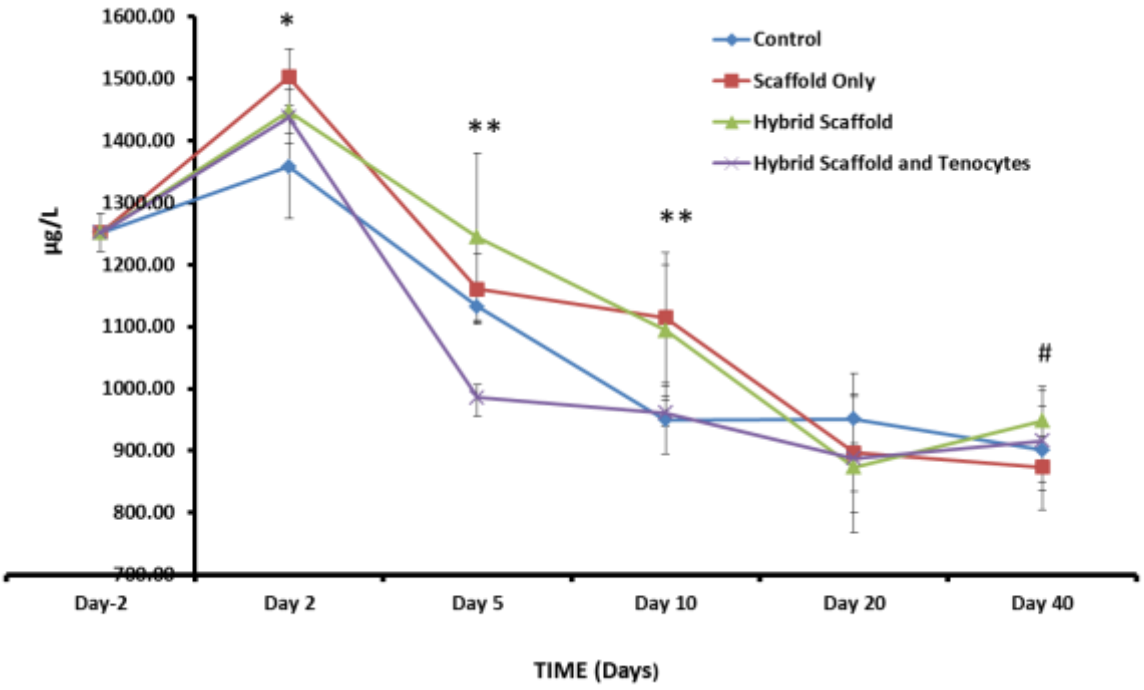

Figure 0.9 Immune Response to Implanted Scaffold.

CRP base values were obtained prior to implantation (n=20). Post implantation, all experimental groups were sampled (n=5) and measured at time points 2, 5, 10, 20 and 40, and then compared to previous time points and day.

2.3.3 Restoration of Function

Prior to implantation Achilles functional index scores were calculated for the healthy animals prior to implantation. Further analysis was taken at 0, 2, 5, 10, 20 and 40 days

post implantation and compared against the pre-implantation values which were used as baseline scores.

2.3.3.1Achilles Functional Index

Initial AFI scores were taken 2 days prior to surgery (-24.83 ± 1.29) (Figure 2.10). At day +2 all groups displayed a dramatic decrease in AFI (Control -86.32 ± 14.05), PHBHHx only (-95.36 ± 9.56), PHBHHx-collagen (-84.21 ± 12.50) and tenocyte-PHBHHx-collagen (-103.31 ± 12.04) where all groups had a significantly lower AFI when compared do day -2 ($p<0.05$). All groups showed a continuous improvement from day +5 to day + 10 excepting the PHBHHx-collagen group at day +5 (-84.90 ± 14.90). The greatest improvement was noted in the PHBHHx-collagen group at day +10 (-47.42 ± 33.68), and the tenocyte-PHBHHx-collagen group (-49.44 ± 13.81). The least improved group at day +10 was the scaffold only group (-67.25 ± 11.03) (with all groups having a significantly lower AFI when compared to day -2, $p<0.04$). By day +20 the tenocyte-PHBHHx-collagen group had improved over the pre implantation AFI score (-18.95 ± 17.00). By day +40 the tenocyte-PHBHHx-collagen group had improved further (-5.16 ± 6.95) followed by the scaffold only group (-14.79 ± 3.97), PHBHHx-collagen group (-15.22 ± 5.12) and finally by the control group (-19.67 ± 23.12).

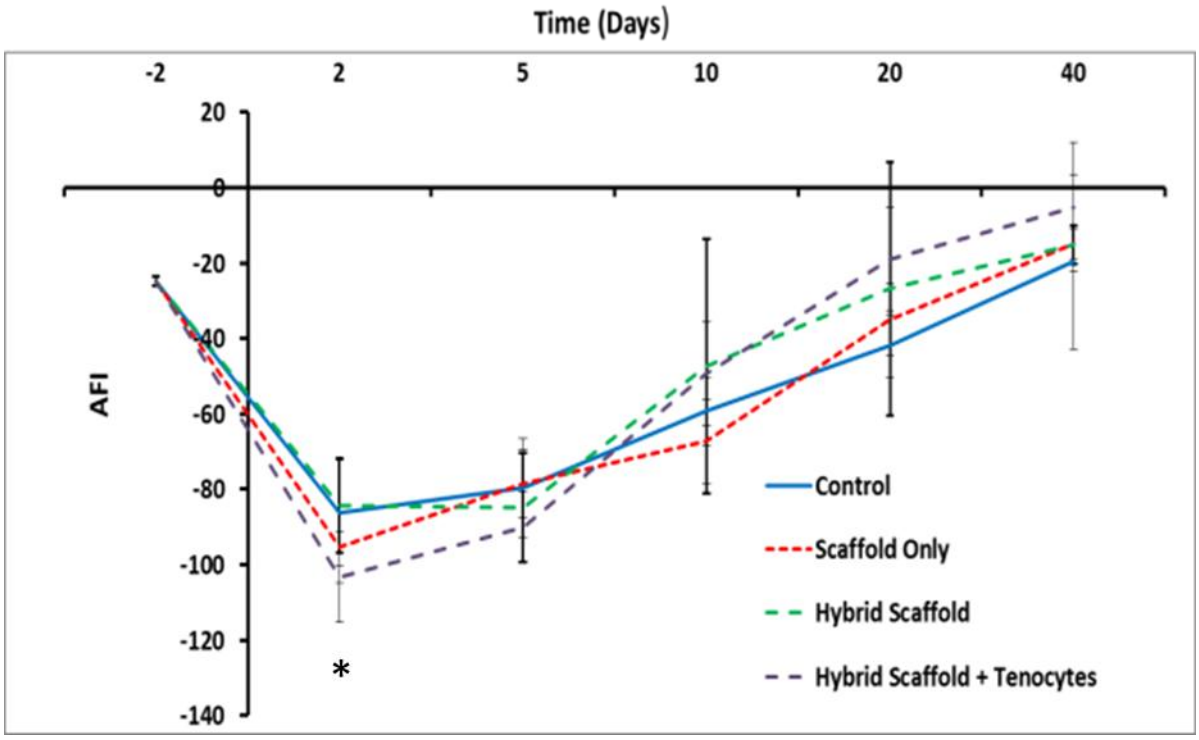

Figure 0.10 AFI Data Against Time

AFI analysis was undertaken on pre implantation rats to produce a baseline for comparison. All implant groups were then compared to the control group, with all implant groups showing a return of function to pre-implantation values by day 40 (* p<0.05).

2.3.4 Molecular Properties of Explanted Scaffolds

Prior to implantation the molecular properties of the scaffolds were analysed using GPC. This data formed the baseline for comparison. After 40 days post implantation each implant group had the scaffold removed for GPC analysis and the molecular properties were compared to the original scaffold properties prior to implantation.

Pre-implant tubes had a molecular weight (Mw) of 224,742 ± 23,975 Da (Figure 2.12), Mean chain length (Mn) of 399,732 ± 73,540 Da (Figure 2.13) and Polydispersity Index (Mw/Mn) of 0.58 ± 0.042 (Figure 2.14). After 40 days all groups displayed reduced Mw and slightly elevated Mn; tenocyte-PHBHHx-collagen (212,381 ± 10,515 Da and 412,412 ± 19,433 Da, respectively), scaffold only (212,623 ± 11,879 Da and 416,436 ± 46,612 Da,

respectively), and PHBHHx-collagen (222,204 ± 16,415 Da and 442,200 ± 22,054 Da, respectively). However, PDI was reduced after 40 days in scaffold only group (0.51 ± 0.043) and significantly reduced in the PHBHHx-collagen (0.50 ± 0.012), and tenocyte-PHBHHx-collagen group (0.52 ± 0.021) in comparison to non-implanted scaffold ($p<0.03$)

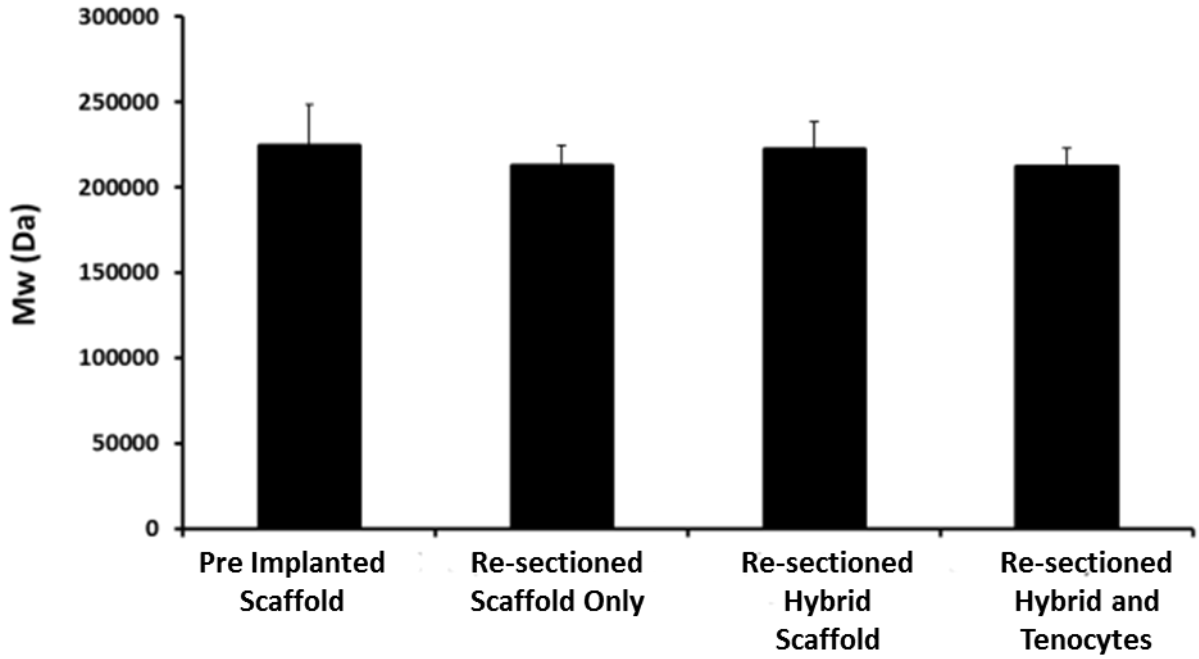

Figure 0.11 Re-sectioned Scaffold Degradation Measurement of Molecular Weight.

Molecular weight analysis was performed on pre and re-sectioned implants and showed no significant decrease in values obtained when compared to the pre-implantation values.

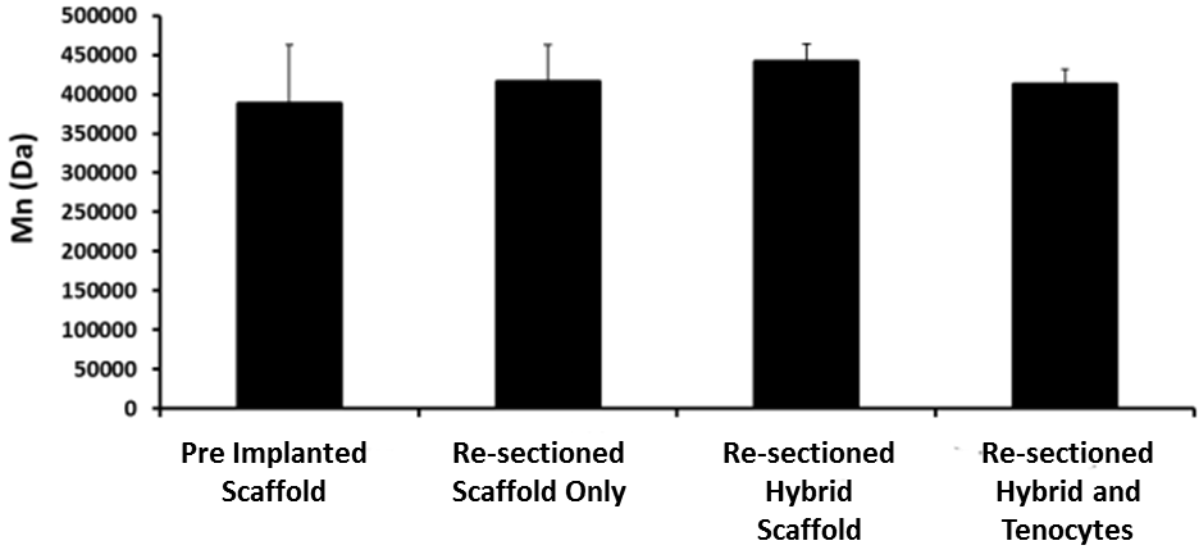

Figure 0.12 Re-sectioned Scaffold Degradation Measurement of Mean Chain Length Molecular Weight (Mn)

Mean Chain analysis was performed on pre and re-sectioned implants and showed no significant decrease in values obtained when compared to the pre-implantation values.

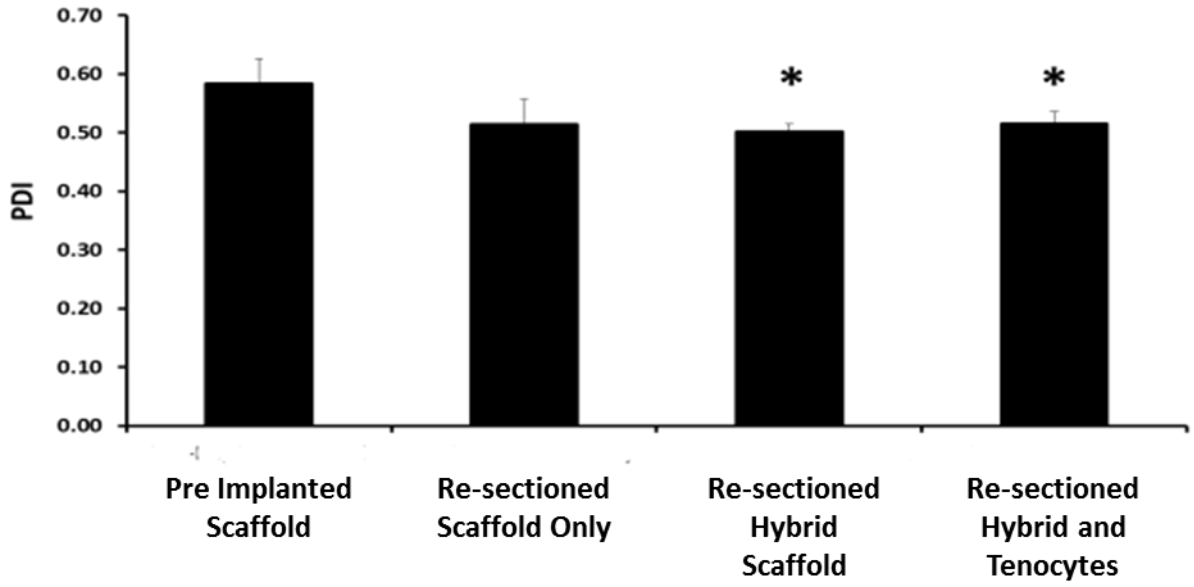

Figure 0.13 Re-sectioned Scaffold Degradation Measurement of PDI

PDI analysis was performed on pre and re-sectioned implants and showed significant decrease in values for re-sectioned hybrid scaffold and explanted hybrid scaffold that contained tenocytes when compared to the pre-implantation values (*p<0.05).

2.3.5 Re-sectioned Mechanical Properties of implanted scaffolds

Mechanical testing, namely stretch to break (force to break) and elastic modulus determination was performed after the implant removal on day 40 (Figure 2.14 and Figure 2.15). Pre-implanted scaffold had a maximum force of 9.4 ± 2.2N and elastic modulus of 24.3 ± 13.2 MPa. All explanted scaffolds had a reduction in both maximum force and elastic modulus (PHBHHx only: 7.5 ± 1.1N and 18.7 ± 2.7 MPa, PHBHHx and Collagen: 5.6 ± 2.4N and 14.0 ± 6.0 MPa, and tenocyte-PHBHHx-collagen: 4.8 ± 0.1N and 12.1 ± 0.2MPa). All groups had a significantly lower force to break (PHBHHx only, $p<0.05$; PHBHHx and collagen, $p<0.05$; and tenocyte-PHBHHx-collagen, $p<0.003$) with no observed difference in elastic modulus.

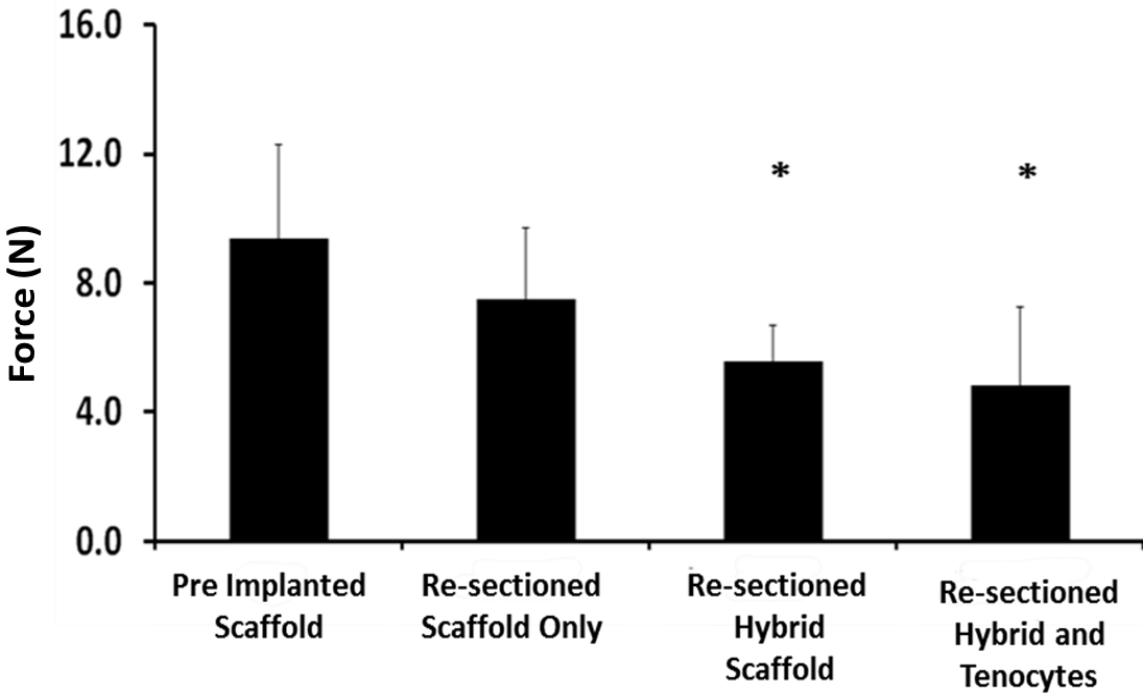

Figure 0.14 Re-sectioned Scaffold Mechanical Testing

Comparison of ultimate tensile strength (N) of pre implantation scaffold and re-sectioned scaffolds removed after 40 days implantation (*p<0.05).

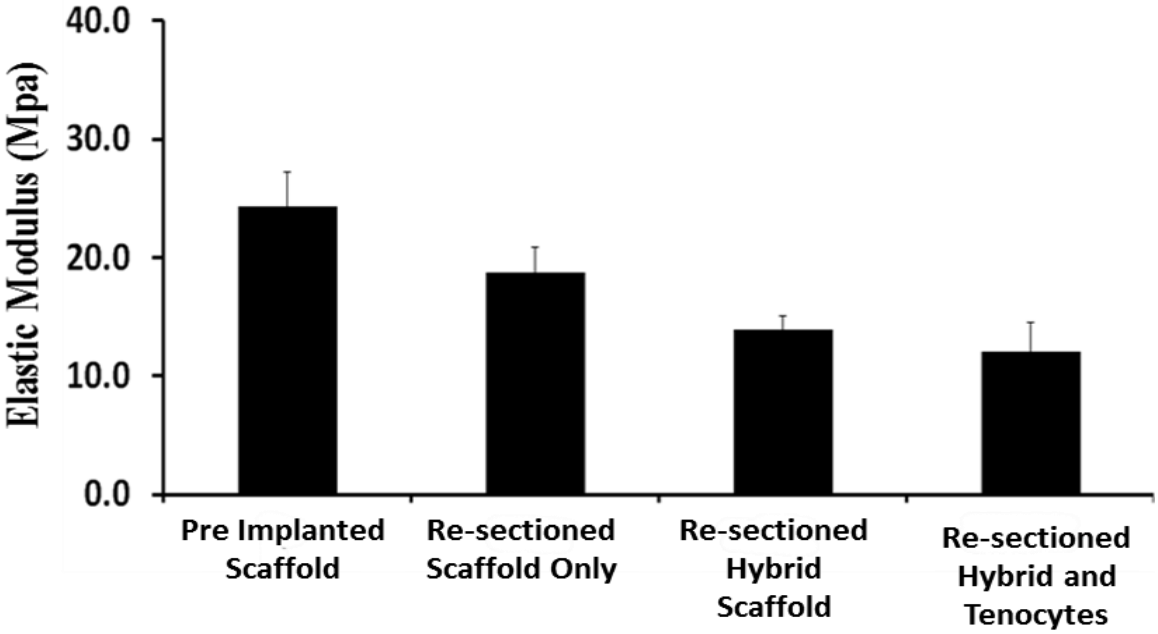

Figure 0.15 Re-sectioned Scaffold Young's Modulus.

Comparison of elastic modulus (MPa) of pre implantation scaffold and re-sectioned scaffolds removed after 40 days implantation.

2.3.6 Histological Analysis

One re-sectioned scaffold was taken from each experimental group for histological analysis. Each section underwent paraffin wax imbedding and sectioned to a thickness of 10µm. Post sectioning each sample was stained using Haematoxylin and Eosin staining protocol as outlined in Section 2.2.13 and imaged for analysis.

2.3.6.1Haematoxylin and Eosin Staining

Microscopic evaluation of the damaged tendon sites with Haematoxylin and Eosin demonstrated evidence of cellular infiltration and partial structure regeneration to varying degrees dependent upon the scaffold implanted. Cellular migration into the defect site was apparent throughout where increased migration was observed where a PHBHHx-collagen only implant had been introduced to the wound site when compared to

either healthy tendon (Figure. 2.16) or a wound site with PHBHHx scaffold only (Figure. 2.16). A characteristic of tendon tissue is the crimp pattern which is presented by the elongated sinusoidal wave like patterning of the nuclei and cytoplasm of the cells as apparent in the undamaged tendon sample .The emergence of the wave-like patterning was observed in both the PHBHHx-collagen and tenocyte-PHBHHx-collagen implants, however a greater structural organisation was observed in the tenocyte-PHBHHx-collagen implants. The tenocyte-PHBHHx-collagen implant displayed increased cellular alignment along the force-bearing axis; this feature was also observed in all other implants with less organisation along the fibre axis (Figure. 2.16). Cells formed a consistent wave pattern when in contact/close proximity to the fibre or tube component of the implant. This demonstrates that tendon-like tissue was being created around the implant, rather than just overlaying fibrous tissue. This was less evident in the scaffold only group (Figure 2.16), indicating that tendon regeneration was more efficient in the tenocyte-PHBHHx-collagen and PHBHHx-collagen implant groups. The implant was not discernible in the scaffold only group, providing further evidence of weaker interaction, leading to slight detachment from the tissue resulting in reduced integration This finding shows the use of collagen within the implant construct plays a vital role not only for remodelling of the implant but also integration

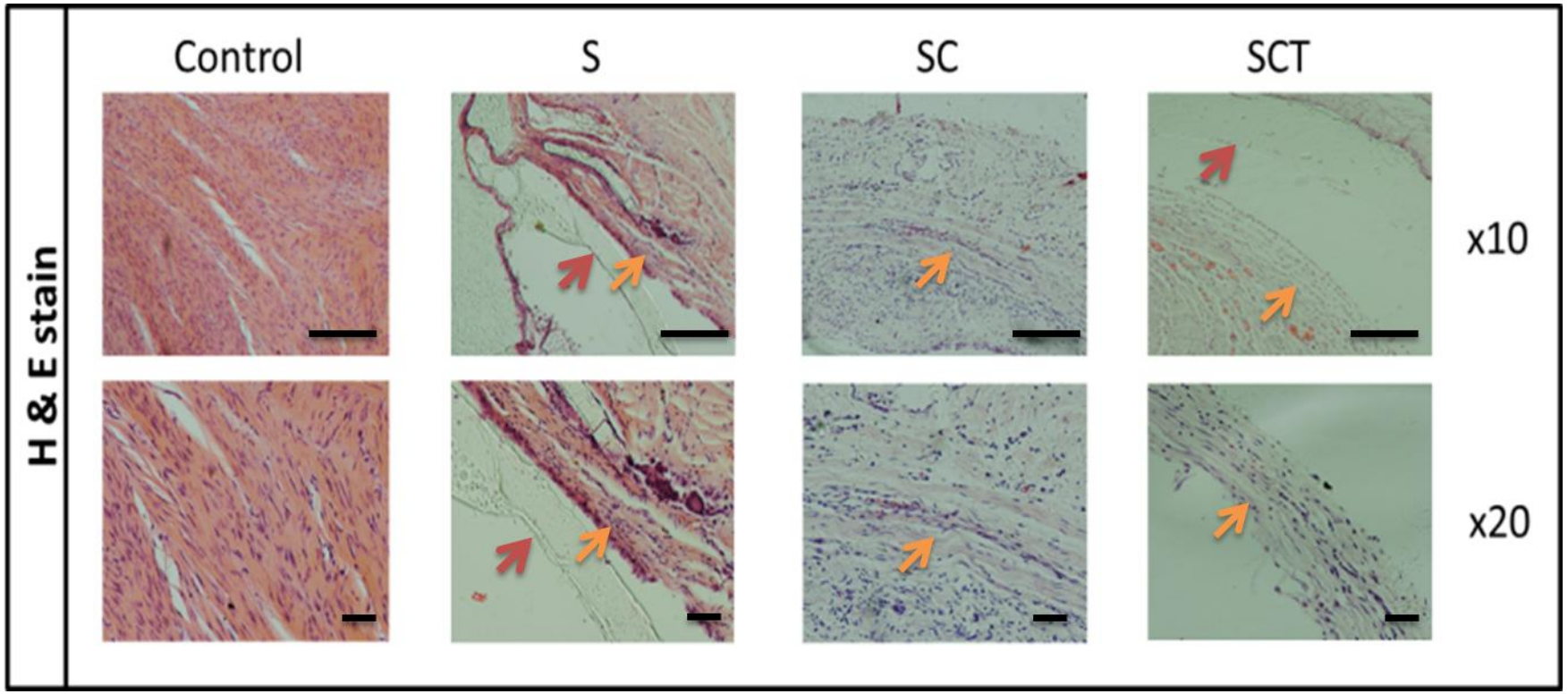

Figure 0.16 Histological Staining of Explanted Scaffold (H&E staining)

Shows microscopic images of Control (healthy rat tendon), PHBHHx Scaffold only group (S), PHBHHx Scaffold and Collagen (SC) and PHBHHx Scaffold, Collagen and rat tenocytes (SCT) using 10x and 20x magnifications. Red arrows indicate PHBHHx fibres, Orange arrows indicate cellular alignment (error bars=500µm)

2.4 Discussion

The aim of this investigation was to identify a PHBHHx scaffold design that could be used to facilitate repair of damaged tendon tissue while not initiating an immune response or prolonging inflammation. A composite scaffold was developed which featured a PHBHHx tube, a collagen core, and PHBHHx fibres which would facilitate cellular migration and tissue remodelling, while at the same time allowing for limited restoration of movement. The design was mechanically similar to the rat Achilles tendon and to other commercially available human tendon repair materials [117, 297]. Furthermore, this study has shown that PHBHHx scaffold encourages cellular infiltration, proliferation and cellular alignment/organisation along the force barring fibre without initiating a prolonged immune response.

C-reactive protein (CRP) is a well conserved member of the pentraxin family of proteins and is secreted by the liver in response to an array of inflammatory cytokines [316, 317]. CRP binds to damaged tissue and increases rapidly in response to trauma, infection and inflammation and also decreases rapidly with the resolution of the condition [318-320]. CRP also has the ability to activate the complement pathway and has been shown to bind to the Fc receptors used by IgG (FcγRI and FcγRII) [317, 319-321]. CRP-Fc receptor binding leads to a pro-inflammatory response similar to that observed with IgG complexes[321]. Not only does CRP activation precede IgG antibodies by approximately one week, CRP has also been shown to play a crucial role in the activation of the adaptive immune response early in the inflammatory and infectious process [318]. CRP has been used to measure an array of immune responses such as inflammation in implanted biomaterials in animals and both total knee replacement and hip replacements in humans [322]. This study

employed multiple time point analysis which included pre and post implantation levels of serum C-reactive protein (CRP) in response to the 40 day exposure of PHBHHx implanted scaffold in the rat model. CRP level grossly elevated on Day +2 which agrees with previous studies [323] However, by day +5 CRP levels had rapidly decreased to below pre-implantation levels in all experimental groups and continued to remain below pre-implantation levels in all experimental groups throughout the remainder of the study, which agrees with previous studies in both rodents and humans [324]. The decrease in CRP to below pre-implantation levels indicates that no long term immunological/inflammatory reaction was occurring due to the presence of the implanted PHBHHx scaffold and its components; improving on similar conclusions made by previous studies [325]. This study has also shown for the first time prolonged exposure to PHBHHx or PHBHHx breakdown products does not prolong an immunological/inflammatory response in the rat model when monitored using CRP.

AFI testing showed a continued improvement for all groups over the 40 day investigation, with complete return of function being as early as day +20 in the tenocyte-PHBHHx-collagen group which was a full 20 days prior to the PHBHHx only and PHBHHx-collagen group, with the control group remaining below pre-surgical implantation levels. These results show the implanted scaffolds are capable of withstanding the forces which are exposed to native tendon and the implantation of a scaffold returns function to the limb faster than the absence of an implant which agrees with previous studies [314].

Mechanical testing of tube samples recovered from the rats at day +40, found that all group had a reduced mechanical load capability of the scaffold tubes when compared to pre-implanted scaffold tube, suggesting that the fibre component of the scaffold was the

major contributor to the delivery of the mechanical properties displayed in the AFI. Histological examination showed cellular infiltration into the PHBHHx lumen, which would show PHBHHx provides favourable conditions for cellular migration and proliferation which adds to the findings in previous studies [307-311]. Cellular infiltration into the scaffold was observed in both the PHBHHx only and Collagen-PHBHHx scaffold designs with sinusoidal cellular alignment which is a key marker in the histological analysis of tendon tissue, signifying the presence of crimp angles between collagen fibrils [33, 43]. However, the collagen-PHBHHx scaffold showed a denser cellular presence with limited sinusoidal morphology along the surface of the PHBHHx fibre, this would imply a more favourable environment for cells is produced when a collagen lumen is present within the scaffold design [114, 300, 312]. The tenocyte-PHBHHx-collagen scaffold cells appeared to be more elongated and sinusoidal in morphology, when compared to the other implanted scaffold designs, as with the PHBHHx only and collagen-PHBHHx scaffold designs, when cells were in direct contact with the scaffold, especially the fibre component this feature was more apparent and the sinusoidal-elongated morphology could possibly indicating that force transmission resulting in mechanotransduction from the fibre to the cells promoted tendon cell proliferation and alignment [90, 301, 312]. However, the cellular density observed in the tenocyte-PHBHHx-collagen group was less apparent than that of the PHBHHx only and collagen-PHBHHx containing scaffold which would imply the addition of tenocytes cells had proliferated and become organised earlier, resulting in decrease in time required for functionality to return to the tendon and would account for the results in AFI measurements. Earlier studies have highlighted the addition of collagen within the scaffold design can aid integration within the implanted tissue. This further highlights the importance of collagen not only in the tissue integration and remodelling of

tendon but in a means of delivering cells to a point of repair and further adds to previous studies suggesting collagen is a beneficial inclusion in tendon graft material [114, 300, 326].

GPC analysis of explanted tube component of the scaffold showed an increase in number average chain length (Mn) and lower molecular weight (Mw). These findings suggest that the shorter chain length and low molecular weight component of the scaffold (namely the hydroxybutyrate) component may be being metabolised/broken down, which would account for the decrease in overall molecular weight which agrees with an earlier PHBHHx study [310]. The increase in Mn indicates that the polymer has a greater ratio of longer chain lengths than shorter chain lengths, which would correspond with the shorter chain length component of the polymer being metabolised/broken down. This is further evident in the changes of polymer dispersity index (PDI) (calculated by Mw/Mn) which is attributed to the dissolution of degraded polymer chain from the polymer bulks [327].The scaffold only group which lacked the presence of collagen, showed the greatest decrease in the Mw, we hypothesis the collagen component does in-fact delay the breakdown of the polymer [328]. The tenocyte-PHBHHx-collagen implant (212,381 Da ± 10,515 Da, after 40 days) already contained a cellular component and therefore the requirement for cellular infiltration is removed and cells were able to actively proliferate, remodel the collagen component and breakdown the polymer at an earlier stage with similar values to that of the PHBHHx only (212,623 Da ± 23,975 Da after 40 days) than the PHBHHx-collagen scaffold lacking the cellular component. Furthermore, the decrease in molecular weight would convey mechanical changes in the scaffold observed in explant mechanical testing of the scaffolds tube component, such as ultimate tensile strength and Young's modulus [327].

When considered together, these results suggest that this scaffold is biocompatible; inferring ability to perform its desired function without eliciting any undesirable local or systemic effects whilst facilitating a regenerative cellular response capable of contributing mechanical properties of the scaffold [329].

2.5 Conclusion

This study has demonstrated for the first time that PHBHHx in conjunction with collagen and tenocytes can be used as a scaffold material for the treatment of damaged tendon tissue *in vivo,* and with no prolonged immunological/inflammatory response in the rat model. It has also shown that cells not only migrate into, but implanted tenocytes proliferate within the PHBHHx scaffold *in vivo* and are capable of remodelling damaged tissue, with a tenocyte-PHBHHx-collagen scaffold aiding regeneration and the recently generated tissue being able to contribute to mechanical properties of the implant 40 days post implantation.

Chapter 3: Growth Factor induced Tenogenesis of Human Stem Cells

3.1 Introduction

Tendon injury due to ageing tendon and over use continues to be a burden on western health care. The current shortage in donor tissue and inadequate synthetic implants provides a niche for the development of a tissue engineered approach for the treatment of damaged tendons.

Tendon injuries and the subsequent repair continues to be an under researched topic area. Currently, the treatment options employed are limited to two major options, namely: conservative approach and surgical approach. Both methodologies have produced limited degrees of success with no consensus on which approach produces the best outcome for the patient.

Surgical repair is restricted to the size of injury with the use of xenobiotic implants also producing limited success. Autologous implants are limited by the induced morbidity at the donor site. The use of allograft is also limited to donor availability and also the age of the donor material. Therefore, an alternative approach to the treatment of tendon ruptures is highly desirable. In the previous chapter we have identified a PHBHHx based scaffold which is capable of restoring function of an induced tendon injury in the rat model. This chapter aims to identify a unique combination of growth factors capable of inducing and maintaining stem cell differentiation towards a tenocyte lineage.

A stem cell based approach to the treatment of tendon ruptures may provide a unique treatment opportunity. This can be patient specific by the utilisation of the patients' mesenchymal stem cells or a broader "off-the-shelf" approach which may utilise embryonic stem cells

Growth factors have been shown to be powerful mediators and initiators of tissue formation [174].The utilisation of embryogenesis as a means of mapping tendon development has been limited to species such as rats, murine and chicks [197, 198, 201, 202].

However, observations of such developmental pathways may not be conserved to human development [330]. One possible example is in tendon development in humans. To date there is very little evidence to the tendon transcription factor scleraxis activity in growth factor initiated human tendon development. However, there is evidence indicating scleraxis activity post mechanical stimulation [331].

This chapter will focus on the possibility of: FGF-4, FGF-6, FGF-8 and there combinations as being candidates for initiating stem cell differentiation towards a tenocyte-like cell lineage. Also, this chapter will build upon previous studies within the group in regards the potential of the combination of BMP-12 and BMP-13 as initiators of hESC differentiation towards a tenocyte-like cell lineage

3.2 Materials and Methods

The primary cells used in the experiments are described below (Table 3.1).

Cell Lines	Description	Origin	Age	Sex
MEFs	Mouse Embryonic fibroblasts isolated from 12.5-13.5 days gravid uteri of Black CB1 hybrid mice	Keele University Small Animal Facility	11 – 14 day old pups	M/F
SHEF-1	Human Embryonic Stem cell line	Sheffield University, UK; used under license from the UK Stem Cell Bank	n/a	Male
hMSC	Human mesenchymal stem cells isolated from bone marrow aspirates	Human bone marrow aspirates from Lonza, USA	32 Year old	M
rtTenocytes	Rat tenocytes isolated from 8 week old Sprague-Dawley rats	Keele University Small Animal Facility	8 weeks Old	M/F
rtTenocytes(TU)	Rat tenocytes isolated from 8 week old Sprague-Dawley rats	Tsinghua University Small Animal Facility	8 Weeks Old	M/F
rtTenocytes(SU)	Rat tenocytes isolated from 8 week old Sprague-Dawley rats	Sichuan University Small Animal Facility	8 Weeks Old	M/F
rtMSC(SU)	Rat mesenchymal stem cells isolated from bone marrow aspirates	Sichuan University Small Animal Facility	8 Weeks Old	M/F

Table 0.1 Cell lines

The following materials were used in cell culture unless otherwise stated (Table 3.2)

Material	Details
DMEM	Dulbeccos Modified Eagles media (4.5g/L glucose) (12-604F, Lonza, UK)
FBS	Foetal Bovine Serum (12-501F, Lonza, UK)
bFGF	basic Fibroblast Growth Factor (FGF-2) (100-18B, Peprotech, UK)
BMP-12	Bone Morphogenic Protein -12 (recombinant mouse GDF-7,CF, R5240 A572, R &D Systems, UK)
BMP-13	Bone Morphogenic Protein-13/CDMP-2 (120-04, Peprotech, UK)
FGF-4	Fibroblast Growth Factor -4 (100-31, Peprotech, UK)
Dorsomorphin	6-(4-(2-Piperidin-1-ylethoxy)phenyl]-3-pyridin-4-ylpyrazolo[1,5-a)pyrimidine (P5499-5mg, Sigma-Aldrich, UK)
FGF-6	Fibroblast Growth Factor -6 (100-30, Peprotech, UK)
FGF-8	Fibroblast Growth Factor -8 (100-25, Peprotech, UK)
NEAA	Non-Essential Amino Acids (13-114E, Lonza, UK)
L-Glut	L-Glutamine (17-605E, Lonza, UK)
PSA	Penicillin, Streptomycin and AmphotericinB (15240112, Invitrogen, UK)
Typsin	Trypsin/EDTA Solution (CC-5012, Lonza, UK)
KO DMEM	Knockout DMEM (03382, Gbico, UK)
Matrigel™	354277, SLS, UK
Fibronectin	F0895, Sigma Aldrich, UK
SR	Serum Replacement (10828-028, Gibco, UK)
DMSO	Dimethyl Sulphoxide (R00550, Invitrogen,UK)
PBS	Phosphate Buffered Saline (17-516F, Lonza, UK)
BME	β-Mercaptoethanol (31350010, GIBCO, UK)
ASC	L-Ascorbic Acid (A4403-100MG, Sigma-Ardich, UK)
T-25	Corning 25cm^2 tissue culture flask 430639 (43021, SLS, UK)
T-75	Corning 75cm^2 tissue culture flask 4306 (354639, SLS, UK)
6 well plates	Costar 3516 (SLS, UK)
96 well Plates	Costar 96 (SLS, UK)
Centrifuge tube 15ml	SLS8002 (SLS, UK)
Centrifuge tube 50ml	SLS8110 (SLS, UK)
IMS	Industrial Methylated Spirit (64-17-5, Genta Medical, UK)
PFA	Paraformaldehyde (P6418, Sigma-Aldrich, UK)
BSC	Biological Safety Cabinet Class II (W05318, Envair, UK)

Table 0.2 General cell Culture Consumables

3.2.1 Mouse Embryonic Fibroblast

3.2.1.1 Mouse Embryonic Fibroblast Harvest

Mouse embryonic fibroblasts were harvested from 12.5 – 13.5 days pregnant black CB1 hybrid mice. The hybrid mice were sacrificed and the embryos were harvested and eight to ten embryos collected from each pair of uteri. Post collection the Viscera and head were identified and removed from the embryos using aseptic techniques by Keele University animal house staff. The resulting embryos were then placed in PBS containing 1% PSA and transferred to ISTM facilities at the Guy Hilton Research Centre.

Once at the Guy Hilton research centre, the embryos were then washed three times in 1% PSA containing PBS to remove remaining fragments of the viscera and blood clots. Embryo fibroblasts were then isolated from the embryos by placing 5 embryos into a 7ml Bijou bottle containing 5ml of trypsin/EDTA.

Trypsinised embryos were then vortexed twice at 5 minute intervals during the incubation process. Post incubation, cell supernatants were collected and re-suspended in 10ml of DMEM supplemented with 10% FBS, 1% L-Glutamine, 1% NEAA and 1% PSA in 15ml centrifuge tubes. The cell suspensions were then centrifuged at 200g for 3 minutes. The supernatants were discarded and the cell pellets re-suspended in 10ml of DMEM media mentioned above. 2 ml of MEFs cell suspension was then seeded into T75 culture flasks in 18 ml of media and incubated at 37^{o}C in the presence of 5% CO_2 and 95% air in a humidified cell culture incubator. 24 hours later the media was replaced with antibiotic-free complete culture media, with media changes twice weekly until the MEFs became confluent.

3.2.1.2 Mouse Embryonic Fibroblast Cryopreservation

After isolation from the mouse embryo and post expansion, MEF at passage 1 were cryopreserved for future use. Confluent T-75 flasks of MEF were harvested by aspirating the culture media from the T-75 and washing twice with 10ml PBS. Once the PBS was aspirated from the T-75, 3ml of 1% trypsin/PBS solution was added to disassociate the cells from the culture plastic. Once the cells had disassociated from the T-75 flask, 3ml of MEFs culture media was added to the trypsin-cell suspension to quench the effects of trypsin. The media-cell-trypsin suspension was then placed into a 15ml centrifuge tube and centrifuged for 3 minutes at 200g. After 3 minutes had elapsed the media- trypsin solution was aspirated from the centrifuge tube to leave a cell pellet. The cell pellet was then re-suspended in 1ml of 90% FBS and 10% DMSO at room temperature. The DMSO-FBS-cell suspension was then placed into a 1.5ml cryovial and placed in a 'Mr Frosty' (C1562 Sigma Aldrich, UK) and placed into a -80^{o}C freezer for 24hrs.. After 24hrs had elapsed the cryovial was then transferred into liquid nitrogen.

3.2.1.3 Mouse Embryonic Fibroblast Expansion

Mouse embryonic fibroblast cells (MEF) were cultured in T-75 culture flasks in MEF media (DMEM, 10% FBS, 1% NEAA and 1% L-glutamine) with a media change twice weekly until confluent. Once confluent MEFs were washed twice with PBS, the PBS aspirated from the T-75 and 3ml of 1% trypsin/PBS solution was added to disassociate the cells from the culture plastic. Once the cells had disassociated from the T-75 flask, 3ml of MEFs culture media was added to the trypsin-cell suspension to quench the effects of trypsin. The media-cell-trypsin suspension was then placed into a 15ml centrifuge tube and centrifuged for 3 minutes at 200g. After 3 minutes had elapsed the media-cell-trypsin was

aspirated from the centrifuge tube to leave a cell pellet. The cell pellet was then re-suspended in 5ml of MEFs media and 1ml of the cell suspension was added to five, T-75 with a further 14ml of MEF media added. MEFS were then cultured with a twice weekly media change until 50 -60 % confluent.

3.2.1.4 Mouse Embryonic Fibroblast Preparation of Conditioning Media for use with Embryonic Stem Cells

Once the MEFs reached 50-60% confluent the T-75 flasks were washed twice with PBS and media changed to Conditioning Media (KO-DMEM, 20% SR, 1% NEAA, 1% L-Glut, 4ng/ml bFGF (1µl per ml) and 910µl BME for 24hrs. After 24hrs media was removed and 4ng/ml FGF-2 was added prior to filtration using Millipore Express^{TM} Plus 0.22µm vacuum filter. The filtered media (CM+) is then ready for use for the culture of hESC.

3.2.2 Human Embryonic Stem Cell Culture

3.2.2.1 Matrigel Coating of T-25 Culture Flasks

Culture surfaces of T-25 tissue culture flasks were coated with 1:100 diluted ice cold KO-DMEM. Coating was undertaken by adding 4ml matrigel/KO-DMEM solution to each T25 flask (160µl/cm2) and incubated at room temperature for 2 hours. Before use, matrigel containing flasks were incubated at 37^{0}C for 30 minutes in the incubator, after incubation the matrigel media was discarded and hESC culture media was added. Prepared matrigel coated culture flasks were stored at 4^{0}C for later use.

3.2.2.2 Human Embryonic Stem Cell Expansion

SHEF-1 embryonic stem cells were then cultured on matrigel-coated T-25 culture flasks in conditioned media (CM^{+}) changed every 24hrs. Once confluent the media was aspirated

from the T-25 and subsequently washed with PBS. After washing 1% Trypsin/PBS solution was added to induce cell detachment. Once the cells had detached the trypsin was quenched with 1ml of CM+ media. The cell suspension was then pipetted into a centrifuge tube, centrifuged (200g, 2 minutes), media aspirated and cell pellet re-suspended in 1ml CM^+ and 500ul pipetted into 2 x T-25 flasks.

3.2.2.3 Human Embryonic Stem Cell Cryopreservation

80-90% confluent T-25 flasks of hESC were harvested by aspirating the culture media from the T-25 and washing twice with 3ml PBS. Once the PBS was aspirated from the T-25, 1ml of 1% trypsin/PBS solution was added to disassociate the cells from the culture plastic. Once the cells had disassociated from the T-25 flask, 1ml of CM+ culture media was added to the trypsin-cell suspension to quench the effects of trypsin. The media-cell-trypsin suspension was then placed into a 15ml centrifuge tube and centrifuged for 3 minutes at 200g. After 3 minutes had elapsed, the media –trypsin solution was aspirated from the centrifuge tube to leave a cell pellet. The cell pellet was then re-suspended in 1ml of 90% SR and 10% DMSO at room temperature. The DMSO-SR-cell suspension was then placed into a 1.5ml cryovial and placed in a 'Mr Frosty' (C1562 Sigma Aldrich, UK) and placed into a -80^{o}C freezer for 24hrs. After 24hrs had elapsed the cryovial was then transferred into liquid nitrogen.

3.2.3 hESC BMP- Driven *in vitro* Differentiation

Sub-confluent (80-90%) T-25 of hESC were trypsinised, centrifuged (200g, 3 minutes), re-suspended and distributed evenly across matrigel-coated 6-well plates and 2 ml of CM+ media added to each well. The following day the CM^+ media was aspirated from each of the six wells and differentiation media (DMEM, 10% FBS, 1% NEAA and 1% L-Glut)

supplemented with 10ng/ml BMP-12, 10ng/ml BMP-13 and 10mM ASC. Media was replenished twice weekly and RNA lysates collected or cells fixed for immunocytochemistry or histology at multiple time points (Days 0, 1, 5, 10, 20 and 40).

3.2.4 hESC FGF-Driven *in vitro* Differentiation

Sub-confluent (80-90%) T-25 of hESC were trypsinised, centrifuged (200g, 3 minutes), re-suspended and distributed evenly across matrigel-coated 6-well plates and 2ml of CM+ was added. The following day the CM^{+} was aspirated from the wells and differentiation media (DMEM, 10% FBS, 1% NEAA and 1% L-Glut) supplemented with either FGF4 +/- 10mM Ascorbic acid, FGF6 +/- 10mM ASC, or FGF8 +/- 10mM Ascorbic acid. Growth factors were supplemented to final concentrations of 0, 20, and 50ng/ml. Media was replaced with fresh twice weekly and RNA lysates collected or cells fixed for immunocytochemistry or histology at multiple time points (Days 0, 1, 5, 10, 20 and 40).

3.2.5 Human Mesenchymal Stem Cells

3.2.5.1 Fibronectin Coating of Tissue Culture Flasks

10ml of 10ng/ml fibronectin/PBS solution was added to each T-75 tissue culture flask and incubated at room temperature for 2 hours. Prior to use the fibronectin solution was aspirated from the T-75 tissue culture flasks.

3.2.5.2 Human Mesenchymal Stem Cell Isolation

hMSCs were isolated and expanded from human bone marrow aspirates (BMA) using the plastic adherent technique following the previously published protocols [332, 333]. The whole bone marrow was seeded at a density of 1 x 10^5 mononuclear cells/cm^2 on fibronectin coated T-75 flasks in 20ml of DMEM supplemented with 10% FBS, 1% NEAA,

1% L-glut and 1% PSA. The whole bone marrow containing non-adherent (mononuclear cells) and adherent (MSC) were maintained in a continuous co-culture for three weeks in a humidified incubator at 37^{o}C in the presence of either 2% O_2 or 21% O_2. After seven days of culture 50% of the DMEM supplemented with 10% FBS, 1% NEAA, 1% L-glut and 1% PSA was aspirated from the T-75 flask and replenished with DMEM supplemented with 5% FBS, 1% NEAA, 1% L-glut and 1% PSA media (10ml). After 14 days, a complete media change was undertaken, the 20ml of media was aspirated and the T-75 tissue culture flask was rinsed once with PBS and 20ml of fresh DMEM media supplemented with 5% FBS, 1% NEAA, 1% L-glut and 1% PSA was added to the T-75 tissue culture flask. After, three weeks the adherent hMSC populations were either cryopreserved.

3.2.5.3 Human Mesenchymal Stem Cell Expansion

hMSC were cultured in T-75 culture flasks in hMSC media (DMEM, 5% FBS, 1% NEAA and 1% L-glutamine) with a media change twice weekly until confluent. Once confluent hMSC were washed twice with PBS, the PBS aspirated from the T-75 and 3ml of 1% trypsin/PBS solution was added to disassociate the cells from the culture plastic. Once the cells had disassociated from the T-75 flask, 3ml of hMSC culture media was added to the trypsin-cell suspension to quench the effects of trypsin. The media-cell-trypsin suspension was then placed into a 15ml centrifuge tube and centrifuged for 3 minutes at 200g. After 3 minutes had elapsed the media-cell-trypsin was aspirated from the centrifuge tube to leave a cell pellet. The cell pellet was then re-suspended in 2ml of hMSC media and 1ml of the cell suspension was added to two, T-75 with a further 14ml of hMSC media added. hMSC were then cultured with a twice weekly media change until confluent.

3.2.5.4Human Mesenchymal Stem Cell Cryopreservation

After isolation from the Bone marrow aspirate a substantial number of hMSC cultured at 2% and 21% O_2 at passage 1 were cryopreserved for future use. Confluent T-75 flasks of hMSCs were harvested by aspirating the culture media from the T-75 and washing twice with 10ml PBS. Once the PBS was aspirated from the T-75, 3ml of 1% trypsin/PBS solution was added to disassociate the cells from the culture plastic. Once the cells had disassociated from the T-75 flask, 3ml of hMSC culture media was added to the trypsin-cell suspension to quench the effects of trypsin. The media-cell-trypsin suspension was then placed into a 15ml centrifuge tube and centrifuged for 3 minutes at 200g. After 3 minutes had elapsed the media- trypsin solution was aspirated from the centrifuge tube to leave a cell pellet. The cell pellet was then re-suspended in 1ml of 90% FBS and 10% DMSO at room temperature. The DMSO-FBS-cell suspension was then placed into a 1.5ml cryovial and placed in a 'Mr Frosty' (C1562 Sigma Aldrich, UK) and placed into a -80^{o}C freezer for 24hrs.. After 24hrs had elapsed the cryovial was then transferred into liquid nitrogen.

3.2.6 hMSC FGF-Driven *in vitro* Differentiation

Sub-confluent (80-90%) T-75s of hMSC were trypsinised, centrifuged (200g, 3 minutes), re-suspended and distributed evenly across Fibronectin-coated 6-well plates and 2ml of hMSC media was added. The following day the hMSC was aspirated from the wells and differentiation media (DMEM, 10% FBS, 1% NEAA and 1% L-Glut) supplemented with either FGF4 +/- 10mM ASC, FGF6 +/- 10mM Ascorbic acid, or FGF8 +/- 10mM ASC. Growth factors were supplemented to final concentrations of 0, 20, and 50ng/ml. Media was

replaced with fresh twice weekly and RNA lysates collected or cells fixed for immunocytochemistry or histology at multiple time points (Days 0, 1, 5, 10, 20 and 40).

3.2.7 Dorsomorphin Supplementation Optimisation

Dorsomorphin was reconstituted to a concentration of 10mM using 1.25ml DMSO. 750ul of stock solution was added to 15ml of differentiation) to produce a secondary stock solution of 500ug/ml. Subsequent serial dilutions were undertaken to produce experimental concentrations of 500 µM/ml, 200 µM/ul, 100 µM/ml, 10 µM/ml and 1 µM/ml. hESC (hMSC in the absence of Matrigel™) were seeded at a density of $3x10^5$ cells per well and cultured on matrigel™ coated 6 well plate. hESC (hMSC in the absence of Matrigel™) C were cultured for 7 days with a media change being undertaken after 3 days. On day 7 the wells were fixed using 95% methanol (Sigma) and Giemsa's staining was undertaken to evaluate cell survival.

3.2.7.1hESC Growth Factor Inhibition by Dorsomorphin

hESC were seeded at a density of $3x10^5$ cells per well and cultured on matrigel™ coated 6 well plate. hESC were cultured for 40 days with differentiation media (10% FBS, 1% L-glutamine, 1% NEAAand 10mM ASC) which was supplemented with 10ng/ml BMP-12/BMP-13 and 1µM Dorsomorphin or 50ng/ml of FGF-4 and 1µM Dorsomorphin, 50ng/mL of the combination of FGF-4 & FGF-8 and 1µM Dorsomorphin or FGF-4, FGF-6 & FGF-8 and 1µM Dorsomorphin) and cultured at 2% O_2 environment. Cell lysates were collected at time points: Day 0, Day 2, Day 5, Day 10, Day 20 and Day 40 along with cells being fixed at the same time points for immunocytochemistry.

3.2.7.2hMSC Growth Factor Inhibition by Dorsomorphin

hMSC were seeded at a density of 6 x 10^5 cells per well and cultured on fibronectin coated 6 well plate. hMSC were cultured for 40 days with differentiation media (10% FBS, 1% L-glutamine, 1% NEAA and 10mM ASC) which was supplemented with 50ng/mL of the combination of FGF-4 & FGF-8 and 1µM Dorsomorphin or FGF-4, FGF-6 & FGF-8 and 1µM Dorsomorphin and cultured at 2% O_2 environment. Cell lysates were collected at time points: Day 0, Day 2, Day 5, Day 10, Day 20 and Day 40 along with cells being fixed at the same time points for immunocytochemistry.

3.2.8 Rat Tenocyte Harvest and Culture

Please refer to previous sections 2.2.7.1 – 2.2.7.3

3.3 Ribonucleic Acid Extraction and Processing

Listed below are the materials used for RNA extraction:

Reagent/Kit	Supplier
QIA Shredder	79654, Qiagen, UK
RNesay minikit	74104, Qiagen, UK
Superscript III one-step hi-fi RTPCR	12574030, Invitrogen, UK
RNAse ZAP	R2020-250ml, Sigma Aldrich, UK
β-mercaptoethanol	3150010, Invitrogen, UK
Ethidium Bromide Solution	E1510-10ML, Sigma Aldrich, UK
Agarose (High resolution electrophoresis quality) molecular biology grade	A4718, Sigma Aldrich, UK
Directload Wide Range DNA marker	D7058, Sigma Aldrich, UK
Gel loading Solution	G2526-5ml, Sigma Aldrich, UK
50x TAE	B9-0030, Geneflow, UK

Table 0.3 Molecular Biology Reagents

3.3.1 Cell Lysis and RNA Extraction

RNA lysates were obtained by aspiration of media from the 6 wells followed by a PBS wash, followed by the addition 700µl of lysis buffer (contained in the RNEasy kit) to the well and samples scraped using a well scraper to encourage detachment of the cells from the well. The lysis buffer-cell suspension was then transferred in to a QIAshredder spin column, which was placed into a collection tube. The column/ collection tube was then centrifuged for 2 minutes at 16000g. After 2 minutes the shredder column was removed and the collection tube capped and stored at -80^{o}C until RNA extraction could be undertaken.

RNA was extracted using the RNeasy kit (Qiagen). Samples were retrieved from the -80^{o}C and thawed at room temperature. Once thawed, 350µl of 70% ethanol (EtOH) was added to the eppendorff containing the lysed sample and mixed well by pipetting. The sample was then decanted into a spin column which sits on a 2ml collection tube. The collection tube/column was then centrifuged at 9000g for 15 seconds and the flow-through was discarded. 700µl of buffer RW1 (supplied as part of the Qiagen RNeasy Kit) was placed into the RNeasy spin mini column; this was then centrifuged for 15 seconds at 9000g and the flow-through was discarded. 500µl of RPE buffer was then added (supplied as part of the Qiagen RNeasy Kit) to the RNeasy spin column and centrifuged for 15 seconds at 9000g discarding the flow-through and repeated. The spin column was then placed into a new collection tube and centrifuged at 9000g for 2 minutes to remove excess EtOH. The RNeasy mini spin column was then placed into a new 1.5ml collection tube and 15µl of RNase-free water added and left to stand for 3 minutes prior to being centrifuged on full power for 1 minute at 9000g. The flow through was then pipetted directly back onto the RNeasy mini column and allowed to stand for a further 3 minutes and then centrifuged at full power for 1 minute at 9000g. The RNeasy mini spin column was then discarded and the flow through retained for quantification and subsequent gene expression analysis. Samples were frozen at -80^{o}C until analysis could be undertaken.

3.3.2 Quantitative Analysis of RNA Extraction

After RNA extraction quantitative analysis of the RNA sample was performed using Nanodrop (ND-200) spectrophotometer to enable correct RNA sample concentration for RT-PCR (30ng/µl).Briefly 1µl of RNA sample was loaded onto the pedestal analysis stand and read using the RNA quantification tool as part of the ND-2000 software. RNA

concentration (ng/ml), 260/280 260/230 measurements were recorded. Pre and post sample analysis the Nanodrop pedestal was cleaned before each sample run (all samples were kept on ice whilst RNA quantitative analysis was performed).

The following calculation was applied to each reading to calculate the dilution of RNA samples to the 30ng/µl required for RT-PCR.

The following calculation was applied to each reading to calculate the dilution of RNA samples to the 5ng/µl required for RT-PCR (Figure 3.1).

1. Desired RNA = (sample reading)/5 = ***X***

2. Dilution = 1*y + (1*y)*(***X***)

Where y= volume of RNA

Figure 0.1 RNA Dilution Calculation

3.3.3 Reverse Transcription Polymerase Chain Reaction

The PCR reaction solution: were set up as below:

Chemical	**Sample Mix** **Volume**	**Blank Mix** **Volume**
Reaction Mix	6.75µl	6.75 µl
RNA free H_2O	2.5 µl	2.5 µl
Forward Primer	1 µl	1 µl
Reverse Primer	1 µl	1 µl
Enzyme	0.25 µl	0.25 µl
Sample	1 µl	0 µl
RNA free H_2O	0 µl	1 µl

Table 0.4 PCR Reaction Mix Volumes

3.3.4 Primer Sequences Design

The primers for this thesis were designed using human gene sequences from NCBI Map Viewer or Ensemble Genome Browser and Primer 3. Designed primers were evaluated in NCBI Primer-BLAST to check binding specificity. Customised primer sets were purchased from Invitrogen, UK. Primers are show below (Table 3.5). RT-PCR was performed with a one-step protocol.

Gene		Primer (5' - 3')	Annealing Temp (°C)	Amplicon Size (bp)
POU5F1 (Oct-4)	F	GCAATTTGCCAAGCTCCTGAAGCAG	55	536
	R	CATAGCCTGGGGTACCAAAATGGGG		
NANOG (Nanog)	F	GGTGGCAGAAAAACAACTGGC	55	300
	R	TGCAGGACTGCAGAGATTC		
TERT (hTERT)	F	GCAGCTCCCATTTCATCAGC	53	343
	R	CAGGATGGTCTTGAAGTCTG		
COL1A2(Collagen 1)	F	GACTTTGTTGCTGCTTGC	50	242
	R	CAAGTCCAACTCCTTTTCC		
COL3A1 (Collagen 3)	F	AAGGACACAGAGGCTTCG	51	210
	R	CTGGTTGACCATCAATGC		
TNMD (Tenomodulin)	F	GCACTGATGAAACATTGG	47	274
	R	ATCCAATACATGGTCAGG		
THBS-4 (Thrombospondin-4)	F	CCCCAGGTCTTTGACCTTCTCCC	59	245
	R	ACCTTCCCATCGTTCTTCAGGT		
TENC (Tenascin C)	F	AAGAGCATTCCTGTCAGC	50	217
	R	CAGTTTGCCGGTAAGAGG		
DCN (Decorin)	F	CTGCTTGCACAAGTTTCC	48	372
	R	TTCCAACTTCACCAAAGG		
ACTB (β-actin)	F	GCCACGGCTGCTTCCAGC	55	504
	R	AGGGTGTAACGCAACTAAGTC		

Table 0.5 Table of Primers sequences, annealing temperatures and amplicon size

3.3.5 Thermocycler Set Up

The gene amplification were run on the DNA Engine thermal cycler (PTE-200) the table below shows the cycle temperature, time and number of cycles used in the amplification of the specific genes shown in Table 3.6.

Sub Cycle	Temperature	Time	Number of Cycles
cDNA Synthesis and	50°C	30 mins	1
pre-denaturing	94°C	2 mins	1
Denaturing	94°C	15 secs	40 Cycles
Anneal	Gene Specific *	30 secs	
Extend	68°C	30 secs	
Extend	68°C	5 mins	1
* Gene specific temperature for annealing			

Table 0.6 PCR Thermal Cycler gene amplification Reagent Set up

The PCR reaction tubes are set up using 1µl of sample to be amplified along with 11.5µl of the reaction mix (including enzyme, gene specific primers and reaction mix). The reaction tubes are then capped and placed in the thermal cycler for the PCR reaction to be initiated.

Once the PCR reaction is complete the reaction tubes are removed from the thermal cycler and 2µl of gel loading solution using a fresh pipette tip for each of the samples.

3.3.6 Agarose Gel

The agarose gel was prepared 1 hour prior to the electrophoresis run by adding 2g agarose (electrophoresis quality) to 1 x TAE (20ml 50xTAE buffer is added to 980ml of dH_2O to get a working concentration of 1 x TAE buffer. This was heated using a laboratory microwave set to full power until the agarose was fully dissolved and the solution was completely clear. Once the agarose was dissolved 5µl of Ethidium bromide solution was added, and the solution poured into the gel mould and allowed to set with a gel comb in place for 45mins to allow the gel to set.

3.3.7 Electrophoresis

The gel was removed from the mould and placed in the electrophoresis tank containing excess 1 x TAE buffer ensuring the buffer completely covers the gel to a depth of around 5mm. The comb was removed from the gel and the wide range ladder loaded into the first well and samples are loaded in all other wells allowing for a blank and second wide range ladder to be placed in the final 2 wells. Samples and blanks were loaded at a volume of 6µl per well with fresh pipette tips for each sample and blank. The wide range ladders were loaded at a volume of 5µl. The electrophoresis tank was then connected to the Biorad Powerpac 300 (92Volts/400mAMPS/37W) and allowed to run for 45 minutes.

3.3.8 Gel Imaging

After the allotted 45 minutes for electrophoresis the power pack was switched off and the gel removed from the tank. Gels were imaged on the Syngene Gel UV illuminator and focused using Genimage™ software. Once the gel was focused the image was printed and saved.

3.4 Immunocytochemistry

3.4.1 hMSC (BMA-12) Characterisation

hMSC (P-1) were seeded at a density of 5 x 10^4 cells to each well of a 24 well plate and cultured until 80-90% confluent prior to immunophenotyping. Once 80-90% confluency was achieved each well was fixed with 4% PFA for 5 minutes. After 30 mins had elapsed the PFA was aspirated from each well and each well was subsequently washed twice with 2mL of PBS before adding 0.5% Triton-X 100 for 5 mins to induce membrane permeability. After 5 mins had elapsed the 0.5% Triton X 100 was aspirated from the wells and the wells washed twice with PBS. After which, 3% BSA and allowed to stand for 1 hour at room temperature to block non-specific antibody binding. After 1 hour had elapsed each well was washed twice with PBS and cells were characterised using human MSC characterisation kit which contained anti-human mouse anti-CD-44, anti-CD90, anti-CD146, anti-CD14 and anti-STRO-1 primary antibodies at 1:500 dilutions (Cat. No. SCR067, Millipore). Cells were then incubated at 4^{o}C overnight. Secondary antibodies used were anti-mouse IgG-NL557 for anti-human mouse anti-CD-44, anti-CD90, anti-CD146 and anti-CD14, with anti-mouse IgM-NL493 for STRO-1(both sets of secondary antibodies dilutions of 1:200. DAPI was used at a dilution of 1:500 as a nuclear stain. Once staining was complete the samples were immediately imaged using a fluorescent microscope (Nikon Eclipse Ti-ST, Japan).

3.4.2 hESC (SHEF-1) Characterisation

SHEF-1 (hESC (P-37)) were seeded at a density of 2.5 x 10^4 cells to each well of a 48 well plate and cultured to 80-90% confluency prior to immunophenotyping. Once 70-80% confluency was achieved each well was fixed with 4% PFA for 5 minutes. After 30 mins had elapsed the PFA was aspirated from each well and each well was subsequently washed twice with 2mL of PBS (Lonza, Belgium) before adding 0.5% Triton-X 100 for 5 mins to induce membrane permeability. After 5 mins had elapsed the 0.5% Triton X 100 was aspirated from the wells and the wells washed twice with PBS. After which, 3% BSA and allowed to stand for 1 hour at room temperature to block non-specific antibody binding. After 1 hour had elapsed each well was washed twice with PBS and cells were characterised using "human embryonic stem cell marker antibody panel" kit which contained anti-human mouse anti-alkaline phosphatase (ALP), goat anti-OCT-4, goat anti-Nanog, mouse anti-SSEA-1 and mouse anti-SSEA-4 primary antibodies at 1µg/100µL concentration (each well was covered with 150µL) (Cat. No. SC008, R&D systems). Cells were then incubated at 4^{o}C overnight. Secondary antibodies used were anti-goat IgG-NL493 (1:200, Northern Lights, R & D Systems) for OCT-4 and Nanog. TRITC-conjugated anti mouse IgG (1:200, ab6787, Abcam) was used for ALP and SSEA-4. DAPI was used at a dilution of 1:500 as a nuclear stain. Once staining was complete the samples were immediately imaged using a fluorescent microscope (Nikon Eclipse Ti-ST, Japan).

3.4.3 Tenomodulin Staining

PBS was aspirated and the wells were washed twice using fresh PBS (Lonza). After washing, 1ml of 0.5% triton X 100 (Sigma) was added to each well for 5 minutes to permeate the cell membrane. After the 5 minutes had elapsed, the triton X 100 was aspirated and the wells washed twice with PBS. Once washed, the PBS was aspirated and each well was covered with 500µl of 3% Albumin (A8806, Sigma Aldrich, UK)/PBS solution for 1 hour at room temperature then washed twice with PBS. After washing, 500µl of Primary tenomodulin antibody (SC98875, Santa Cruz Biotechnologies, Germany, 1:500 dilution in PBS) was added to each well and left overnight at 4^{o}C. The next day the primary antibody was aspirated off and each well washed twice with PBS (and the secondary (detection) antibody was added (SC2090 Santa Cruz Biotechnologies, Germany, 1:500 dilution in PBS) and left for 1 hour at room temperature. After 1 hour had elapsed, the secondary antibody was aspirated off and each well washed twice with PBS (Lonza) and 500ul of 4', 6-diamidoino-2-phenylindole (DAPI) (D9542 Sigma Aldrich, UK) (1:500 dilution.) and left for 5 minutes room temperature. After 5 minutes had elapsed the DAPI solution was aspirated and then each well was washed twice with PBS and imaged immediately on the Nikon Eclipse T1 microscope.

3.5 Histological Staining

3.5.1 Giemsa's Staining

Cells were fixed using 95% EtOH and then washed twice with PBS. After wash 750µl of Giemsa's stain was placed into each well and placed for 2 hours on a motorised rocker. After 2 hours had elapsed the Giemsa's stain was aspirated off and each well was washed with PBS until clear. The 6 well plates where then allowed to dry overnight before imaging.

3.5.2 Alcian Blue Staining

PBS was aspirated from the wells and then 50µl of Alcian Blue stain (A3157-10G, Sigma Aldrich, UK) was placed into each well and kept at room temperature for 24hrs on an R100 Rotateck shaker (Luckham) to maximise stain uptake.

After 24hrs had elapsed the Alcian Blue stain was aspirated off each well and each well washed with 150µl of sterile double filtered H_2O until excess Alcian Blue stain was removed (if required, a third wash with sterile double filtered H_2O was performed). Once all the excess Alcian Blue stain was removed the plates were left for 24hrs to dry before imaging and image analysis was performed using Image J.

3.5.3 Masson's Trichrome Staining

PBS was aspirated from the wells and then 50µl of Bouins Solution (Sigma Aldrich HT15-1KT) to completely cover the cells at the case of the wells and placed on the R100 Rotateck shaker (Luckham) for 24hrs to maximise stain uptake.

After 24hrs had elapsed the Bouins solution was aspirated from all the wells and each well was washed with 150µl of double filtered H_2O (multiple washes if required) as to

remove the residual Bouins solution. The wells were then counterstained with 50µl Haematoxylin (Sigma HT15-1KT). After 5mins had elapsed the Haematoxylin was aspirated from the wells which were then washed with 150µl of double filtered H_2O (multiple washes if required) to remove excess residual red colour. The wells were then stained with 50µl of Biebrich Scarlet-Acid Fuschin solution (Sigma Aldrich HT15-1KT) and allowed to stand at room temperature for 5 mins.

After 5 mins had elapsed the Biebrich Scarlet-Acid Fuschin solution was aspirated from the wells and the wells washed with 150µl of double filtered H_2O (multiple washes if required). The wells were then stained with 50µl of Phosphotugstic/Phosphomolybdic Acid solution (Sigma HT15-1KT freshly constituted by adding 25% ($^{v}/_{v}$) Phosphotungstic Acid, 25% ($^{v}/_{v}$) Phosphomolybdic Acid and 50% ($^{v}/_{v}$) dH_2O) and allowed to stand for 5 mins. After 5 mins had elapsed the Phosphotugstic/Phosphomolybdic Acid solution was aspirated from the wells and 50µl of Aniline Blue Solution (Sigma HT15-1KT) was added to cover the base of the wells and allowed to stand at room temperature for 5 mins.

After a further 5 mins had elapsed the Aniline Blue solution was aspirated from the wells and 50µl of 1% Acetic Acid (8.8ml of 1M Acetic (Ethanoic) Acid was added to 41.2ml of dH_2O) and allowed to stand for 2 minutes. After an additional 2 mins had elapsed the 1% Acetic acid was aspirated from the wells and the wells were washed with 150µl double filtered H_2O. The H_2O was then aspirated for the wells and the 96 well-plate was allowed to stand and dry for 24hrs, prior to imaging.

3.5.4 Image Analysis

After air drying (24 hrs) the individual wells were imaged using X4 magnification on a Nikon Eclipse TD100 inverted microscope. Once the cells/colony had been located an

image was taken using a Canon EOS400D digital camera and saved as a TIF file, this process was repeated for all wells stained with Alcian Blue and Masson's Trichrome.

3.5.5 Image J Software Set-up

Image J software was obtained as a free download and for Alcian Blue analysis the following settings were used to extract colour analysis which were part of the analysis pack.

COLOUR	SETTING
Red	**0.6371708**
Green	**07683354**
Blue	**0.06061394**

Table 0.7 Colour Settings for Alcian Blue Data Analysis

To Undertake Alcian blue analysis we open the image J software package and choose the image to be analysed (Figure 3.2A). Once the image opens, we then choose Plugin, analyse and then Alcian blue (Figure .2B). From the choices made 4 small windows will open we close the windows named "Colour 3" and "Colour 2" (Figure 3.2C). We then choose the window "Colour 1" and select measure which will produce a table window containing the data (Figure 3.2D). This data is then transferred to Excel for future analysis. this process is utilised for all Alcian Blue Images.

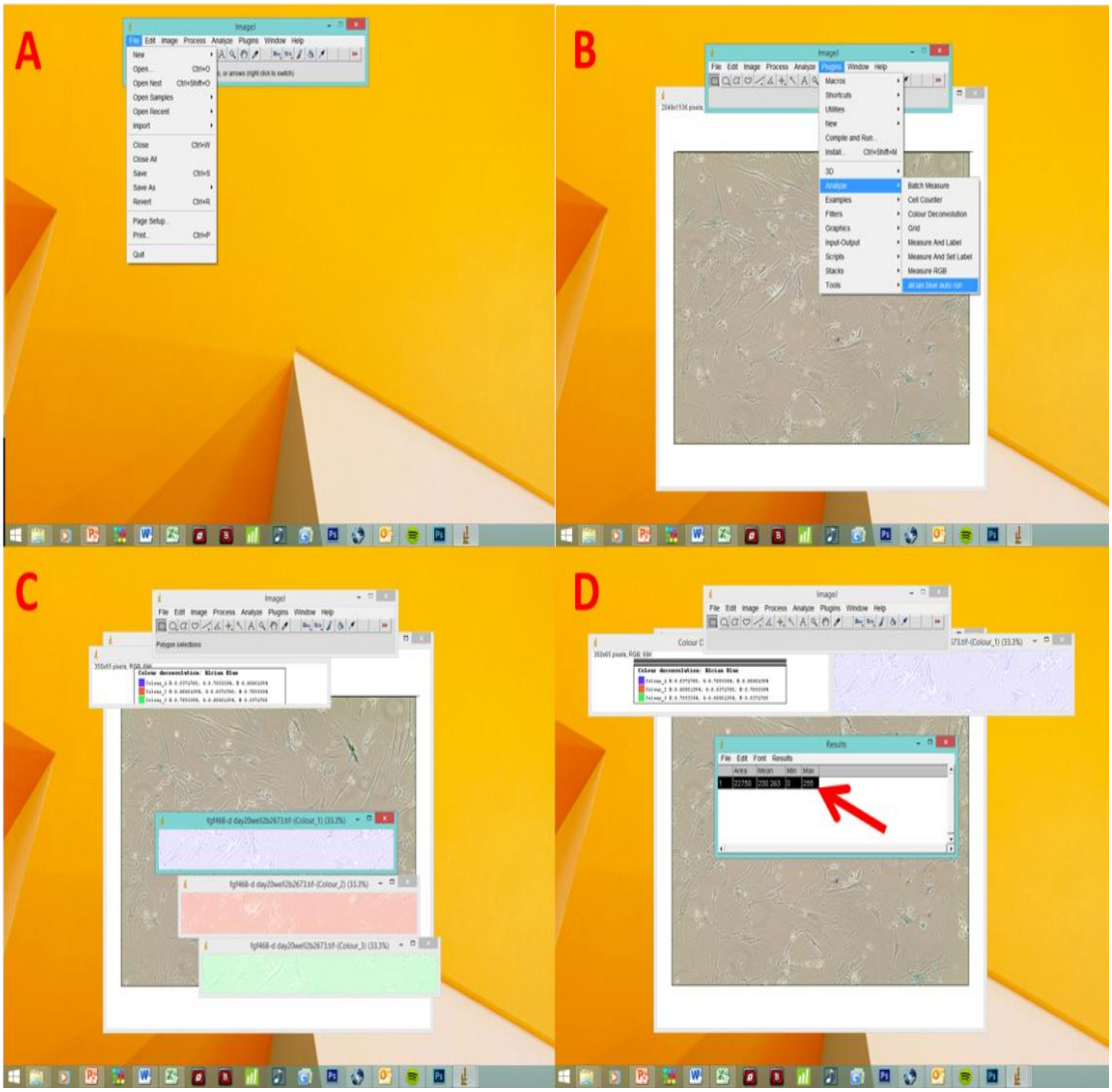

Figure 0.2 Image J Alcian Blue Analysis set up

For Masson's Trichrome Analysis the following Macro was used:

To Undertake Masson's Trichrome analysis we open the image J software package and choose the image to be analysed (Figure 3.3A). Once the image opens (Figure .3.3), we then choose measure which will produce a table window containing the data (Figure 3.3C). This data is then transferred to Excel for future analysis. This process is utilised for all Masson's Trichrome Images.

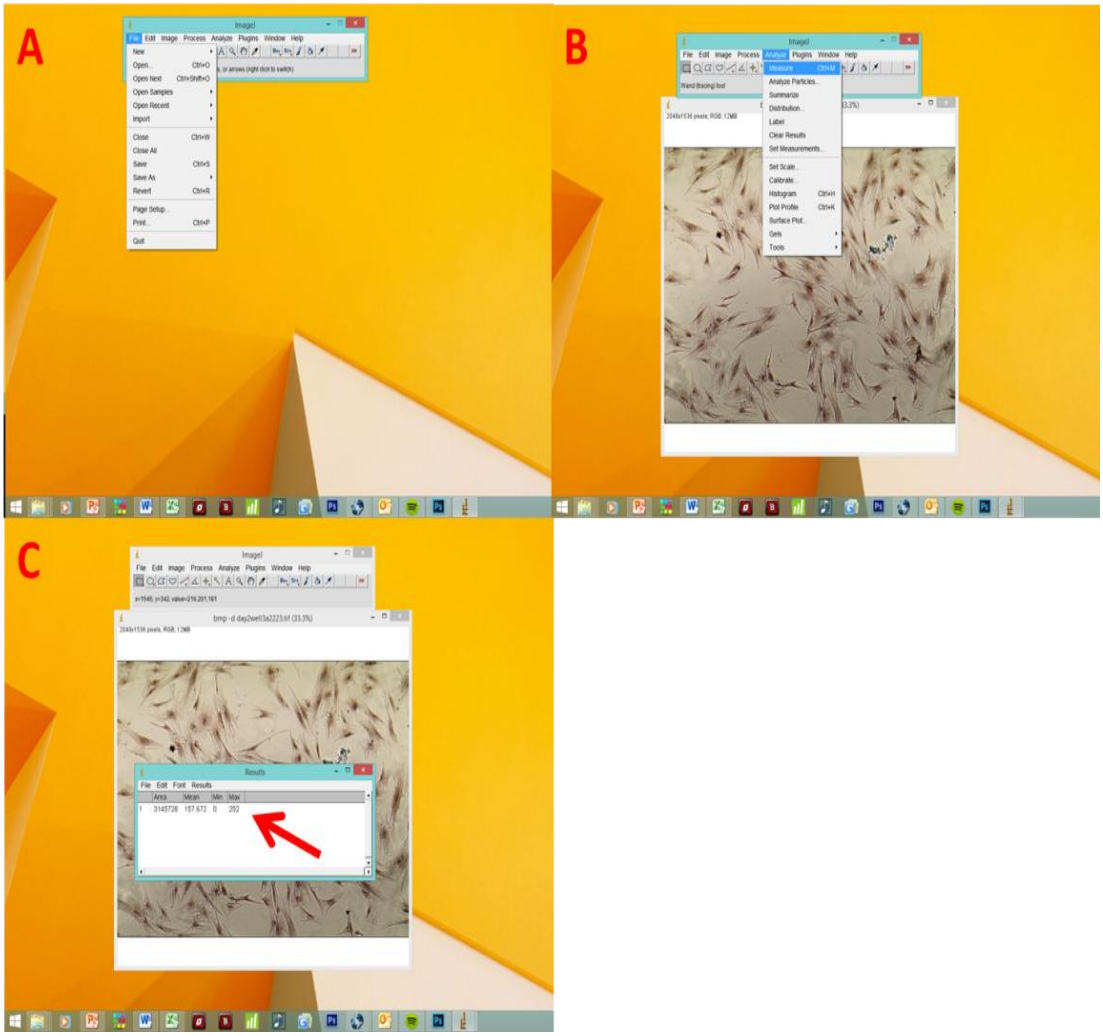

Figure 0.3 Image J Masson's Trichrome Set up

3.5.6 Statistical Testing

The significance of difference between groups (n=3 per group) was determined by one-way ANOVA two factor two tailed comparison analysis. A p value less than 0.05 was considered to indicate statistical significant. Data are presented as mean ± standard deviation (SD). All statistical analysis was performed using Minitab® 16 (Minitab Inc., Pennsylvania, USA).

3.5.7 Experimental Plan

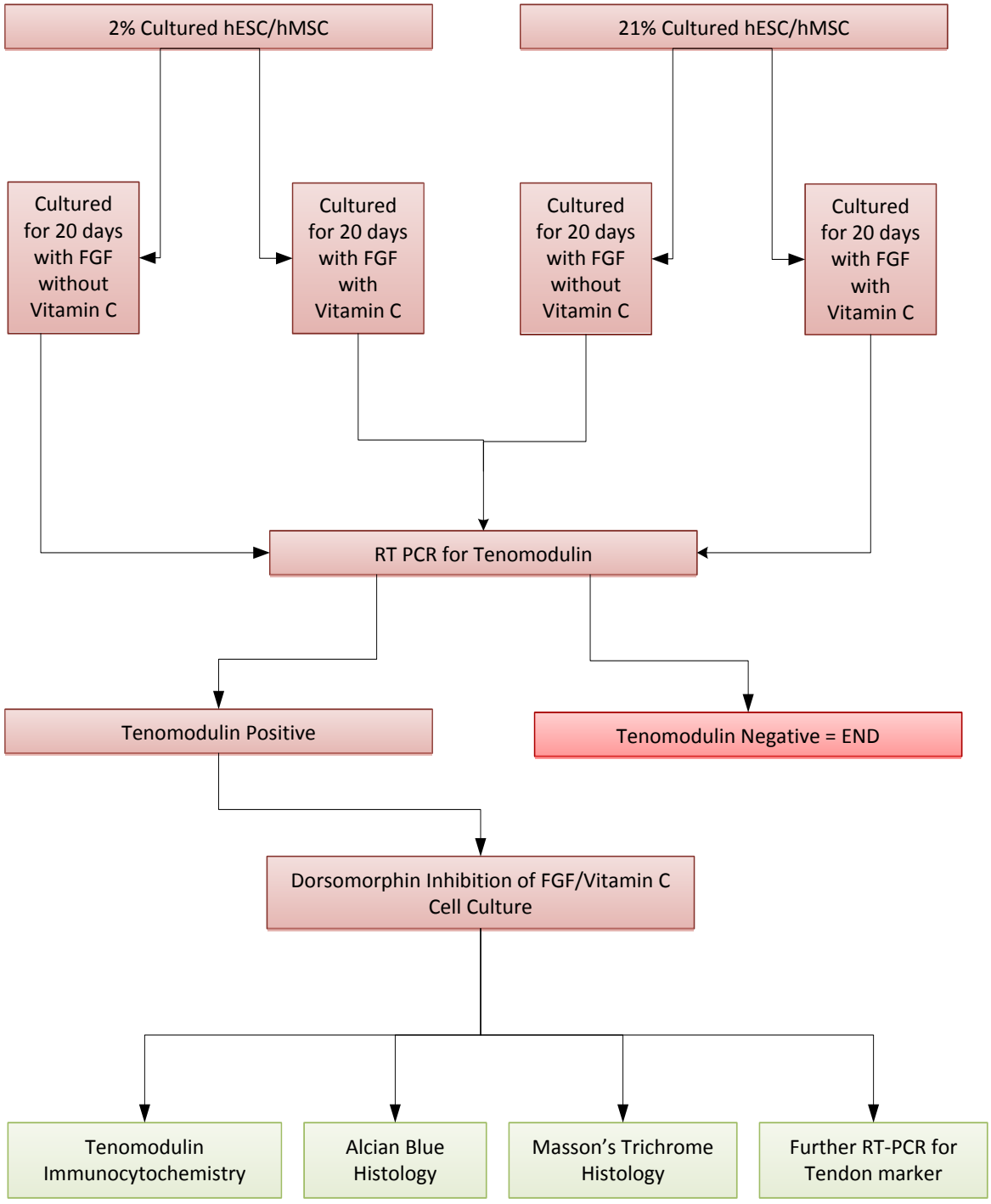

Figure 0.4 FGF driven human MSC and hESC differentiation experimental plan

Flow chart of work plan showing initial screening for TNMD gene expression. After identification of TNMD gene expression, Dorsomorphin inhibition of BMP signalling and full tendon gene expression for growth factor supplementation of differentiation media along with TNMD immunocytochemistry and histological analysis.

3.6 Results

3.6.1 hESC Characterisation

Prior to experimental set up we sought to confirm the expression of pluripotent markers for human embryonic stem cells (SHEF-1) utilising immunocytochemistry previously described in Section 3.4. This was undertaken by expanding a 2 x T-25 and seeding the confluent T-25 to a 6 well plate. The remaining T-25 was then utilised for RNA extraction using the Qiagen RNEasy kit previously described in Section 3.3.

3.6.1.1hESC Phenotyping

hESC cell line SHEF-1 was utilised for this experimental chapter and cultured in a feeder-free, culture condition using MEFs-CM media following the protocol described in the Section- 3.2.2. SHEF-1 cells grew in a steady manner and did not show any apparent sign of senescence.

Immunocytochemistry (Figure 3.5) SHEF-1 cells were highly positive for alkaline phosphatase (ALP) and stage-specific embryonic antigen-4 (SSEA-4) markers [336]. Supplementary to the immunocytochemistry, RT PCR analysis showed SHEF-1 cells displayed high levels of hTERT gene expression as detected by RT-PCR (Figure 3.6) (Section- 3.3), a common criterion for hESC (Thomson et al., 1998). Cells were also positive for pluripotent nuclear markers Octamer-binding protein-4 (Oct-4) and Nanog again detected by RT-PCR (Figure 3.6).

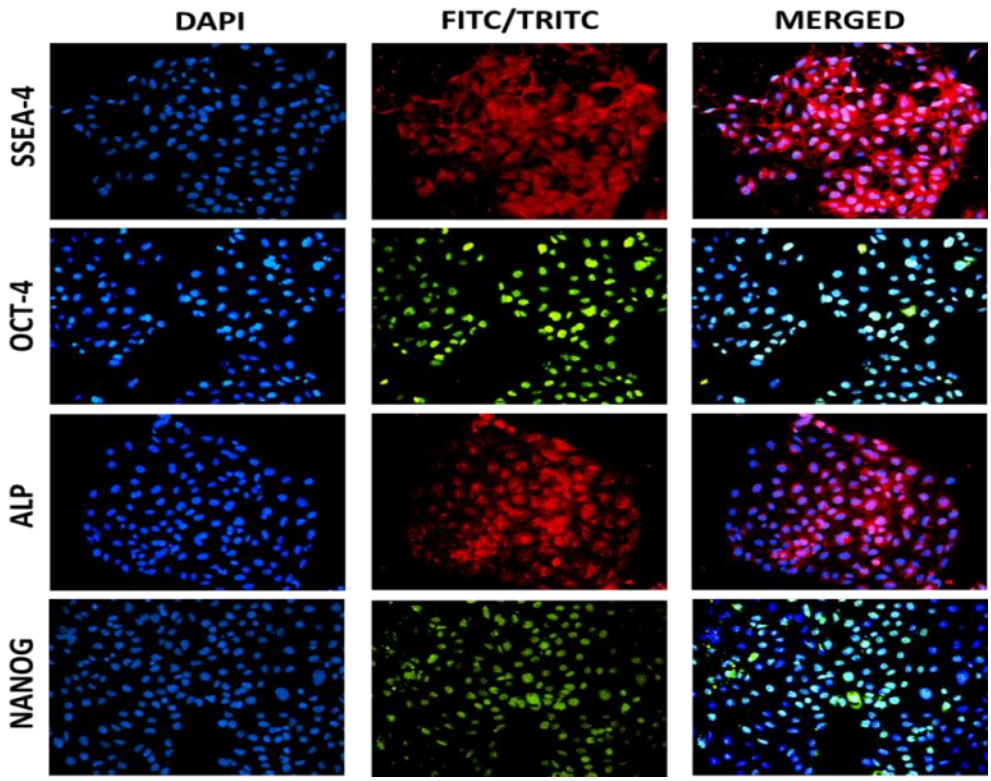

Figure 0.5 Immunocytochemistry Profiling of Human Embryonic Stem cells (SHEF-1)

Pluripotent characterisation for embryonic stem cell markers produced positive for NANOG, Alkaline Phosphatase (ALP), OCT-4 and Stage specific embryonic antigen-4 (SSEA-4) protein markers for SHEF-1 cells, during cell expansion.

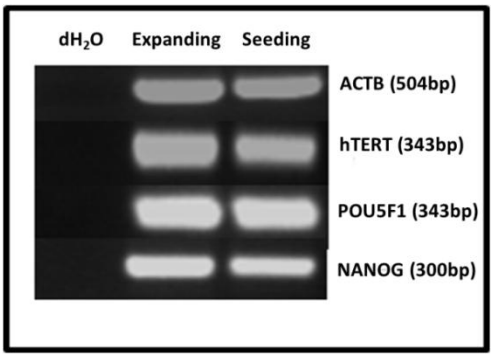

Figure 0.6 RT-PCR Pluripotent gene expression of SHEF-1.

RT-PCR was undertaken during expansion (passage 32) and on seeding (passage 35) the hESCs on the day prior to the addition of FGF supplemented media.

3.6.2 hESC Tenomodulin Expression After FGF Driven Differentiation

After identifying the SHEF-1 (hESCs) expressed pluripotent markers the next phase of the investigation was to investigate the effects of FGF-4, FGF-6 and FGF-8 supplementation of differentiation media (DMEM supplemented with 10% FBS, 1% L-GLUT and 1% NEAA) in the presence and absence of Vitamin C (10µM) at two different oxygen environments (2% and 21%). SHEF-1 cells were seeded as shown in Section 3.2.4.

This phase of the investigation utilised the time points 0, 2, 5, 10 and 20 days for RT-PCR to detect the presence of Tenomodulin (a known tendon marker).

Preliminary RT-PCR showed. FGF-4 & 8 when cultured in the presence of Vitamin C and cultured at 2% O_2 was capable of maintaining TNMD expression through to day 20 (Figure 3.7). However, the expression post day 10, did appear to reduce. FGF-4, 6 & 8 when cultured at 2% O_2 and supplemented with Vitamin C were capable of sustaining TNMD gene expression in hESCs (Figure 3.7) with no apparent reduction in expression. Conversely, FGF-4, FGF-6, FGF-8 FGF-4 & 6, FGF-4 & 8 and FGF-4, 6 & 8 when cultured for 20 days at 21% O_2 were incapable of sustaining TNMD gene expression in hESC when cultured in the presence or absence of Vitamin C (Figure 3.8).

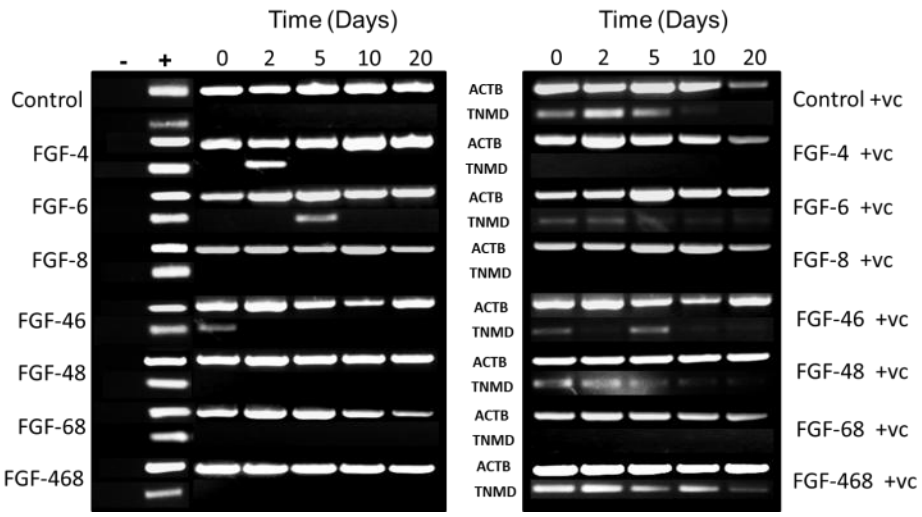

Figure 0.7 Tenomodulin expression of FGF driven differentiation of hESC (SHEF-1) cultured at 2% O_2 supplemented with or without Vitamin C

RT-PCR analysis for Tenomodulin (TNMD) showed that combinations of FGF-4 & 8 and the combination of FGF-4, 6 & 8 induced and maintained the expression of TNMD for 20 days when supplemented with Vitamin C at 10µM per mL. FGF supplemented media which was not supplemented with Vitamin C was unable to initiate and subsequently maintain the expression of TNMD.

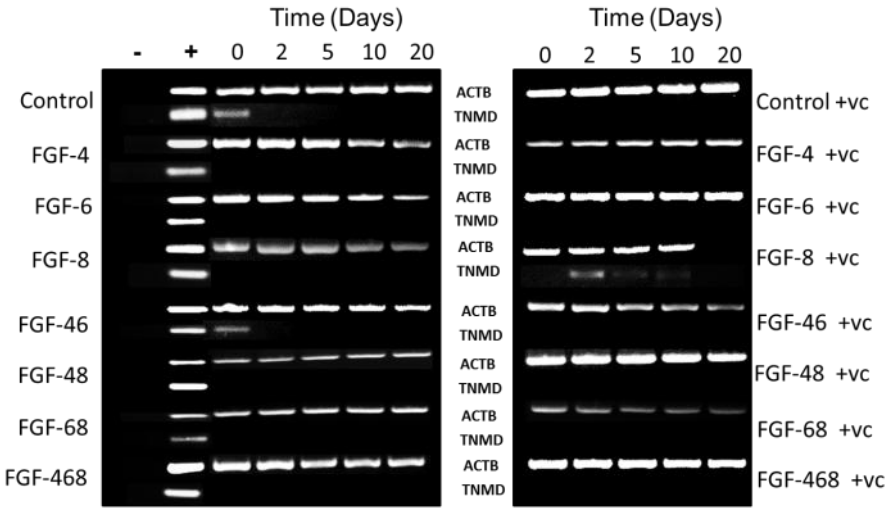

Figure 0.8 *Tenomodulin expression of FGF driven differentiation of hESC (SHEF-1) cultured at 21% O_2 supplemented with or without Vitamin C*

FGF supplemented media with/without Vitamin C was unable to initiate transcription of TNMD when hESC's are cultured at 21% O_2.

Having now identified the FGF growth factor combination capable of initiating and maintaining TNMD expression the next phase was to be initiated. The next investigation was to identify the concentration of Dorsomorphin that allowed cell survival. Then supplement the FGF/Vitamin C differentiation media with Dorsomorphin.

3.6.3 Dorsomorphin Concentration Optimisation

Shef-1 cells were seeded to a 6 well plate as shown in Section 3.2.7 and cultured using CM+ (Conditioned embryonic stem cell media) supplemented with a range of Dorsomorphin concentrations (ranging from 1µM to 500µM) and cultured at 2% O_2 for 5 days and media change every 24 hours.

After 5 days had elapsed cells were fixed and stained with Giemsa's stain for analysis (Section 3.5.1)

The concentration to be used for investigation of Dorsomorphin inhibition of SHEF-1 FGF driven differentiation was 1µM per ml (Figure 3.9). The concentration of 1µM per ml as this concentration impaired cellular proliferation whilst all higher concentrations were shown to have a toxic effect.

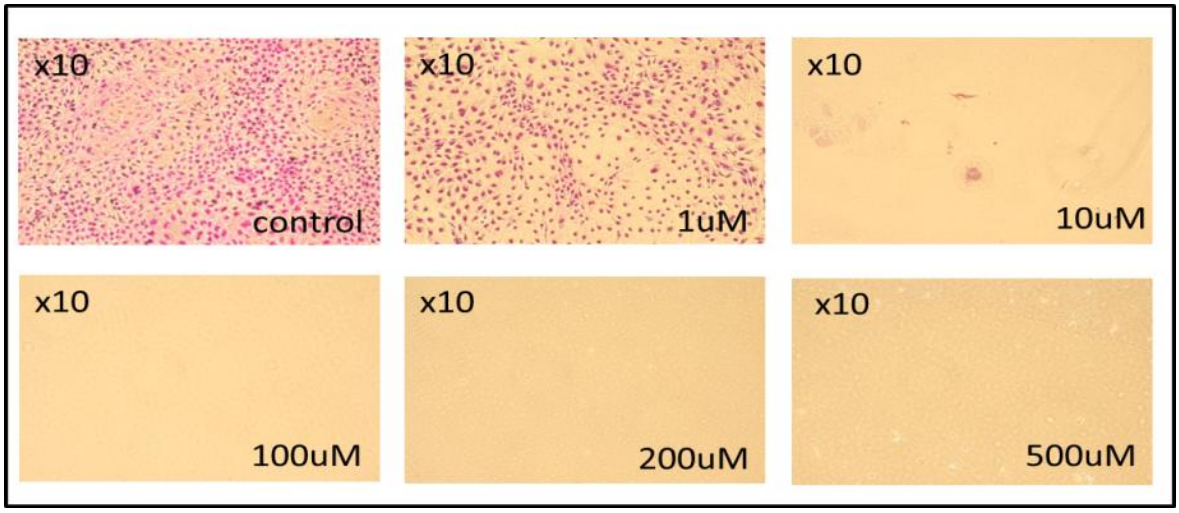

Figure 0.9 SHEF 1 cultured in Dorsomorphin supplemented media at a range of concentrations.

Shows a range of concentrations of Dorsomorphin with concentrations in excess of 1µm having a high level of cellular toxicity.

3.6.4 FGF driven differentiation of hESC cultured with Vitamin C and Dorsomorphin at 2% O_2

hESC when cultured at 2% O_2 in differentiation media containing FGF-4 & 8 and Vitamin C showed a continued expression of both TNMD, THBS-4 genes and COL1A2 genes. COL3A1 expression was present at Day 0, 2 and weakly present at Day 5, by day 10 expression had returned to pre-day 5 levels and COL1A2 was expressed through to day 40. TENC was expressed from day 10 through to day 40. DCN gene expression was only detected at day 40 (Figure 3.10).

Conversely, the addition of Dorsomorphin to the culture media inhibited the gene transcription of THBS-4 and DCN. Furthermore, TENC and TNMD were not detected post day 20. Conversely, both COL1A2 and COL3A1 were detected throughout the investigation (Figure 3.10).

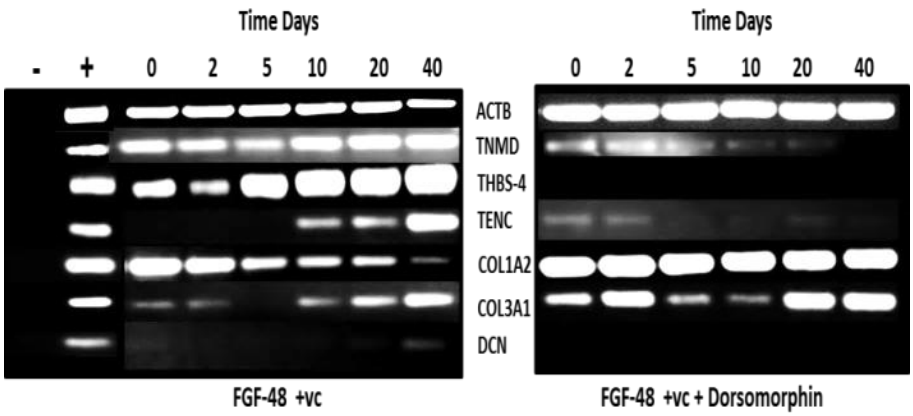

Figure 0.10 Tendon gene expression for hESC FGF-4 & 8 driven differentiation when supplemented with Dorsomorphin at 2% O_2

Tendon gene expression panel for FGF-4 & 8 supplemented differentiation media with Vitamin with and without Dorsomorphin cultured at 2% O_2.

hESC when cultured at 2% O_2 and supplemented differentiation media containing FGF-4, 6 & 8 and Vitamin C showed continued gene expression of TNMD, THBS-4, TENC, COL1A2, COL3A1 with DCN being detected from day 2 through to day 40 (Figure 3.11).

Conversely, the addition of Dorsomorphin to the culture media inhibited the gene transcription of DCN. However, TNMD, THBS-4, TENC, COL1A2, COL3A1 were detected up to day 40, with TNMD being less expressed.

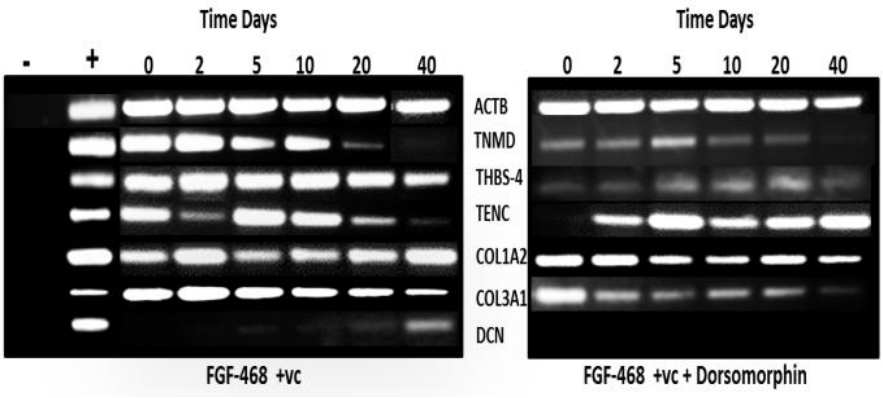

Figure 0.11 Tendon gene expression for hESC FGF-4, 6 & 8 driven differentiation when supplemented with Dorsomorphin at 2% O_2

Tendon gene expression panel for FGF-4, 6 & 8 supplemented differentiation media with Vitamin with and without Dorsomorphin cultured at 2% O_2.

hESC cultured in the presence of BMP-12 & 13 and differentiation media further supplemented with Vitamin C showed TNMD, TENC expression for the duration of the investigation (Figure 4.9). However, THBS-4 was detected until day 2 although the signal was weak. COL1A2 was detected throughout the 40 day investigation again this was a weak signal. COL3A1 was detected from day 5 through to day 40 with increasing levels with DCN only being detected on day 10 and day 20 (Figure 3.12).

Conversely, the addition of Dorsomorphin to the differentiation media containing BMP-12 & 13 and Vitamin C inhibited the gene transcription of TNMD and COL3A1. Furthermore, THBS-4 and COLA2 were detected up until day 20 and TENC until Day 10, whilst DCN was only detected on day 2 and day 5 (Figure 3.12).

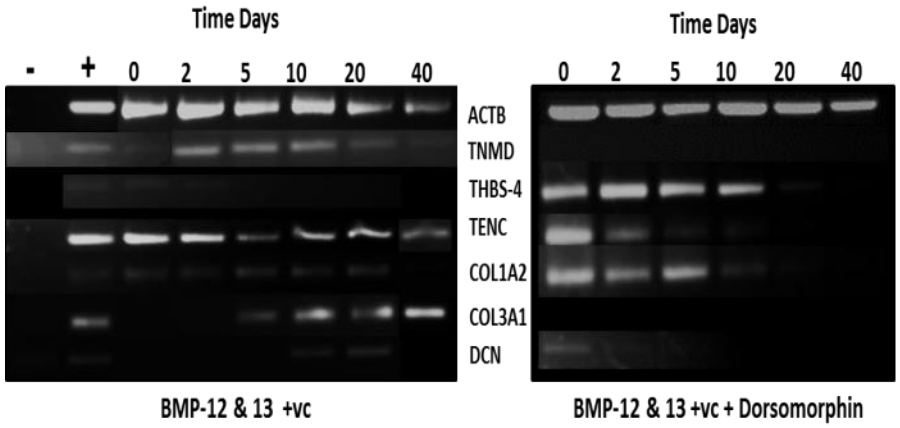

Figure 0.12 Tendon gene expression for BMP-12 & 13 driven differentiation when supplemented with Dorsomorphin at 2% O_2

Tendon gene expression panel for BMP12 & 13 supplemented differentiation media with Vitamin with and without Dorsomorphin cultured at 2% O_2.

Having now established the gene expression for both Dorsomorphin supplemented growth factor differentiation media. We then used immunocytochemistry to identify the expression of TNMD protein this phase of the investigation utilised TNMD Immunocytochemistry.

3.6.5 Immunocytochemistry

Immunocytochemistry was undertaken to detect the presence of tenomodulin protein expression after growth factor driven differentiation of hESC. Also, to evaluate the effect of further supplementation of differentiation media with Dorsomorphin and its subsequent affect upon TNMD expression.

Prior to undertaking the immunocytochemistry staining for TNMD we looked at utilising rat tenocytes as a positive control.

3.6.5.1 Tenomodulin Antibody Staining of Rat Tenocytes

Rat tenocytes (rt-tenocytes) were harvested and expanded following the protocol shown in Section 3.4.3. After expansion the rt-tenocytes were seeded into a six well plate and subsequently immunocytochemistry stained for tenomodulin utilising the protocol in Section 3.4.3.

The immunofluorescence showed positive expression for TNMD (confirming the cells were tenocytes), with a DAPI (blue) nuclear stain (Figure 3.13). The Cells appeared to show the presence of synapse-like morphology and fibroblast like appearance.

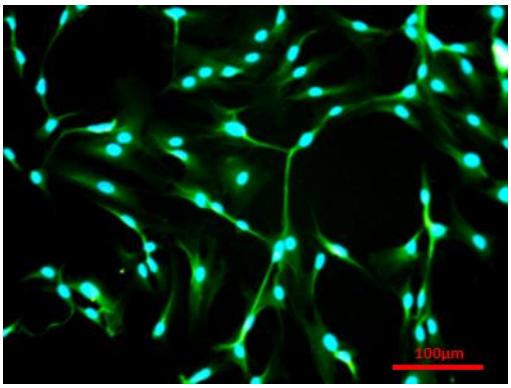

Figure 0.13 Tenomodulin positive stained rat tenocyte

Rat Tenocytes at passage 1 showing positive TNMD (green) and DAPI nuclear staining (Blue).

3.6.5.2 Tenomodulin Staining of FGF Driven Differentiation of hESCs.

FGF driven differentiation of hESC cells were cultured for 40 days in FGF or BMP (n=3), Vitamin C supplemented differentiation media (Section 3.2.3 & 3.2.4) in the presence and absence of Dorsomorphin. Cells were fixed for staining (Section 3.4.3) at time-points 0, 2, 5, 10, 20 and 40 days exposure to the respective media.

hESCs supplemented with the combination of FGF-4 & 6 with Vitamin C showed the presence of TNMD stain which was localised to the nucleus which indicates a presence of TNMD throughout the investigation (Figure 4.11). However, there appeared to be little to no TNMD staining on the cellular membrane and the cells lacked the fibroblast like morphology observed in the rat tenocytes and appeared more cobble stone “like” (Figure 3.14)

hESCs supplemented with the combination of FGF-4 & 8 with Vitamin C and Dorsomorphin appeared to have reduced TNMD signalling (Figure 3.15) compared to the absence of Dorsomorphin (Figure 3.14). The addition of Dorsomorphin appeared to inhibit morphological change towards a fibroblast like appearance which the cells appearing to remain “embryonic-like”.

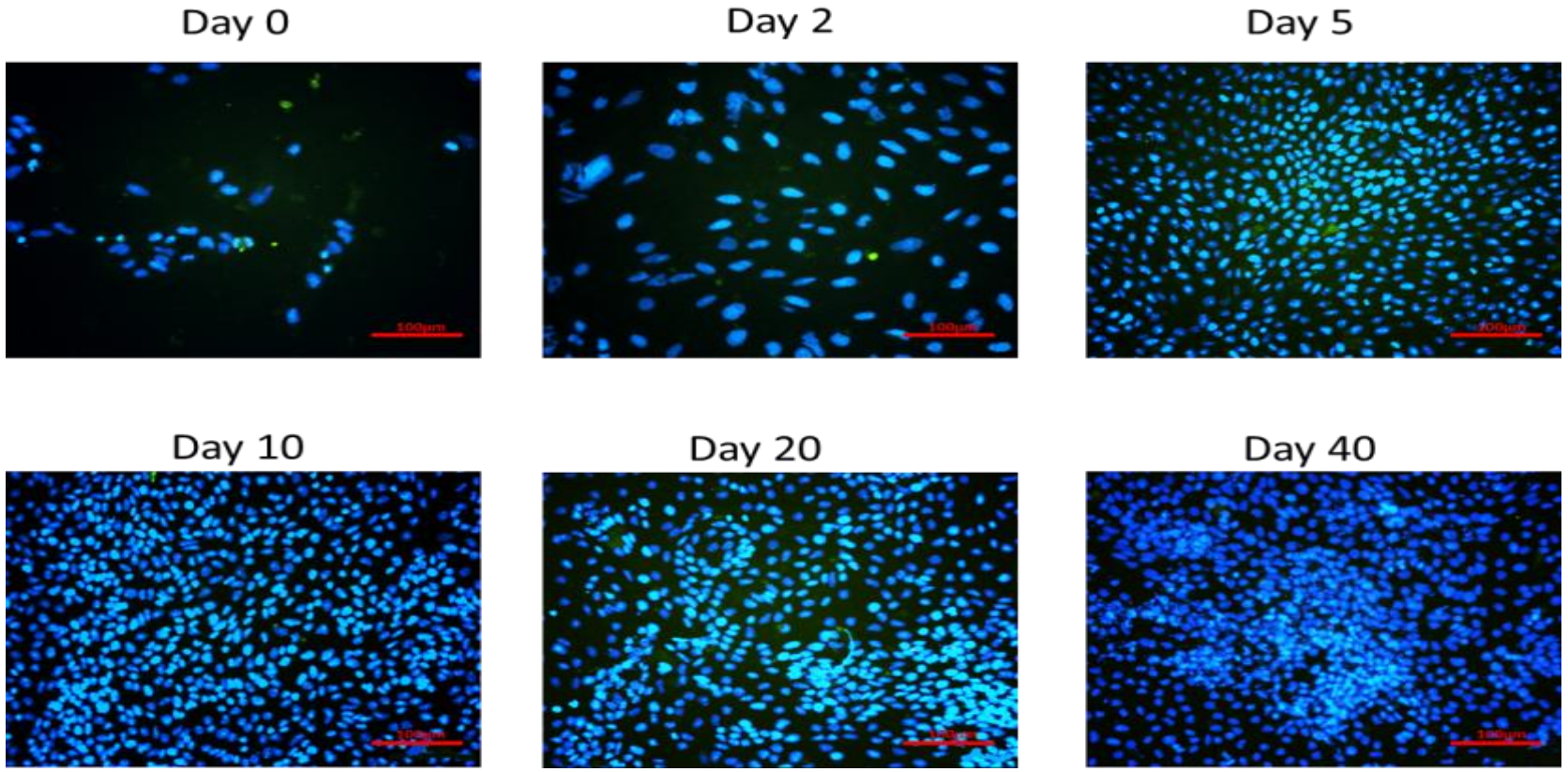

Figure 0.14 hESC FGF-4 & 8 with Vitamin C cultured at 2% O_2

TNMD (green) staining with DAPI (blue) nuclear stain of hESC cultured in differentiation media supplemented with FGF-4 & 8 with Vitamin C over 40 days (Time points 0, 2, 5, 10, 20 and 40 days).

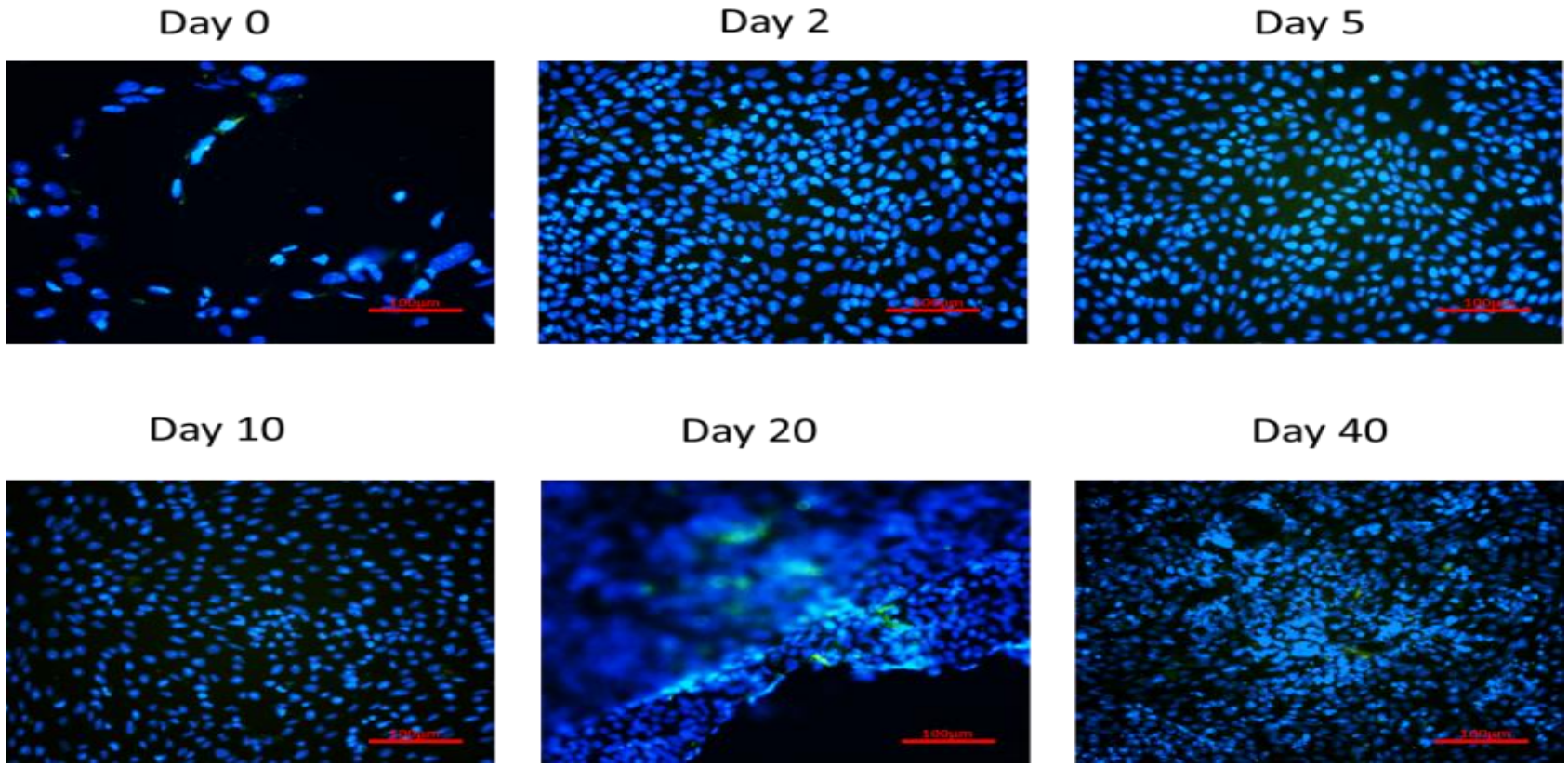

Figure 0.15 hESC FGF-4 & 8 with Vitamin C cultured at 2% O_2 supplemented with Dorsomorphin

TNMD (green) staining with DAPI (blue) nuclear stain of hESC cultured in differentiation media supplemented with FGF-4 & 8 with Vitamin C and Dorsomorphin over 40 days (Time points 0, 2, 5, 10, 20 and 40 days).

hESCs supplemented with the combination of FGF-4, 6 & 8 with Vitamin C showed TNMD staining within the cytoplasm of the cells (Figure 3.16). However, the cells lacked the fibroblast-like morphology observed in rat tenocytes (Figure 3.13). As the investigation progressed in time the TNMD staining appeared as back ground staining which may indicate the TNMD protein being expressed within the cellular matrix, but lacking the morphological appearance of tenocytes and more spherical (cobble stone like).

hESCs supplemented with the combination of FGF-4, 6 & 8 with Vitamin C and Dorsomorphin showed reduced TNMD staining within the cytoplasm of the cells (Figure 3.17) when compared to the absence of Dorsomorphin (Figure 3.16). The addition of Dorsomorphin appeared to inhibit morphological change towards a fibroblast like appearance which the cells appearing to remain “embryonic-like”.

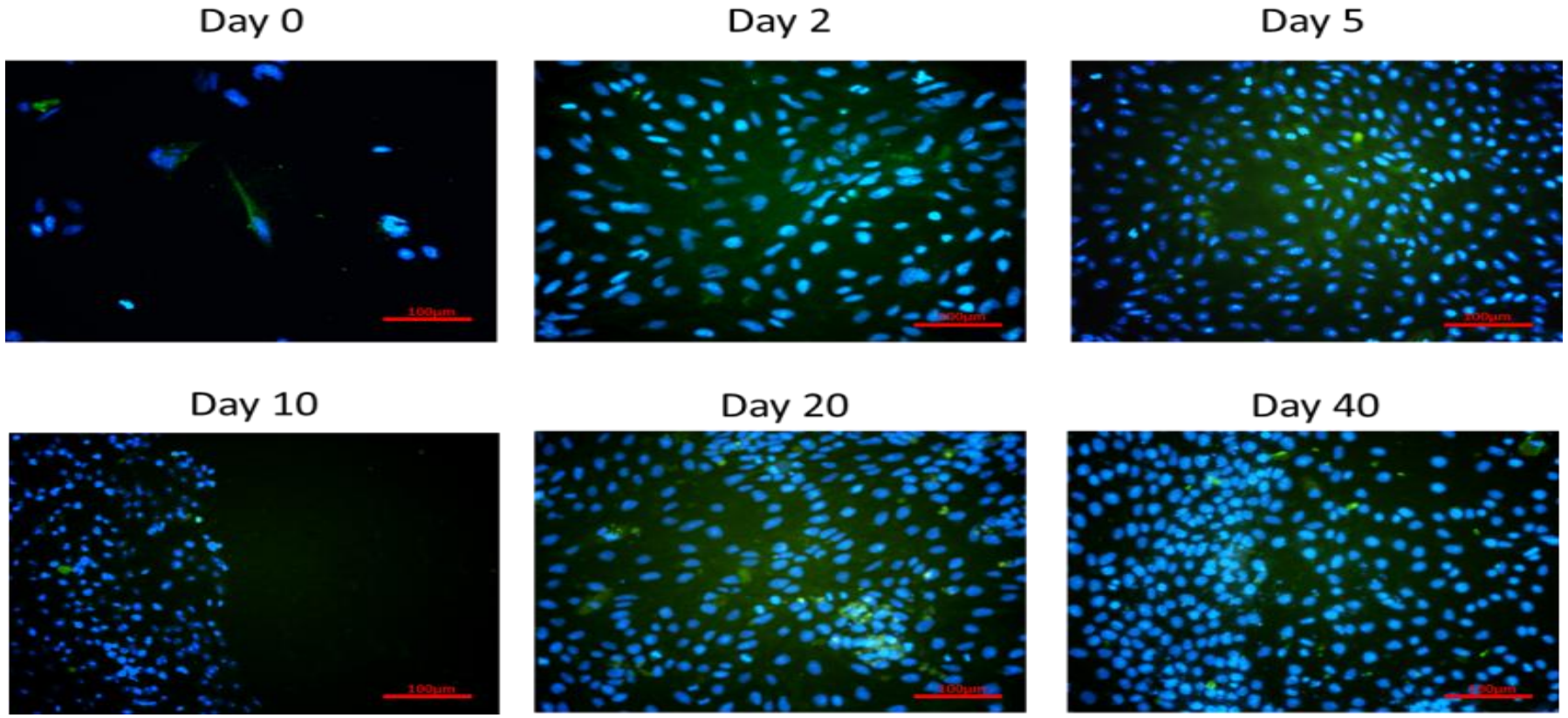

Figure 0.16 hESC supplemented with FGF-4, 6 & 8, Vitamin C and cultured at 2% O_2

TNMD (green) staining with DAPI (blue) nuclear stain of hESC cultured in differentiation media supplemented with FGF-4, 6 & 8 with Vitamin C and Dorsomorphin over 40 days (Time points 0, 2, 5, 10, 20 and 40 days).

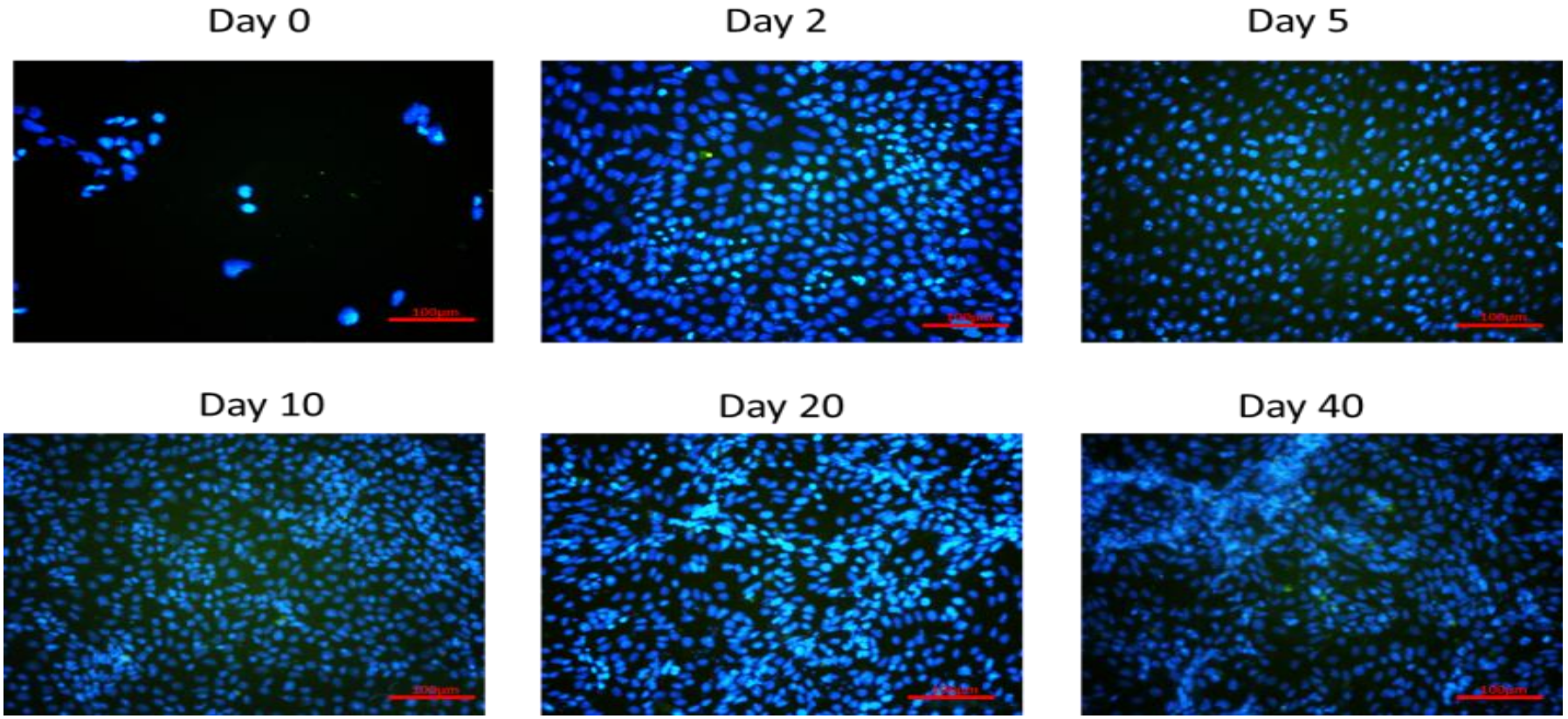

Figure 0.17 hESC Supplemented with FGF-4, 6 & 8, Vitamin C and Dorsomorphin Cultured at 2% O_2

TNMD (green) staining with DAPI (blue) nuclear stain of hESC cultured in differentiation media supplemented with FGF-4, 6 & 8 with Vitamin C and Dorsomorphin over 40 days (Time points 0, 2, 5, 10, 20 and 40 days).

hESCs supplemented with the combination of BMP-12 & 13 with Vitamin C showed TNMD staining within the cytoplasm of the cells at day 5 (Figure 3.18). The BMP differentiated cells appeared to be fibroblast-like morphology similar to that observed in rat tenocytes (Figure 3.13) with distinct synapsing with other cells. Prior to day 5 and between the time points 10 -20 the cells appeared to lack TNMD staining.

hESCs supplemented with the combination of BMP-12 & 13 with Vitamin C and Dorsomorphin showed no positive TNMD staining over the 40 day investigation (Figure 3.19). This indicates that Dorsomorphin inhibited the effects of BMP12 & 13 observed in Figure 3.18.

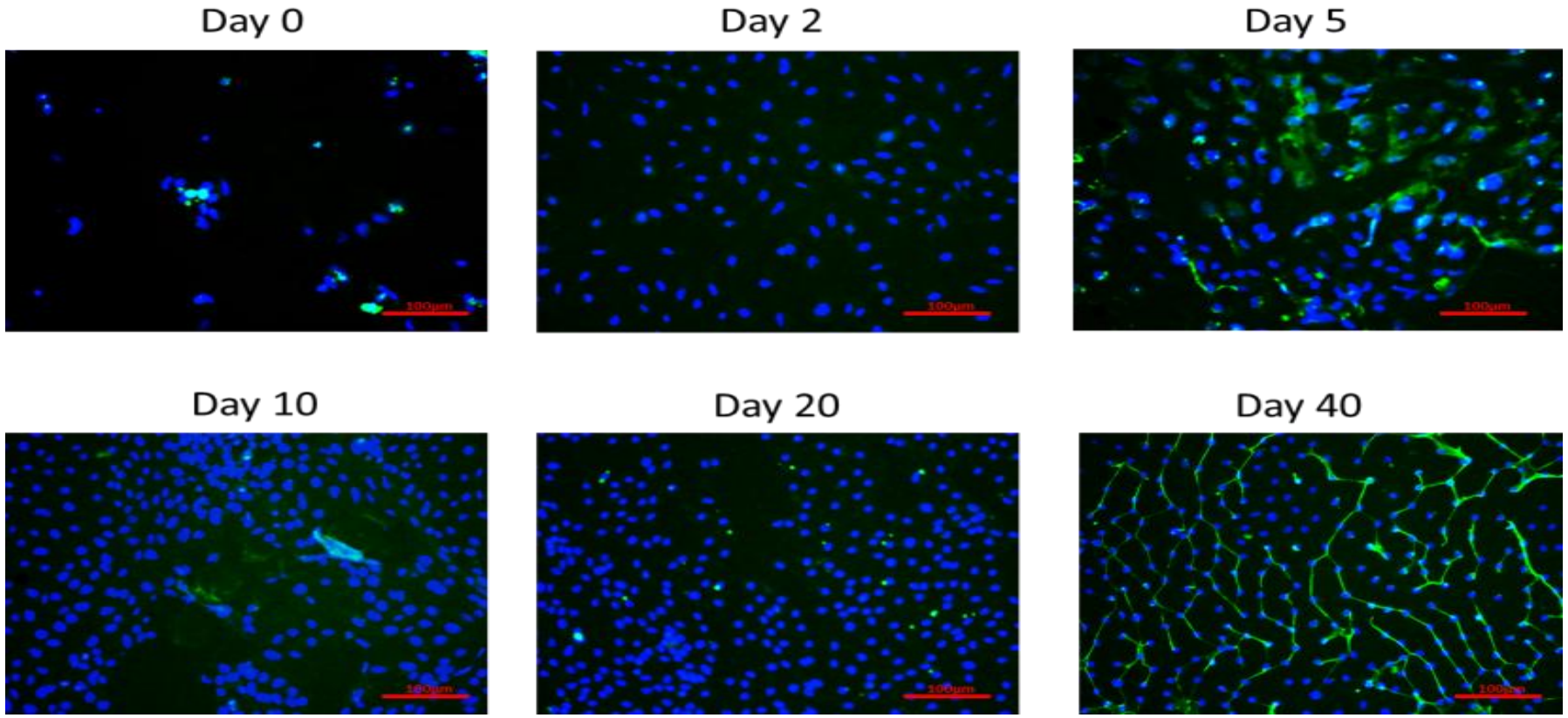

Figure 0.18 hESC Supplemented with BMP-12 & 13 and Vitamin C and cultured at 2% O_2

TNMD (green) staining with DAPI (blue) nuclear stain of hESC cultured in differentiation media supplemented with BMP-12 & 13 with Vitamin C and Dorsomorphin over 40 days (Time points 0, 2, 5, 10, 20 and 40 days).

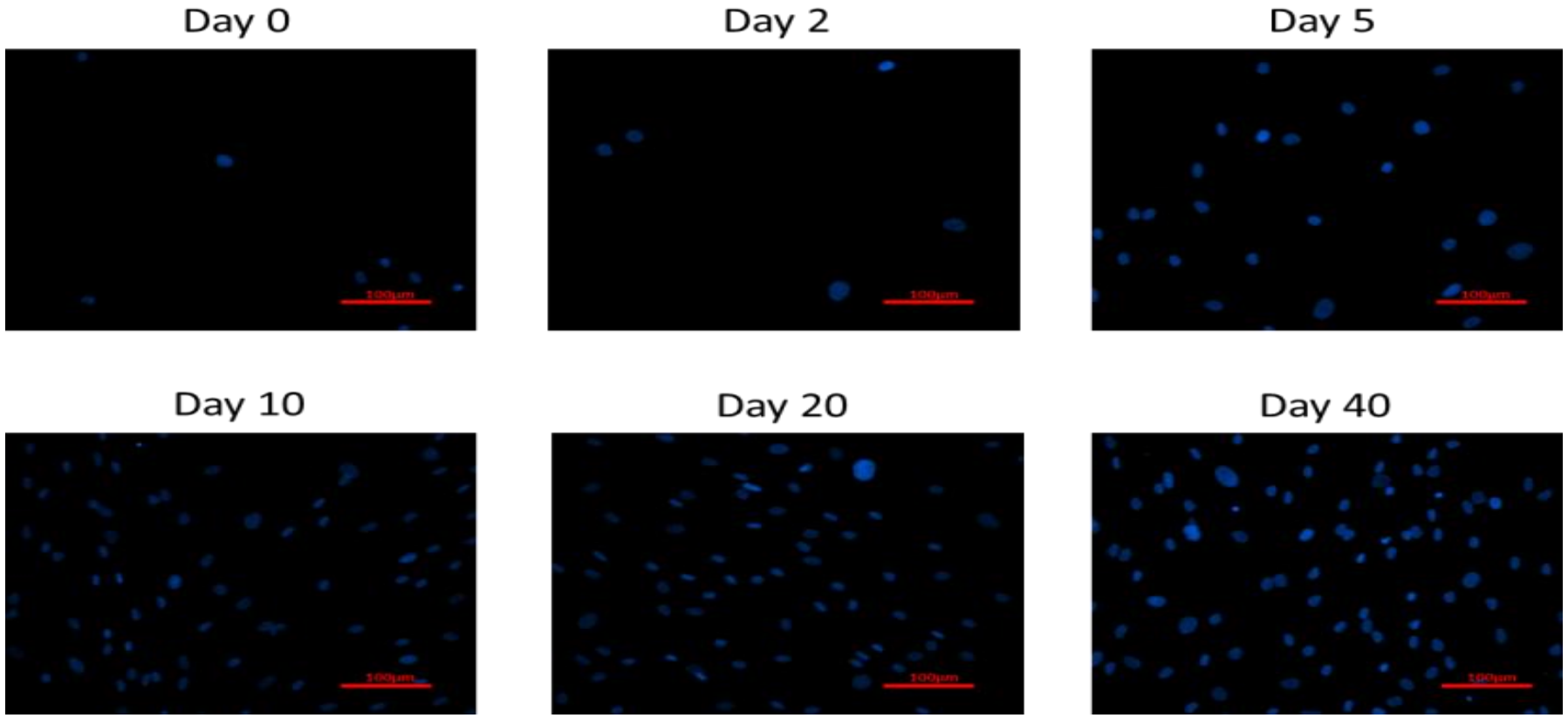

Figure 0.19 hESC BMP-12 & 13 cultured at 2% O_2 and Supplemented with Dorsomorphin

TNMD (green) staining with DAPI (blue) nuclear stain of hESC cultured in differentiation media supplemented with BMP-12 & 13 with Vitamin C and Dorsomorphin over 40 days (Time points 0, 2, 5, 10, 20 and 40 days).

3.6.6 Histological Analysis

Histological staining of growth factor (and Vitamin C supplemented differentiation media) driven differentiation of hESC towards a tenocyte lineage was undertaken in parallel to immunocytochemistry and rt-PCR. Growth factor driven differentiation of hESC was undertaken utilising the procedure shown in Section 3.2.3– 3.2.6.

Glycosaminoglycans were stained utilising Alcian Blue stain procedure shown in Section 3.5.2 and analysed utilising Image J analysis shown in Section 3.5.4– 3.5.5.

Collagen was stained using Masson's Trichrome staining procedure shown in Section 3.5.3 and image J analysis was undertaken utilising the procedure outlined in Section 3.5.4– 3.5.5.

A selection of growth factor driven hESC stained with Masson's Trichrome is shown in Figure 3.20. Each time point had a n=3 and each well imaged 3 times to produce the data shown in Table 3.8.

From the Data shown in Table 3.8 comparisons were made between growth factor in the absence of Dorsomorphin and the presence of Dorsomorphin in the differentiation media.

3.6.6.1 Masson's Trichrome Staining

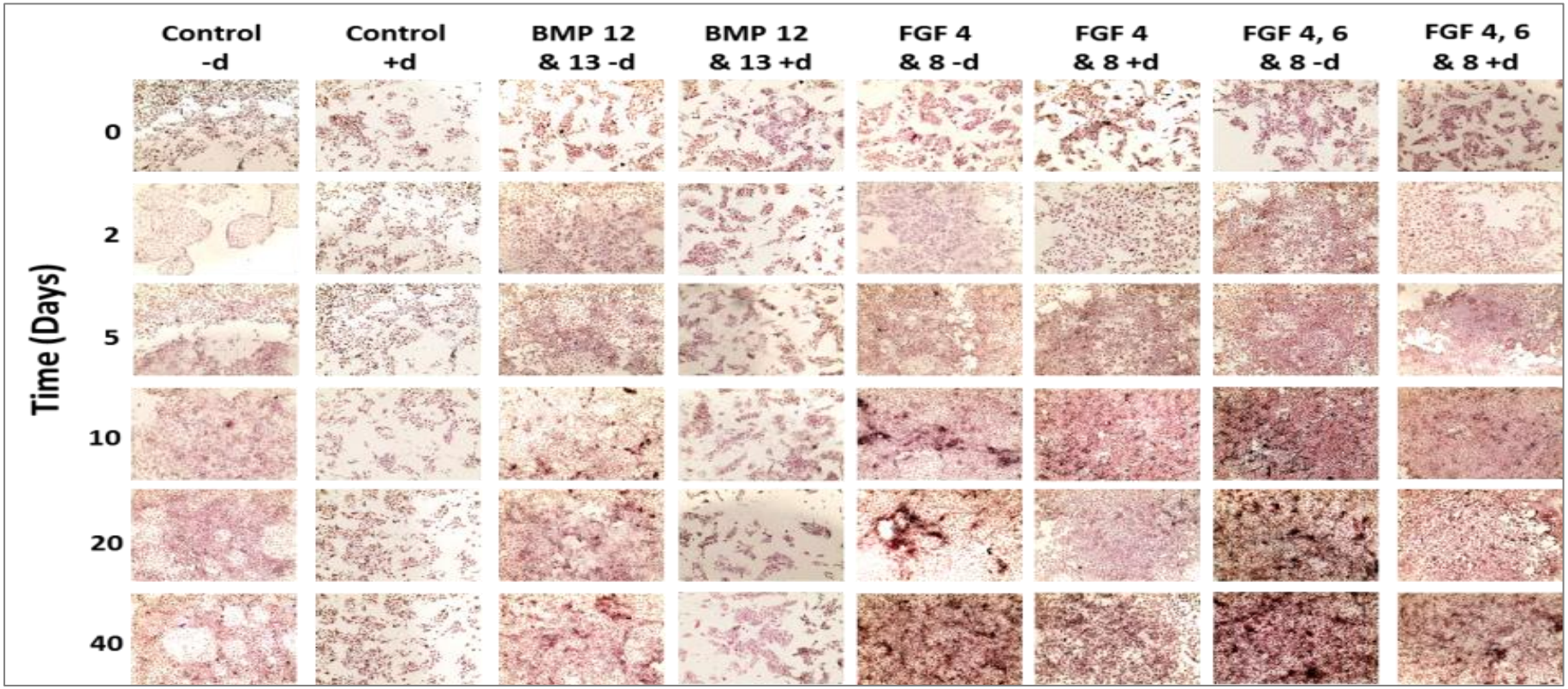

Figure 0.20 Masson's Trichrome staining for each group of Shef-1 over 40 Days.

All groups showed Masson's Trichrome staining. All time points (n=9) were analysed and data extracted from the images. From the data extracted each time point for each condition was compared and statistically tested and the data is shown in Table 3.8.

Time (Days)	hESC Control – d	hESC Control +d	hESC BMP-12 &13 -d	hESC BMP-12 &13 +d	hESC FGF-4 & 8 -d	hESC FGF-4 & 8 +d	hESC FGF-4, 6 & 8 -d	hESC FGF-4,6 & 8 +d
0	52.77	52.63	52.77	52.57	52.67	52.57	52.77	52.57
	±3.39	±3.22	±3.39	±3.66	±3.13	±3.66	±3.31	±3.66
2	49.41	49.85	61.70	53.41	61.23	52.79	56.58	54.59
	±1.36	±1.26	±2.65	±1.42	±1.99	±1.49	±6.85	±2.22
5	49.52	50.60	65.35	53.96	64.79	52.97	66.56	64.55
	±1.48	±2.22	±3.05	±2.53	±2.52	±1.62	±3.18	±5.23
10	50.23	49.24	68.55	54.29	69.30	53.50	69.62	68.72
	±2.81	±1.19	±3.55	±2.93	±4.21	±4.21	±3.70	±5.44
20	60.82	49.86	74.48	54.29	75.17	54.24	79.24	73.54
	±2.91	±2.28	±6.71	±2.38	±4.96	±2.44	±5.00	±6.56
40	64.87	49.62	79.72	57.86	77.89	56.75	86.62	74.98
	±4.13	±1.16	±3.66	±3.06	±1.92	±1.87	±2.27	±6.22

Table 0.8 Masson's Trichrome data extraction from Image J for human Embryonic Stem cells

The data shown is obtained from Image J and is a total colour extraction of images taken from growth factor driven differentiation.

From the data shown in Table 3.8 the following observations were made:

hESC cultured in control differentiation media (DMEM supplemented with: 10% FBS, 1% NEAA, 1% L-Glut) displayed a Masson's Trichrome colour extraction value of 52.77±3.39 on day 0, which decreased by day 2 (49.41±1.36). A slight increase in value was observed by day 5 (49.52±1.48), with further increases on day 10 (50.23±2.81), day 20 (60.82±2.91) and Day 40 (64.87±4.13).

Conversely, hESC cultured in control differentiation media supplemented with Dorsomorphin had a Masson's Trichrome colour extraction value of 52.63±3.22 on day 0, which decreased by day 2 (49.85±1.26). A slight increase in value was observed by day 5 (50.60±2.22), with further decreased at day 10 (49.24±1.19), an increase on day 20 (49.86±2.28) and a subsequent decrease on Day 40 (49.62±1.16).

Statistical testing between Control differentiation media against control differentiation media plus Dorsomorphin showed significant difference between Control-d and Control +d day 20 ($p<0.0001$) and day 40 ($p<0.0001$) time points (Figure 3.21).

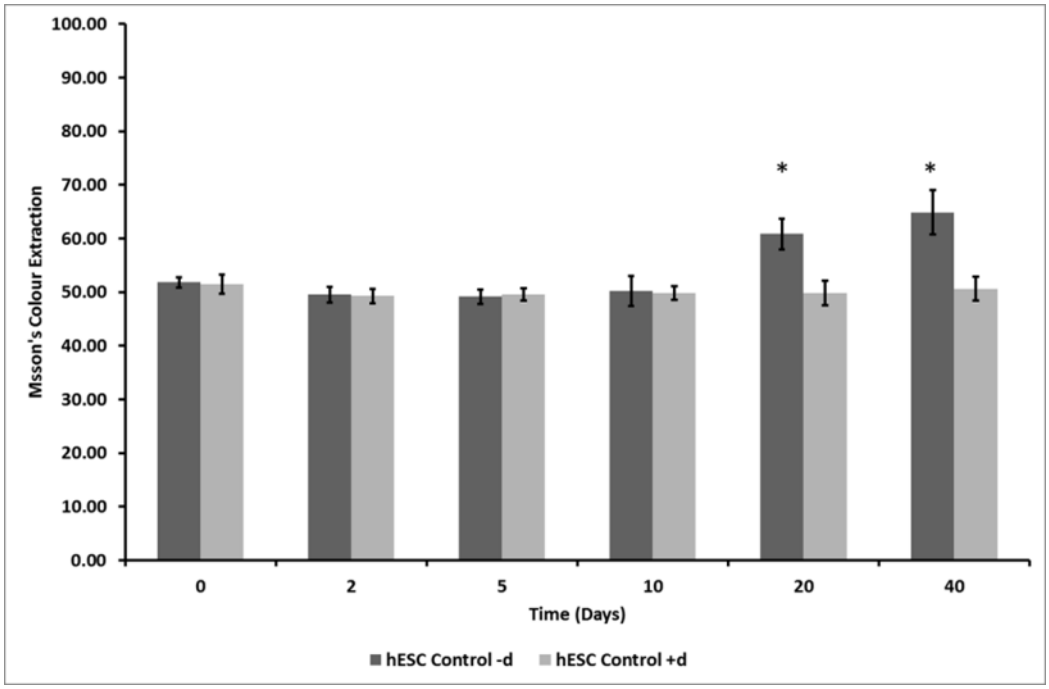

Figure 0.21 Masson's Trichrome analysis of hESC supplemented with control differentiation media in the presence and absence of Dorsomorphin

hESC cultured using differentiation media and differentiation media supplemented with Dorsomorphin over 40 days (*p<0.0001).

Further, supplementation of differentiation media with BMP-12 & 13 produced a Masson's Trichrome colour extraction value of 52.77±3.39 at day 0. Which increased continuously on: day 2 (61.70±2.65), day 5 (65.35±3.05), day 10 (68.55±3.55), day 20 (74.48±6.71) and day 40 (79.72±3.66).

Conversely, supplementation of differentiation media with BMP-12 & 13 and Dorsomorphin produced a Masson's Trichrome colour extraction value of 52.57±3.66 at day 0. Which decreased on day 2 (53.41±1.42) and increase on day 5 (53.96±2.53).a further increase was observed on day 10 (54.29±2.93) and day 20 reporting similar values to day 10 (54.29±2.38) and day 40 showing a slight increase 57.86±3.06).

Further testing of BMP-12 & 13 –d and BMP-12 & 13 +d showed significant difference at day 2 ($p<0.0005$), day 5 ($p<0.00001$), day 10 ($p<0.00001$), day 20 ($p<0.00001$) and day 40 ($p<0.000001$). FGF-4 & 8-d and FGF-4 & 8+d showed significant difference at day 2 ($p<0.0005$), day 5 ($p<0.00001$), day 10 ($p<0.0005$), day 20 ($p<0.00001$) and day 40 ($p<0.00001$). FGF-4, 6 & 8 –d and FGF-4, 6 & 8+d significant difference was observed at day 20 ($p<0.05$) and day 40 ($p<0.001$) (Figure 3.22)

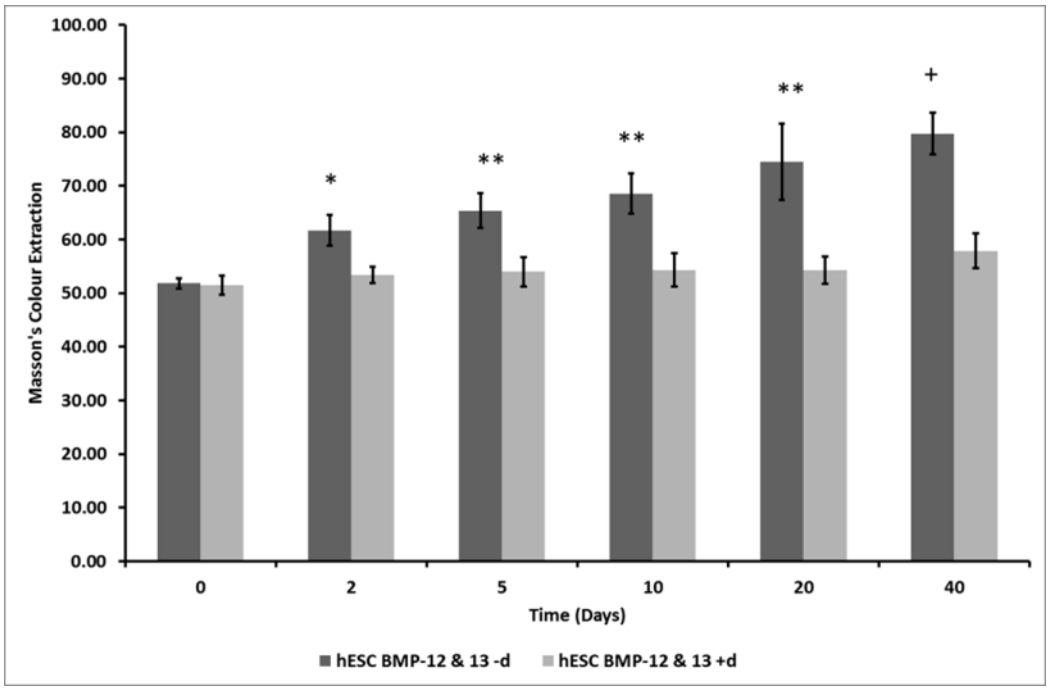

Figure 0.22 Masson's Trichrome analysis of hESC supplemented with BMP-12 & 13 differentiation media in the presence and absence of Dorsomorphin

hESC cultured using differentiation media supplemented with BMP-12 and 13 (Vitamin C) and differentiation media supplemented with BMP-12 and 13 (Vitamin C) and Dorsomorphin cultured for 40 days (*p<0.0005, **p<0.00001 and +p<0.001).

When hESC differentiation media was supplemented with FGF-4 & 8, an initial day 0 value for Masson's Trichrome colour extraction of 52.67±3.13 was observed. By day 2 this value had increased to 61.23±1.99 with further increases observed on day 5 (64.79±2.52), day 10 (69.30±4.21), day 20 (75.17±4.96) and day 40 (77.89±1.92).

Conversely, hESC differentiation media was supplemented with FGF-4 & 8 and Dorsomorphin, an initial day 0 value for Masson's Trichrome colour extraction of 52.57±3.66 was observed. By day 2 this value had increased to 52.49±1.49 with further increases observed on day 5 (52.97±1.62), day 10 (53.50±4.21), day 20 (54.24±2.44) and day 40 (56.75±1.87).

On statistically testing hESC cultured in differentiation media supplemented with FGF-4 & 8 and Vitamin C against hESC cultured in differentiation media supplemented with FGF-4 & 8, Vitamin C and Dorsomorphin. Revealed a significant difference at all time points from Day 2 days through to 40 days where the absence of Dorsomorphin had significantly higher level of Masson's Trichrome staining which implies increased collagen formation (Figure 3.23).

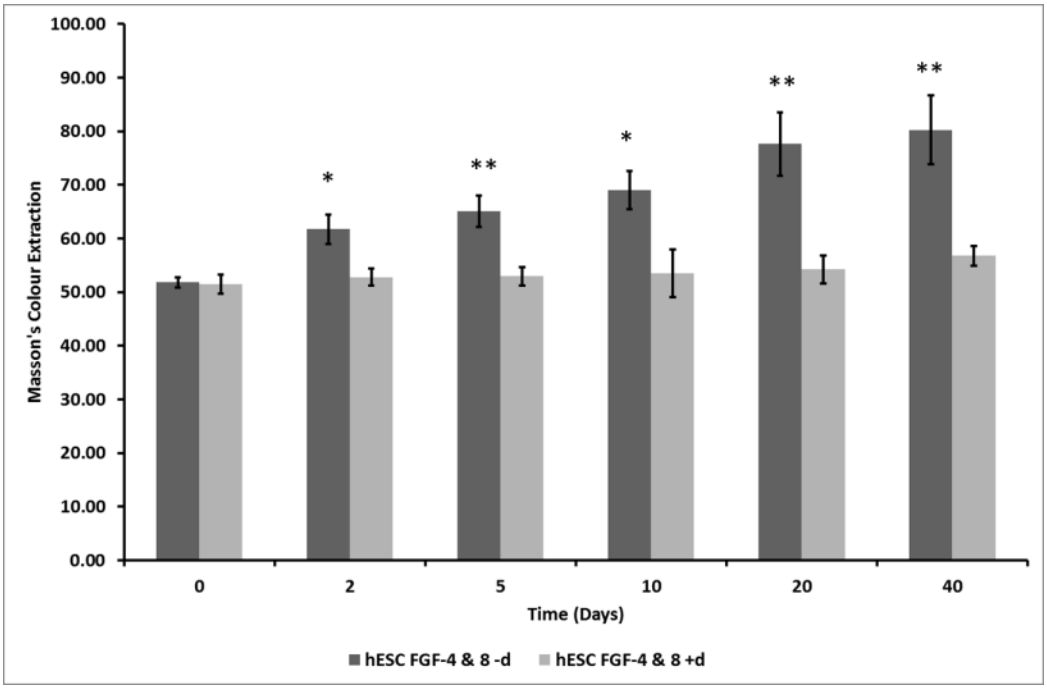

Figure 0.23 Masson's Trichrome analysis of hESC supplemented with FGF-4 & 8 differentiation media in the presence and absence of Dorsomorphin

hESC cultured using differentiation media supplemented with FGF-4 & 8 (Vitamin C) and differentiation media supplemented with FGF-4 & 8 (Vitamin C) and Dorsomorphin cultured for 40 days (*p<0.0005, **p<0.00001).

hESC cultured in differentiation media supplemented with FGF-4, 6 & 8 had an initial day 0 Masson's Trichrome value of 52.77±3.31. Which increased further on: day 2 (56.58±6.85), with further increases on Day 5 (66.56±3.18), day 10 (69.62±3.70), day 20 (79.24±5.00) and day 40 (86.62±2.27) (Figure 4.21).

Conversely, hESC cultured in differentiation media supplemented with FGF-4, 6 & 8 and Dorsomorphin had an initial day 0 Masson's Trichrome value of 52.57±3.66. Which increased further on: day 2 (54.59±2.22), with further increases on Day 5 (64.55±5.23), day 10 (68.72±5.44), day 20 (73.54±6.56) and day 40 (74.98±6.22) (Figure 3.24).

On statistically testing hESC cultured in differentiation media supplemented with FGF-4, 6 & 8 and Vitamin C against hESC cultured in differentiation media supplemented with FGF-4, 6 & 8, Vitamin C and Dorsomorphin. Revealed a significant difference at time points 20 days and 40 days where the absence of Dorsomorphin had significantly higher level of Masson's Trichrome staining which implies a increased collagen formation (Figure 3.24).

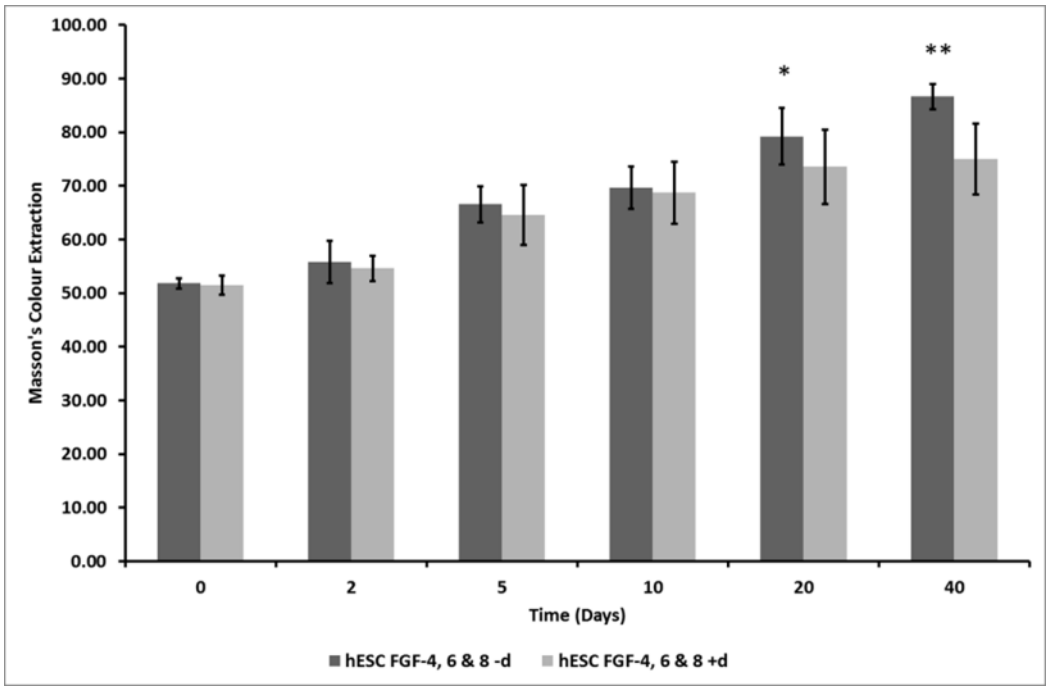

Figure 0.24 Masson's Trichrome analysis of hESC supplemented with FGF-4, 6 & 8 differentiation media in the presence and absence of Dorsomorphin

hESC cultured using differentiation media supplemented with FGF-4, 6 & 8 (Vitamin C) and differentiation media supplemented with FGF-4, 6 & 8 (Vitamin C) and Dorsomorphin cultured for 40 days (*p<0.005, **p<0.00005).

Further statistical testing was undertaken by comparing BMP-12 & 13-d against both FGF-4 & 8-d and FGF-4, 6 & 8-d, and also testing FGF-4 & 8-d against FGF-4, 6 & 8-d. On testing BMP-12 & 13 –d against FGF-4 & 8-d, no significant difference was observed. Conversely on testing BMP-12 & 13-d with FGF-4, 6 & 8-d significant difference was observed at day

40 ($p<0.05$). FGF-4 & 8-d testing against FGF-4, 6 & 8-d produced significant difference at Day 40 ($p<0.05$) (Figure 3.25).

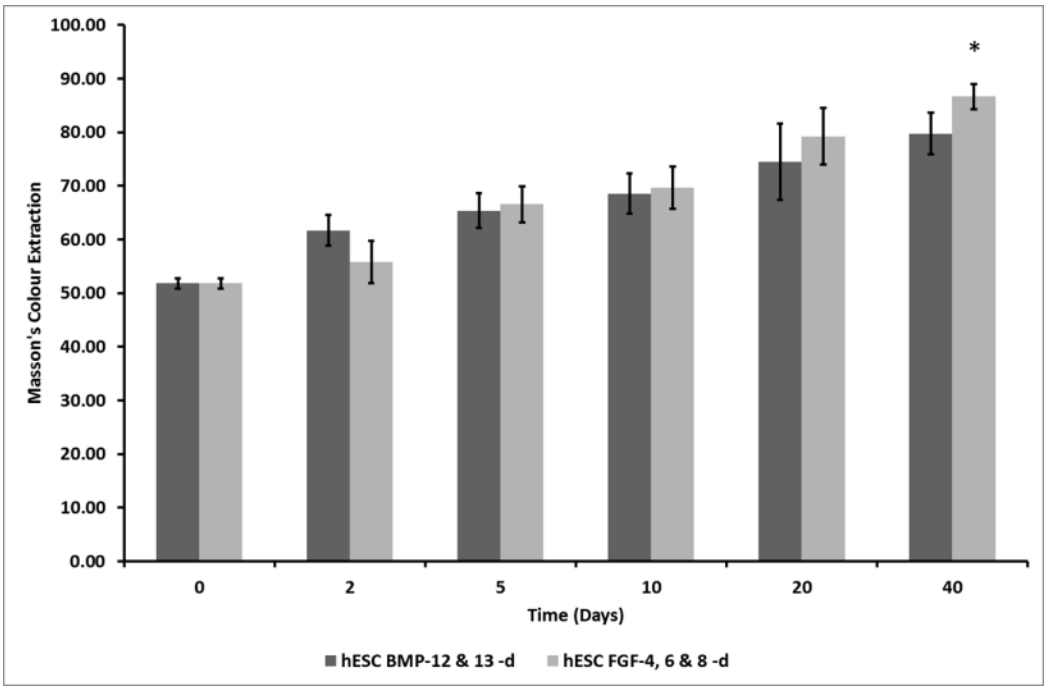

Figure 0.25 Masson's Trichrome analysis of hESC supplemented with FGF-4, 6 & 8 and BMP12 & 13 differentiation media in the and absence of Dorsomorphin

hESC cultured using differentiation media supplemented with BMP-12 & 13 (Vitamin C) and differentiation media supplemented with FGF-4, 6 & 8 (Vitamin C) cultured for 40 days (*$p<0.05$).

Further statistical testing was undertaken by comparing BMP-12 & 13+d against both FGF-4 & 8+d and FGF-4, 6 & 8+d, and also testing FGF-4 & 8+d against FGF-4, 6 & 8+d. On testing BMP-12 & 13+d against FGF-4 & 8+d, no significant difference was observed. Conversely on testing BMP-12 & 13+d with FGF-4, 6 & 8+d significant difference was observed at: day 5 ($p<0.005$), day 10 ($p<0.0005$), day 20 ($p<0.0005$) and day 40 ($p<0.0005$). FGF-4 & 8+d testing against FGF-4, 6 & 8+d produced significant difference on day 5 ($p<0.005$), day 10 ($p<0.0005$), day 20 ($p<0.0005$) and day 40 ($p<0.0005$) (Figure 3.26).

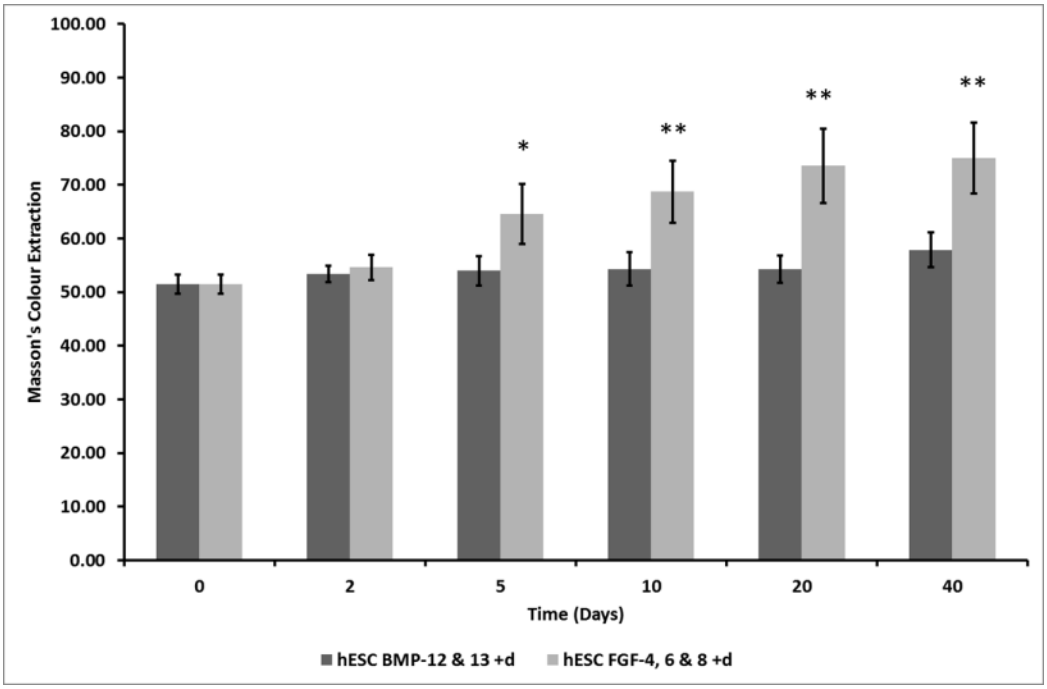

Figure 0.26 Masson's Trichrome analysis of hESC supplemented with FGF-4, 6 & and BMP12 & 13 differentiation media in the and presence of Dorsomorphin

hESC cultured using differentiation media supplemented with BMP-12 & 13 (Vitamin C) and Dorsomorphin differentiation media supplemented with FGF-4, 6 & 8 (Vitamin C) and Dorsomorphin cultured for 40 days (*p<0.005 and **p<0.0005).

On statistically testing FGF-4 & 8 and FGF-4,6 & 8 in the absence of Dorsomorphin revealed Masson's Trichrome stain to be higher at day 2 for FGF-4 & 8 (Figure 4.24)($p<0.05$). Conversely on day 40, FGF-4,6 & 8 in the absence of Dorsomorphin had a higher Masson's Trichrome staining ($p<0.05$) (Figure 3.27).

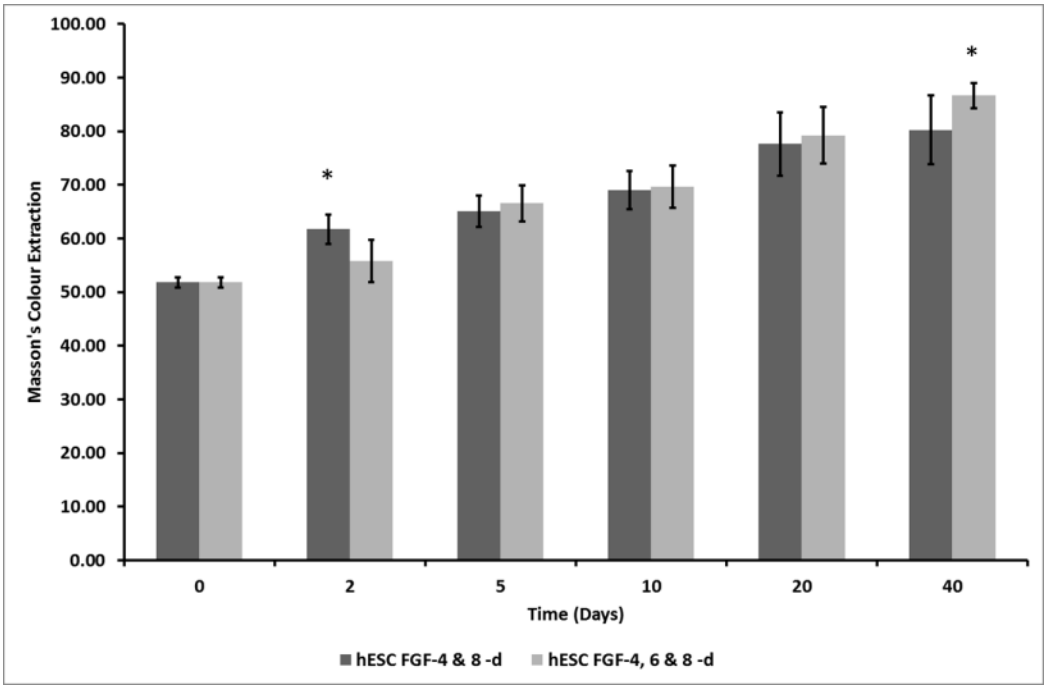

Figure 0.27 Masson's Trichrome analysis of hESC supplemented with FGF-4 & 8 and FGF-4,6 & 8 differentiation media in the absence of Dorsomorphin.

hESC cultured using differentiation media supplemented with FGF-4 & 8 (Vitamin C) and differentiation media supplemented with FGF-4, 6 & 8 (Vitamin C) cultured for 40 days (*p<0.005).

Further statistical analysis revealed that from Day 5 through to day 40 that a higher level of collagen staining was observed in FGF-4, 6 & 8 samples than in FGF-4 and 8 when both differentiation media contained Dorsomorphin ($p<0.005$ and $p<0.0005$) (Figure 3.28)

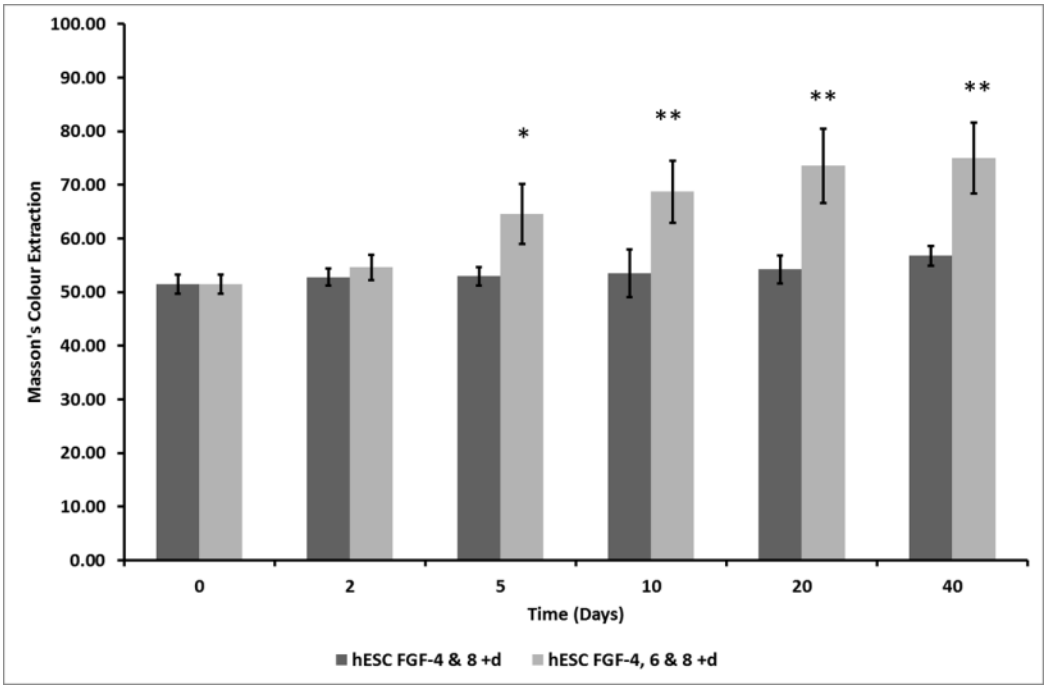

Figure 0.28 Masson's Trichrome analysis of hESC supplemented with FGF-4 & 8 and FGF-4,6 & 8 differentiation media in the presence of Dorsomorphin.

hESC cultured using differentiation media supplemented with FGF-4 & 8 (Vitamin C and Dorsomorphin) and differentiation media supplemented with FGF-4, 6 & 8 (Vitamin C and Dorsomorphin) cultured for 40 days (*p<0.005 and **p<0.0005).

3.6.6.2 Alcian Blue Staining

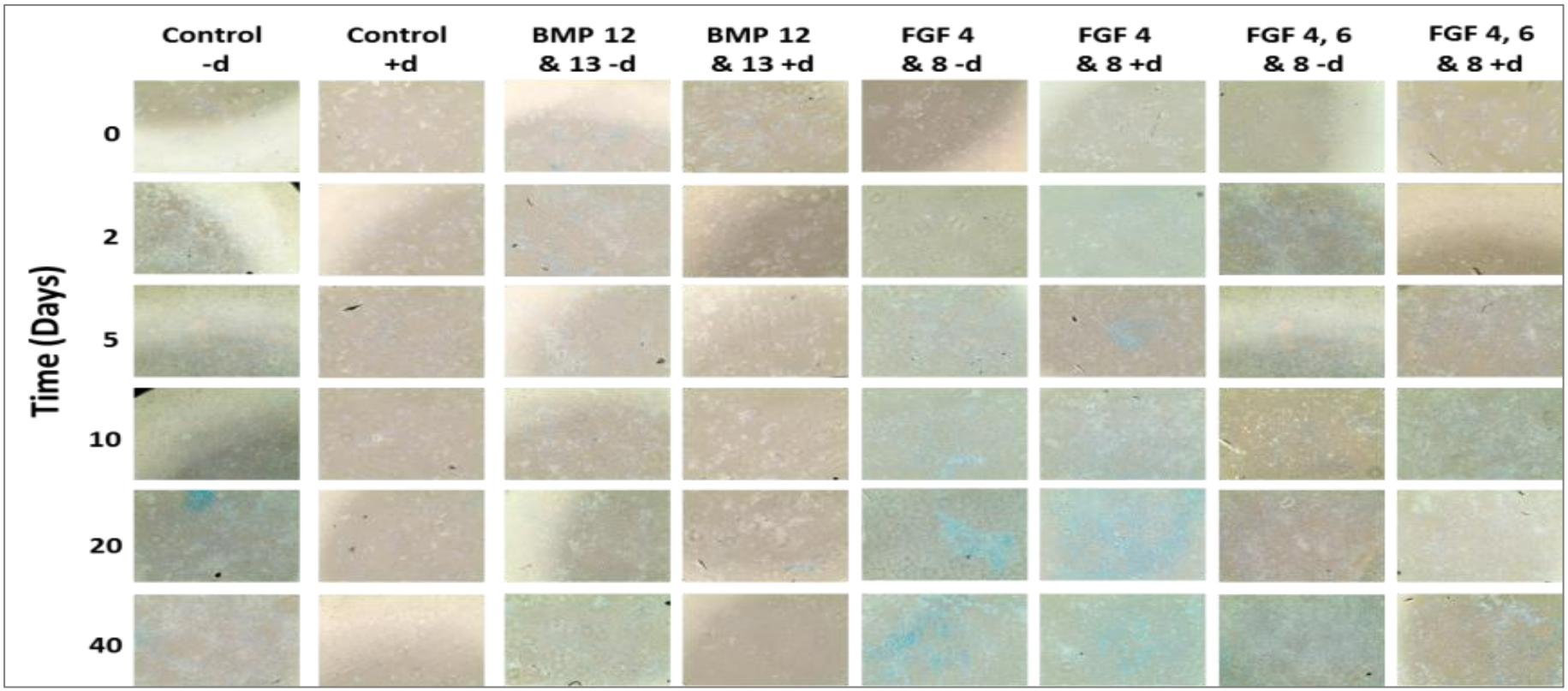

Figure 0.29 Alcian Blue staining for each group of Shef-1 over 40 Days.

All groups showed Alcian Blue staining. All time points (n=9) were analysed and data extracted from the images. From the data extracted each time point for each condition was compared and statistically tested and the data is shown in Table 3.9.

Time (Days)	hESC Control -d	hESC Control +d	hESC BMP-12&13 -d	hESC BMP-12&13 +d	hESC FGF-4 & 8 -d	hESC FGF-4 & 8 +d	hESC FGF-4,6 & 8 -d	hESC FGF-4,6 & 8 +d
0	39.94	40.42	41.70	40.00	39.67	39.98	39.98	40.01
	±0.63	±0.79	±1.20	±0.64	±0.75	±0.36	±0.63	±0.72
2	43.41	40.42	47.45	42.93	46.32	44.37	47.13	44.70
	±0.36	±0.91	±1.28	±0.44	±0.43	±0.60	±0.72	±0.58
5	44.56	40.30	50.53	45.08	47.89	46.01	48.77	47.31
	±0.48	±0.47	±0.67	±0.58	±0.50	±0.23	±1.04	±1.03
10	45.90	40.44	52.01	46.52	49.40	47.14	51.27	49.63
	±0.32	±0.78	±0.37	±0.67	±0.76	±1.36	±0.64	±0.27
20	47.02	40.60	52.97	47.89	50.36	49.15	54.59	51.04
	±0.53	±0.84	±0.27	±1.45	±0.50	±0.30	±0.69	±0.62
40	48.48	40.58	56.36	50.44	52.48	51.30	58.79	54.90
	±1.13	±1.11	±2.04	±0.64	±0.72	±0.62	±1.78	±1.82

Table 0.9 Alcian Blue data extraction from Image J for human Embryonic Stem cells (SHEF-1)

The data shown is obtained from Image J and is Alcian blue colour extraction of images taken from growth factor driven differentiation.

From the data shown in Table 3.9 the following observations were made:

hESC cultured in differentiation media had an Alcian blue colour extraction value of 39.94±0.63 on day 0, which decreased by day 2 (43.41±0.36). A slight increase in value was observed by day 5 (44.56±0.48), with further decreased at day 10 (45.90±0.32), an increase on day 20 (47.02±0.53) and a subsequent decrease on Day 40 (48.48±1.13) (Figure 3.30).

hESC cultured in differentiation media supplemented with Dorsomorphin had a Alcian Blue colour extraction value of 40.42±0.79 on day 0, which decreased slightly by day 2 (40.42±0.91). A slight in value was observed by day 5 (40.30±0.47), with an increase at day 10 (40.44±0.78), with continued increase on day 20 (40.60±0.84) and a subsequent decrease on Day 40 (40.58±1.11) (Figure 3.30

Statistical testing between Control differentiation media against control differentiation media plus Dorsomorphin showed significant difference between Control-d and Control

+d: Day 2 (p<0.0001), day 5 (p<0.0001), day 5 (p<0.0001), day 20 (p<0.0005) and day 40 (p<0.0005) time points (Figure 3.30).

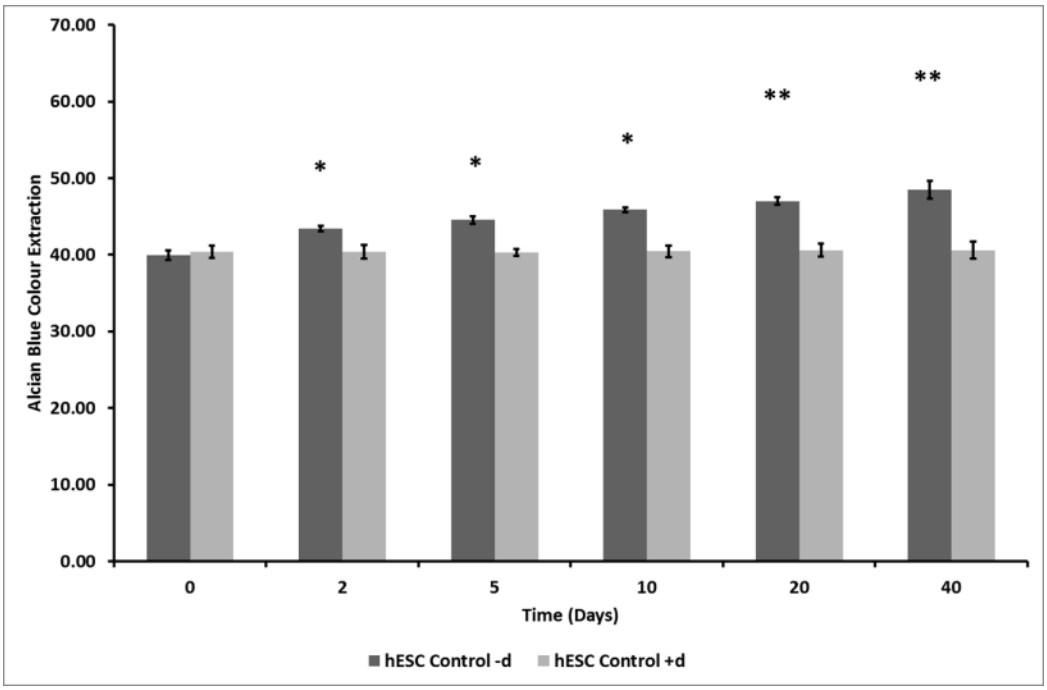

Figure 0.30 *Alcian Blue analysis of hESC supplemented with control differentiation media in the presence and absence of Dorsomorphin*

hESC cultured using differentiation media and differentiation media supplemented with Dorsomorphin over 40 days (*p<0.0001 and **p<0.0005).

Further supplementation of differentiation media with BMP-12 & 13 produced Alcian Blue colour extraction value of 41.70±1.20 at day 0. Which on day 2 had a value of (47.45±01.28) and on day 5 (50.53±0.67).a further increase was observed on day 10 (52.01±0.37) and day 20 reporting a further increase (52.97±0.27) and day 40 showing a slight decrease (56.36±2.04).

Further supplementation of differentiation media with BMP-12 & 13 and Dorsomorphin produced Alcian Blue colour extraction value of 40.00±0.64 at day 0. Which an increase on day 2 (42.93±0.44) and increase on day 5 (45.08±0.58).a further increase was observed

on day 10 (46.52±0.67) and day 20 increased values to day 10 (47.89±1.45) and day 40 showing a slight increase 50.44±0.64).

Further testing of BMP-12 & 13 –d and BMP-12 & 13 +d showed significant difference at day 2 ($p<0.00001$), day 5 ($p<0.00001$), day 10 ($p<0.00001$), day 20 ($p<0.00005$) and day 40 ($p<0.00005$

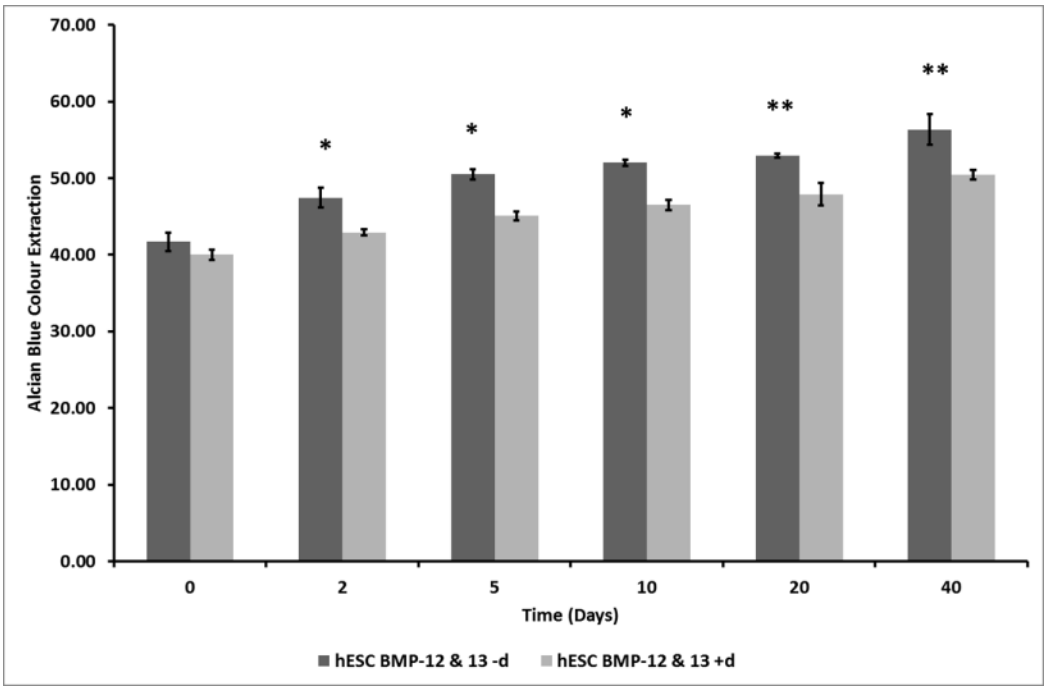

Figure 0.31 Alcian Blue analysis of hESC supplemented with control ifferentiation media Supplemented with BMP-12 & 13 in the presence and absence of Dorsomorphin.

hESC cultured using differentiation media and differentiation media supplemented with BMP-12 & 13 and Dorsomorphin over 40 days (*p<0.00001 and **p<0.00005).

When hESC differentiation media was supplemented with FGF-4 & 8, an initial day 0 value for Alcian Blue colour extraction of 39.67±0.75 was observed. By day 2 this value had increased to 46.32±0.43 with further increases observed on day 5 (47.59±0.50), day 10 (49.40±0.76), day 20 (50.36±0.50) and day 40 (52.48±0.72).

When hESC differentiation media was supplemented with FGF-4 & 8 and Dorsomorphin, an initial day 0, value for Alcian Blue colour extraction of 39.98±0.36 was observed. By day 2 this value had increased to 44.37±0.60 with further increases observed on day 5 (46.01±0.23), day 10 (47.14±1.36), day 20 (49.15±0.30) and day 40 (51.30±0.62).

On statistically testing FGF-4 & 8-d and FGF-4 & 8+d showed significant difference with a decrease in Alcian Blue staining in Dorsomorphin supplemented media at day 2 ($p<0.00005$), day 5 ($p<0.01$), day 10 ($p<0.00005$), day 20 ($p<0.00005$) and day 40 ($p<0.005$).

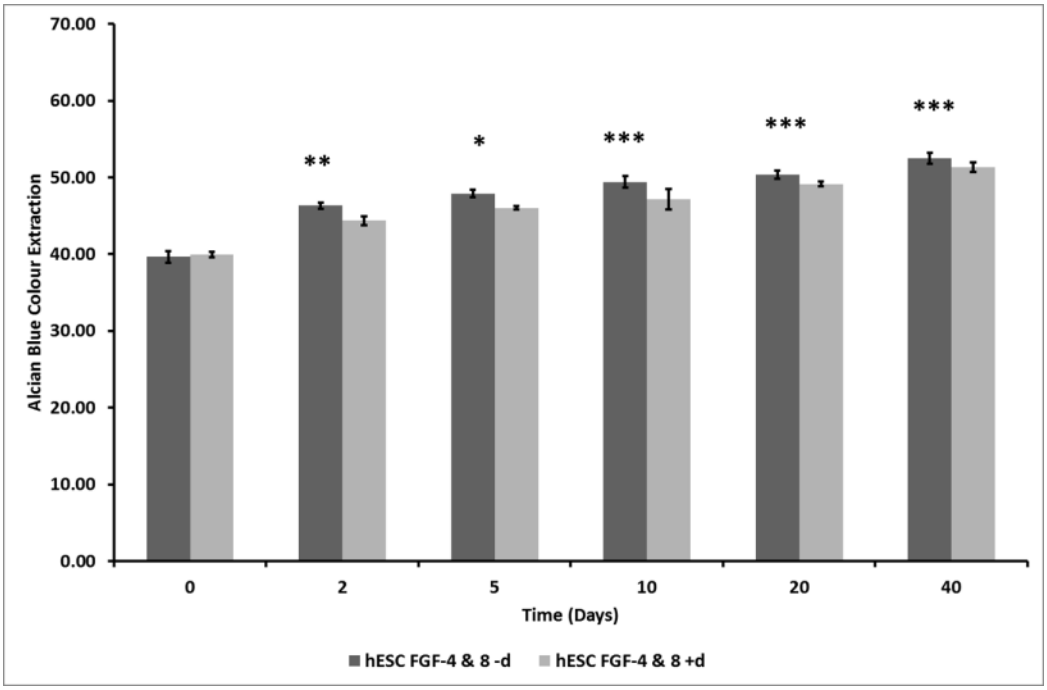

Figure 0.32 Alcian Blue analysis of hESC supplemented with control differentiation media Supplemented with FGF-4 & 8 in the presence and absence of Dorsomorphin.

hESC cultured using differentiation media and differentiation media supplemented with FGF-4 & 8 and Dorsomorphin over 40 days (*p<0.00005, **p<0.01 and ***p<0.05).

hESC cultured in differentiation media supplemented with FGF-4, 6 & 8 had an initial day 0 Alcian Blue value of 39.98±0.63. Which increased further on: day 2 (47.13±0.72), with further increases on Day 5 (48.77±1.04), day 10 (51.27±0.64), day 20 (54.59±0.69) and day 40 (58.79±1.78).

hESC cultured in differentiation media supplemented with FGF-4, 6 & 8 and Dorsomorphin had an initial day 0 Alcian Blue value of 40.01±0.72. Which increased further on: day 2 (44.70±0.58), with further increases on Day 5 (47.31±1.03), day 10 (49.63±0.27), day 20 (51.04±0.62) and day 40 (54.90±61.82).

On statistically testing FGF-4, 6 & 8 –d and FGF-4, 6 & 8+d significant difference with a decrease in Alcian Blue staining in Dorsomorphin supplemented media was observed at day 2 ($p<0.0005$), day 5 ($p<0.01$), day 10 ($p<0.0005$), day 20 ($p<0.00001$) and day 40 ($p<0.00005$)

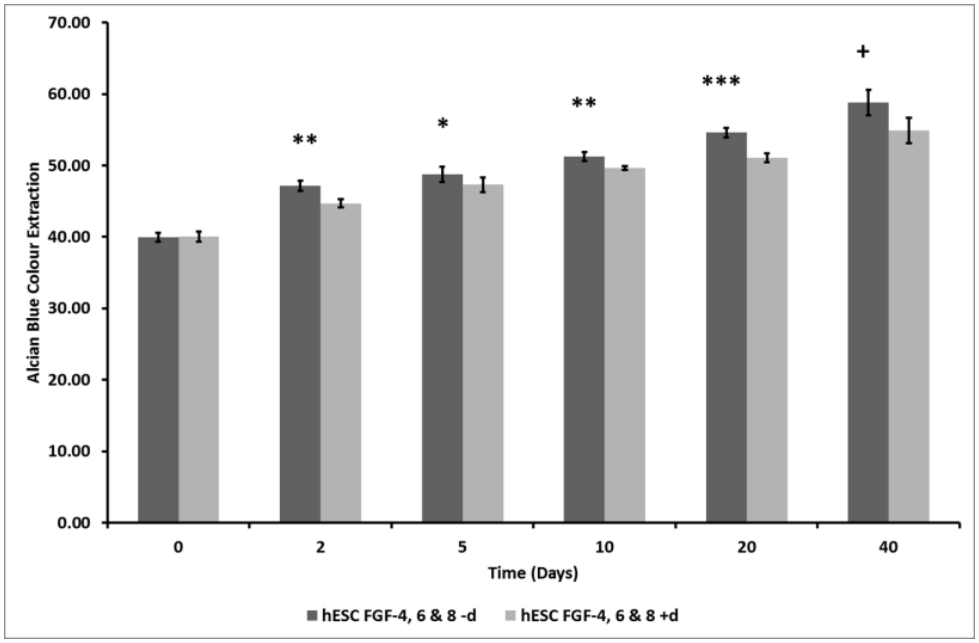

Figure 0.33 Alcian Blue analysis of hESC supplemented with control differentiation media Supplemented with FGF-4 & 8 in the presence and absence of Dorsomorphin.

hESC cultured using differentiation media and differentiation media supplemented with FGF-4 & 8 and Dorsomorphin over 40 days (*p<0.01, **p<0.0005,*p<0.0001 & +p<0.0005).**

Further statistical testing was undertaken by comparing BMP-12 & 13-d against both FGF-4 & 8-d (Figure 3.34) and FGF-4, 6 & 8-d (Figure 3.35), and also testing FGF-4 & 8-d against FGF-4, 6 & 8-d (Figure 3.36). On testing between groups produced significant difference ($p<0.05$)

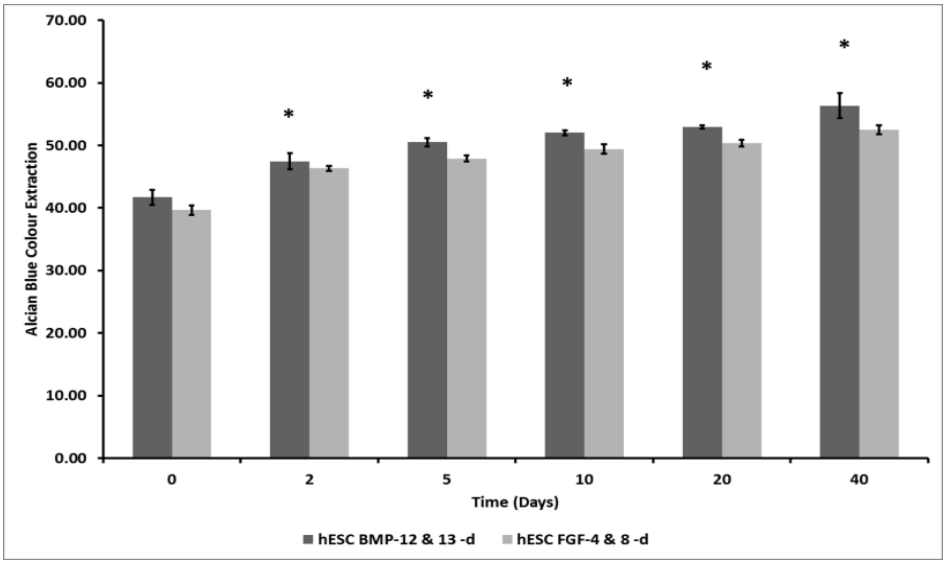

Figure 0.34 Alcian Blue analysis of hESC supplemented with FGF-4& 8 and BMP12 & 13 differentiation media in the and absence of Dorsomorphin

hESC cultured using differentiation media supplemented with BMP-12 & 13 (Vitamin C) and differentiation media supplemented with FGF-4 & 8 (Vitamin C) cultured for 40 days (*p<0.05).

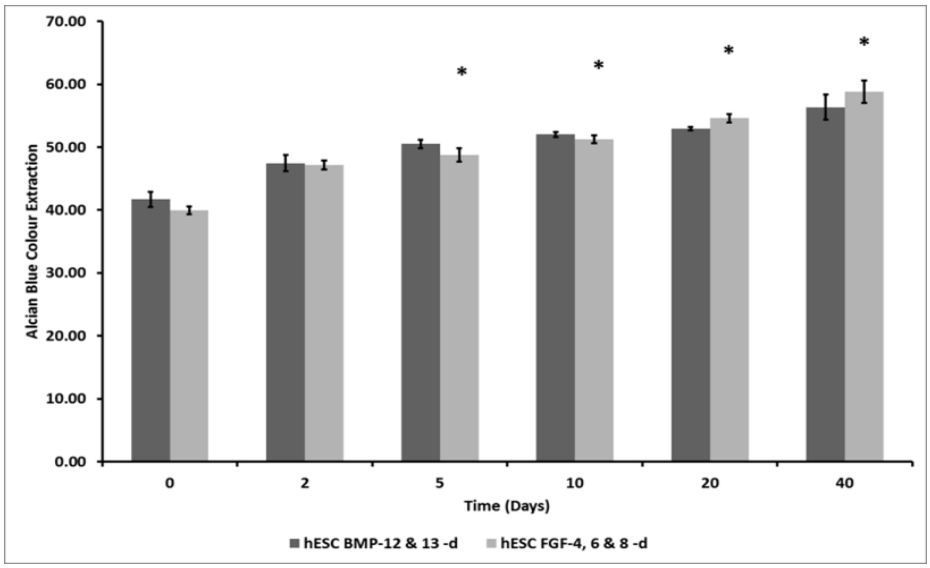

Figure 0.35 Alcian Blue analysis of hESC supplemented with FGF-4, 6 & 8 and BMP12 & 13 differentiation media in the and absence of Dorsomorphin

hESC cultured using differentiation media supplemented with BMP-12 & 13 (Vitamin C) and differentiation media supplemented with FGF-4, 6 & 8 (Vitamin C) cultured for 40 days (*p<0.05).

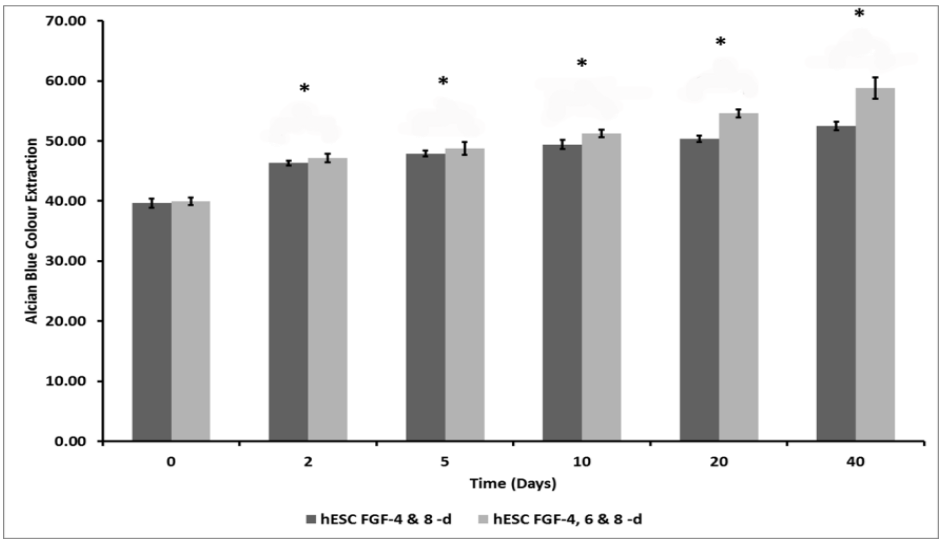

Figure 0.36 Alcian Blue analysis of hESC supplemented with FGF-4 & 8 and FGF-4, 6 & 8 differentiation media in the and absence of Dorsomorphin

hESC cultured using differentiation media supplemented with FGF-4 & 8 (Vitamin C) and differentiation media supplemented with FGF-4, 6 & 8 (Vitamin C) cultured for 40 days (*p<0.05).

Further statistical testing was undertaken by comparing BMP-12 & 13+d against, both FGF-4 & 8+d (Figure 3.37) and FGF-4, 6 & 8+d (Figure 3.38), and also testing FGF-4 & 8+d against FGF-4, 6 & 8+d (Figure 3.39). On statistically testing BMP-12 & 13 –d against FGF-4 & 8-d, significant difference was observed on Day 2 ($p<0.0005$), Day 5 ($p<0.005$), day 20 ($p<0.05$) and day 40 ($p<0.01$). On testing BMP-12 & 13-d with FGF-4, 6 & 8-d significant difference was observed at day 2, Day 5, Day10, Day 20 and day 40 ($p<0.001$). FGF-4 & 8-d testing against FGF-4, 6 & 8-d produced significant difference on day 5, day 10, day 20 and day 40 ($p<0.05$).

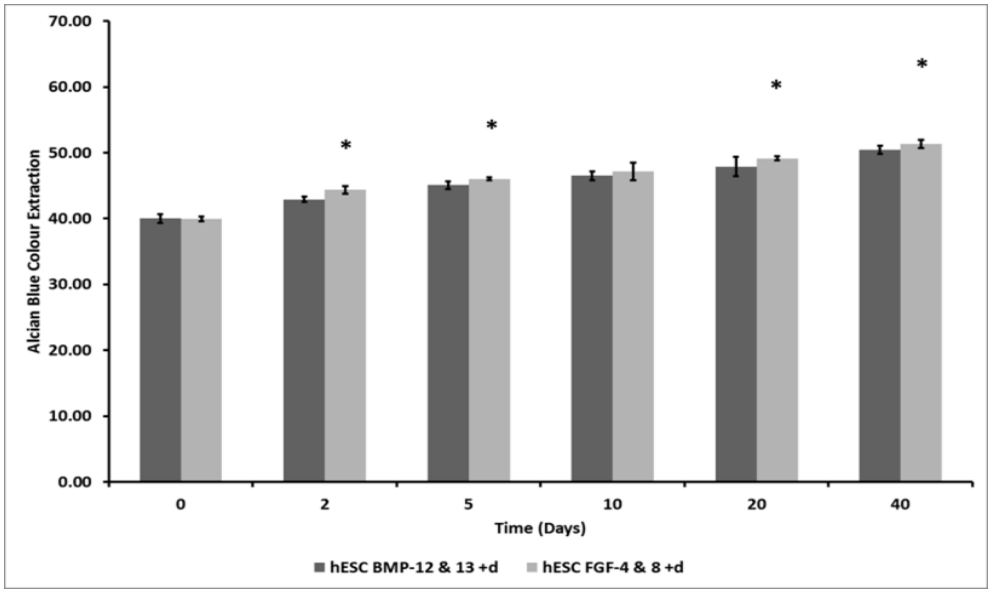

Figure 0.37 Alcian Blue analysis of hESC supplemented with BMP-12 & 13 and FGF-4 & 8 differentiation media in the presence of Dorsomorphin

hESC cultured using differentiation media supplemented with BMP-12 & 13 (Vitamin C) and differentiation media supplemented with FGF-4 & 8 (Vitamin C) cultured for 40 days (*p<0.05).

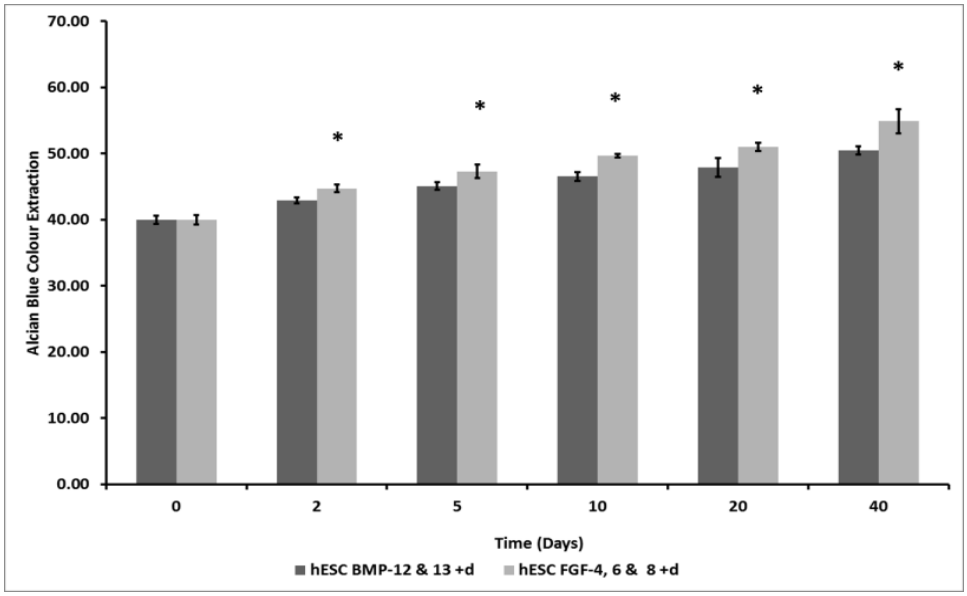

Figure 0.38 Alcian Blue analysis of hESC supplemented with BMP-12 & 13 and FGF-4, 6 & 8 differentiation media in the presence of Dorsomorphin

hESC cultured using differentiation media supplemented with BMP-12 & 13 (Vitamin C) and differentiation media supplemented with FGF-4, 6 & 8 (Vitamin C) cultured for 40 days (*p<0.05).

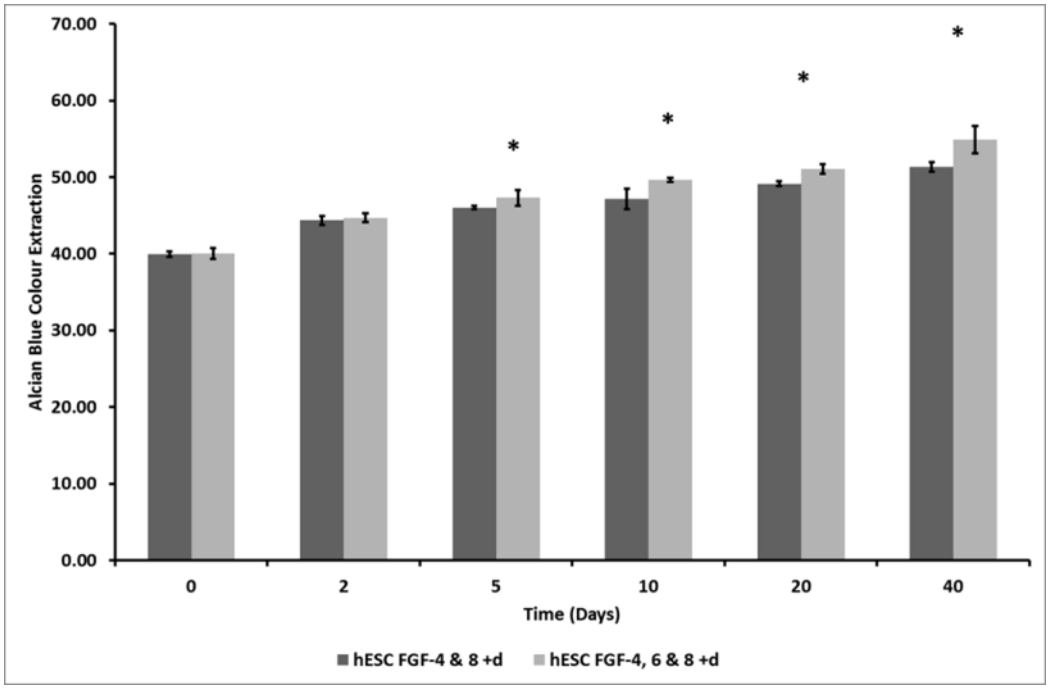

Figure 0.39 Alcian Blue analysis of hESC supplemented with FGF-4 & 8 and FGF-4, 6 & 8 differentiation media in the presence of Dorsomorphin

hESC cultured using differentiation media supplemented with FGF-4 & 8 (Vitamin C) and differentiation media supplemented with FGF-4, 6 & 8 (Vitamin C) cultured for 40 days (*p<0.05).

Statistical testing was undertaken by comparing growth factor supplemented groups against the control groups (Figure 3.40). Statistical difference was observed with all growth factor supplemented groups from day 2 ($p<0.00005$), day 5 ($p<0.00005$), day 10 ($p<0.00005$), day 20 ($p<0.00005$) and day 40 ($p<0.00005$) with FGF-4, 6 & 8 combination having the greatest significant difference on day 40 ($p<0.00001$).

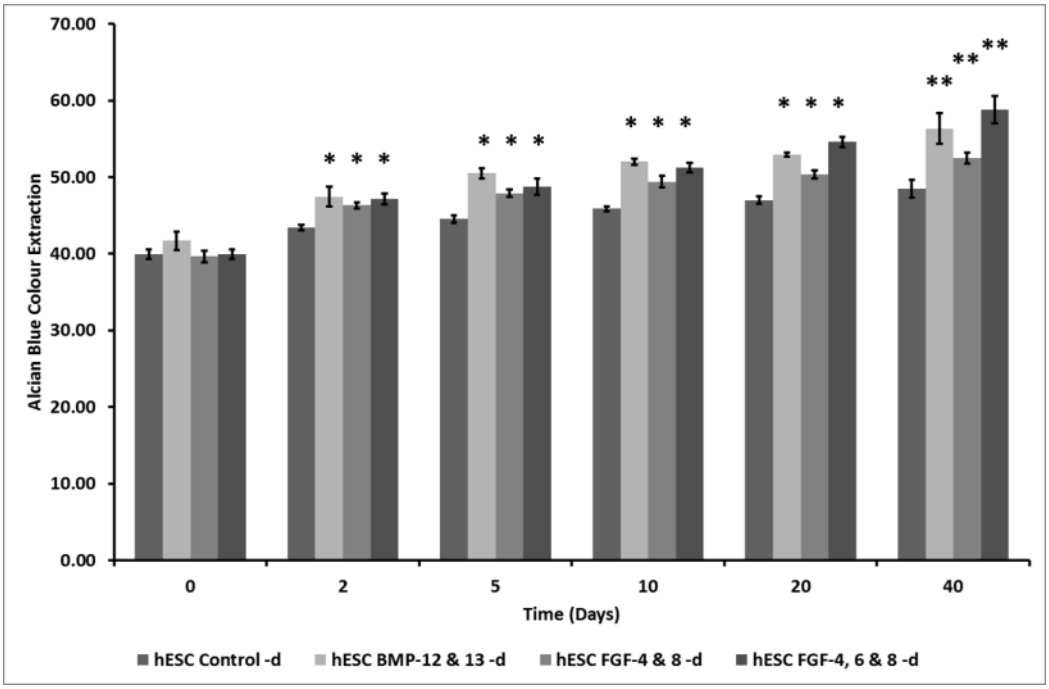

Figure 0.40 Alcian Blue colour extraction Comparison between all hESC cultured with growth factors and Vitamin C without Dorsomorphin

Comparisons were made against the control group (*p<0.00005 & **p<0.00001).

Statistical testing was undertaken by comparing growth factor supplemented groups against the control groups. Statistical difference was observed with all growth factor supplemented groups from day 2 ($p<0.00005$), day 5 ($p<0.00005$), day 10 ($p<0.00005$), day 20 ($p<0.00005$) and day 40 ($p<0.00005$), with FGF-4, 6 & 8 combination having the greatest significant difference on day 40 ($p<0.00001$).

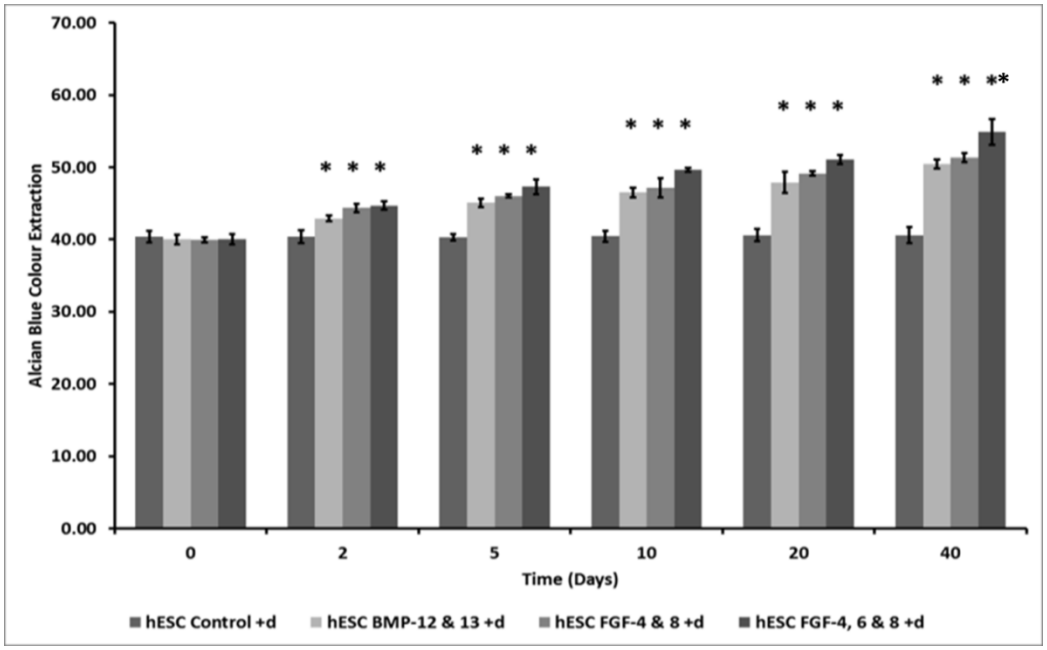

Figure 0.41 Alcian Blue colour extraction Comparison between all hESC cultured with growth factors and Vitamin C with Dorsomorphin

Comparisons were made against the control group (*p<0.00005 & **p<0.00001).

3.7 hMSC Characterisation

3.7.1 Immunocytochemistry Profiling of hMSC Markers (BMA-12)

hMSC were isolated from bone marrow aspirate following the previously described methodology [332, 333] (Section 3.2.5). Prior to experimentation, the phenotypic surface markers of hMSC were confirmed by immunocytochemistry (Section- 3.4.1). The hMSC surface markers were detected on passage-1 cells. Isolated hMSC were positive for surface antigens CD44, CD90, CD146, STRO-1 and negative for haematopoietic markers CD14 and CD19 (Figure 3.42).

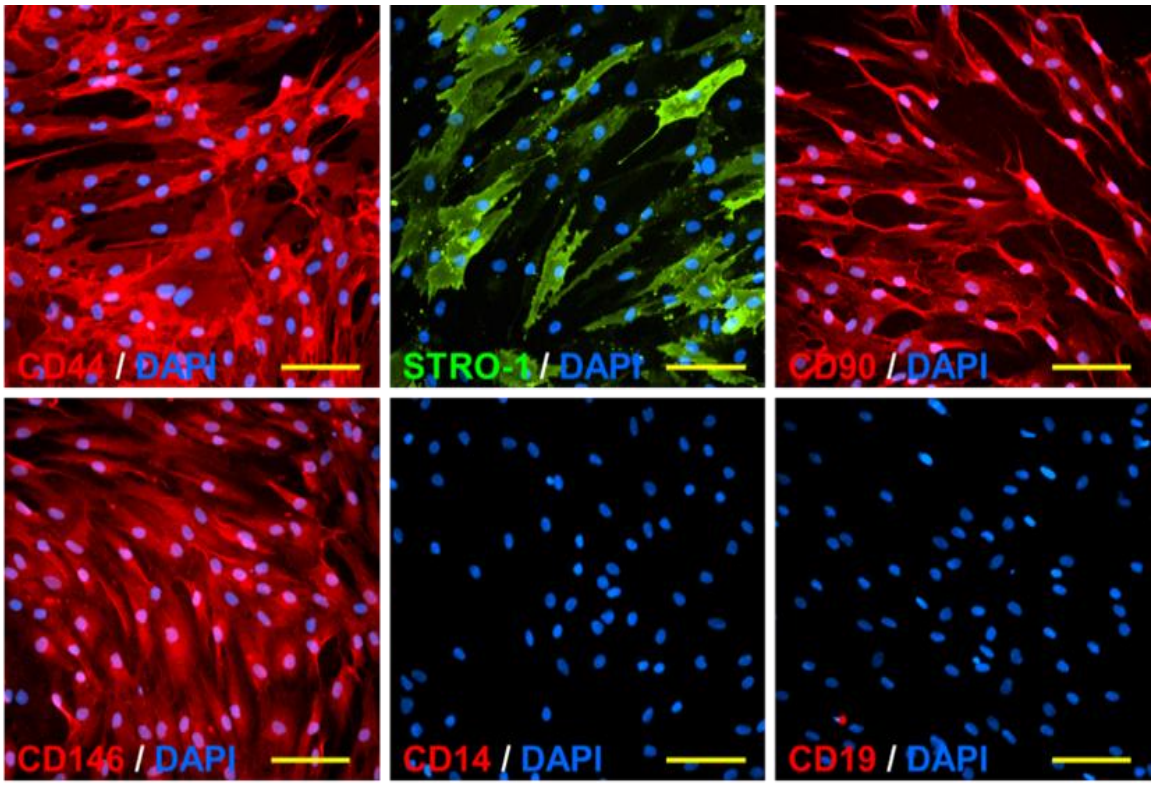

Figure 0.42 Immunophenotyping of hMSC

hMSC showed positive expression of the surface antigens CD44, STRO-1, CD90 and CD146 and negative for the haemopoietic markers CD14 and CD19. DAPI was utilised as a nuclear counter stain. Scale bar 100µm.

3.8 Tenomodulin Expression

After identifying the BMA-12 (hMSCs) expressed hMSC markers the next phase of the investigation was to investigate the effects of FGF-4, FGF-6 and FGF-8 supplementation of differentiation media (DMEM supplemented with 10% FBS, 1% L-GLUT and 1% NEAA) in the presence and absence of Vitamin C (10µM) at two different oxygen environments (2% and 21%). SHEF-1 cells were seeded as shown in Section 3.2.6.

This phase of the investigation utilised the time points 0, 2, 5, 10 and 20 days for RT-PCR to detect the presence of Tenomodulin (a known tendon marker).

Preliminary hMSC RT-PCR showed. FGF-4 when cultured in the presence of Vitamin C and cultured at 2% O_2 was capable of maintaining TNMD expression from day 2 to day 20 (Figure 3.43). However, the expression post day 5, did appear to reduce. FGF-4, 6 & 8 when cultured at 2% O_2 and supplemented with Vitamin C were capable of sustaining TNMD gene expression in hMSCs (Figure 3.43) with no apparent reduction in expression. Conversely, FGF-4, FGF-6, FGF-8 FGF-4 & 6, FGF-4 & 8 and FGF-4, 6 & 8 when cultured for 20 days at 21% O_2 were incapable of sustaining TNMD gene expression in hESC when cultured in the presence or absence of Vitamin C (Figure 3.43 – Figure 3.44).

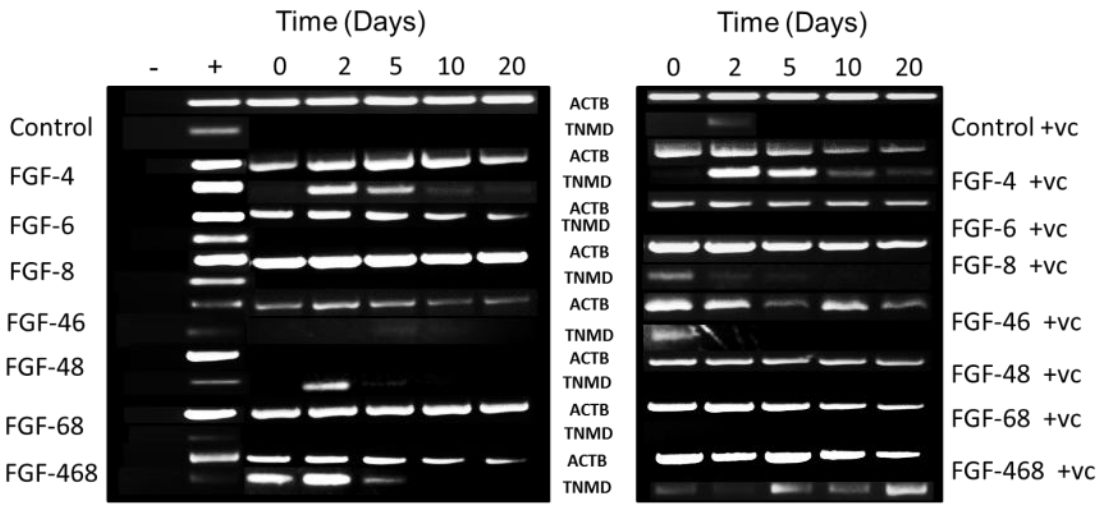

Figure 0.43 Tenomodulin expression of FGF driven differentiation of hMSC cultured at 2% O_2 supplemented with or without Vitamin C

RT-PCR analysis for Tenomodulin (TNMD) showed that combinations of FGF-4 and the combination of FGF-4, 6 & 8 induced and maintained the expression of TNMD for 20 days when supplemented with Vitamin C at 10µM per mL. FGF supplemented media which was not supplemented with Vitamin C was unable to initiate and subsequently maintain the expression of TNMD.

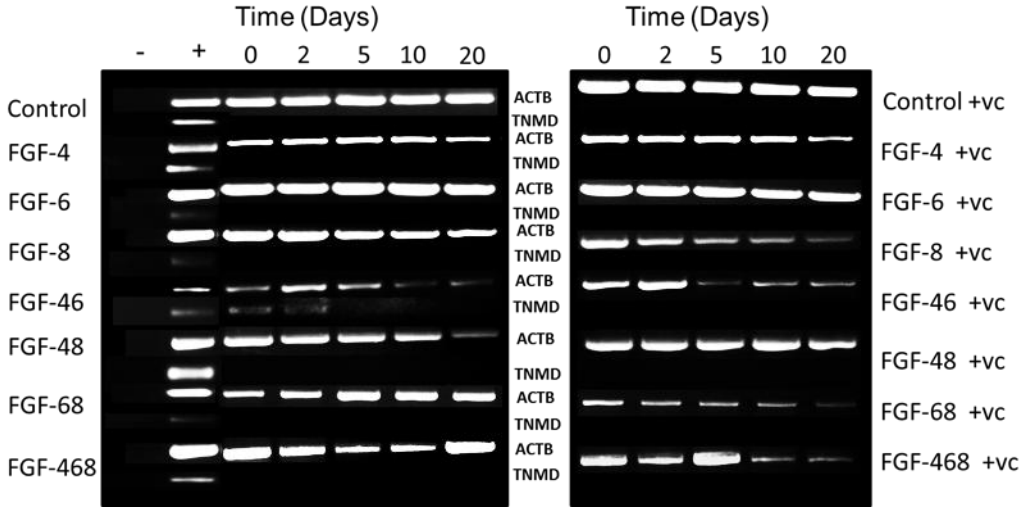

Figure 0.44 Tenomodulin expression of FGF driven differentiation of hMSC cultured at 21% O_2 supplemented with or without Vitamin C

FGF supplemented media with/without Vitamin C was unable to initiate transcription of TNMD when hESC's are cultured at 21% O_2.

Having now identified the FGF growth factor combination capable of initiating and maintaining TNMD expression the next phase was to be initiated. The next investigation was to identify the concentration of Dorsomorphin that allowed cell survival. Then supplement the FGF/Vitamin C differentiation media with Dorsomorphin.

3.8.1.1 Dorsomorphin Optimisation

BMA-12 cells were seeded to a 6 well plate as shown in Section 3.2.7 and cultured using CM+ (Conditioned embryonic stem cell media) supplemented with a range of Dorsomorphin concentrations (ranging from 1µM to 500µM) and cultured at 2% O_2 for 5 days and media change every 24 hours.

After 5 days had elapsed cells were fixed and stained with Giemsa's stain for analysis (Section 3.5.1).

The concentration to be used for investigation of Dorsomorphin inhibition of BMA-12 FGF driven differentiation was 1µM per ml (Figure 3.45). The concentration of 1µM per ml as this concentration impaired cellular proliferation whilst all higher concentrations were shown to have a toxic effect

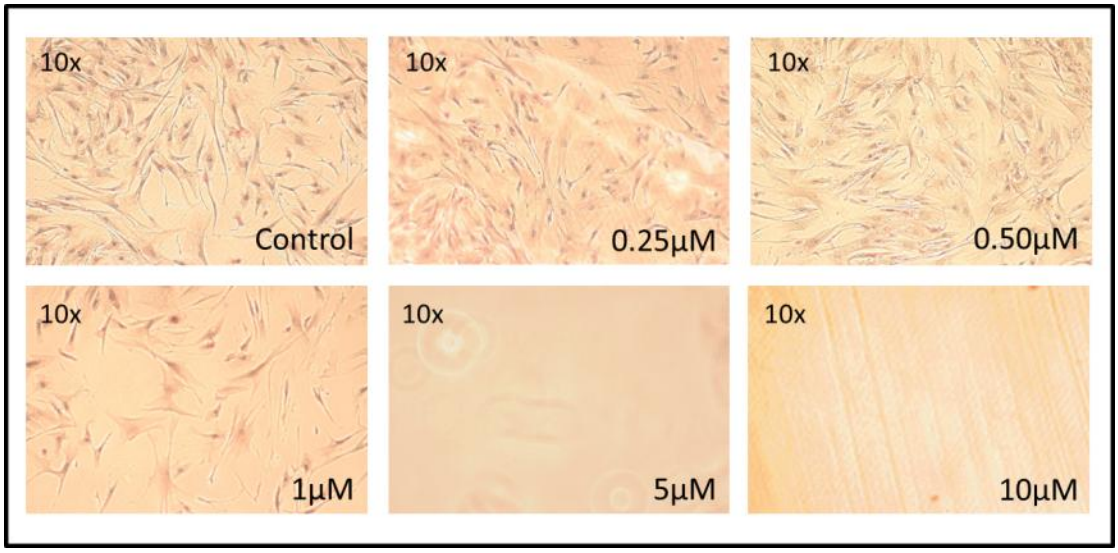

Figure 0.45 hMSC cultured in Dorsomorphin supplemented media at a range of concentrations.

Shows a range of concentrations of Dorsomorphin with concentrations in excess of 1um having a high level of cellular toxicity. Where a concentration of 1um showed reduced cellular proliferation, therefore, the concentration of 1uM was utilised in further investigations into the effects of FGF and BMP signal transduction using MSC human embryonic stem cells.

3.8.1.2 RT-PCR of Tendon markers for FGF driven differentiation of hMSC cultured with Vitamin C and Dorsomorphin at 2% O_2

hMSC (BMA-12) cultured in differentiation media supplemented with: FGF-4 and Vitamin C showed the presence of: THBS-4, TENC, COL1A2, COL3A1 and DCN throughout the 40 day investigation. Conversely, TNMD was detected up until day 20 and extremely weak detection at day 40. hMSC (BMA-12) cultured in differentiation media supplemented with: FGF-4, Vitamin C and Dorsomorphin showed the presence of: THBS-4, TENC, COL1A2, COL3A1 and DCN throughout the 40 day investigation. Conversely, TNMD was detected up until day 10, day 20 and 40 showed no transcription of TNMD (Figure 3.46).

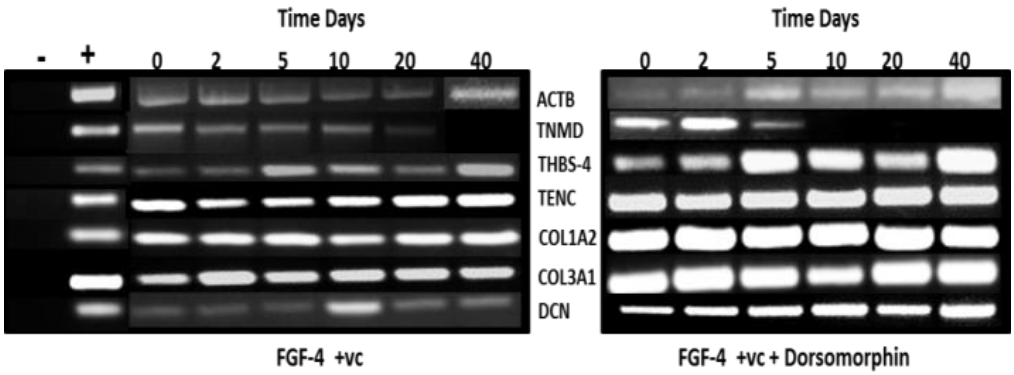

Figure 0.46 Tendon gene expression for hMSC FGF-4 driven differentiation when supplemented with and without Dorsomorphin at 2% O_2

Tendon gene expression panel for FGF-4 supplemented differentiation media with Vitamin with and without Dorsomorphin cultured at 2% O_2

hMSC (BMA-12) cultured in differentiation media supplemented with: FGF-4, 6 & 8 and Vitamin C showed the presence of: THBS-4, TENC,TNMD, COL1A2 and COL3A1 throughout the 40 day investigation. DCN was expressed from day 2 through to day 40 (Figure 3.47). hMSC (BMA-12) cultured in differentiation media supplemented with: FGF-4, 6 & 8, Vitamin C and Dorsomorphin showed the presence of: THBS-4, TENC,DCN, COL1A2 and COL3A1 throughout the 40 day investigation. TNMD was expressed from day 2 through to day 20, with day 10 and day 20 showing reduced expression and lack of expression on day 40 (Figure 3.47).

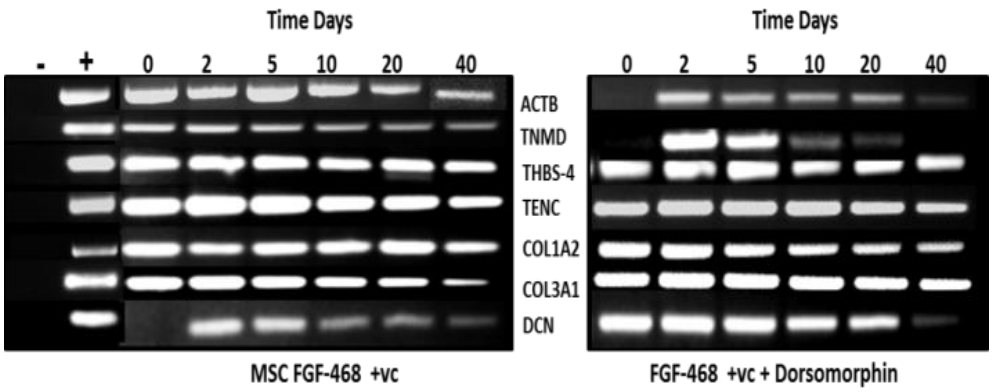

Figure 0.47 Tendon gene expression for hMSC FGF-4, 6 & 8 driven differentiation when supplemented with and without Dorsomorphin at 2% O_2

Tendon gene expression panel for FGF-4, 6 & 8 supplemented differentiation media with Vitamin with and without Dorsomorphin cultured at 2% O_2

Having now established the gene expression for both Dorsomorphin supplemented growth factor differentiation media. We then used immunocytochemistry to identify the expression of TNMD protein this phase of the investigation utilised TNMD Immunocytochemistry.

3.8.2 Immunocytochemistry

Immunocytochemistry was undertaken to detect the presence of tenomodulin protein expression after growth factor driven differentiation of hMSC. Also, to evaluate the effect of further supplementation of differentiation media with Dorsomorphin and its subsequent affect upon TNMD expression.

Prior to undertaking the immunocytochemistry staining for TNMD we looked at utilising rat tenocytes as a positive control.

3.8.2.1 Tenomodulin staining of hMSC

FGF driven differentiation of hMSC cells were cultured for 40 days in FGF, Vitamin C supplemented differentiation media (Section 3.2.6) in the presence and absence of Dorsomorphin. Cells were fixed for staining (Section 3.4.3) at time-points 0, 2, 5, 10, 20 and 40 days exposure to the respective media (n=3).

hMSCs cultured in differentiation media in the absence of Dorsomorphin (Figure 3.48) and in the presence of Dorsomorphin (Figure 3.49) showed no apparent TNMD protein expression.

hMSCs supplemented with the combination of FGF-4 with Vitamin C and FGF-4, 6 & 8 and Vitamin C, showed the presence of TNMD stain which was shown to be cytoplasmic in presence of TNMD throughout the investigation (Figure 3.50 & Figure 3.51). FGF-4 and FGF-4, 6 & 8 further supplemented with Dorsomorphin and Vitamin C showed continued TNMD staining (Figure 3.52 & Figure 3.53) Furthermore, there appeared to be TNMD staining on the cellular membrane and the cells appeared to have fibroblast like morphology at day 20 which was similar to that observed in the rat tenocytes (Figure 4.10).

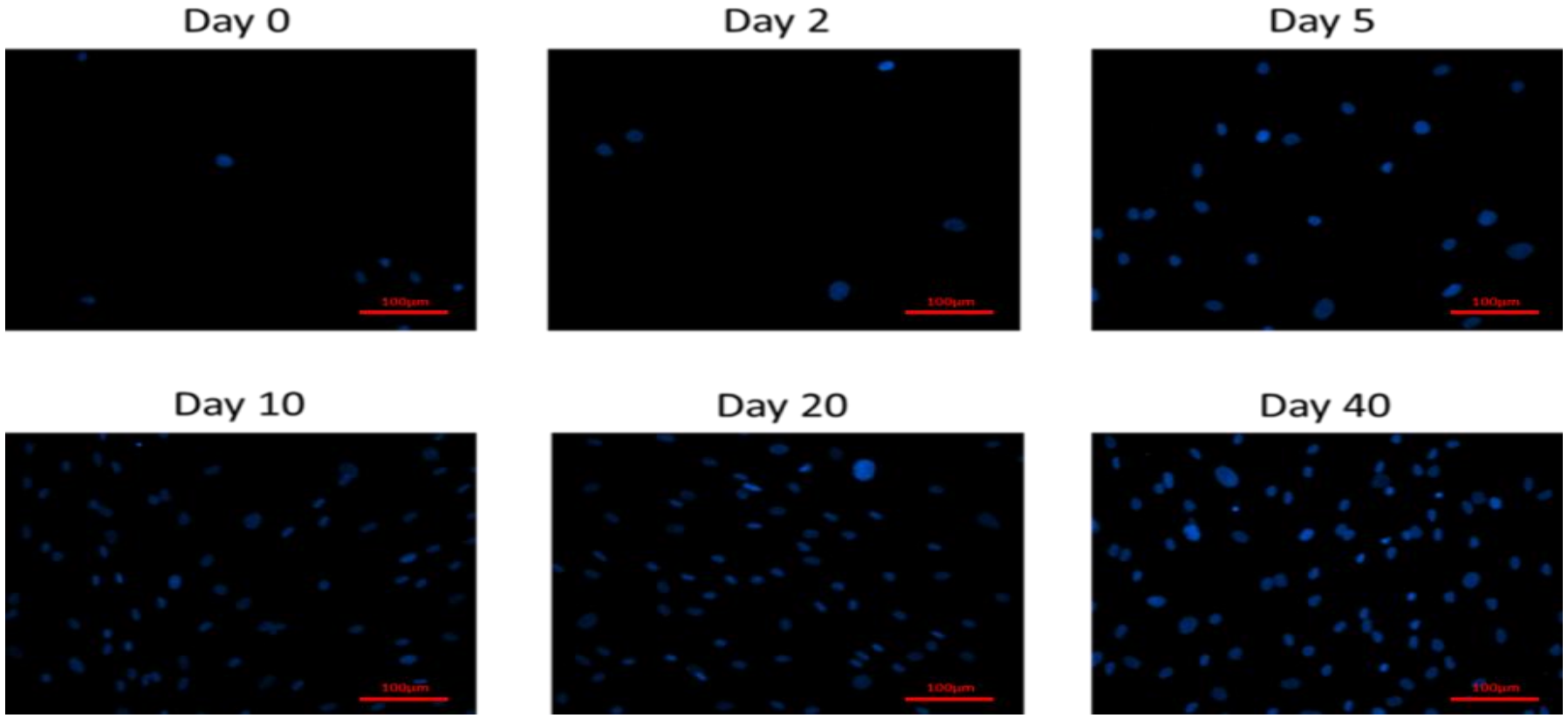

Figure 0.48 hMSC Cultured in differentiation media.

hMSC (BMA-12) when cultured in differentiation media supplemented with Vitamin C lacked the presence of TNMD staining as observed in Figure 3.47.

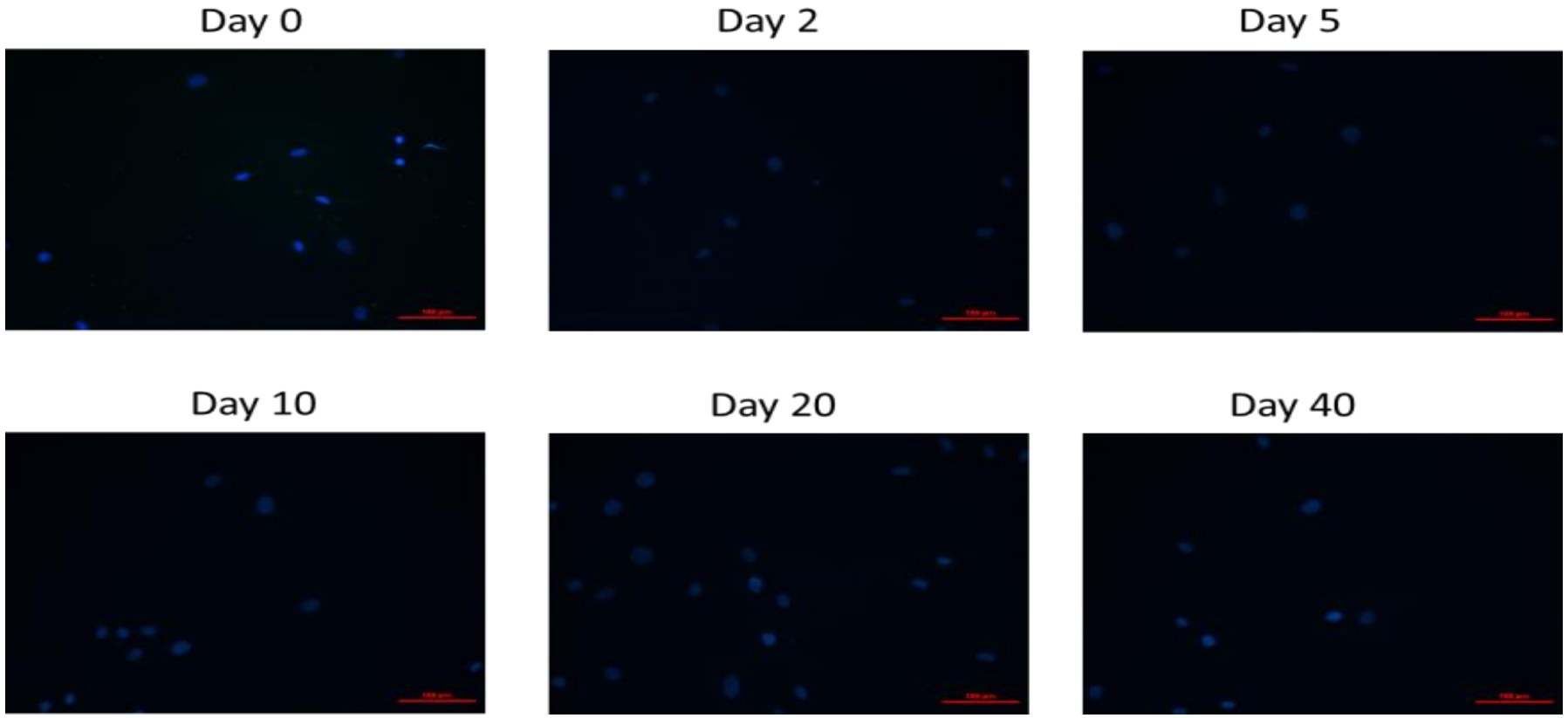

Figure 0.49 MSC Cultured with differentiation media supplemented with Dorsomorphin

hMSC (BMA-12) when cultured in differentiation media supplemented with Vitamin C and Dorsomorphin lacked the presence of TNMD staining as observed in Figure 3.47.

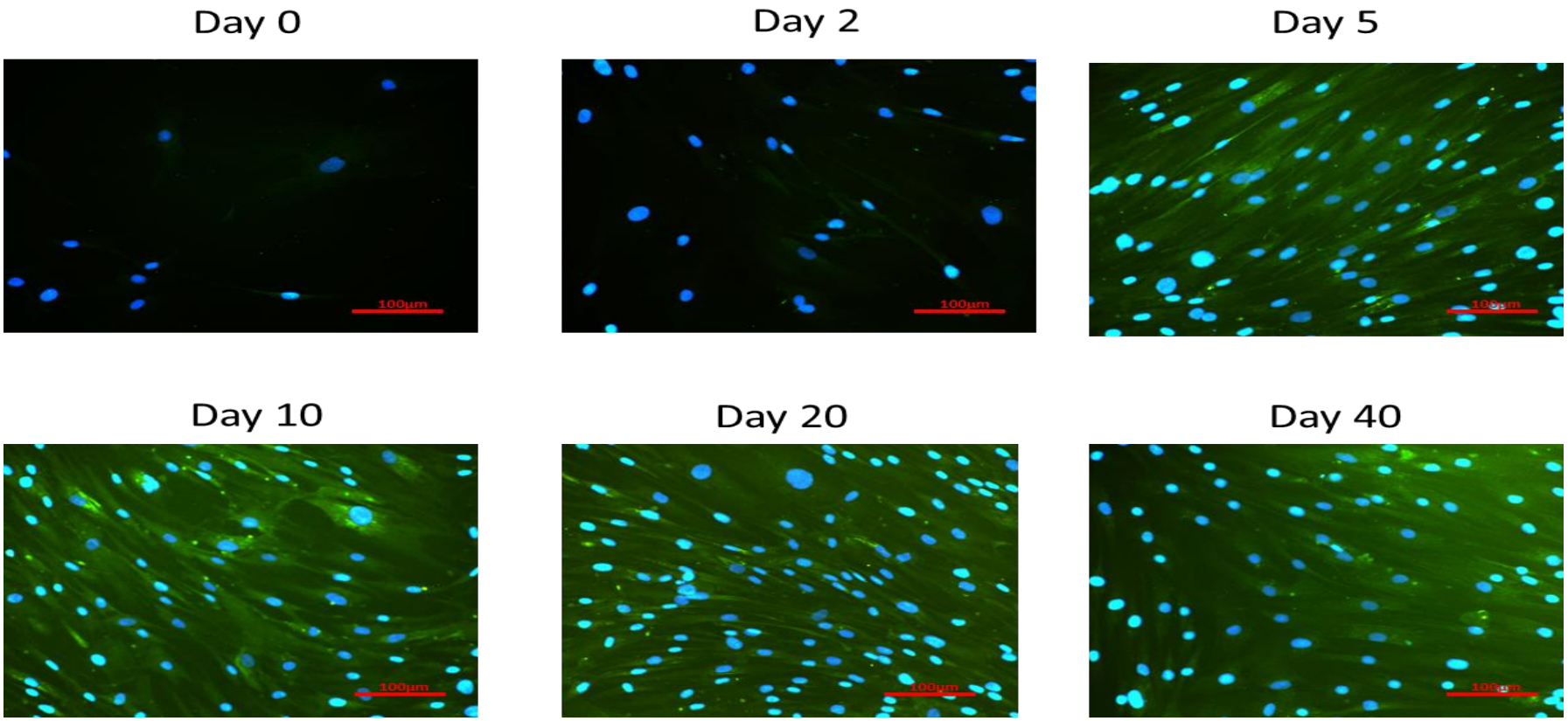

Figure 0.50 hMSC FGF-4 with Vitamin C cultured at 2% O_2

hMSC (BMA-12) when cultured in differentiation media supplemented with FGF-4 and Vitamin C showed the presence of TNMD protein staining.

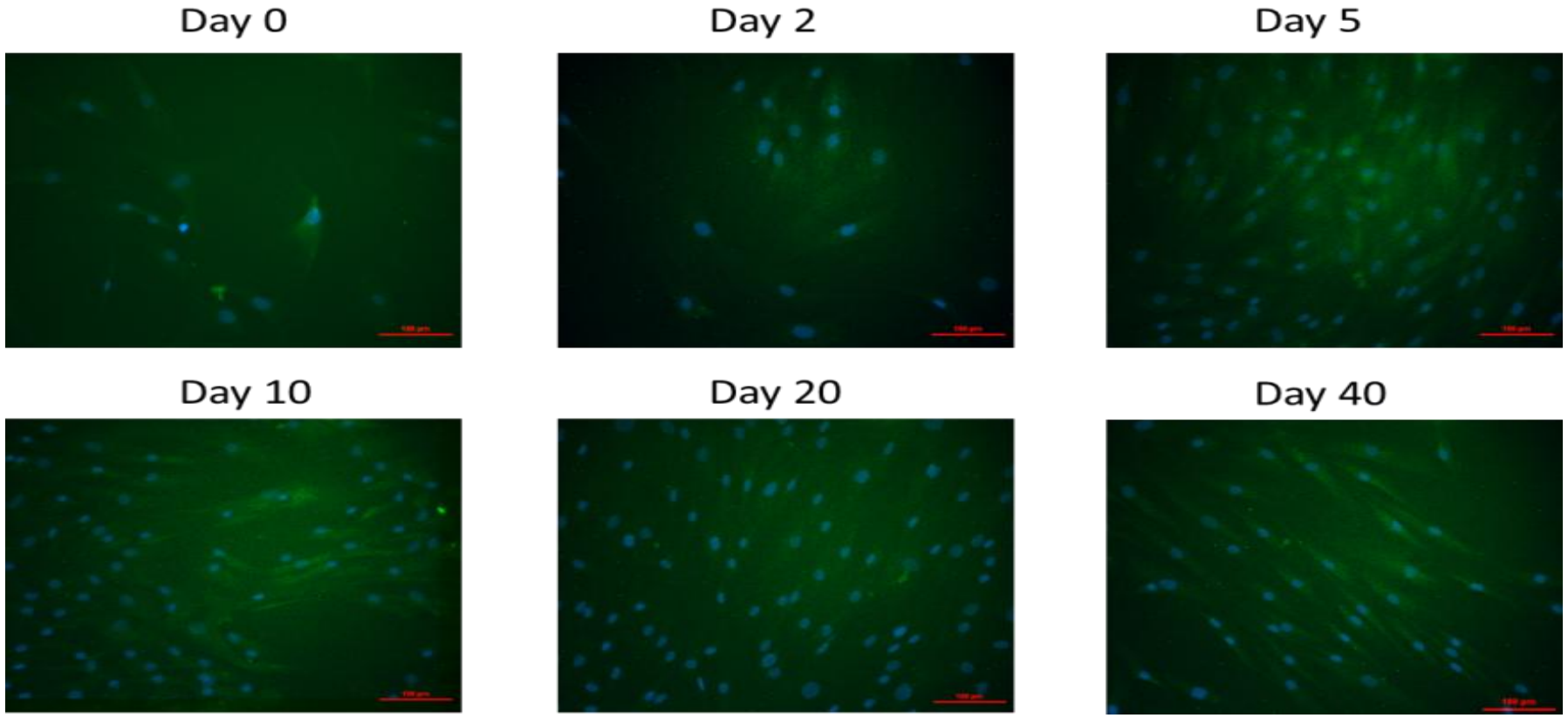

Figure 0.51 MSC FGF-4 with Vitamin C cultured at 2% O_2 supplemented with Dorsomorphin.

hMSC (BMA-12) when cultured in differentiation media supplemented with FGF-4, Vitamin C and Dorsomorphin showed the presence of TNMD protein staining.

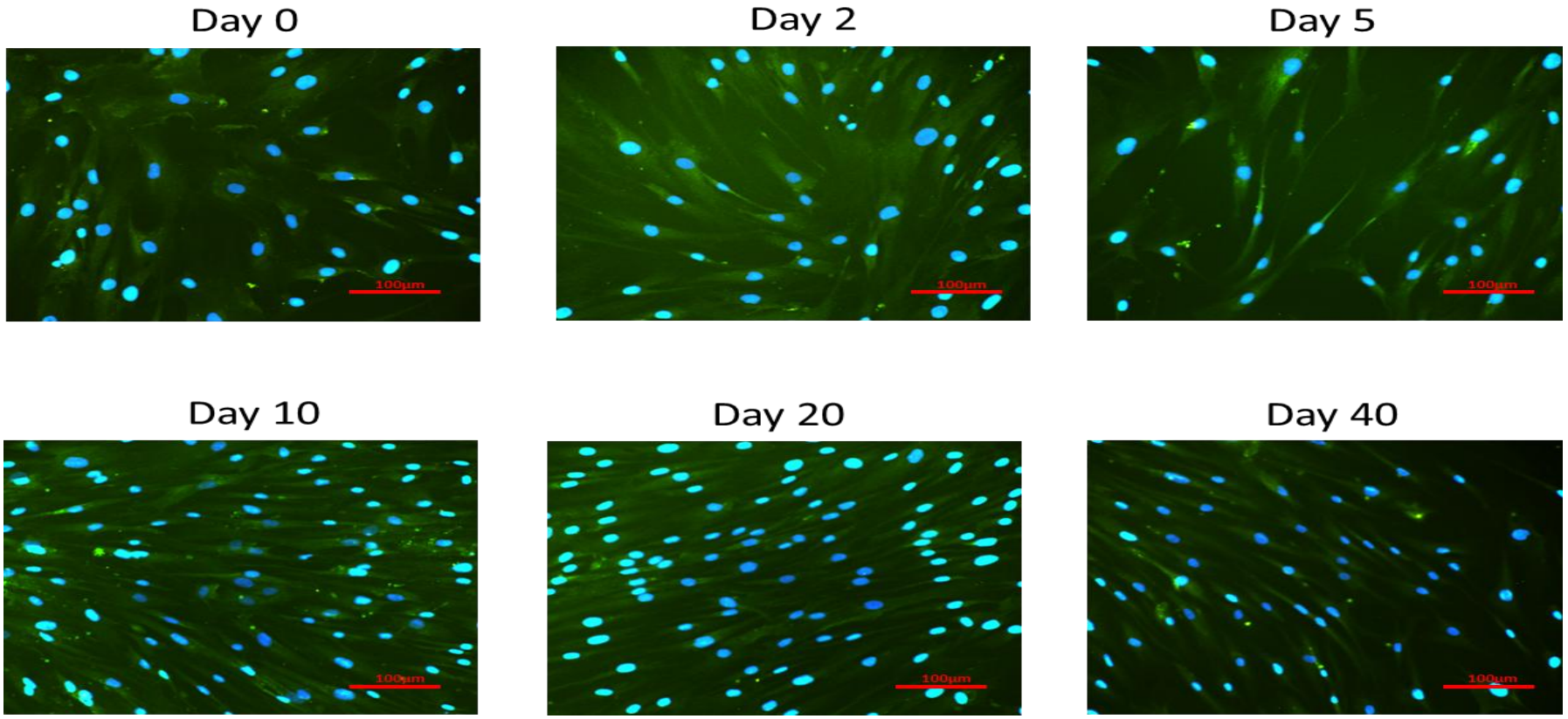

Figure 0.52 hMSC FGF-4, 6 & 8 with Vitamin C cultured at 2% O_2

hMSC (BMA-12) when cultured in differentiation media supplemented with FGF-4, 6 & 8 and Vitamin C showed the presence of TNMD protein staining.

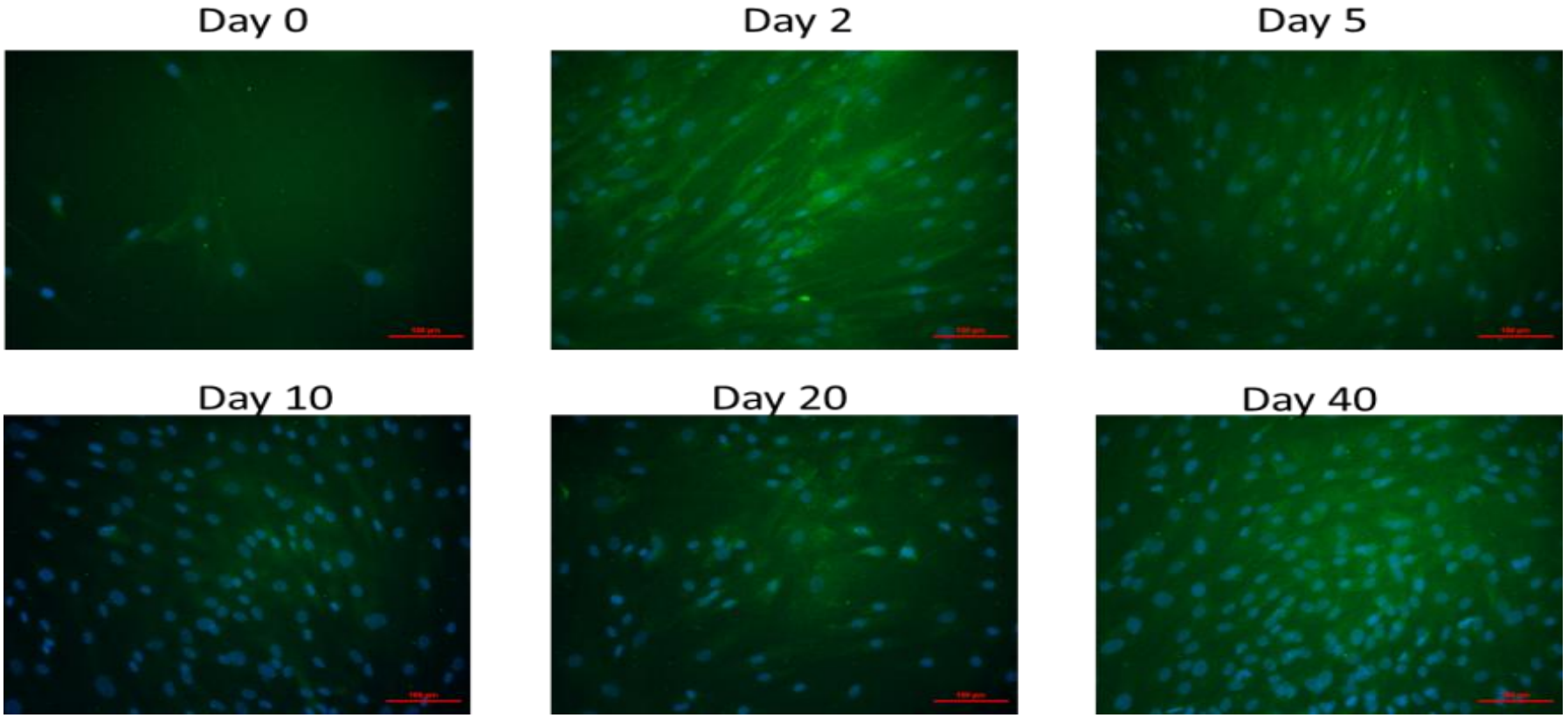

Figure 0.53 MSC FGF-4, 6 & 8 with Vitamin C cultured at 2% O_2 and supplemented with Dorsomorphin.

hMSC (BMA-12) when cultured in differentiation media supplemented with FGF-4, 6 & 8, Vitamin C and Dorsomorphin showed the presence of TNMD protein staining.

3.8.3 Histological Analysis

Histological staining of growth factor (and Vitamin C supplemented differentiation media) driven differentiation of hMSC towards a tenocyte lineage was undertaken in parallel to immunocytochemistry and rt-PCR. Growth factor driven differentiation of hMSC was undertaken utilising the procedure shown in Section 3.5.

Glycosaminoglycans were stained utilising Alcian Blue stain procedure shown in **S**ection 3.5.2 and analysed utilising Image J analysis shown in Section 3.5.4 – 3.5.6.

Collagen was stained using Masson's Trichrome staining procedure shown in Section 3.5.3 and image J analysis was undertaken utilising the procedure outlined in Section 3.5.4 – 3.5.6

A selection of growth factor driven hESC stained with Masson's Trichrome is shown in Figure 3.54. Each time point had a n=3 and each well imaged 3 times to produce the data shown in Table 3.10.

From the Data shown in Table 3.10 comparisons were made between growth factor in the absence of Dorsomorphin and the presence of Dorsomorphin in the differentiation media.

3.8.3.1Masson's Trichrome

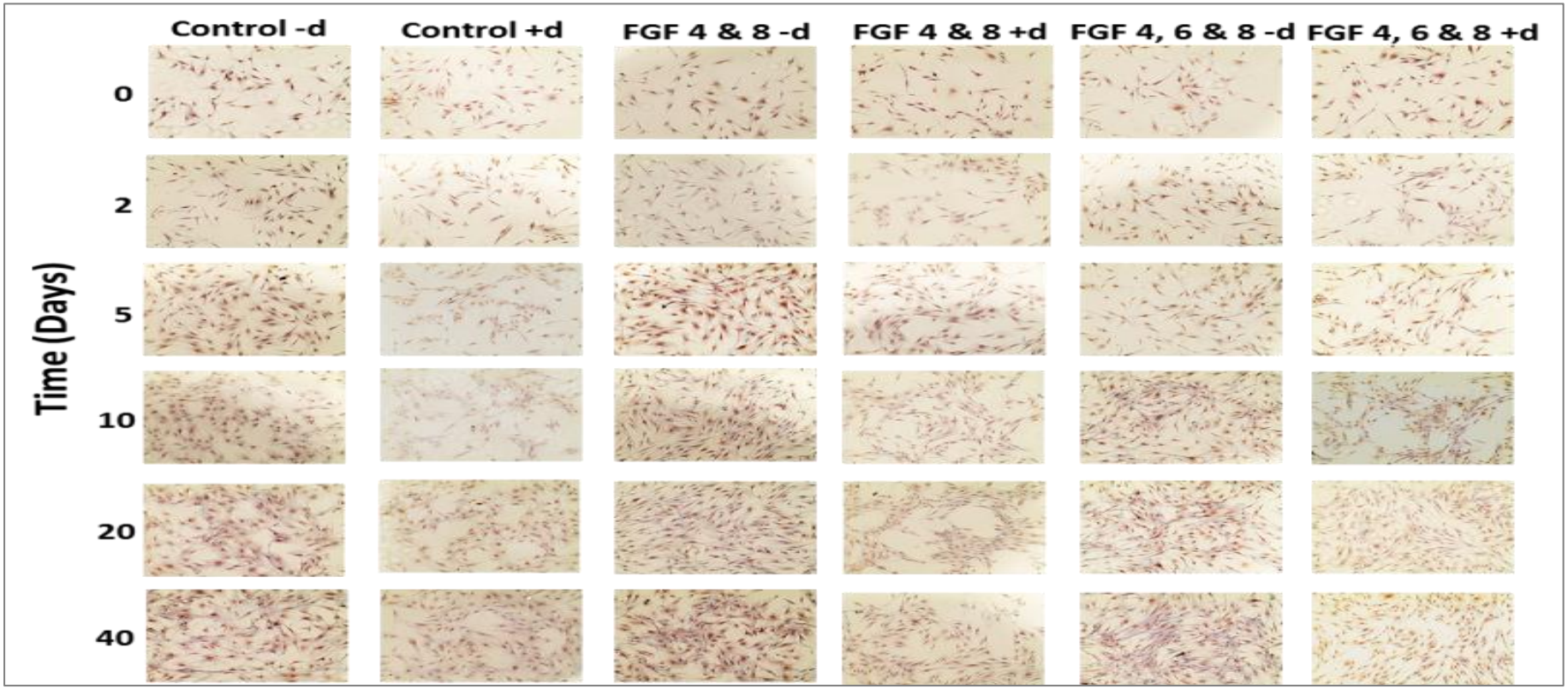

Figure 0.54 Masson's Trichrome staining for each group of MSC over 40 Days.

All groups showed Masson's Trichrome staining. All time points (n=9) were analysed and data extracted from the images. From the data extracted each time point for each condition was compared and statistically tested and the data is shown in Table 3.10.

Time (Days)	MSC Control -d	MSC Control +d	MSC FGF-4 –d	MSC FGF-4 +d	MSC FGF-4, 6 & 8 -d	MSC FGF-4, 6 & 8 +d
0	56.82 ±1.86	57.08 ±2.05	56.82 ±1.96	56.88 ±2.13	56.13 ±1.78	57.16 ±2.05
2	59.44 ±1.53	57.41 ±2.66	59.40 ±2.89	58.89 ±2.88	58.51 ±2.64	58.77 ±4.26
5	59.47 ±3.15	58.19 ±1.71	60.17 ±4.80	59.55 ±1.89	60.03 ±3.93	59.75 ±3.73
10	59.87 ±4.86	58.69 ±2.08	60.25 ±1.14	60.67 ±2.79	61.11 ±2.38	61.42 ±3.56
20	61.59 ±2.77	58.96 ±1.94	61.05 ±1.67	61.28 ±2.52	62.97 ±3.14	61.71 ±1.89
40	61.78 ±4.00	60.38 ±3.51	62.77 ±3.14	61.84 ±2.26	65.25 ±3.21	63.03 ±3.04

Table 0.10 Masson's Trichrome data extraction from Image J for human Mesenchymal Stem cells

The data shown is obtained from Image J and is a total colour extraction of images taken from growth factor driven differentiation.

From the data shown in table 3.10 the following observations were made:

hMSCs cultured in the absence of Dorsomorphin in differentiation culture media had a colour extraction value for Masson's Trichrome of 56.82 ± 1.86 at day 0 which increased to 61.78 ± 4.00 by day 40. Further supplementation of differentiation culture media with Dorsomorphin had an initial value of 57.08 ± 2.05 which increased to a value of 60.38 ± 3.51 by day 40. Supplementation of differentiation media with FGF-4 had an initial value of 56.82 ± 1.96 at day 0, which increased to 62.77 ± 3.14. Further supplementation of FGF-4 differentiation media with Dorsomorphin had an initial value of 56.88 ± 2.13 which increased continuously over the investigation to a value of 61.84 ± 2.26 by da 40. Supplementation of differentiation media with FGF4, 6 & 8 had an initial day 0 value of 56.13 ± 1.78 which produced the greatest increase over the 40 day investigation producing a value of 65.25 ± 3.21 at day 40. Further supplementation of FGF-4, 6 & 8 differentiation media had an initial day 0 reading of 57.16 ± 2.05 which increased over the 40 day investigation to a value of 63.03 ± 3.04.

Statistical analysis was undertaken between groups (Figure 3.55 and Figure 43.56) and individual groups against the controls with no significant difference being observed.

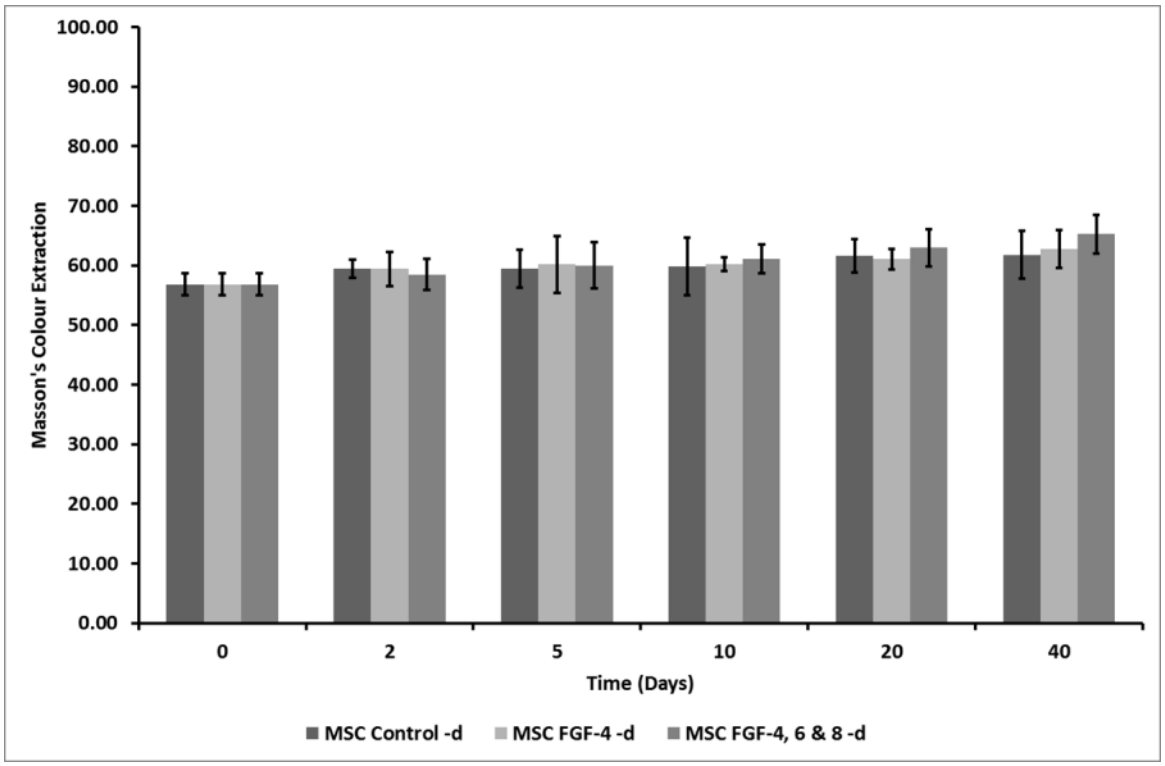

Figure 0.55 Masson's Trichrome growth factor driven differentiation of hMSC in the absence of Dorsomorphin.

Masson's Trichrome data extraction for all growth factor driven differentiation of hMSC with no significant difference observed.

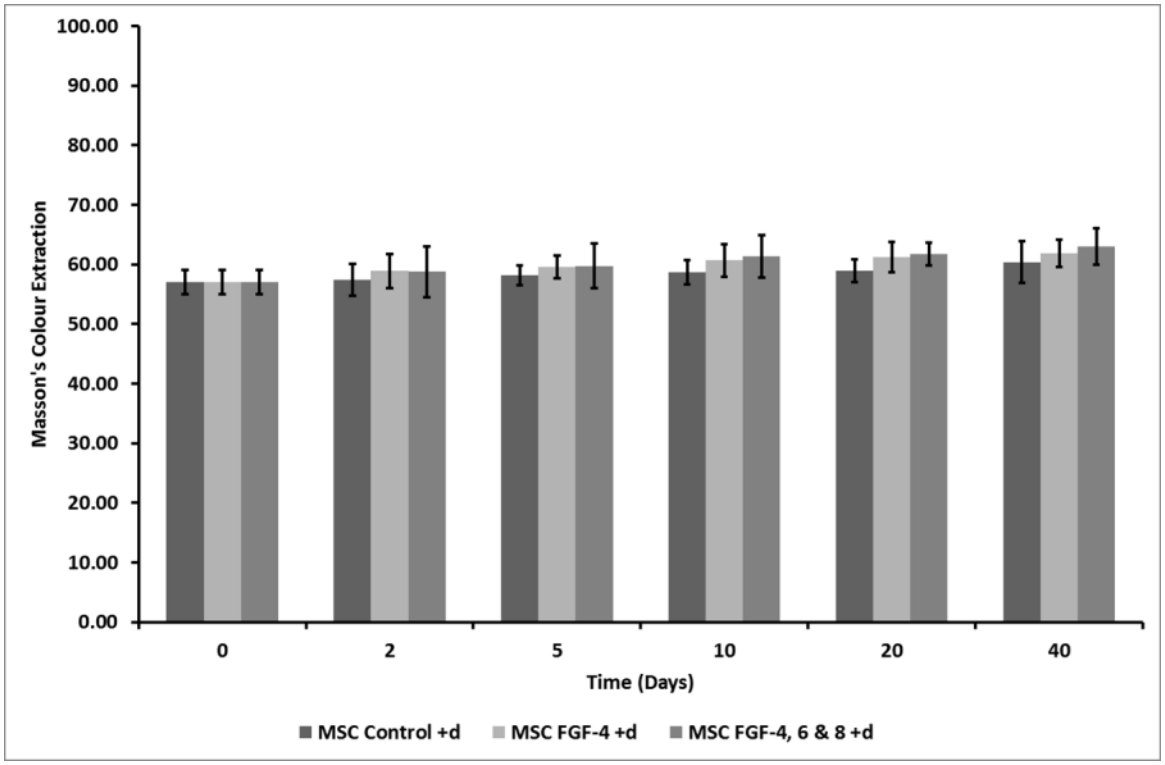

Figure 0.56 Masson's Trichrome growth factor driven differentiation of hMSC in the presence of Dorsomorphin.

Masson's Trichrome data extraction for all growth factor and Dorsomorphin driven differentiation of hMSC with no significant difference observed.

3.8.3.2 Alcian Blue Analysis

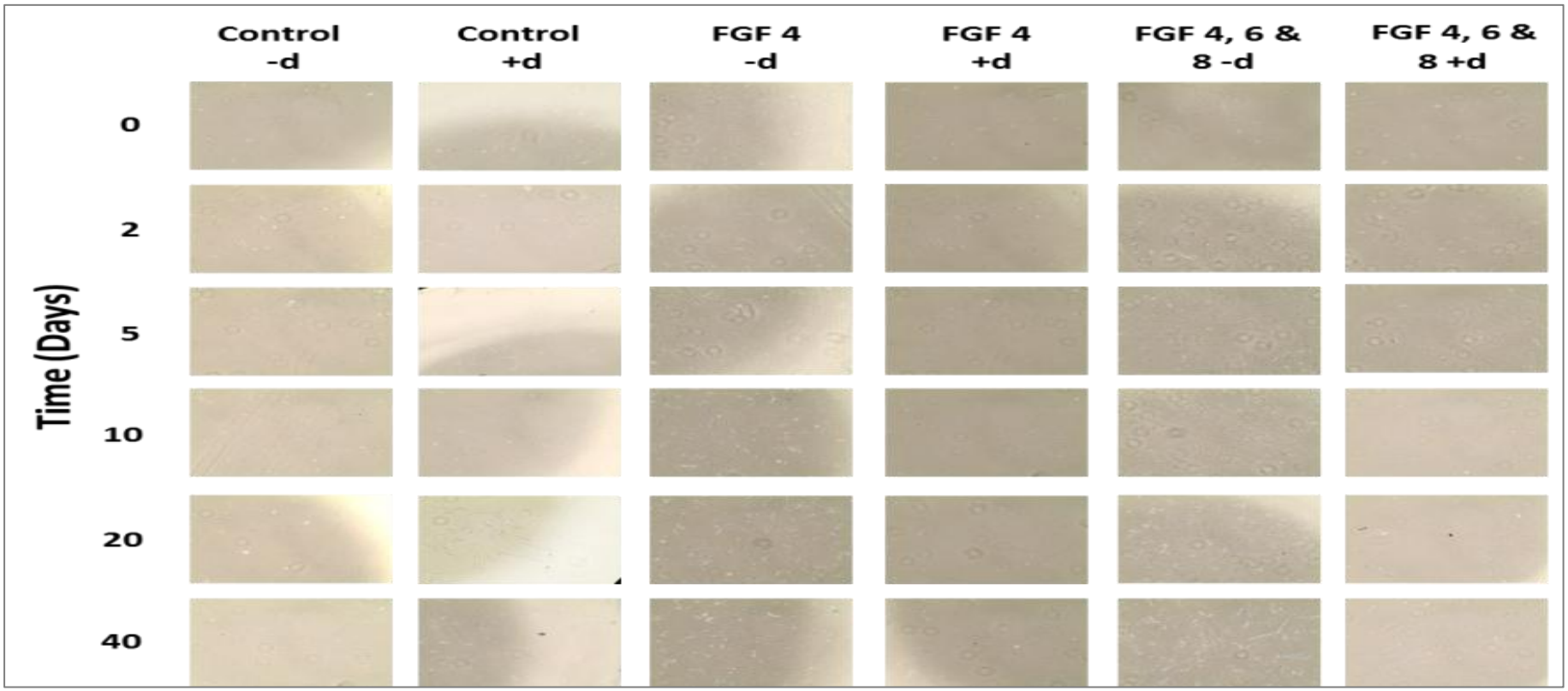

Figure 0.57 Alcian Blue staining for each group of MSC over 40 Days.

All groups showed Alcian Blue staining. All time points (n=9) were analysed and data extracted from the images. From the data extracted each time point for each condition was compared and statistically tested and the data is shown in Table 3.11.

Time (Days)	MSC Control -d	MSC Control +d	MSC FGF-4 -d	MSC FGF-4 +d	MSC FGF-4, 6 & 8 –d	MSC FGF-4,6 & 8 +d
0	40.84	41.12	40.12	41.10	40.93	40.74
	±0.56	±0.22	±0.34	±0.38	±0.38	±0.28
2	43.99	42.30	41.20	42.11	43.10	41.11
	±0.44	±0.37	±0.43	±0.31	±0.23	±0.13
5	44.96	44.18	42.34	43.33	43.77	41.43
	±0.34	±0.39	±0.61	±0.42	±0.17	±0.07
10	46.05	45.23	43.37	44.35	44.30	43.67
	±0.52	±0.22	±1.02	±0.26	±0.13	±0.06
20	48.27	45.59	47.53	44.87	50.71	49.80
	±0.78	±0.08	±1.23	±0.29	±0.14	±0.69
40	51.74	45.82	54.66	50.49	55.31	50.89
	±2.08	±0.10	±0.97	±1.44	±0.26	±0.61

Table 0.11 Alcian Blue data extraction from Image J for human Mesenchymal Stem cells (hMSC)

The data shown is obtained from Image J and is Alcian blue colour extraction of images taken from growth factor driven differentiation.

From the data shown in table 3.11 the following observations were made:

hMSC cultured in differentiation in the absence of Dorsomorphin (Control-d) media had a Alcian blue colour extraction value of 40.84±0.56 on day 0, which decreased by day 2 (43.99±0.44). A slight increase in value was observed by day 5 (44.96±0.34), with further increase at day 10 (46.05±0.52), day 20 (48.27±0.78) and a subsequent decrease on Day 40 (51.74±2.08).

hMSC cultured in differentiation media supplemented with Dorsomorphin (Control +d) had a Alcian blue colour extraction value of 41.12±0.22 on day 0, which decreased by day 2 (42.30±0.37). A slight increase in value was observed by day 5 (44.18±0.39), with further increase at day 10 (45.23±0.22), day 20 (45.59±0.08) and on Day 40 (45.82±0.10).

Statistical testing between Control differentiation media against control differentiation media plus Dorsomorphin showed significant difference between Control-d and Control +d: Day 2 ($p<0.0005$), day 5 ($p<0.005$), day 5 ($p<0.005$), day 20 ($p<0.005$) and day 40 ($p<0.0005$) time points.

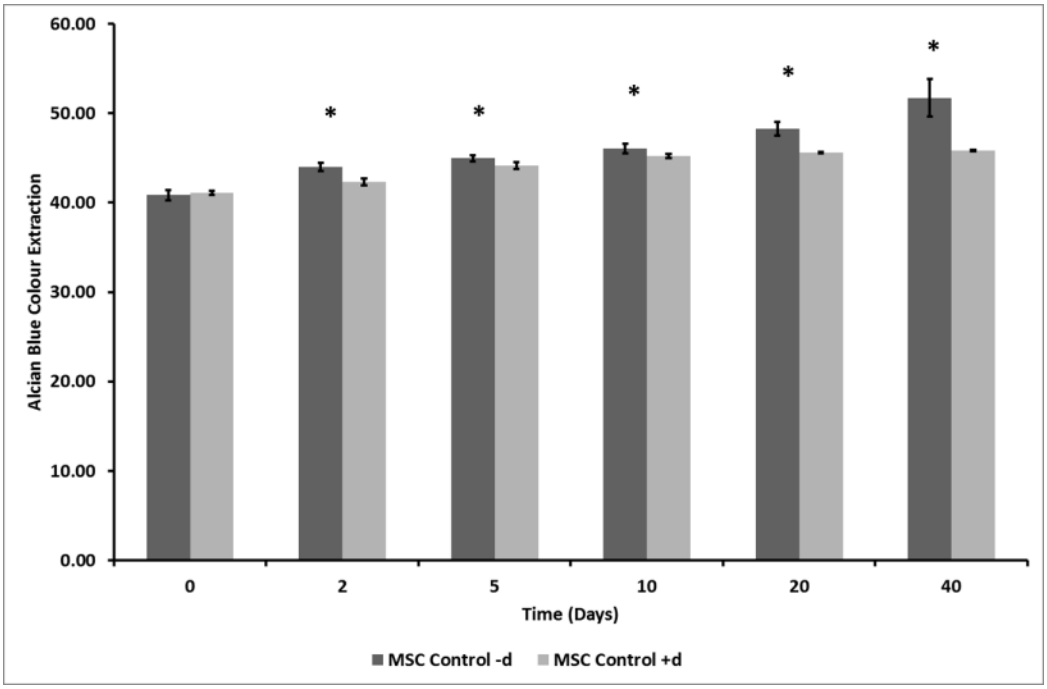

Figure 0.58 *Alcian Blue analysis of hMSC supplemented with control differentiation media in the presence and absence of Dorsomorphin*

hMSC cultured using differentiation media and differentiation media supplemented with Dorsomorphin over 40 days (*p<0.0001).

When hMSC differentiation media was supplemented with FGF-4-d, an initial day 0 value for Alcian Blue colour extraction of 40.12±0.34 was observed. By day 2 this value had increased to 41.20±0.43 with further increases observed on day 5 (42.34±0.61), day 10 (43.37±1.02), day 20 (47.53±1.23) and day 40 (54.66±0.97).

When hMSC differentiation media was supplemented with FGF-4 and Dorsomorphin (FGF-4+d), an initial day 0 value for Alcian Blue colour extraction of 41.10±0.38 was observed. By day 2 this value had increased to 42.11±0.31 with further increases observed on day 5 (43.33±0.42), day 10 (44.35±0.26), day 20 (44.87±0.29) and day 40 (50.49±1.44).

Further testing of FGF-4 –d and FGF-4 +d showed significant difference at day 2 ($p<0.0005$), day 5 ($p<0.05$), day 10 ($p<0.0005$), day 20 ($p<0.0005$) and day 40 ($p<0.0005$) (Figure 3.59).

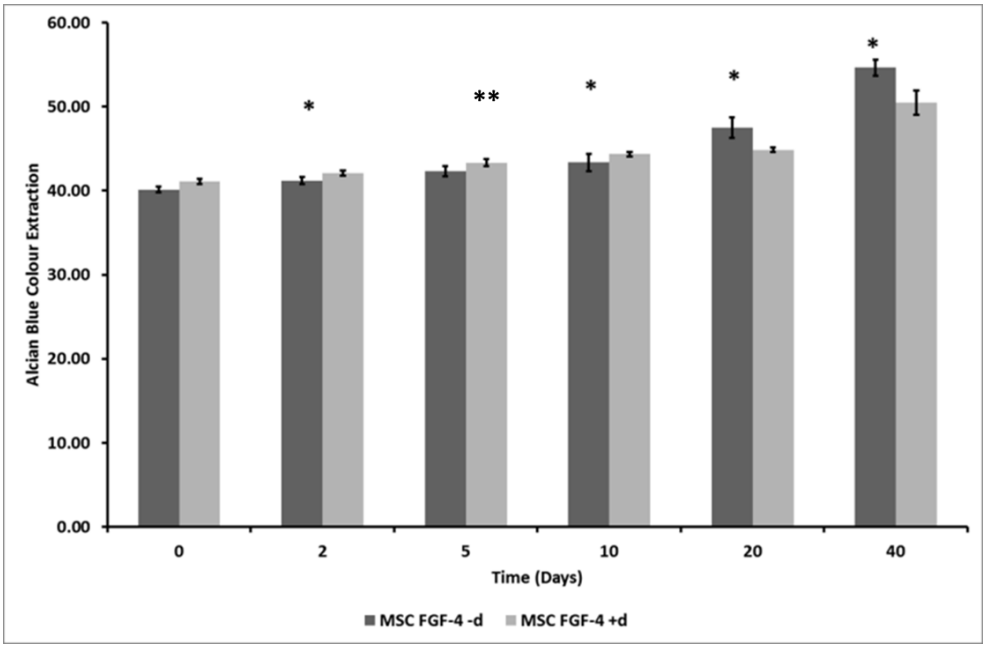

Figure 0.59 Alcian Blue analysis of hMSC supplemented with FGF-4 and Control Differentiation media in the presence and absence of Dorsomorphin

hMSC cultured using differentiation media with FGF-4 and differentiation media supplemented with FGF-4 & Dorsomorphin over 40 days (*p<0.0005 and **p<0.05).

hMSC cultured in differentiation media supplemented with FGF-4, 6 & 8-d had an initial day 0 Alcian Blue value of 40.93±0.38. Which increased further on: day 2 (43.10±0.23), with further increases on Day 5 (43.77±0.17), day 10 (44.30±0.13), day 20 (50.71±0.14) and day 40 (55.31±10.26).

hMSC cultured in differentiation media supplemented with FGF-4, 6 & 8 and Dorsomorphin (FGF-4, 6 & 8+d) had an initial day 0 Alcian Blue value of 40.74±0.28.

Which increased further on: day 2 (41.11±0.13), with further increases on Day 5 (41.43±0.07), day 10 (43.67±0.06), day 20 (49.80±0.69) and day 40 (50.89±0.61).

FGF-4, 6 & 8-d and FGF-4, 6 & 8+d showed significant difference at day 2 ($p<0.01$), day 5 ($p<0.01$), day 10 ($p<0.01$), day 20 ($p<0.01$) and day 40 ($p<0.01$).

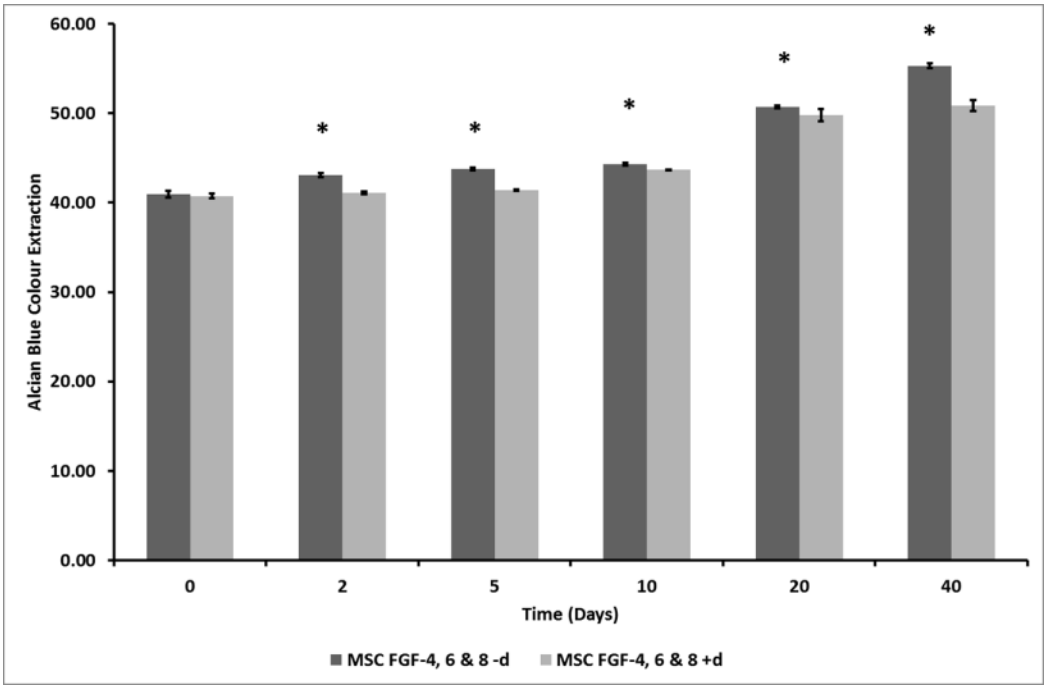

Figure 0.60 *Alcian Blue analysis of hMSC supplemented with FGF-4, 6 & 8 and control differentiation media in the presence and absence of Dorsomorphin*

hMSC cultured using differentiation media and FGF-4,6 & 8 differentiation media supplemented with FGF-4, 6 & 8 and Dorsomorphin over 40 days (*p<0.001).

Further statistical testing was undertaken comparing FGF-4-d against FGF-4, 6 & 8-d, significant difference was observed on day 2, day 5, day 10 and day 20 ($p<0.05$). On testing FGF-4+d against FGF-4, 6 & 8+d significant difference was observed on Day 2, day 5, day 10 and day 20 ($p<0.05$) (Figure 3.61 and Figure 3.62).

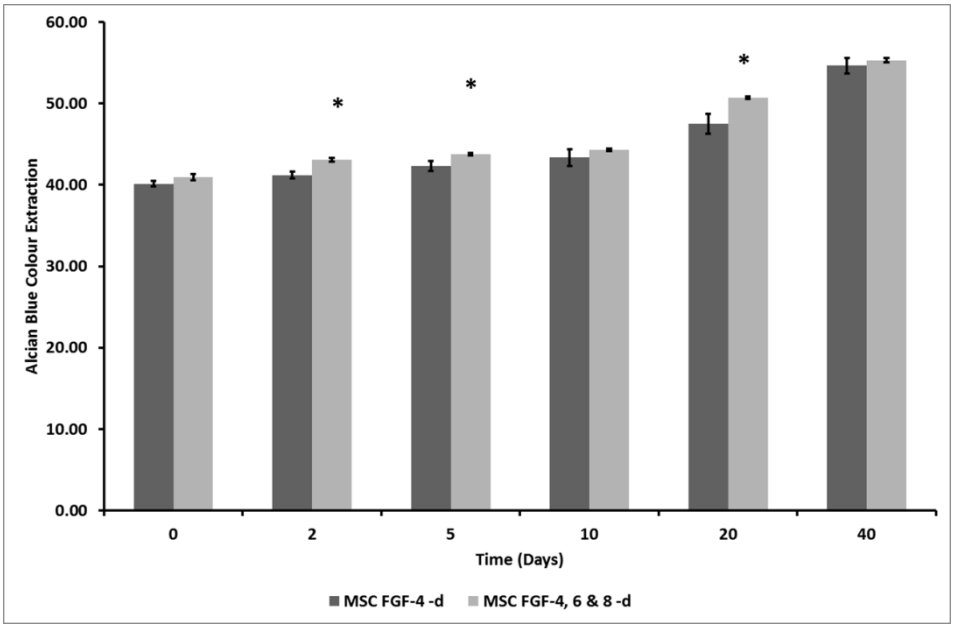

Figure 0.61 Alcian Blue analysis of hMSC supplemented with FGF-4 differentiation media compared with FGF-4, 6 & 8 differentiation media in the absence of Dorsomorphin

hMSC cultured using differentiation media and FGF-4 differentiation media against differentiation media supplemented with FGF-4, 6 & 8 over 40 days (*p<0.05).

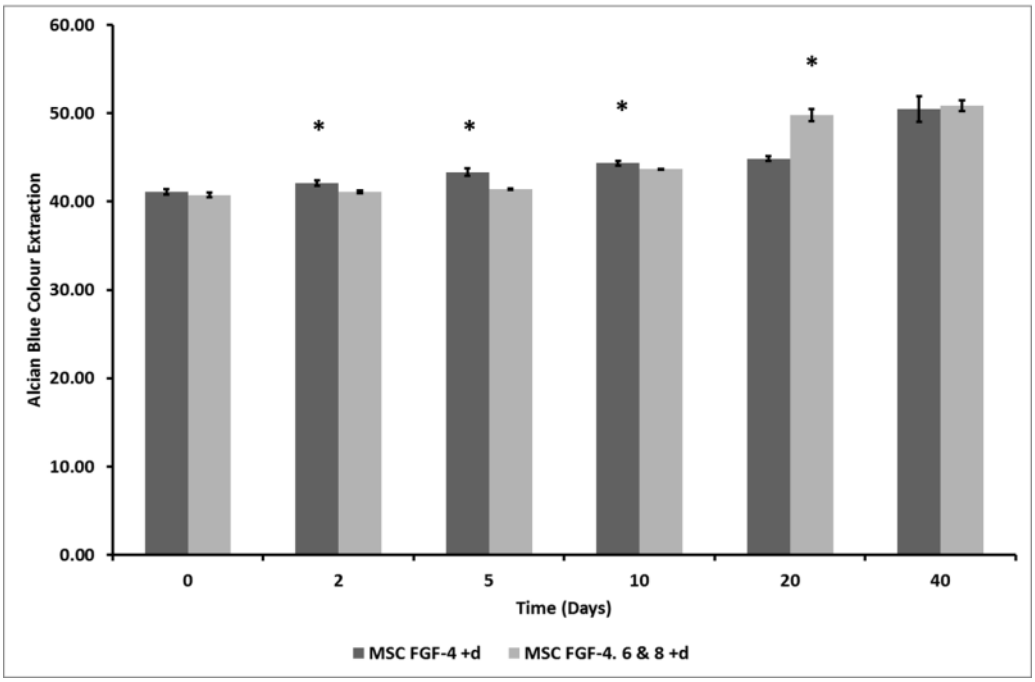

Figure 0.62 Alcian Blue analysis of hMSC supplemented with FGF-4 and differentiation media compared with FGF-4, 6 & 8 differentiation media in the presence of Dorsomorphin

hMSC cultured using differentiation media and FGF-4 differentiation media against differentiation media supplemented with FGF-4, 6 & 8 in the presence of Dorsomorphin over 40 days (*p<0.05).

Statistical testing was undertaken by comparing growth factor supplemented groups against the control-d. When testing control-d against FGF-4-d statistical difference was observed on Day 2, day 5 and day 10 ($p<0.0005$) as the control group values were higher. By day 40 the FGF-4-d group value was significantly higher than the control group ($p<0.005$). On statistically testing the control group against FGF-4, 6 & 8-d the control group reported higher values with a significant difference being observed for day 2, day 5 and day 10 ($p<0.001$). By day 20 and day 40 FGF-4, 6 & 8-d was reporting higher than control values which were significantly different ($p<0.005$) (Figure 3.63)

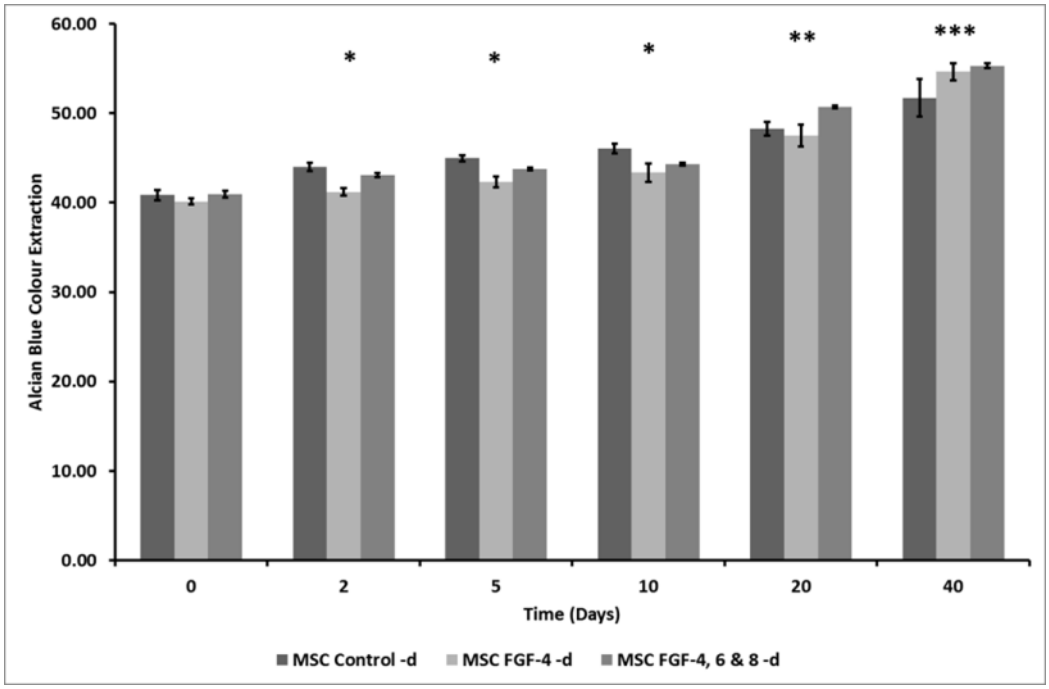

Figure 0.63 Alcian blue comparison of all groups supplemented in the absence of Dorsomorphin.

Statistical testing was undertaken by comparing growth factor supplemented groups against the control groups. When testing control +d against FGF-4+d statistical difference was observed on Day 2, day 5 and day 10 and day 30 ($p<0.0005$) as the control group values were higher. By day 40 the FGF-4+d group value was significantly higher than the control group ($p<0.0001$). On statistically testing the control group against FGF-4, 6 & 8+d the control +d group reported higher values with a significant difference being observed for day 2, day 5 and day 10 ($p<0.0005$). By day 20 and day 40 FGF-4, 6 & 8-d was reporting higher than control values which were significantly different ($p<0.0005$) (Figure 3.64)

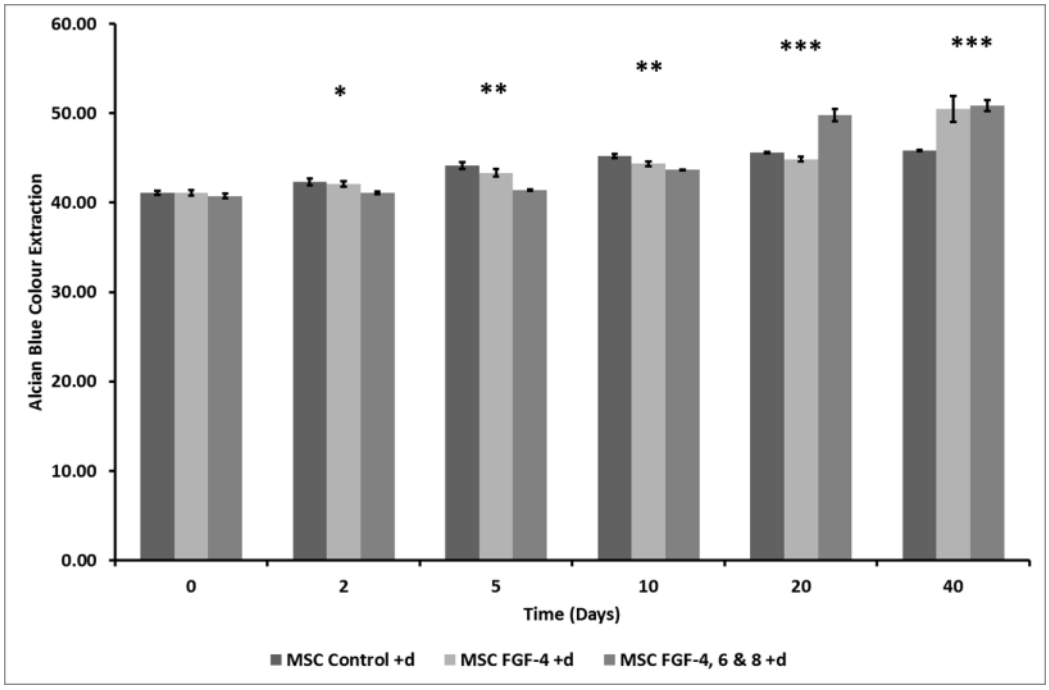

Figure 0.64 Alcian blue comparison of all groups supplemented in the absence of Dorsomorphin.

3.9 Discussion

Tissue engineering and stem cell technologies aims to provide treatment regime for disease and damaged tissue were current therapeutical options are limited or inadequate. Tissue engineering specifically aims to deliver a regime whereby full function is restored to damaged and diseased tissue. The use of stem cells as a means to deliver a functional tendon is highly desired. This study investigated the use of a combination of growth factors, stem cells, Vitamin C along with normoxic and hypoxic cell culture to differentiate human embryonic stem cells and adult mesenchymal stem cells towards a tenocyte like cell lineage. This study employed the gene combination of TNMD and THBS-4 expression as a marker of tendon differentiation first identified by Jelinsky *et al* [68].

Both hESC's and hMSC's were cultured supplemented with individual FGF's and in the presence and absence of Vitamin C under both normoxic and hyperoxic conditions. RT-PCR was undertaken on all samples over 20 days (time intervals 0, 2, 5, 10 and 20 Days). The results obtained showed FGF-4 and the combination of FGF-4, FGF-6 & FGF-8 were capable of maintaining TNMD expression in hMSC when cultured in the presence of Vitamin c under hypoxic conditions. The combinations of FGF-4 & FGF-8 and FGF-4, FGF-6 & FGF-8 were both capable of maintaining TNMD expression over 20 days when cultured in the presence of Vitamin C under normoxic conditions.

Vitamin C is well documented to play an active role in collagen synthesis [337] which is required or muscular skeletal tissue development and also more specifically tendon [338]. Previous unpublished studies conducted by our laboratory have highlighted the requirement for Vitamin C in tendon differentiation when using BMP-12 & 13. This study has shown that the supplementation of media with Vitamin C and the specific growth

factors of FGF-4 or FGF-4, 6 & 8 in mesenchymal stem cells, FGF-4 + 8 or FGF-4, 6 + 8 in embryonic stem cells can induce and maintain the expression of the tendon linked genes TNMD and THBS-4. The use of Vitamin C in this study agrees with previous studies using Vitamin C as a component of differentiation media which enhances differentiation towards cardiomyocytes [339], chondrogenic lineage [340] and osteogenic lineage [341].

On comparing 21% O_2 and 2% O_2 culture of both hESC and hMSC cells supplemented with growth factors and Vitamin C. 2% O_2 showed continued expression of TNMD and THBS-4 tendon markers when hESC and hMSC cells were cultured with the growth factor combination of FGF-4, FGF-6 and FGF-8 with Vitamin C. ESC cultured at 2% O_2 with differentiation media supplemented with BMP-12, BMP-13 & Vitamin C (previous unpublished data) and FGF-4 + 8 and Vitamin C was also capable of maintaining TNMD and THBS-4 expression. Furthermore, FGF-4 and Vitamin C was capable of maintaining TNMD and THBS-4 gene expression with MSC cultured at 2% O_2. Reduced oxygen levels have been previously been shown to play a role in differentiation control especially in embryogenesis. During embryogenesis with oxygen diffusion in the embryo is limited by size with the natural progression of tissue-genesis involves hypoxia. The cellular response to hypoxia involves HIF proteins. HIF proteins especially HIF-1 and HIF-2, which are activated during development and many genes involved in differentiation being effected by hypoxia such as; POU5F1 (HIF-2α) and NANOG (HIF-1α) [342, 343]. Recently studies have found evidence of classical hypoxia response pathways in tendon injury where rota cuff injuries express high levels of HIF-1α [344]. This study has shown oxygen level plays a critical role in the differentiation of both embryonic and mesenchymal stem cells towards a tenocyte-like cell lineage. HIF-1α has previously been shown to up regulate the

transcription of COL1A2 [345]. Furthermore, HIF-1α has also been shown to up regulate TENC in human small cell lung carcinoma [346]. This study has shown that hypoxic stem cell culture is vital for the differentiation of stem cells towards tenocyte lineage and the possible role of HIF proteins in differentiation of both embryonic and mesenchymal stem cells towards a tenocyte-like lineage.

The results of a previous unpublished study showed that BMP-12 & 13 could induce for hESCs *in vitro* tenogenic differentiation under normoxic conditions (2% O_2). Distinct up-regulation of tendon-linked genes (i.e. COL1A2, COL3A1, TENC, TNMD, THBS-4 and DCN) being observed in BMP-12 & 13 treated samples cultured under normoxic conditions (2% O_2).

Previous studies suggested that the transcriptional control of tendon-specific genes relied on BMP signalling pathway and Smad1, 5 & 8 activation [179, 183, 347-349]. As ligands, BMP-12 & 13 bind to Type II BMP serine/threonine kinase receptor followed by the activation of Type I receptor and subsequently activate the SMAD1, 5 & 8 which leads to tenocyte-like gene expression [350, 351]. This might be the explanation for the signal transduction pathway for the genes up-regulation observed in BMP-12 and 13 supplemented differentiation media.

FGF-4 has previously been shown to play an active and pivotal role in embryonic development. FGF-4 is expressed in pre-implantation murine blastocysts and is also present in the ICM [197, 198]. Previous studies focusing of the effect of FGF-4 on chick wing bud tendon development has shown overexpression FGF-4 was capable of up-regulation of scleraxis a known tendon transcription factor. FGF-6 Studies conducted using the murine model has shown FGF-6 presence at E9.5 and to be exclusively present

in the myotomal compartment of the somite [201, 202]. FGF-6 has been shown to play a significant role in myogenesis employing knockdown murine model [201, 202]. Due to the highlighted importance of interactions between muscle and tendon during limb development FGF-6 was investigated as a possible signalling molecule in tendon development. Early investigation into the role of FGF-8 in limb development was conducted by Moon and Capecchi in 2000 were they undertook experimental work to assess the role of FGF-8 during mouse limb development [203]. Further, investigations utilising chick embryos highlighted the presence of FGF-8 transcripts in tendon of the developing limb in a chick [352]. Our findings agree in that both FGF-6 and FGF-8 are required for tenocyte differentiation, in that tendon is a constituent part of a limb.

The individual FGF signal pathways are under researched along with FGF combinational studies in tendon differentiation. FGF's are known to bind to one of the FGF receptors of which there are 4 (namely FGFR1-4) with subclass receptors. Post receptor ligation results in the activation of either PKC (Protein Kinase C) by means of activation of FGFR1/FGFR2 signal cascade via FGF-4 ligation, ERK1/2 via activation of FGFR2 by FGF-4. JNK activation via FGFR1 by FGF-4 Ligation,FGFR2-FGF-4 ligation activation of p38 or Akt all of which can induce gene transcription by means of regulation of transcriptional promoters and enhancers [353]. However, the biochemical cues required for *in vitro* tenogenesis are poorly defined since the signalling pathways during the differentiation are complex and under-investigated.

THBS-4 is an adhesive glycol protein that mediates cell-cell and cell-matrix interactions which has been identified that together with TNMD can be considered as tendon markers [68]. TNMD, as one of the type II transmembrane glycoproteins, was found to be

predominantly in dense connective tissue such as tendon and ligament [68], and thus was considered as a marker for tendon maturation when used in conjunction with COL1A2, COL3A1, TENC and DCN [354]. In our study, we observed distinct TNMD, THBS-4 transcription over 2 days in the untreated SHEF-1 cells. This may due to the spontaneous differentiation progress of hESCs. Conversely, the SHEF-1 samples supplemented with BMP-12 & 13 or FGF-4 & 8 or FGF-4, 6 & 8 and hMSC supplemented with either: FGF-4 or FGF-4, 6 & 8, TNMD and THBS-4 transcription was observed to be transcribed throughout the 40-day differentiation. FGF-4 & 8 (hESC) and FGF-4 (hMSC) showed TNMD and THBS-4 transcription up to day 20. Also, the clear synapsing of the cells observed at day 40 with the supplementation of BMP-12 & 13 with hESC indicated by the positive green TNMD staining which was not observed with FGF-4, 6 & 8 supplemented hESC or MSC although the expression of TNMD was observed. Taken together, these results suggested that BMP1-12 & 13 and FGF-4, 6 & 8 are capable of maintaining TNMD expression in hESC and FGF-4, 6 & 8 is also capable of maintaining expression of TNMD expression in hMSC. Both BMP-12 & 13 and FGF-4, 6 & 8 are capable of inducing tenocyte-like morphology when cultured at 2% O_2, with FGF-4,6 & 8 is also capable of inducing a tenocyte-like gene expression in hMSC when cultured at 2% O_2.

This study agreed with previous studies as FGF-4 alone was capable to induce or maintain the tendon marker TNMD and THBS-4 up to 20 days in hMSC. This study showed FGF-6 alone was incapable of inducing or maintain TNMD and THBS-4 expression in hESC and hMSC (post day 10). In this study FGF-8 alone was incapable of initiating and maintaining TNMD and THBS-4 expression past day 10 in hESC and was not detected in hMSC. FGF-4 and FGF-6 have both been detected in AER and provide the signals to maintain

mesenchymal cells in the proliferative state in the PZ during limb development. As mentioned previously, FGF-4 has been shown to initiated scleraxis and FGF-6 having a role in myogenesis. However, the combination of FGF4 & FGF-6, were unable to maintain TNMD and THBS-4 expression past day 10 in hESC and again was not detectable in hMSC. On investigating the combination of FGF-4 and FGF-8, both THBS-4 and TNMD transcription was detected at day 40 in hESC supplemented media.

The combination of FGF-4, 6 & 8 in this study provides the strongest expression of TNMD and THBS-4 in both hESC and hMSC over 40 day cultured at 2% O_2. Understanding the close relationship between bone, cartilage, muscle and tendon development would underpin a stem cell based tissue engineered approach to tendon injuries.

Further investigation employed the known SMAD inhibitor Dorsomorphin which was supplemented into growth factor supplemented media. FGF-4 & 8+d (hESC) and BMP-12 & 13+d (hESC) showed inhibition of THBS-4 and therefore impaired tenogenesis. FGF-4+d (hMSC) showed inhibition of TNMD expression post 10 days. Conversely, FGF-4, 6 & 8 +d (hESC and hMSC) showed change to Tenogenic gene expression in that both TNMD and THBS-4 were both expressed. BMP signalling is known to utilise the SMAD signalling pathway and due to the inhibition of FGF-4 and FGF-4 + 8 by Dorsomorphin would infer that FGF-4 and FGF-4 +8 stimulate BMP production and subsequent signalling which would agree with previous studies linking FGF and BMP signalling and the requirement of both growth factors for cardiomyocyte differentiation [355, 356].

Histological comparisons made between growth factor supplementation and growth factor and Dorsomorphin supplementation of differentiation media highlighted subtle differences. hESC cultured in the presence of both BMP12 & 13 and Dorsomorphin

showed a distinct reduction in Collagen staining (Masson's Trichrome) which highlights a inhibition of the SMAD signalling pathway results in a decrease in collagen synthesis. hESC cultured with BMP-12 & 13 and Dorsomorphin also a distinctive reduction in GAG staining (Alcian Blue) further highlighting that media supplemented with Dorsomorphin and inhibition of the SMAD signalling cascade also resulted in impaired GAG synthesis and secretion, which is confirmed by rt-PCR showing distinctive reduction in the gene transcripts for DCN, TENC, THBS-4, TNMD, COL3a1 and COL1a2. Similar down regulation was observed in the FGF-4 & 8 hESC cultured with the further supplementation of Dorsomorphin showed a distinct reduction in GAG staining and with THBS-4, DCN and TENC down regulation. Masson's Trichrome staining for collagen also showed a distinctive reduction. However, both collagen 1a2 and Collagen 3a1 RNA were detected at all-time points using rt-pcr. hESC supplemented with both FGF-4, 6 & 8 and Dorsomorphin showed a distinct reduction at day 40 when compared with FGF-4, 6 & 8 only supplementation. Although, the alican blue measurements were reduced in the Dorsomorphin supplemented media from day 5 to day 40. Rt-pcr showed inhibition of the GAG decorin (DCN) with both THBS-4 and TNMD being detected throughout all time points. Masson's Trichrome measurements showed a reduction in collagen staining at all time-points. However both COL1a2 and COL3a1 transcription were detected at all-time points. The effects of Dorsomorphin on BMP-12 & 13 supplementation agree with previous SMAD inhibition. However, the effects of Dorsomorphin on FGF induced hESC response indicates, the distinct possibility of FGF-BMP signalling cross talk.

hMSC cultured with both FGF-4 or FGF-4, 6 & 8 and Dorsomorphin no significant difference in Masson's Trichrome staining when compared to hMSC cultured with FGF-4

or FGF-4, 6 & 8 only. However, Alcian blue measurement revealed significant difference between FGF-4 and FGF-4 & Dorsomorphin and FGF-4, 6 & 8 and FGF-4, 6 & 8 with Dorsomorphin at day 40. Rt-PCR analysis showed Dorsomorphin to inhibit TNMD when supplemented into FGF-4 and FGF-4, 6 & 8 media at day 40. This further adds to the hypothesis that there is a distinct possibility of FGF-BMP cross talk.

Morphological comparisons between FGF-4, 6 & 8 supplemented hESC and hMSC revealed the differentiated hESC cells to have a “cobble stone” like appearance. Conversely, the hMSC had a distinct fibroblastic morphology, similar to that of native tenocytes. The natural differentiation pathway for tenocytes would be embryonic stem cells to mesodermal to tenocyte stem cell to mature tenocyte. We hypothesis that the hESC have partially differentiated to a tenocyte derived “like” stem cell as the cobble stone like morphology [357] is not dissimilar to that observed in FGF-4, 6 and 8 supplemented hESC differentiation. These distinct finding may be due to mesenchymal stem cells specialisation and differentiation having already occurred when compared to embryonic stem cells?

This study has shown Vitamin C in conjunction with FGF-4, 6 & 8 cultured at 2% O_2 was capable of inducing and maintaining tendon like gene markers such as tenomodulin (TNMD) and Thrombospondin-4 (THBS-4) over a 40 day culture period.

3.10 Conclusion

In this study we have shown for the first time that FGF-4, 6 & 8 being capable of maintaining tendon specific genes TNMD and THBS-4 in both embryonic stem cells and mesenchymal stem cell when cultured at 2% O_2. Furthermore, this study has for the first time shown FGF-4 as being capable of maintaining TNMD and THBS-4 gene expression in human mesenchymal stem cells and FGF 4 & 8 being capable of maintaining TNMD and THBS-4 gene expression in embryonic stem cell when cultured at 2% O_2 for a limited time periods.

Chapter 4: PHBHHx Nanoparticle Production

4.1 Introduction

This study aims to control nanoparticle size to deliver a growth factor concentration previously identified in chapter 4. The multidisciplinary field of nanomedicine aims to produce materials in the nanometre range to restore or maintain tissues, deliver drugs and proteins as well as combination products for the purpose of improving human health. Nanotechnology has quickly evolved within medical engineering due to its ability to produce structures mimicking the dynamic biological micro environment, combining cells, scaffolds and drug releasing nanoparticles to efficiently produce functional tissue [358-360] as well as effective destruction of diseased tissue [361-364] for medical applications. Nanoparticles have been shown to have an array of applications ranging from nanosensing, drug delivery, and gene transfection to growth factor delivery [365-370]. The ability to manipulate nanoparticle size to fit the needs of a desired application would provide increased utility to treat a range of diseases, including cardiovascular disease [371], osteoarthritis [372], diabetes [373], cancer [371, 374-377] and neurodegenerative disease [378] to mention but a few. Recently, nanoparticles have been shown to pass across the blood-brain barrier which is a major obstacle when delivering chemotherapeutical drugs for the treatment of nervous system tumours [379] as well as neurodegenerative diseases. For controlled drug release, linking nanoparticle size to a drug release rate would create a system whereby a specified drug release rate and duration could be achieved via a controlled manufacturing process. This would lead to improved treatment methods by removing drug metabolism and loss via administration route (i.e. the digestive tract) as the nanoparticle would serve to protect the encapsulated drug allowing for reduced drug loading. An immediate benefit of improved delivery would be in cost reduction of drug due to reduced concentration requirements

to meet efficacious dosage compared to oral administration. More importantly, limiting the administered dose would potentially reduce the risk of toxicity and non-specific side effects in the patient and could be combined with a targeted drug release systems [380-384] for advanced drug delivery.

The ability to control the size of nanoparticles during production would allow for the reliable and reproducible creation of smaller nanoparticles for applications such as nanoparticle-mediated gene transfection and direct low does growth factor delivery. This holds much promise in regenerative medicine as non-viral gene vectors present a significantly reduced safety hazard compared to viral based gene vectors [374]. The nanoparticle-mediated cellular response is critical for successful therapies with particles below 100nm actively mediating biological effects such as the binding and activation of membrane receptors and subsequent protein expression [385], a critical aspect within a variety of nanoparticle applications. The advantage of the use of smaller particles in clinical practise include easier intravenous injection, sterilisation by filtration [386, 387] and the avoidance of spleen filtration [388-390] which are critical for treating and managing the disease state. Isolating the key production variables affecting the size of nanoparticles would allow for more effective fabrication of smaller nanoparticles and promote efficient utilisation of their biological and practical benefits.

Here, the controlled production of PHBHHx nanoparticles was investigated via the DOE method to determine the sensitivity of process variables and the repeatability of producing PHBHHx nanoparticles of a desired size. The DOE approach uses parallel multivariate designed experiments to investigate the action and interaction of variables in order to improve understanding, and therefore control of complex processes [391]. A key aspect of this is identifying controlled and uncontrolled variables, which affect the

response from the process, with preliminary studies aimed at highlighting which input variables affect the desired process output. Heperzine-A, Paclitaxel and ALB-PLC encapsulated nanoparticles showed conformity to this trend with high process repeatability. This study shows that controlled manufacture of PHBHHx nanoparticles via the solvent evaporation method is achievable and has been utilised to produce nanoparticles of below 100 nm. Demonstrating this level of controlled manufacture is essential for developing products in the tightly regulated medical industry where precision manufacture is essential for successful commercialisation and also increasing the control of desired drug delivery and drug concentration.

4.2 Materials and Methods

4.2.1 Nanoparticle Formulation

A range of PHBHHx w/v Chloroform solutions were prepared at a volume of 2mL (Organic Phase), 0.5% w/v of F68 (150mg)(Nanjing Well Chemical Co., Ltd. Nanjing, China) and 0.5% w/v of Sodium deoxycholate (150mg) (Amresco, Solon, USA) were prepared in a volume of 28ml of 0.22µm filtered Water (Aqueous Phase). Once both the organic and aqueous phases were dissolved, the aqueous phase was filtered and added drop-wise to the organic phase. The aqueous/organic phase were then sonicated (Scientz JY92 – II) for various cycles whilst on ice (sonication cycle was 1 second sonication at a range of power settings and 1 second rest).The nanoparticle emulsion was then placed on a rotary evaporator(Buchi Rotavapor R-3) set at 30^{o}C until all the organic phase was evaporated (emulsion becomes transparent).

4.2.2 Phospholipid Entrapment of Bovine Serum Albumin/FITC Albumin

Phospholipid, namely, soybean lecithin containing 70-97% phosphatidylcholine (PC), was purchased from Shanghai Tai-wei Pharmaceutical Co. Ltd. (Shanghai, China). Bovine serum albumin Fraction V was purchased from Xuzhou Wanbang Bio- Chemical Co. Ltd. (Jiangsu, China). Poloxamer188 (F68) was provided by Nanjing Well Chemical Co., Ltd. (Nanjing, China). Sodium deoxycholate (DOC-Na) was supplied by Amresco (Solon, USA). PHBHHx (MW 174,000) containing 14 mol% of R-3-hydroxyhexanoate (HHx) was kindly donated by Professor G. Chen (Tsinghua University, China). All other chemical reagents were of analytical grade or better.

4.2.3 Preparation of PHBHHx Encapsulated Nanoparticles

PHBHHx nanoparticles were prepared with adjustments from a previous study [373] 0.5% (1mg) of ALB-PLC/FITC-Albumin or drug and 3% (7.5mg) PHBHHx w/v Chloroform solution were prepared at a volume of 2mL (Organic Phase), 0.5% w/v of F68 (150mg) (Nanjing Well Chemical Co., Ltd. Nanjing, China) and 0.5% w/v of Sodium Deoxycholate (150mg) (Amresco, Solon, USA) were prepared at a volume of 28ml of 0.22µm filtered Water (Aqueous Phase). Once both the organic and aqueous phases were dissolved, the aqueous phase was filtered and added drop-wise to the organic phase. The aqueous/organic phase were then sonicated (Scientz JY92 – II) for various cycles whilst on ice (sonication cycle was 1 second sonication at a range of power settings and 1 second rest).The nanoparticle emulsion was then placed on a rotary evaporator(Buchi Rotavapor R-3) set at 30^{O}C until all the organic phase was evaporated (emulsion becomes transparent).

4.2.4 Nanoparticle Characterization: Size, Zeta Potential and Poly-dispersity Index

The mean particle size, size distribution and zeta potential of the resulting PHBHHX nanoparticles were characterized using dynamic light scattering (DLS) and electrophoretic light scattering (ELS) technology, respectively, with a Zetasizer Nano ZS90 instrument (Malvern Instruments Ltd., U.K.), using water as a dispersant at 25°C with each cycle of the measurement automatically determined by the instrument system. The particle size was displayed by intensity distribution, and the size distribution was evaluated by polydispersity index (PDI).

4.2.5 Nanoparticle Stability Study

NP and ALB-PLC-NPs were produced as shown previously and zeta sized immediately (time point zero) further measurements were taken at time points 12hrs, 24hrs, 48hrs, 96 hrs and 168 hrs from samples stored at 4°C and room temperature.

4.2.6 Multifactoral Experiment Design

Minitab® (16.2.2) was used to design and evaluate the multifactorial experiment and produce graphical outputs of the data. Three factors were assessed, namely, PHBHHx concentration, sonication power and number of sonication cycles at high and low conditions to bind the key experimental conditions (Table 4.1). This gave a total of eight experimental conditions (cube plot) with a centerpoint to complete the experimental design (Figure 4.1). An N=3 was taken for each run to account for variability in the measurement system and a total of three experimental runs were completed to account for batch-to-batch variability, an assessment of common-cause variation within the nanoparticle production process and an indication of the repeatability of the methodology.

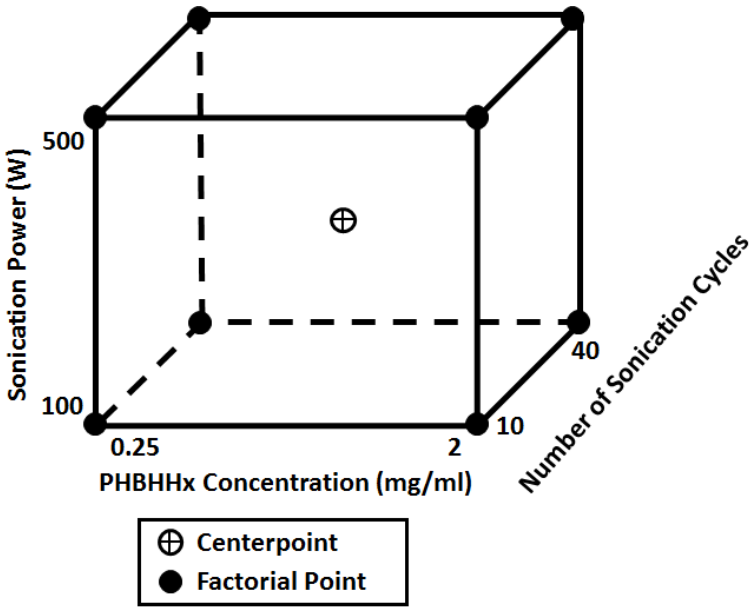

Figure 0.1 Multifactoral Cube illustration of experimental design.

Multifactorial Value	PHBHHx Concentration (mg/ml)	Sonication Power (W)	Number of Sonication Cycles
HIGH	2.000	500	40
MIDDLE	1.125	300	25
LOW	0.250	100	10

Table 0.1 Multifactoral experimental parameters

4.2.7 Encapsulation Efficiency

Briefly, 5 ml of the drug/albumin NPs suspension was mixed with 5 ml NaOH (0.05M). The mixture was stirred for 24 h at room temperature so that the PHBHHx nanoparticles could be degraded by alkaline hydrolysis. The sample was then underwent centrifugation using (100,000 Da molecular weight cut off). The resultant flow-through sample was analysed by GCMS (Drug) or HPLC (Albumin) after a 1:20 dilution. As a result the total added amount of drug/albumin was obtained. Meanwhile, another 0.5 ml drug/albumin NPs suspension was taken, and mixed with 0.5 ml dH_2O. The sample was also analysed by

GCMS after proper dilution. As such the amount of non-encapsulated drug/albumin was obtained. Therefore, the encapsulation efficiency could be calculated according to the following equation

$$\mathrm{EE} = (\frac{\mathrm{Wt} - \mathrm{Wf}}{\mathrm{Wt}}) * 100$$

Equation 1 *Encapsulation Efficiency Formulae*

Where *Wt*= Original concentration at start of encapsulation process, *Wf*= free drug or protein.

4.2.7.1LC-MS/MS Detection of Paclitaxel and Haperzine A

The LC-MS/MS system consisted of an Agilent 1200 series RRLC, which includes an SL auto-sampler, degasser, SL binary pump and an Agilent triple-quadrupole MS (Agilent, USA). The system was controlled with B01.03 software for qualitative analysis and B01.04 software for quantification. Separation was performed in a Diamonsil ODS column (50 × 3.5 mm, 3.4 µm) with a corresponding guard column (ODS, 5 µm). The column was maintained at 30 °C and the injection volume was 1 µl. The mass spectrometer was operated using an electrospray source configured to positive ion mode and the quantification analysis was performed using multiple reaction monitoring (MRM). (M+H) of each analyte was selected as the precursor ion. Instrumental parameters were as follow: gas temperature: 350^{o}C; with a gas flow: 8 ml/min; nebulizer: 30 psi; capillary: 4 000 v.

Gas chromatography separation of Haperzine A was performed using a mobile phase 83% : 17% H_2O and MeOH with 0.1% v/v Formic Acid with a flow rate of 0.4ml/min. Mass spectrometry detection using $(M+H)^+$ m/z 243 - 226, Dwell: 300, fragmentor : 185, collision energy: 4, Polarity: positive.

Gas chromatography separation of Paclitaxel was performed using a mobile phase 30% : 70% H_2O and MeOH with 0.1% v/v Formic Acid with a flow rate of 0.4ml/min. Mass spectrometry detection using $(276)^+$ m/z 876.3 – 308.1, Dwell: 550, Fragmentor : 185, collision energy: 28, Polarity: positive.

4.2.7.2 High Pressure liquid Chromatography detection of Bovine Serum Albumin

Bovine serum albumin fraction V was dissolved in sterile filtered dH2O to make a stock concentration of 1mg/ml. Serial dilutions of the stock solution was undertaken to produce a range of concentration 0.125mg/ml, 0.0625mg/ml, 0.03125mg/ml, 0.015625mg/ml, 0.007825mg/ml, 0.0039025mg/ml and 0mg/ml for production of a standard curve. The samples were then analysed using two phase separation using: mobile phase (A) (double filtered water 99.9% with 0.1% TFA) and mobile phase (B) dH_2O (double filtered acetonitrile 79.95%, 19.95% water and 0.1% TFA). A gradient analysis was set up starting with: 100:0 with a gradient increase to 0:100, over a 20 minute separation using Sepax Bio-C4 protein separation HPLC column. Protein analysis was undertaken using UV analysis at a wavelength of 215nm post separation.

4.2.8 Design of Experiments

Minitab® 16.2.2 was utilised to set-up a 2 level, 3 factor design of experiment (Full Factorial 2^3). Whereby, the upper, median and lower limits of each variable were entered and a randomised run output was created by Minitab®. All samples were then run according to the Minitab® output. Analysis of all factorial data was undertaken utilising the DOE commands in Minitab® 16.2.2 which produced Pareto and interaction plot graphical outputs.

Pareto charts and standardised plots demonstrate the magnitude and importance of an effect in relation to the individual and combinations of variables. The x-axis is dependent upon whether an error term is present. If no error term exists Minitab® uses Lenth's pseudo-standard error which is based upon sparse effect (assumption that the variation in the smallest effect is because of random error, with α=0.05 is set as default).

Interaction plots are a plot of the fitted means (post analysis) for each variable utilising the levels (high, low and median) for each mean and shows the interaction of the variables on the investigated factor.

4.2.9 Experimental Plan

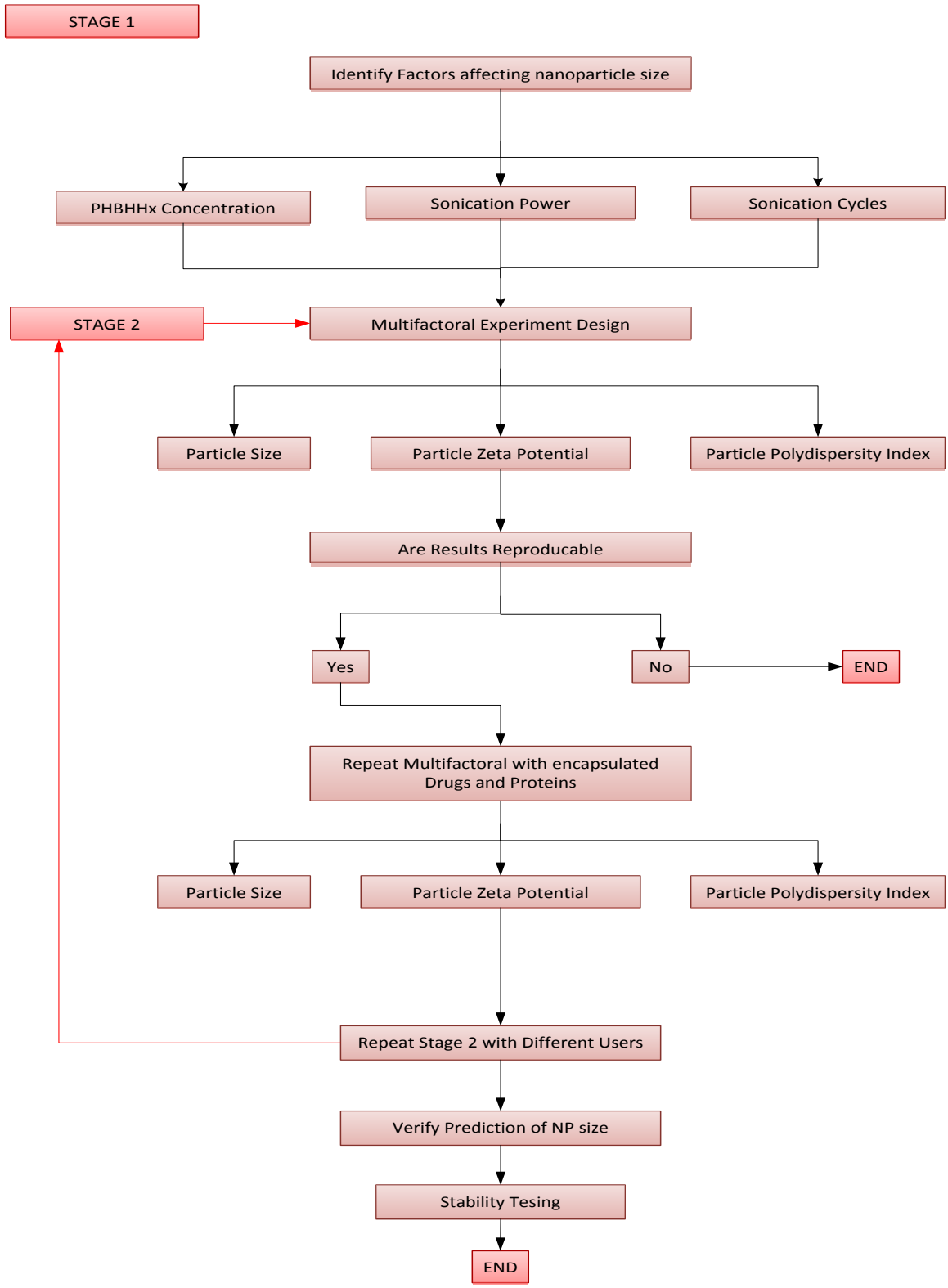

Figure 0.2 Experimental Plan

4.3 Results

4.3.1 Multifactoral Design Blank Nanoparticles

Minitab® (16.2.2) was used to design and evaluate the DOE and produce graphical outputs of the data. Three key factors were assessed, namely, PHBHHX concentration, sonication power and number of sonication cycles at high and low conditions to enclose the experimental.

This gave a total of eight experimental conditions (cube plot) with a centerpoint to complete the experimental design. An N=3 taken for each run to account for variability in the measurement system and a total of three experimental runs were completed to account for batch-to-batch variability, an assessment of common-cause variation within the nanoparticle production process and an indication of the repeatability of the methodology.

From the data obtained from the cube plot shown in Figure 4.3 a range of nanoparticle properties are produced with a size range of 89.5nm – 229.3nm, PDI ranging from 0.1293 – 0.1923 and a zeta potential ranging from -9.8mV - -13.7mV.

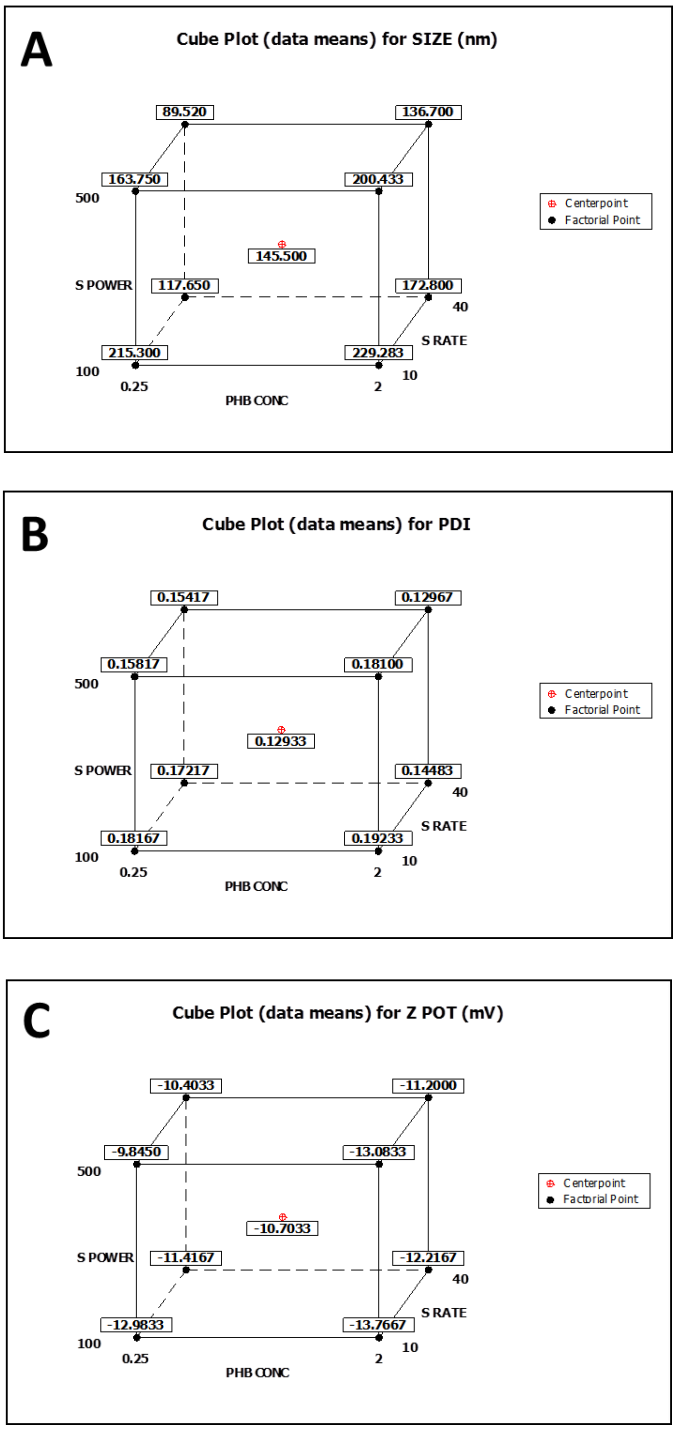

Figure 0.3 Cube plot of the multifactorial designed experiment showing the process variables

Shows high/low values and the centre point for first run. A) Size, B) PDI and C) Zeta potential

From the cube plot in Figure 4.4 nanoparticle properties with a size range of 89.4nm – 234.05nm, PDI ranging from 0.127 – 0.202 and a zeta potential ranging from -10.3mV - -

12.9mV. From both cube plots the major effectors of nanoparticle size can be identified by magnitude of effect.

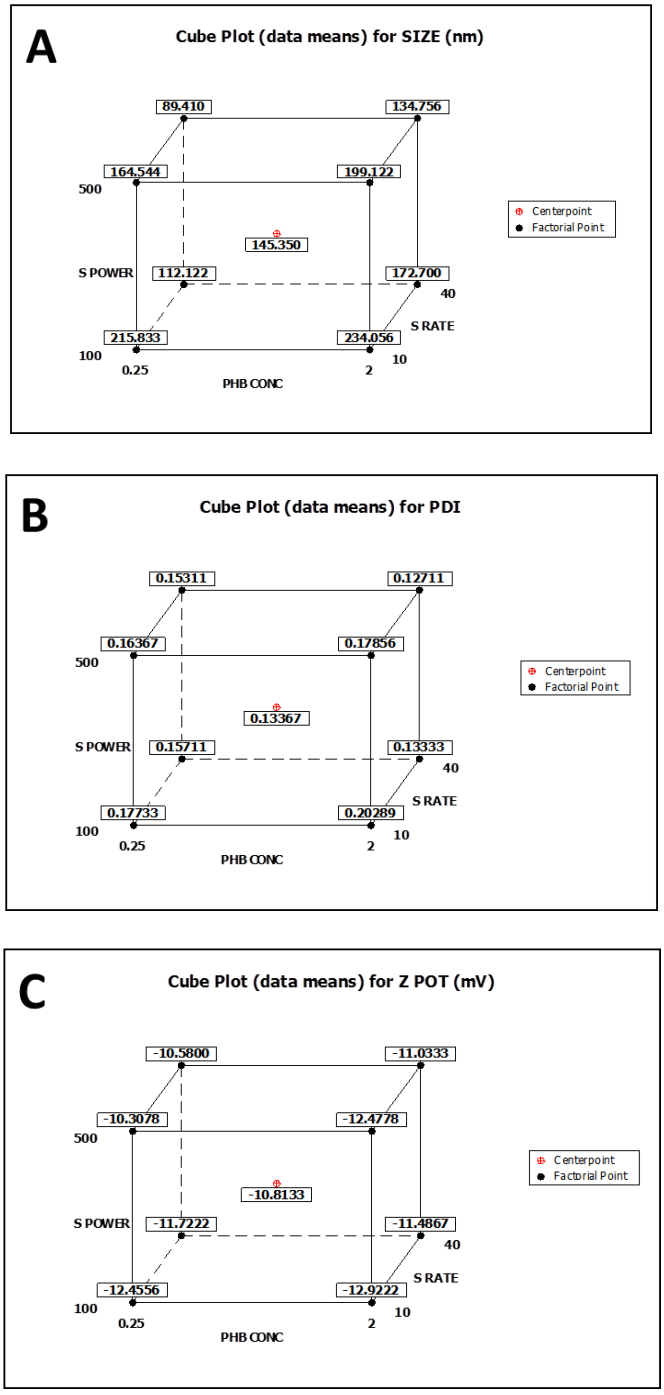

Figure 0.4 Cube plot of the multifactorial designed experiment showing the process variables

Shows high/low values and the centre point for second run. A) Size, B) PDI and C) Zeta potential

From Figure 4.5 the magnitude of effect of each variable can be shown for each nanoparticle property. Sonication rate had the greatest effect on nanoparticle size (Figure 4.5A), followed by PHBHHx concentration then sonication power. However all variables were shown to have an effect on nanoparticle size. The major effector of PDI (Figure 4.5B) was shown to be sonication rate followed by combination of PHBHHx concentration with sonication rate and finally sonication power with PHBHHx concentration and the combinations of PHBHHx and sonication power, sonication power and sonication rate & the combination of sonication power, PHBHHx concentration and sonication rate having no effect. Zeta potential (Figure 4.5C) showed all combinations and individual variables with the exception of the combination of sonication power and sonication rate having no magnitude effects.

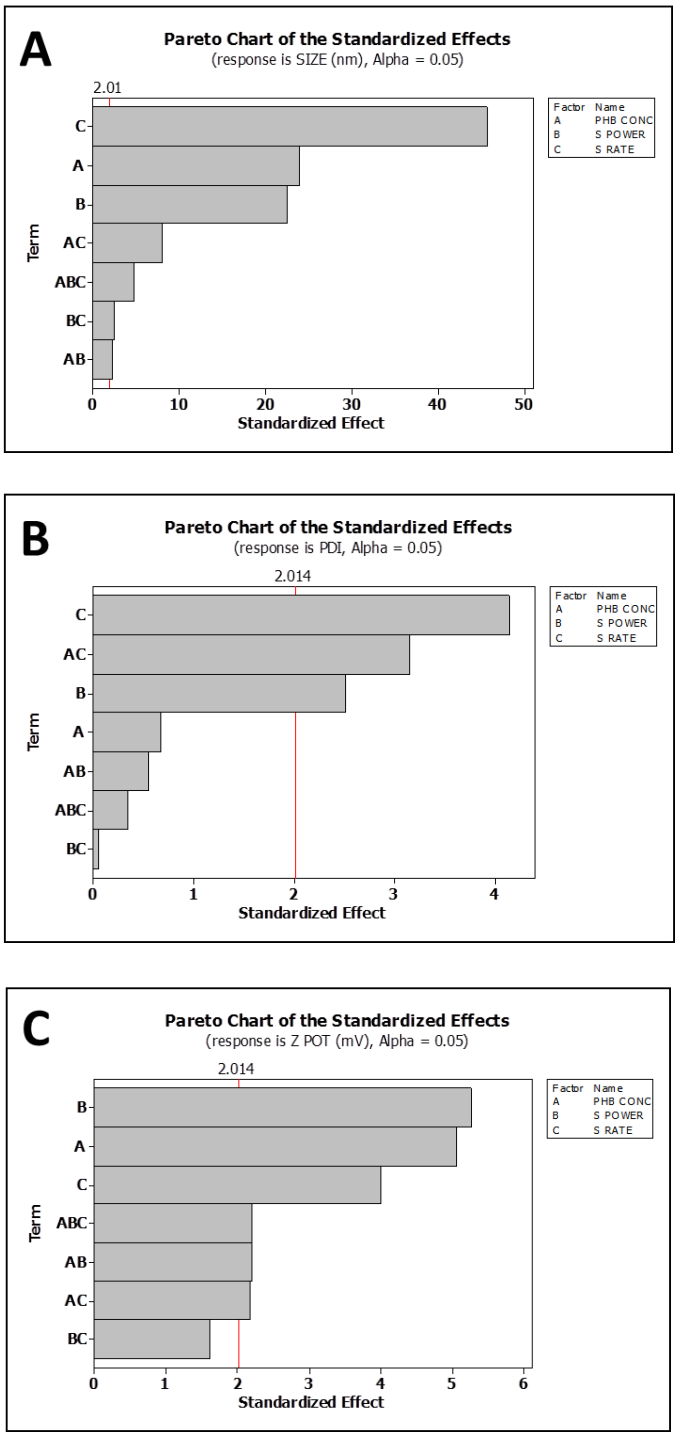

Figure 0.5 Pareto chart of standardised effects for the size production of nanoparticles.

Graph shows single and multi-variable effects with statistical significance shown at p=0.05 for first run. A) Size, B) PDI and C) Zeta potential

From Figure 4.6 the magnitude of effect of each variable can be shown for each nanoparticle property. Sonication rate had the greatest effect on nanoparticle size (Figure 4.6A), followed by PHBHHx concentration then sonication power. However all variables were shown to have an effect on nanoparticle size. The major effector of PDI (Figure 4.6B) was shown to be sonication rate followed by combination of PHBHHx concentration with sonication rate and finally sonication power with PHBHHx concentration and the combinations of PHBHHx and sonication power, sonication power and sonication rate & the combination of sonication power, PHBHHx concentration and sonication rate having no effect. Zeta potential (Figure 4.6C) showed all combinations and individual variables with the exception of the combination of sonication power & sonication rate and the combination of PHBHHx concentration, sonication power and sonication rate having no magnitude effects.

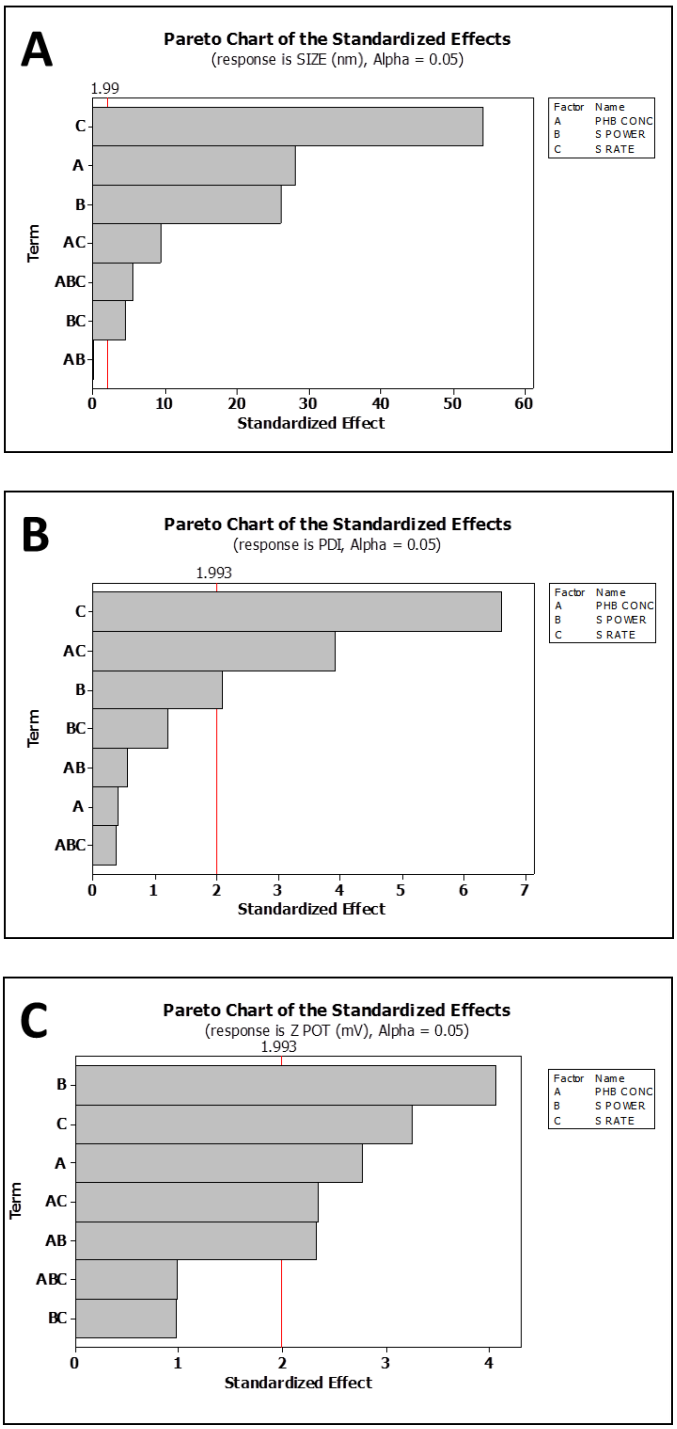

Figure 0.6 Pareto chart of standardised effects for the size production of nanoparticles.

Graph shows single and multi-variable effects with statistical significance shown at p=0.05 for Second run. A) Size, B) PDI and C) Zeta potential

The Standardised plots shown in Figure 4.7A-C, show the variable factors which are significant to the nanoparticle properties of Size (Figure 4.7A), PDI (Figure 4.7B) and Zeta Potential (Figure 4.7 C) for Run 1.

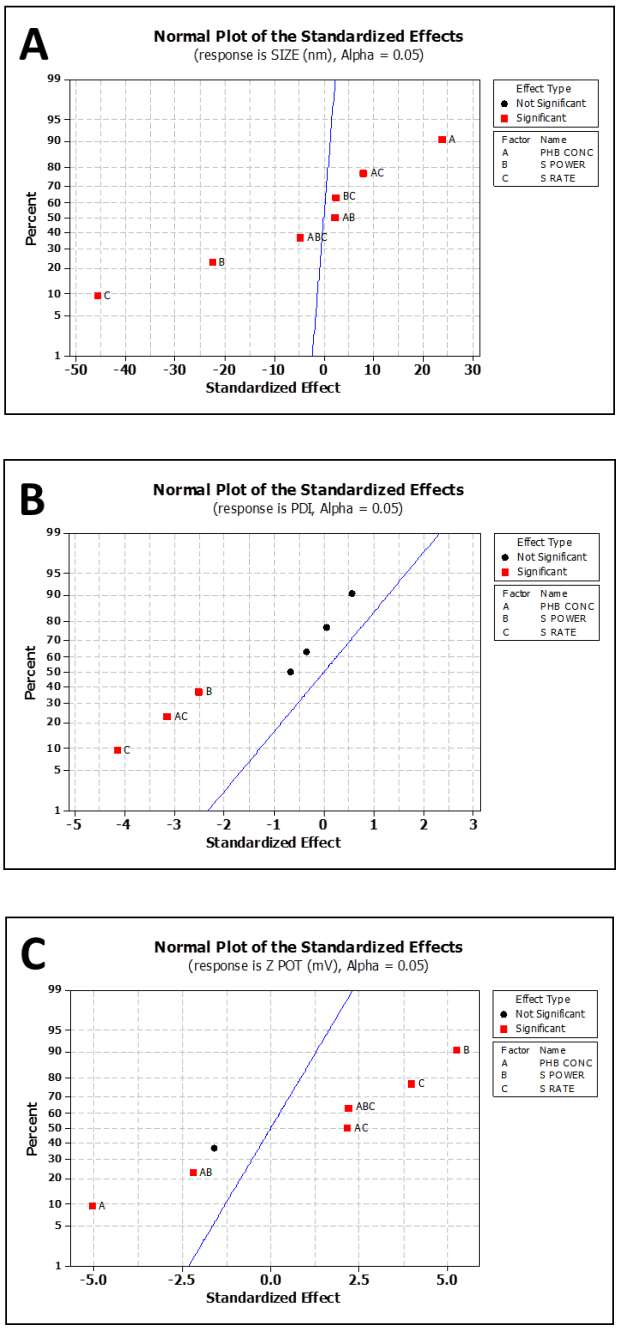

Figure 0.7 Main effects plot showing the effect of the three variables from the first run.

A) Size of nanoparticles during production, B) PDI of nanoparticles during production and C) Zeta Potential.

The Standardised plots shown in Figure 4.8A-C, show the variable factors which are significant to the nanoparticle properties of Size (Figure 4.8A), PDI (Figure 4.8B) and Zeta Potential (Figure 4.8C) for Run 2.

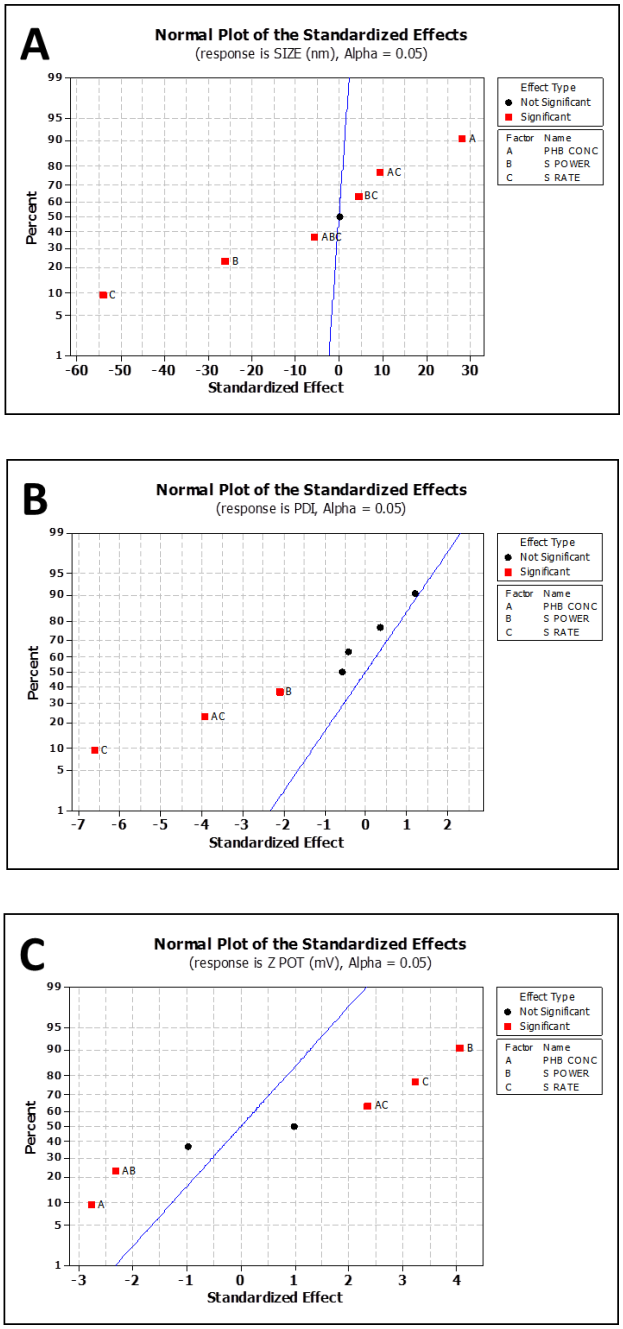

Figure 0.8 Main effects plot showing the effect of the three variables from the second run.

A) Size of nanoparticles during production, B) PDI of nanoparticles during production and C) Zeta Potential

The Interaction plots shown in Figure 4.9A-C, show the interaction of factors (the further the lines are from parallel the greater the interaction) to the nanoparticle properties of Size (Figure 4.9A), PDI (Figure 4.9B) and Zeta Potential (Figure 4.9C) for Run 1.

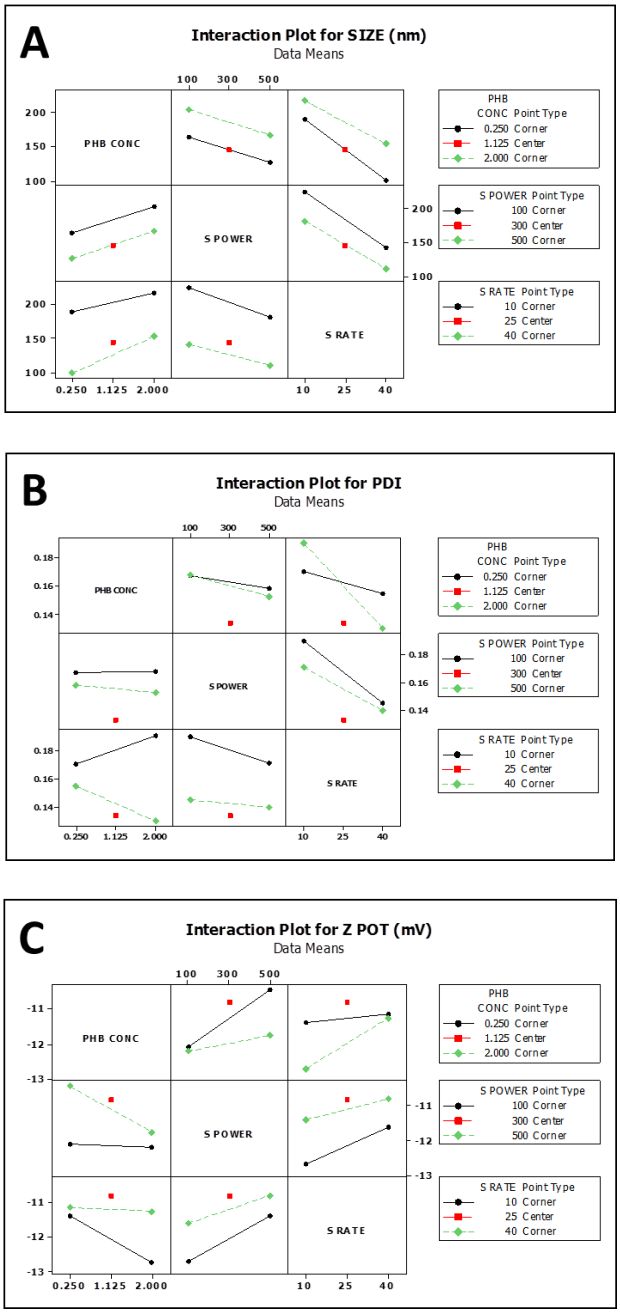

Figure 0.9 Interaction plot showing the effect of the three variables from the first run.

A) Size of nanoparticles during production and B) PDI of nanoparticles during production and C) Zeta Potential.

The Interaction plots shown in Figure 4.10A-C, show the interaction of factors (the further the lines are from parallel the greater the interaction) to the nanoparticle properties of Size (Figure 4.10A), PDI (Figure 4.10B) and Zeta Potential (Figure 4.10C) for Run 2

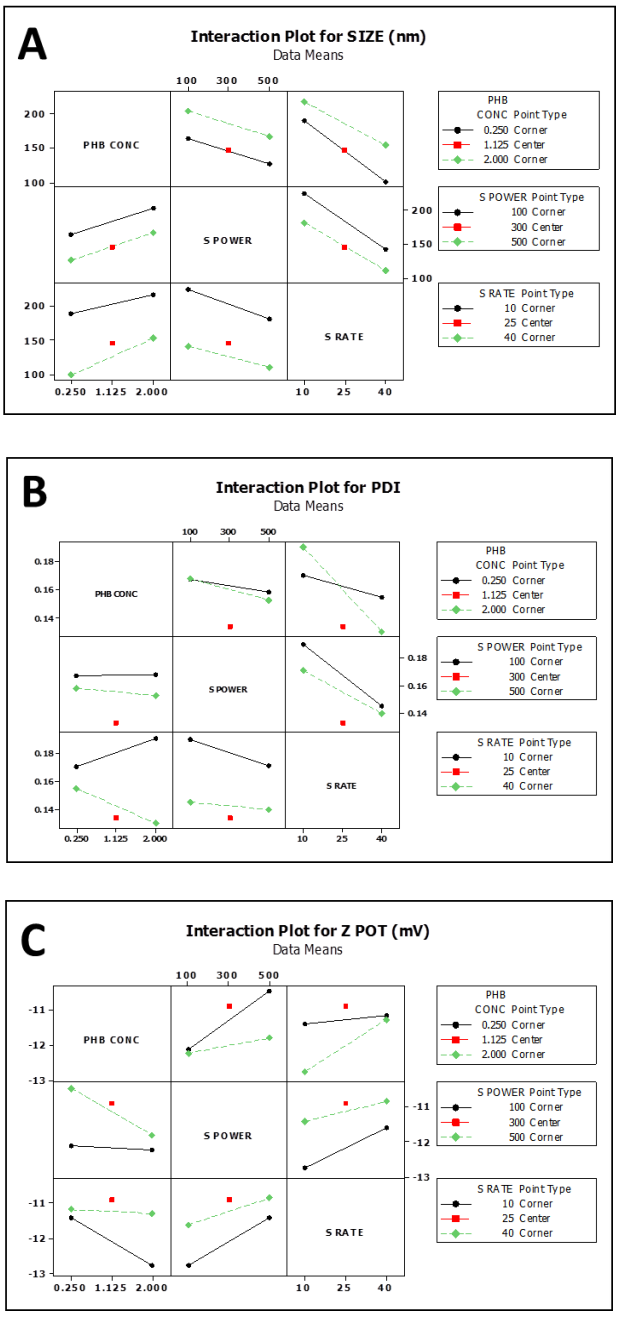

Figure 0.10 Interaction plot showing the effect of the three variables from the second run.

A) Size of nanoparticles during production and B) PDI of nanoparticles during production and C) Zeta Potential.

From the DOE investigation we deduced that by fixing concentration PHBHHx molecular weight and sonication power and introducing variations in sonication cycles we may be able to produce a prediction curve for the production of PHBHHx nanoparticles.

4.3.1.1 Production of a controlled Blank Nanoparticle Size by fixing PHBHHx concentration and Power and varying the number of sonication cycles.

From the preliminary data observed in the multifactorial design the inclusion of 3 extra sonication points were included in production of a standard curve to predict nanoparticle size namely 15, 25 and 35 sonication cycles. The PHBHHx concentration was fixed at 0.25mg/ml and sonication power was fixed at either 100W or 500W (Table 4.2).

Power	10 Sonication Cycles	15 Sonication Cycles	20 Sonication Cycles	25 Sonication Cycles	30 Sonication Cycles	35 Sonication Cycles	40 Sonication Cycles
100W	204.32nm ± 3.74nm	185.00nm ± 2.87nm	167.65nm ± 4.50nm	154.33nm ± 2.75nm	140.07nm ± 1.85nm	132.87nm ± 1.16nm	122.43nm ± 2.79nm
500W	165.78nm ± 1.55nm	134.80nm ± 4.56nm	117.03nm ± 3.37nm	107.07nm ± 0.69nm	98.45nm ± 2.45nm	94.88nm ± 0.67nm	94.26nm ± 0.88nm

Table 0.2 Nanoparticle prediction curve full data set

From the data obtained in the addition of sonication points a standard curve graph for two power settings with fixed PHBHHx concentration was created (Figure 4.11).

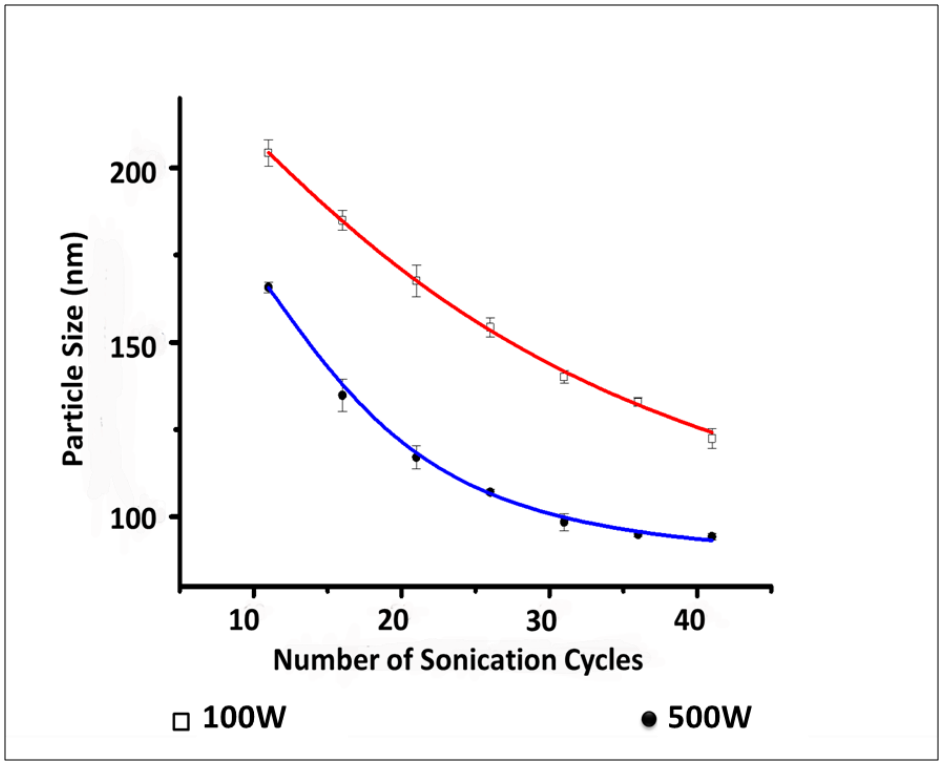

Figure 0.11 Blank Nanoparticle prediction Standard Curve

Blank nanoparticle size prediction curve at high and low sonication power and PHBHHX concentration of 0.25 mg/mL. 100W: Sonication power of 100 W. 500W: Sonication power of 500 W. Graph shows mean values ± 1 standard deviation (N=6) over two batches of N=3. 100W R2= 0.99549, 500W R2= 0.99475.

From the graph in Figure 4.11 an equation was extracted to predict nanoparticle size by fixing PHBHHx concentration, Sonication Power and using sonication cycles as a variable to produce a range of blank nanoparticles to test the logistic dose response curve Table 4.4 and Equation 2).

From the data in Table 4.3 and subsequent graph the following equations were created to predict nanoparticle size for sonication power of both 100W and 500w.

Equation Component	100W	500W
A1 (Initial Value)	241.622	197.357
A2 (Final Value)	67.8974	87.0395
x0 (centre)	25.4944	15.1511
p (Curve constant)	1.54875	2.84045

Table 0.3 Values to be attributed to the equation for nanoparticle prediction

$$\text{Nanoparticle Size Prediction} = \frac{A1 - A2}{1 + \frac{n}{x0}^{p}} + A2$$

Where n=number of Sonication cycles.

Equation 2 Logistic dose response curve

4.3.1.2 Investigating whether encapsulation of a drug/protein has an effect on Nanoparticle size

To validate the standard curve nanoparticles which encapsulated either paclitaxel (Table 4.4 and Figure 4.12), Albumin (Table 4.5 and Figure 4.13) or Haperzine A (Table 4.6 and Figure 4.14) were produced using two power settings of 500W and 100W with fixed PHBHHx concentration of 0.25mg/ml and utilising sonication cycle settings of 10, 20, 30 and 40.

Power	10 Sonication Cycles	20 Sonication Cycles	30 Sonication Cycles	40 Sonication Cycles
100W	199.0nm ± 1.65nm	163.5nm ± 2.87nm	139.8nm ± 4.24nm	124.1nm ± 2.2nm
500W	161.7nm ± 1.85nm	116.8nm ± 2.13nm	99.5nm ± 1.93nm	92.3nm ± 2.77nm

Table 0.4 Paclitaxel Loaded nanoparticle Size validation

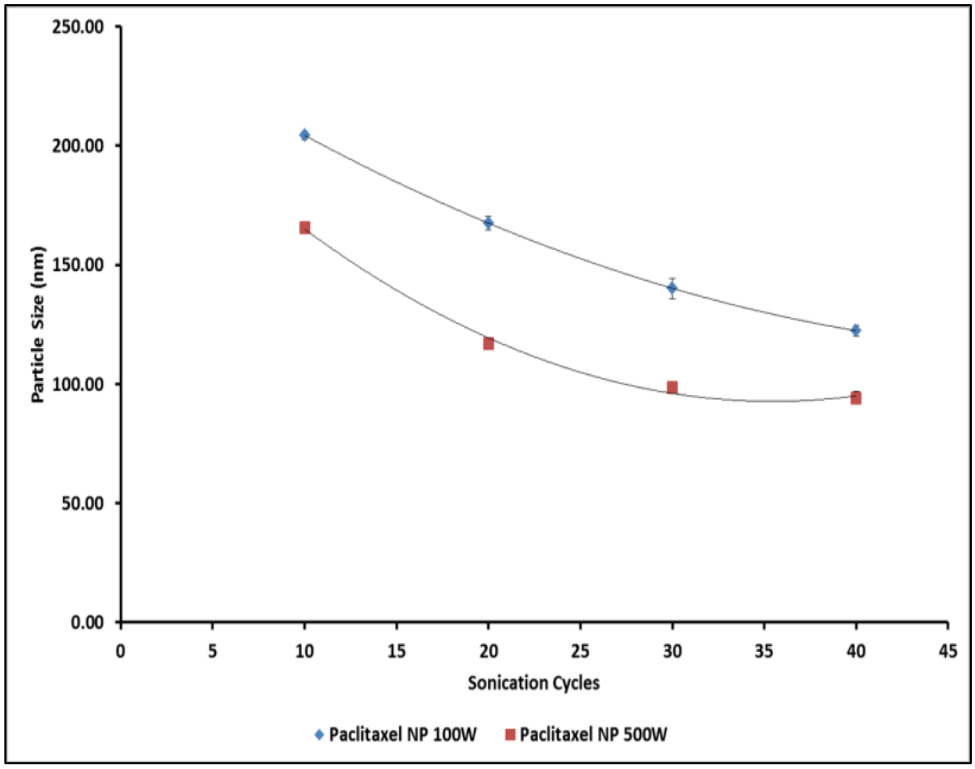

Figure 0.12 Paclitaxel loaded Nanoparticle validation Curve

Size validation compared to original blank PHBHHX nanoparticle curve of Paclitaxel. 100W: Sonication power of 100 W. 500W: Sonication power of 500 W. Graph shows mean values ± 1 standard deviation (N=6) over two batches of N=3.

Power	10 Sonication Cycles	20 Sonication Cycles	30 Sonication Cycles	40 Sonication Cycles
100W	204.0nm ± 5.28nm	164.0nm ± 4.25nm	135.2nm ± 5.13nm	116.4nm ± 2.69nm
500W	161.4nm ± 2.57nm	115.6nm ± 5.33nm	98.6nm ± 3.67nm	93.4nm ± 5.97nm

Table 0.5 Albumin-PLC Loaded nanoparticle Size validation

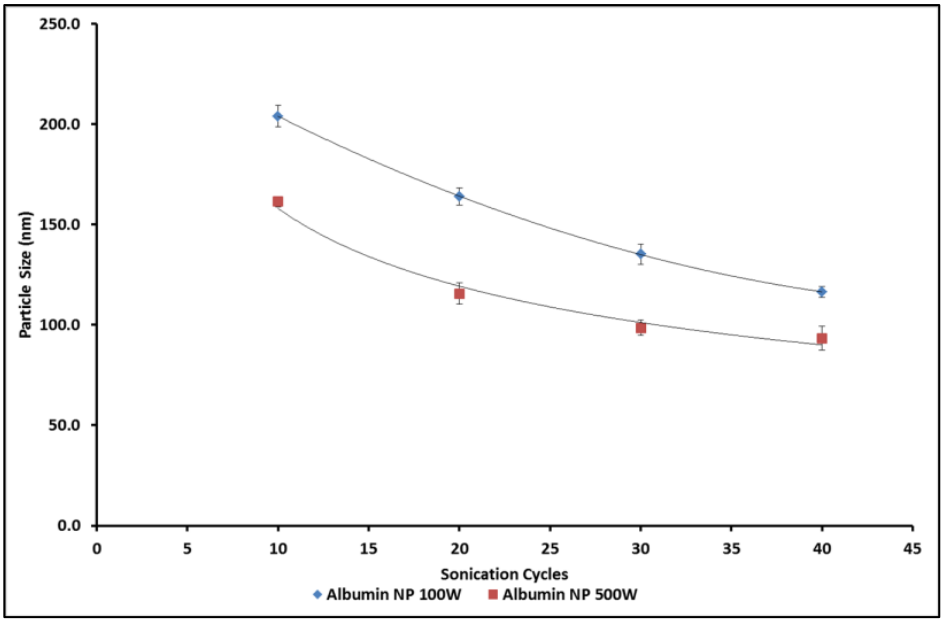

Figure 0.13 Albumin-PLC loaded Nanoparticle validation Curve

Size validation compared to original blank PHBHHX nanoparticle curve of Albumin encapsulated nanoparticles. 100W: Sonication power of 100 W. 500W: Sonication power of 500 W. Graph shows mean values ± 1 standard deviation (N=6) over two batches of N=*3*.

Power	10 Sonication Cycles	20 Sonication Cycles	30 Sonication Cycles	40 Sonication Cycles
100W	210.1nm ± 1.65nm	167.5nm ± 4.60nm	145.5nm ± 2.01nm	132.1nm ± 5.2nm
500W	165.2nm ± 7.08nm	117.8nm ± 1.38nm	98.2nm ± 0.63nm	94.2nm ± 1.46nm

Table 0.6 Haperzine A Loaded nanoparticle Size validation

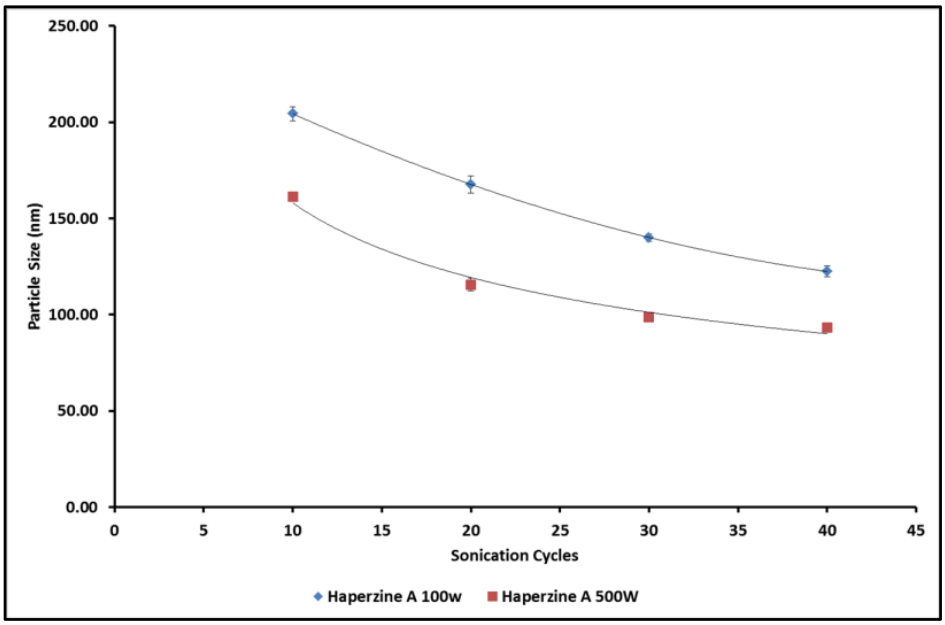

Figure 0.14 Haperzine A loaded Nanoparticle validation Curve

Size validation compared to original blank PHBHHX nanoparticle curve of HaperzineA encapsulated nanoparticles. 100W: Sonication power of 100 W. 500W: Sonication power of 500 W. Graph shows mean values ± 1 standard deviation (N=6) over two batches of N=3.

From the data obtained in tables 4.4 – 4.6 a prediction error (nm) and percentage (%) can be calculated to establish the validity of the nanoparticle prediction curve.

Sonication Power (W)	Curve Prediction (nm)	Paclitaxel		HaperzineA		ALB-PLC-NP	
		Prediction Error (nm)	Prediction Error (%)	Prediction Error (nm)	Prediction Error (%)	Prediction Error (nm)	Prediction Error (%)
100	204.5	5.47	2.67	5.65	2.76	0.44	0.21
	167.7	4.26	2.54	0.26	0.15	3.69	2.20
	141.7	1.96	1.38	4.08	2.86	6.52	4.60
	124.2	0.07	0.06	7.88	6.35	7.75	6.24
500	165.7	3.98	2.40	0.48	0.29	4.28	2.58
	118.3	1.54	1.31	0.54	0.46	2.68	2.26
	99.8	0.30	0.30	1.65	1.66	1.21	1.21
	93.2	0.85	0.91	1.03	1.10	0.16	0.17
Overall Average Prediction Error		**2.30 ± 2.02**	**1.45 ± 1.01**	**2.70 ± 2.84**	**1.96 ± 2.06**	**3.34 ± 2.78**	**2.44 ± 2.10**

Table 0.7 Loaded Nanoparticle Size prediction Evaluation and Error.

Following the evaluation of blank nanoparticles, the process was repeated with Heperzine-A, Paclitaxel and ALB-PL-NPs to see if the same rule applied to these complexes since then the size evaluation can be conducted using blank polymer only nanoparticles and the results extrapolated for drug encapsulated nanoparticles. From Figures 4.15 – 4.17 it can be seen that these encapsulated drugs conformed to the same production size curve as the blank nanoparticles, meaning that the original curve can be used to select a desired nanoparticle size, for a specified application.

The accuracy of this relationship has also been evaluated in Table 4.7, which shows that the maximum overall (mean) prediction error from blank to drug encapsulated nanoparticles as 3.34 $\pm$ 2.78 nm which equates to 2.44 $\pm$ 2.10 %, with a prediction error range of 0.07 – 7.88 nm or 0.06 – 6.35% for the three drugs.

4.3.2 Encapsulation Efficiency

Encapsulation Efficiency was calculated using the following formulae:

Drug Loaded NPs	Size (nm)	PDI	Zeta Potential (mV)	EE (%)
Haperzine A (1:60)	95.2 ± 0.73	0.128 ± 0.007	-12.2 ± 0.35	49.98 ± 1.50
Haperzine A (1:90)	94.2 ± 1.46	0.146 ± 0.012	-13.8 ± 1.85	48.81 ± 1.69
Haperzine A (1:120)	93.3 ± 1.46	0.137 ± 0.013	-15.33 ± 1.10	63.50 ± 1.57

Table 0.8 Haperzine-A loaded nanoparticles optimisation.

Values are mean ± s.d. (n=3).

Drug Loaded NPs	Size (nm)	PDI	Zeta Potential (mV)	EE (%)
Albumin (1:60)	93.4 ± 0.42	0.246± 0.002	-35.9 ± 2.4	59.11 ± 1.50
Albumin (1:90)	95.5 ± 0.25	0.211 ± 0.006	-35.3 ± 0.9	76.63 ± 2.14
Albumin (1:120)	94.2 ± 0.36	0.250 ± 0.010	-37.8 ± 1.7	66.89 ± 2.30

Table 0.9 Albumin loaded nanoparticles optimisation.

Values are mean ± s.d. (n=3).

The encapsulation efficiency of Heperzine-A (Table 4.8) was found to highest at a drug to polymer ratio of 1:120 with 63.50 ± 1.57 % with lower entrapment of around 50% for ratios of 1:60 and 1:90. Transmission electron microscopy (Figure 4.15) showed that the Heperzine-A loaded nanoparticles were spherical in shape and that the size distribution of the nanoparticles was low.

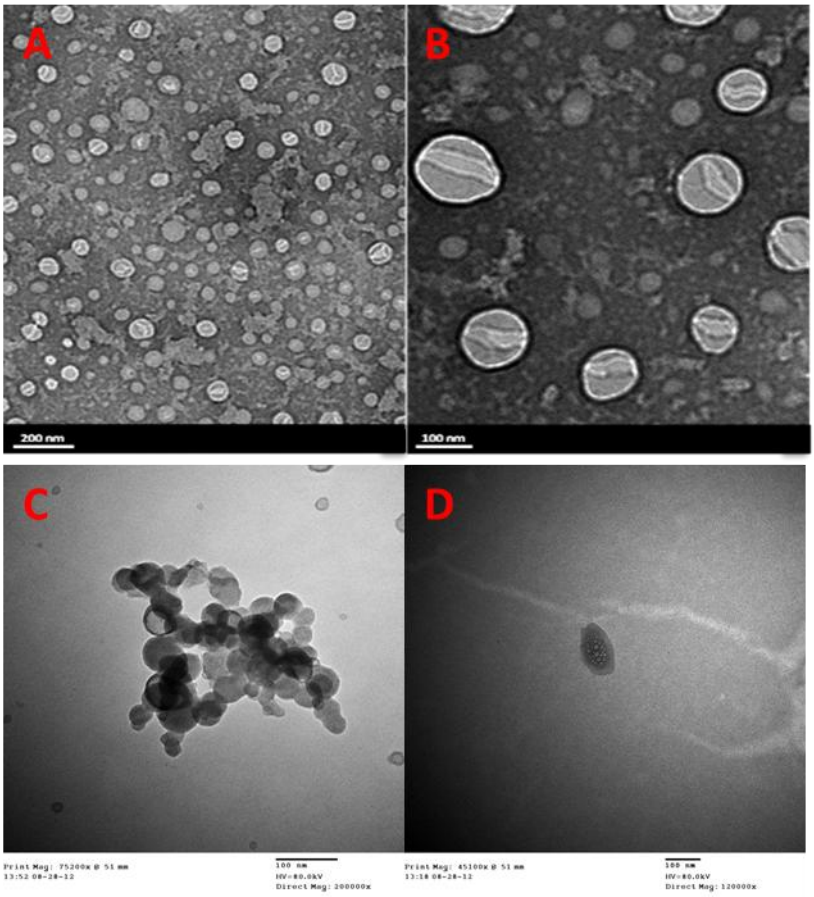

Figure 0.15 Transmission Electron Microscopy (TEM) of PHBHHx nanoparticles

A) Haperzine A loaded PHBHHx nanoparticles (low magnification), B) Haperzine A loaded PHBHHx nanoparticles (high magnification), C) Blank PHBHHx nanoparticles (low magnification) and D) Blank PHBHHx nanoparticles (high magnification). (A & B imaged at West China School of Pharmacy, C & D imaged at School of Medicine, Tsinghua University.)

4.3.3 Effects of controlled manufacture on drug release profiles

Having previously identified that Haperzine A showed a high encapsulation. The next step in the investigation was to evaluate the effects of DOE manufacture of drug containing nanoparticles. This investigation would produce a new batch of 4 haperzine A nanoparticles with varying PHBHHx concentrations and production settings (Table 4.10).

Sample	PHBHHx Concentration (mg/ml)	Sonication Power	Sonication Cycles	Haperzine A Concentration (mg/ml)
1	0.25	500	25	0.000521
2	0.25	100	20	0.000521
3	2	500	35	0.004167
4	2	100	15	0.004167

Table 0.10 Haperzine A loaded nanoparticles for release profile production settings

From the above experimental settings the following Haperzine A loaded nanoparticle profile were obtained and showed a decrease in encapsulation efficiency when PHBHHx concentration was increased (Table 4.11).

Sample	Size (nm)	PDI	Zeta Potential (mV)	Prediction Curve Percentage Error (%)	Encapsulation Efficiency (%)
1	108.33±3.69	0.11±0.03	-17.83±1.39	0.95	60.93±4.85
2	119.93±3.02	0.17±0.04	-21.18±3.08	0.3	75.54±4.5
3	134.77±7.56	0.07±0.02	-23.37±1.14	1.4	22.81±5.44
4	183.27±5.5	0.14±0.06	-32.10±2.38	1.05	21.39±7.27

Table 0.11 Haperzine A nanoparticle properties and Encapsulation Efficiency.

4.4 Multifactoral investigation into the effects of surfactant

From the data obtained from the cube plot shown in Figure 4.16 range of nanoparticle properties are produced with a size range of 77.7nm – 102.8nm, PDI ranging from 0.092 – 0.169 and a zeta potential ranging from -8.37mV - -33.95mV.

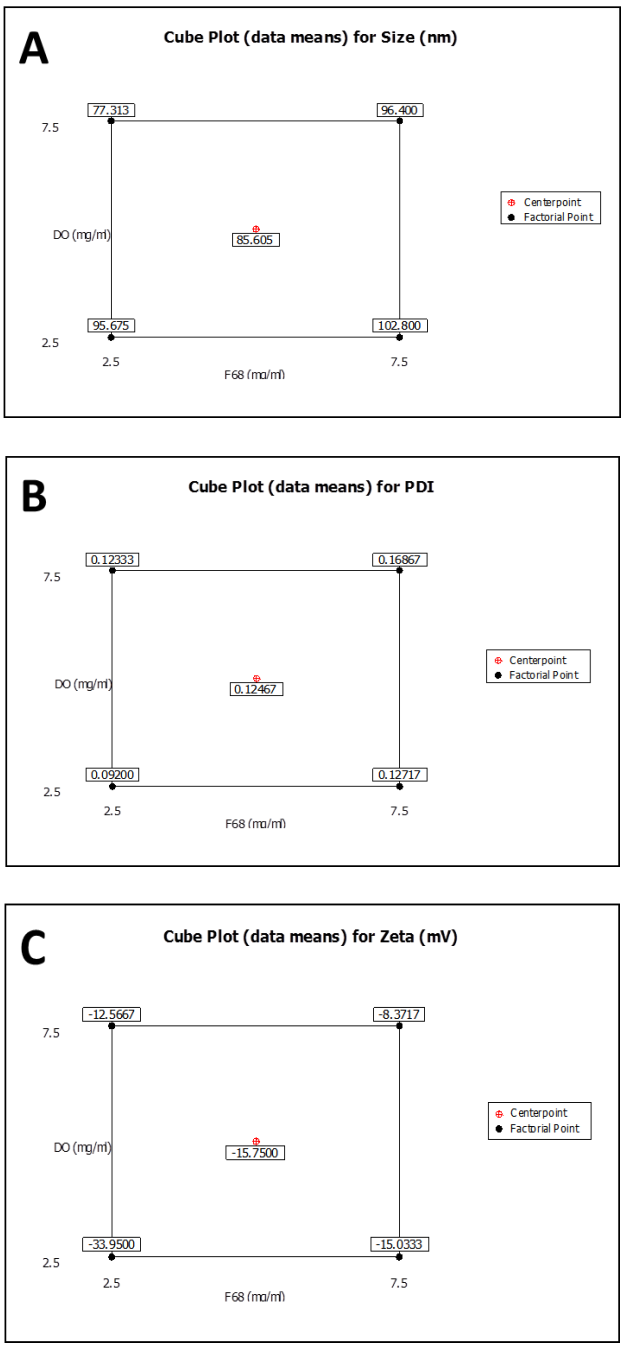

Figure 0.16 Cube plot of the multifactorial DOE for surfactant.

A) Size, B) PDI and C) Zeta potential.

Figure 4.17A and Figure 4.17B shows the magnitude effects of DO and F68. F68 has the greatest magnitude effect on nanoparticle size and PDI. Figure 4.17C shows DO having the greatest effect on zeta potential followed by F68 and the combination of F68 and DO.

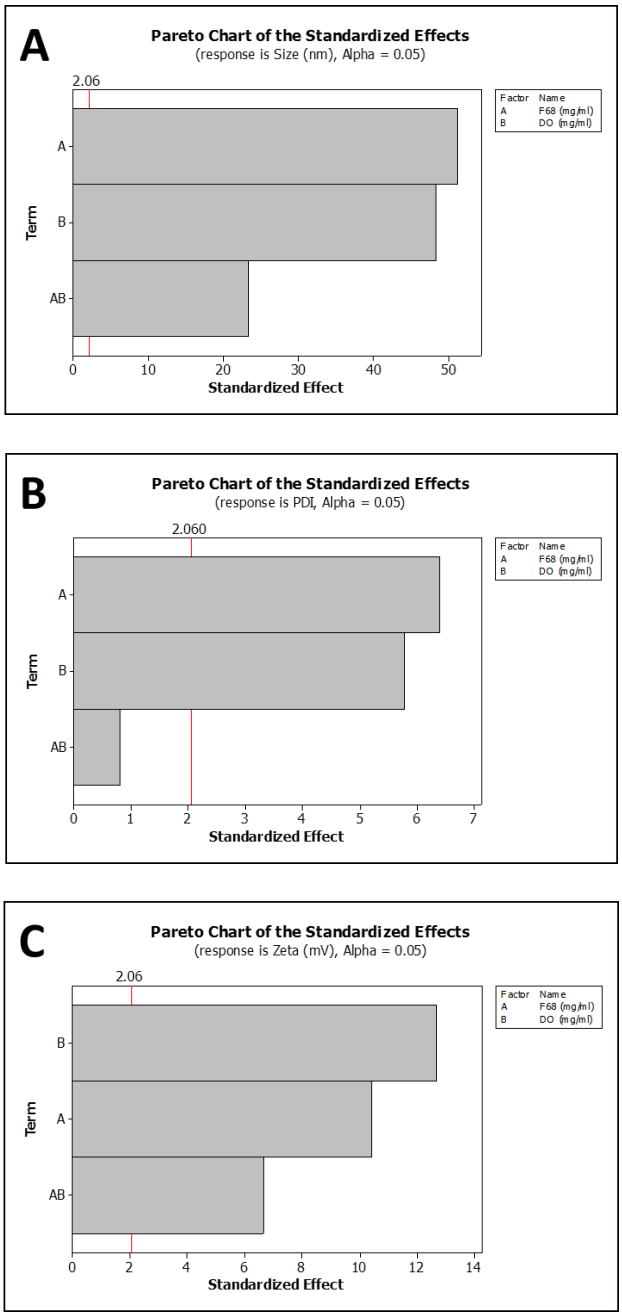

Figure 0.17 Combined and individual effects of surfactants

A) Size, B) PDI and C) Zeta Potential

Figure 4.18A, B & C shows the variables that have a significant effect on nanoparticle properties.

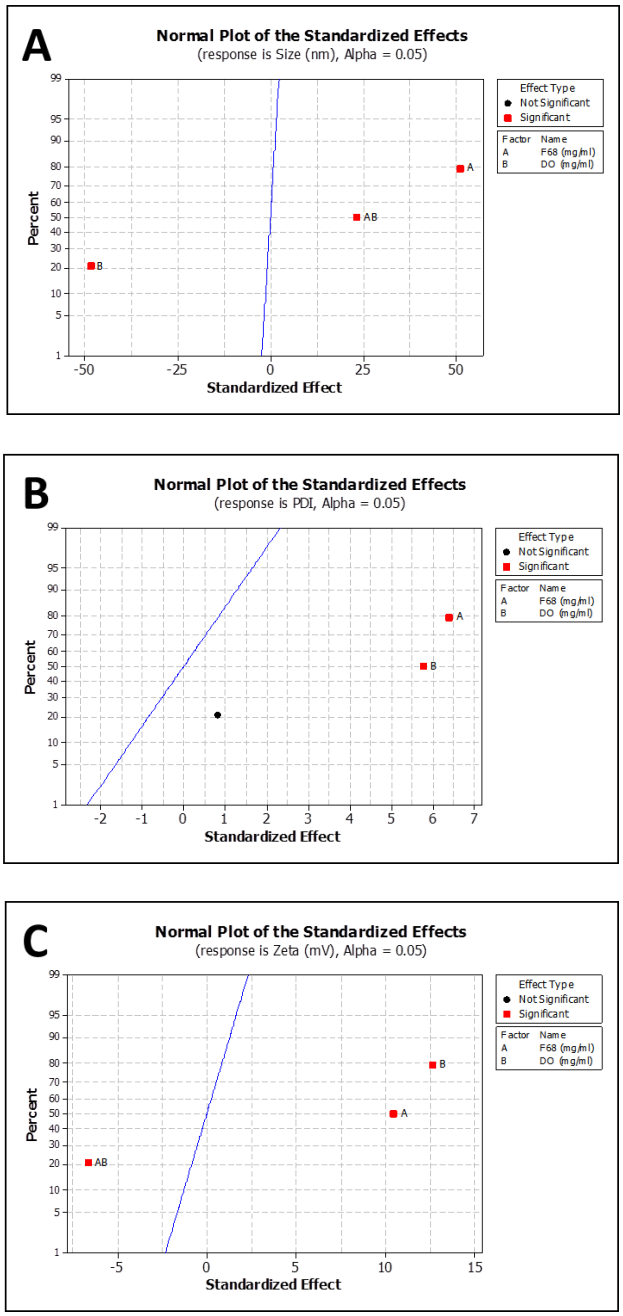

Figure 0.18 Standardised Effects

Shows Standardised effects on A) Size, B) PDI and C) Zeta potential

The Interaction plots shown in Figure 4.19A-C, show the interaction of factors (the further the lines are from parallel the greater the interaction) to the nanoparticle properties of Size (Figure 4.19A), PDI (Figure 4.19B) and Zeta Potential (Figure 4.19C).

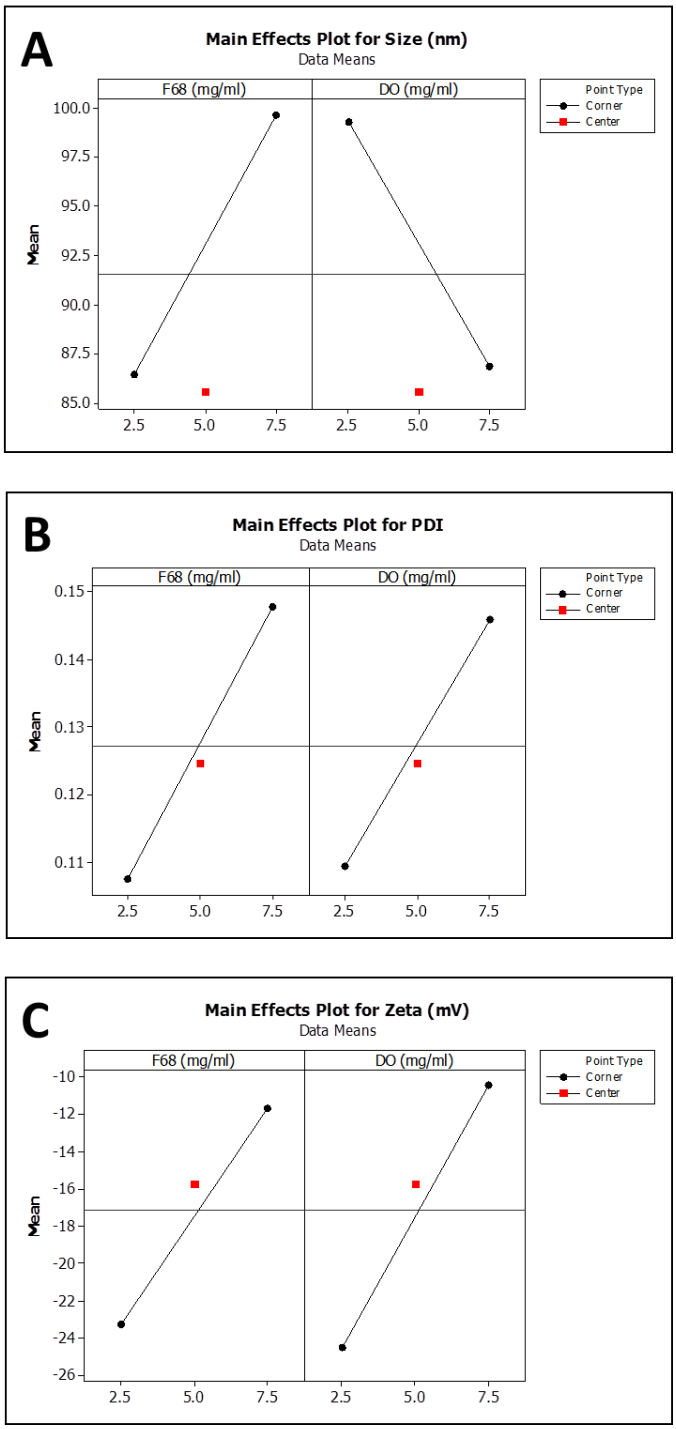

Figure 0.19 Interaction Plot for F68 and Deoxycholate

Shows the interaction of the Surfactants on PDI, Zeta Potential and Size

Figure 4.20 shows the 3D combinational effects of DO and F68 on nanoparticle size (Figure 4.20A), PDI (Figure 4.20B) and nanoparticle zeta potential (Figure 4.20C).

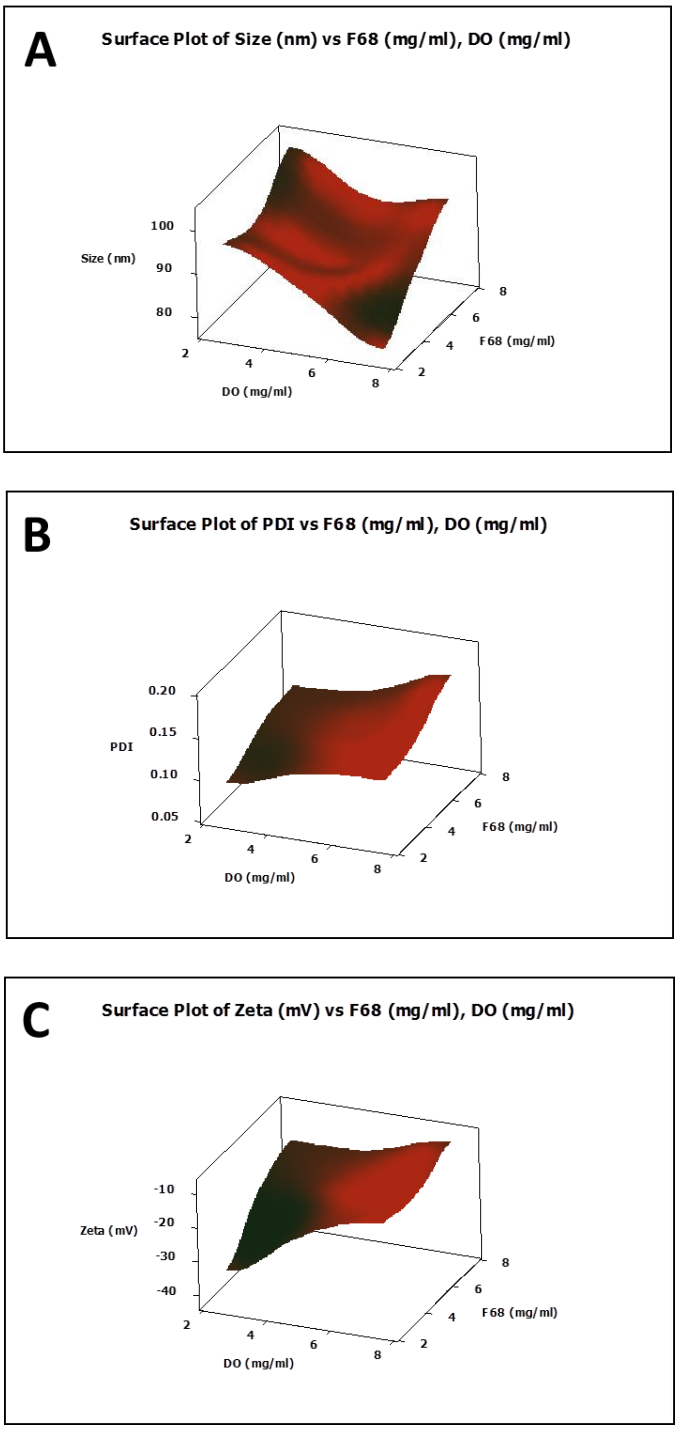

Figure 0.20 Surfactant Surface Plot

showing interactions between surfactant concentration and nanoparticle properties.

By fixing sonication power at 500w, sonication rate at 40 and PHBHHx concentration at 025mg/ml and producing a further two factorial DOE for the surfactants we have

identified a further mechanism of decreasing nanoparticle size to 77.31 ± 0.35 nm and the possibility of control nanoparticle charge (Table 4.12).

Sample	Size (nm)	PDI	Zeta Potential (mV)
0.25mg/ml + 7.5mg of F68 and 7.5mg/ml DO	77.31±0.35	0.123±0.010	-12.57±0.58
0.5mg/ml + 5mg of F68 and 5mg/ml DO	85.61±0.63	0.125±0.005	-15.75±0.80
0.25mg/ml + 7.5mg of F68 and2.5 mg/ml DO	95.68±0.60	0.092±0.022	-33.95±4.96
0.75mg/ml + 7.5mg of F68 and 7.5mg/ml DO	96.40±0.73	0.169±0.017	-8.37±0.50
0.75mg/ml + 7.5mg of F68 and 2.5 mg/ml DO	102.80±0.74	0.127±0.016	-15.03±3.29

Table 0.12 Surfactant multifactorial results for Size, PDI and zeta potential

4.5 Nanoparticle Stability

The blank nanoparticle stability study was conducted over 168 hours (7 days) to assess the change in size, PDI and zeta potential of the nanoparticles (Table 4.13 – Table 4.16 and Figure 4.21A, B and C). The nanoparticle size was stable for the full 168 hours at both high and low sonication settings over the range of nanoparticle sizes. There was also no significant difference seen in the nanoparticle size stability when stored at room temperature compared to 4°C.

The PDI of the blank nanoparticles showed a slight fluctuation over the 168 hour period, resulting in a slightly elevated after 168 hours (Figure 4.21B). The PDI recorded at the end of the 168 hour period was still below the 0.3 benchmark figure for *in vivo* drug delivery applications and there was no significant difference between the nanoparticles PDI after 168 hours stored at room temperature compared to 4°C.

The zeta potential of the blank nanoparticles remained stable over the 168 hour period albeit with minor fluctuations at the measurement intervals (Figure 4.21C). This considered, the zeta potential for the nanoparticles remained in the accepted range of -10 to -40 mv for the duration of the study and there was no observed difference between those stored at 4°C and those stored at room temperature.

Sample number	Sample description
1	0.25mg/ml refrigerated (4°C)100W 40 cycles
2	0.25mg/ml room temperature (4°C)100W 40 cycles
3	0.25mg/ml refrigerated (4°C)500W 40 cycles
4	0.25mg/ml room temperature (4°C)500W 40 cycles

Table 0.13 Sample guide for stability study

Sample	0 hrs	24 hrs	48 hrs	96 hrs	168 hrs
1	189.2±1.1	186.9±5.0	184.0±6.4	181.1±4.2	178.2±1.0
2	189.2±1.1	190.5±0.9	186.3±1.8	185.2±3.1	182.7±4.0
3	97.6±1.0	94.6±0.8	95.3±1.9	96.4±1.4	98.7±2.4
4	97.6±1.0	94.4±0.8	93.9±1.5	97.4±1.7	98.5±2.5

Table 0.14 Stability Study Nanoparticle Size

Shows size of nanoparticles size in nm over 168 hours

Sample	0 hrs	24 hrs	48 hrs	96 hrs	168 hrs
1	0.125±0.033	0.142±0.029	0.108±0.033	0.144±0.020	0.137±0.012
2	0.125±0.033	0.139±0.035	0.170±0.021	0.170±0.017	0.154±0.007
3	0.172±0.009	0.184±0.010	0.242±0.008	0.234±0.006	0.225±0.004
4	0.172±0.009	0.174±0.024	0.183±0.012	0.207±0.007	0.208±0.026

Table 0.15 Stability Study PDI

Sample	0 hrs	24 hrs	48 hrs	96 hrs	168 hrs
1	-13.5±0.2	-18.0±1.2	-18.6±0.7	-23.1±2.3	-37.6±0.9
2	-13.5±0.2	-16.6±1.0	-15.8±1.5	-13.6±0.9	-24.5±1.6
3	-26.3±6.3	-36.9±5.1	-37.5±3.8	-21.6±3.0	-34.3±6.2
4	-26.3±6.3	-31.6±4.0	-36.4±2.1	-34.3±6.0	-37.0±2.1

Table 0.16 Stability Study Zeta Potential

Shows zeta potential over 168 hours values in mV

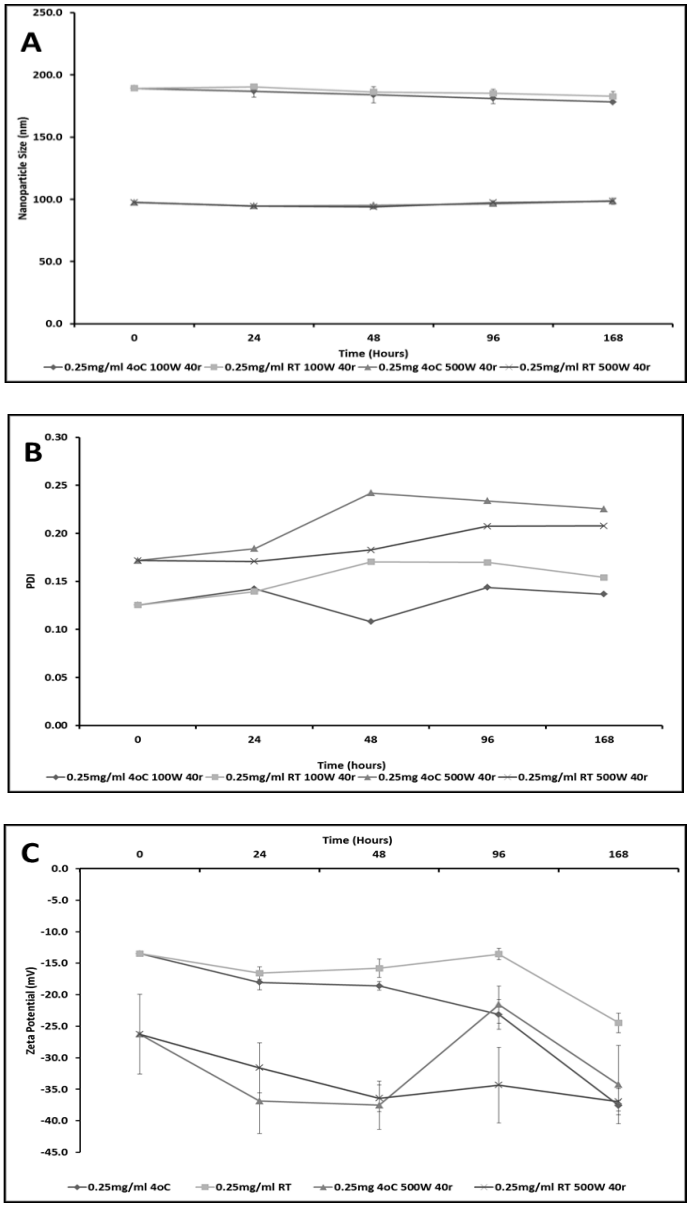

Figure 0.21 Nanoparticle Stability testing.

A) Size stability study of blank PHBHHX nanoparticles at 0.25mg/mL. B) PDI stability study of blank PHBHHX nanoparticles at 0.25mg/mL. C) Zeta potential stability study of blank PHBHHX nanoparticles at 0.25mg/mL. High/low sonication settings at room temperature (rt) and 4°C. Graph shows mean values ± 1 standard deviation(N=3).

4.6 Discussion

To our knowledge there are, no published protocol for controlling nanoparticle size. Controlled drug delivery, more so growth factor delivery over 40 days with an aim to deliver a precise dose being able to control nanoparticle size may well help to deliver a nanoparticle with such properties. To date there has been little focus on controlling nanoparticle properties such as size during the manufacturing process. Experimental design is a vital aspect of any research that is often overlooked but when well executed, has the potential to deliver high impact results with precise planning and reduced cost. A factorial experiment consists of two or more factors, taking into account the effect of each variable on the process as well as the interaction of multiple variables in order to optimise production. Within a manufacturing process such as nanoparticle production, the control of these variables is critical and the knowledge of how they interact as well as which variables have the largest effect on controlling the desired process output will lead to more tightly controlled production. This interaction of variables is often ignored but is critical for a full understanding of the process [392].

Lamprecht et al [393, 394] achieved variation in Poly (lactic-co-glycolic acid) (PLGA) and bovine serum albumin (BSA) nanoparticle size by altering production variables (homogenisation time, polymer concentration and surfactant concentration) using a 'one factor at a time' (OFAT) approach. The absence of consideration of the interaction of competing variables within their process resulted in the production of nanoparticles with a minimum size of 230 nm with no indication of repeatability. A separate study by Gutierro et al [395] also varied PLGA-BSA nanoparticle size by altering the production process and managed to reduce the nanoparticles from 1000 nm to 200 nm which led to a reduced immune response, also using an OFAT approach. Gryparis et al [396] employed

a pseudo-multivariate batch method to vary the size of PLGA nanoparticles and were able to create drug encapsulated nanoparticles with a minimum size of 150 nm and a PDI of close to 0.3, the accepted limit for clinical applications [397].

Perhaps the most rigorous study to date on size control of nanoparticles employed a 5-factor 3-level experimental design for the production of PLGA-BSA nanoparticles [398]. Detailed computer analysis of this factorial design revealed a theoretic minimum nanoparticle diameter for their double emulsion production method of 122.4 nm. As described previously, nanoparticles with a mean diameter of less than 100 nm would be highly desirable to mediate cellular response, for sterilisation via filtration, for use in gene transfection and to actively cross the blood-brain barrier and. By producing a nanoparticle size range of 90 – 205 nm, this study has demonstrated the advantage of using PHBHHx for nanoparticle production to fit a variety of applications. In this study, blank nanoparticles showed the same size trend as encapsulated nanoparticles meaning that various biocompatible polymers can be characterised by this method in the knowledge that the introduction of drugs/growth factors to the nanoparticles will not affect the production size.

From the data in table 5.8 it is evident that the process described is highly repeatable and can accurately produce nanoparticles of a desired size. This is a critical component of any production system, since if a process is not reproducible or repeatable it cannot be used for reliable or commercial production. If batch to batch production is not considered within an experimental process, then common cause variability is not accounted for and the process cannot be reliably evaluated. A large number of experimental methods only account for inter-batch variability which is an assessment of the accuracy of the measurement system in use i.e. an N of three on one occasion, but gives no indication of

the repeatability of the experimental methodology. Bridging the gap between industry and research by implementing a DOE approach in research laboratories is an invaluable way to attract industry and produce high quality research. This is a highly critical consideration for the successful commercialisation of medical products which should be the aspiration of all research groups not only in the field of drug delivery and pharmaceutical research but also regenerative medicine.

One consideration that must be noted in this process is the effect of sonication on the encapsulated protein or drug, since high sonication power may have a destructive effect on the encapsulated protein. Observations from the encapsulation of Albumin and HaperzineA showed a low entrapment efficiency which can be explained by the sonication power being high enough to destroy the drug. This has been highlighted due to the total drug concentration being calculated from the amount of drug input at the start of the process, taking into account the overall efficiency. In contrast, traditional encapsulation efficiency calculations use the total drug concentration after breakdown of the nanoparticles via sonication and therefore do not account for the destruction of drug due to sonication. It can be noted from a previous study that a sonication power of 400 W also had no apparent effect on the encapsulation of insulin [373], however repeat and high power sonication on the formed nanoparticle to release the entrapped drug or protein can cause destruction of the analyte of interest resulting in underestimated encapsulated drug dose, which may have a significant effect on the target whether it is cellular differentiation or diabetic control. At higher sonication power and duration, there was a tighter distribution of particle sizes and a reduction in PDI compared to the lower settings which is consistent with previous studies [399]. This is due to the increased exposure to ultrasonic force, which acts to push the size distribution curve down towards

the lower size limit, reducing the overall range and creating a tighter size distribution. This is advantageous from a process perceptive since creating a tighter size distribution means that the process is inherently more reproducible when creating smaller nanoparticles.

The nanoparticles in this study were assessed over seven days and showed no size deviation for this period as well as small and acceptable changes to PDI and zeta potential which is critical for the viability of the nanoparticles for clinical applications [287]. This was found to be the case for both 4°C and room temperature, showing the viability of this method in terms of stability. Clearly, storage will need to be considered in relation to the encapsulated drug as well, since most proteins will need to be stored at 4°C to retain their integrity.

In this study we created nanoparticles as small as 90 nm with a PDI of well below 0.3, which is far smaller than the theoretical minimum of 122.4 nm using PLGA-BSA as described by Feczkó et al [398]. This shows that the use of PHBHHx as a drug encapsulating polymer has greater potential compared to PLGA, producing smaller nanoparticles as required for precise growth factor concentration delivery.

The bio distribution of nanoparticles on entry into the circulatory system should be considered when embarking on the use of nanoparticles as a delivery vehicle for bioactive molecules. This study investigated the possibility of PHBHHx nanoparticles as a delivery vehicle for growth factors. The growth factors to be delivered were either a combination of BMP-12 & BMP-12 or FGF-4, FGF-6 and FGF-8. Growth factors are well documented to induce and enhance tumour growth. This study aimed to control the production of PHBHHx nanoparticles to produce a desired property namely “nanoparticle Size”, which will then be contained within a PHBHHx hybrid scaffold that would contain a collagen and

stem cell core. As with all implants there is always a risk of implant failure and thus a further risk of growth factor containing nanoparticles entering the circulatory system.

This study showed PHBHHx nanoparticles accumulated in the liver, spleen and brain. Data from this study indicated a higher brain tissue uptake with particles smaller than 100nm. Conversely, the data also suggested that as nanoparticle size increased there was a greater uptake of nanoparticles into liver and spleen tissue which agrees with previous studies [400].

Combining this key attribute with the highly favourable biodegradability of PHBHHx and the potential for cost effective large scale production means that this system has remarkable and unique commercial potential as a drug delivery device and not only growth factor delivery to suit a multitude of applications within the field of nano-medicine.

4.7 Conclusion

It has been shown that the DOE approach can be employed to control the production of nanoparticles to fit a variety of applications within nano-medicine, whereby a size prediction curve can be produced for each polymer which can then be applied to any encapsulated drug to achieve a desired nanoparticle size. The knowledge gained from this preliminary optimisation is important to pave the way for more in depth analysis to obtain a full understanding of the process. This study highlights the most sensitive aspects of nanoparticle production via the solvent evaporation method, which can be used to reduce variability in the production process leading to increased precision within the manufacture of nanoparticles. Reliable production of drug encapsulated nanoparticles provides key evidence that PHBHHx can be used to investigate new applications in the field that require the production of nanoparticles less than 100 nm. Preliminary Investigation into the effect of different surfactant concentration during production using the solvent evaporation method highlighted the potentially lead to the creation of smaller nanoparticles and is a key area for further detailed investigation. This chapter has shown reasonable PHBHHX nanoparticle entrapment efficiency of the hydrophobic drug Heperzine-A and bovine serum albumin which can be combined with this controlled manufacture process for delivery of growth factors. Aligning research practices with those of current commercial research institutions has been highlighted as an invaluable way to attract commercial interest and to allow research to evolve alongside industry which is critical for the success of nano-medicine, controlled drug delivery and regenerative medicine in general.

Chapter 5: Discussion

Tendon injury is an increasing problem in medicine, with between 3 – 5 million tendon related injuries worldwide annually, with over 300,000 tendon procedures performed annually in the United States alone [156, 295]. Tendon is characterised by poor repair following injury or disease, is relatively acellular and has poor blood supply [6]. Treatment can involve many different types of surgical intervention, such as xenograft or allograft to treat large tendon defects, however potential problems with this method (such as foreign body reaction) can occur [296]. A lack of adequate strategies for tendon repair has led to the development of engineered replacement tendon tissue for use in surgical implantation [297]. Tissue engineering could be used to develop a regenerative medicine solution to tendon tissue repair [156].

The aim of this thesis was to investigate three possible components which may lead to the development of a tissue engineered tendon implant:

1. PHBHHx tendon scaffold design (Chapter 2)
2. Growth factor induced differentiation of human stem cells (Chapter 3)
3. Controlled production of nanoparticles to predict the size of nanoparticles to be used in the delivery of growth factors (Chapter 4)

The aim of this investigation (Chapter 2) was to identify a PHBHHx scaffold design that could be used to facilitate repair of damaged tendon tissue while not initiating an immune response or prolonging inflammation. A composite scaffold was developed which featured a PHBHHx tube, a collagen core, and PHBHHx fibres which would facilitate cellular migration and tissue remodelling, while at the same time allowing for limited restoration of movement. The design was mechanically similar to the rat Achilles tendon

and to other commercially available human tendon repair materials [117, 297]. Furthermore, this study has shown that PHBHHx scaffold encourages cellular infiltration and proliferation which agrees with previous studies [119, 312, 313, 329]. Furthermore, cellular alignment was observed along the force baring tube and fibre which agrees with earlier studies indicating cellular alignment with direction of force [401-403].

The ability of any implant to not elucidate an immune response is one of the key components of evaluation of a potential implant [404] .The CRP results from this study clearly indicate that the PHBHHx implant did not induce an immune response and in- fact the immune response 48hrs post-surgery in a natural response to the induced trauma caused by surgery with no subsequent increase in CRP. These findings add to the body of evidence indicating PHBHHx does not elucidate an immune response *in vivo* [318-320, 323].

The ability of a biological implant/scaffold being able to perform as “normal tissue” is highly desired. In this study we utilised AFI testing to measure return of function. AFI testing showed a continued improvement for all groups over the 40 day investigation, with complete return of function being as early as day +20 in the tenocyte-PHBHHx-collagen group which was a full 20 days prior to the PHBHHx only and PHBHHx-collagen group, with the control group remaining below pre-surgical implantation levels. These results show the implanted scaffolds are capable of withstanding the forces which are exposed to native tendon and the implantation of a scaffold returns function to the limb faster than the absence of an implant which agrees with previous studies [314].

Cellular infiltration into the scaffold was observed in both the PHBHHx only and Collagen-PHBHHx scaffold designs with sinusoidal cellular alignment which is a key marker in the histological analysis of tendon tissue, signifying the presence of crimp angles between collagen fibrils [33, 43]. The PHBHHx scaffold which contained tenocytes and collagen the cells appeared to be more elongated and sinusoidal in morphology, when compared to the other implanted scaffold designs, as with the PHBHHx only and collagen-PHBHHx scaffold designs, when cells were in direct contact with the scaffold, especially the fibre component this feature was more apparent and the sinusoidal-elongated morphology could possibly indicating that force transmission resulting in mechanotransduction from the fibre to the cells promoted tendon cell proliferation and alignment [90, 301, 312]. This further highlights the importance of collagen not only in the tissue integration and remodelling of tendon but in a means of delivering cells to a point of repair and further adds to previous studies suggesting collagen is a beneficial inclusion in tendon graft material [114, 300, 326].

However, careful consideration should be given to whether a PHBHHx scaffold can be constructed to deliver the properties that are observed within the human Achilles tendon. The adult Achilles tendon has ultimate force to break in excess of 435N [405]compared with a ultimate force to break in rat Achilles tendon of this study of 17.35N.

This study has potentially identified PHBHHx can be utilised as a tendon scaffold capable of delivering a cellular component to a tendon defect area which was capable of: 1) the return of function to the implant site, 2) did not elucidate an immune response and 3) provided favourable conditions for cellular proliferation and force transmission.

The next stage of this study (Chapter 3) was to identify whether FGF-4, FGF-6 and FGF-8 singularly or as a combination could induce and maintain tendon specific gene expression in human derived stem cells. Therefore, this study employed the gene combination of TNMD and THBS-4 expression as a marker of tendon differentiation first identified by Jelinsky *et al* [68]

This study has shown Vitamin C in conjunction with FGF-4, 6 & 8 cultured at 2% O_2 was capable of inducing and maintaining tendon like gene markers: tenomodulin (TNMD), Tenascin C (TENC), Collagen 3A1 (COL3A1), Collagen 1A2 (COL1A2) and Thrombospondin-4 (THBS-4) over a 40 day culture period in both human embryonic stem cells and human mesenchymal stem cells. However, the mechanisms by which FGF signalling induced and maintained tendon gene expression remain un-identified. FGF's are well documented to bind in an order of hierarchy with many FGF's competitively binding to the same receptors with FGF specificity to a given receptor dictating the order of binding to the FGFR [222, 406].FGF-4, FGF-6 and FGF-8 all bind to FGFR-1, FGFR-2 and FGFR-4. However, competitive affinity to a specific receptor by one of the FGF's will then have a knock on effect on the affinity of the next FGF to its next favourable ligand and so on and so forth with the third FGF. Furthermore, the preferential FGFR binding will have a combined effect on which post receptor signal cascade is active.

FGF's have been previously been shown to preferentially bind to specific FGFR's [222, 406].The hierarchical order/relationship between FGF-4, FGF-6 and FGF-8 with their common receptors is currently poorly defined. The potential of preferential binding to induce a priority of specific FGF-FGFR interactions and subsequent hierarchical shift of preference of other FGF's to bind with a receptor further down its hierarchical order may

well dictate the transcriptional outcomes observed in this investigation. Only in the presence of FGF-4, FGF-6 and FGF-8 in the differential media is a “true” tenocyte-like gene expression observed. Furthermore, the presence of tenocyte-like gene expression may only indicate cellular priming towards a tenocyte-lineage.

The use of Dorsomorphin in this study as a SMAD inhibitor has highlighted the possibility of cross – talk between the FGF-FGFR signal transduction and possible up-regulation of BMP juxtacrine signalling. This study has highlighted the inclusion of Dorsomorphin to FGF supplemented media induced a decrease in both GAG and collagen synthesis in all FGF-4, FGF-4 & 8 and to a lesser extent FGF-4, 6 & 8 supplemented media. These findings agree with previous studies highlighting FGF-BMP signalling cross talk [407, 408].

Previous publications have indicated to the requirement of mechanical force in late tenocyte differentiation and maturation [409]. The Adjunct relationship of mechanical force, cellular positioning and growth factor stimulation remains poorly defined and is a specific area in tendon research that requires further investigation.

Mechanical force has previously been shown to induce tenocyte proliferation with an increased detection of the transcription factor Scleraxis [331, 410]. SCX has previously been shown to directly regulate the transcription of Type I collagen (COL1a1) in the presence of TGF-β (Transforming Growth Factor –β) [411, 412], which encodes for the most abundant protein found in tendon tissue. SCX has been shown to be up-regulated in numerous animal models utilising either TGF-β in the equine model which utilised embryonic derived stem cells [354] or the combination of BMP-12 and BMP-13 in both the rat [181] and canine which utilised adipose derived mesenchymal stem cells [413] model for stem cell differentiation towards a tenocyte lineage.

SCX has shown limited detection in human samples with the majority of finding showing the presence of SCX post mechanical loading [331]. This Study did not focus on SCX, but did focus on the tendon makers TNMD and THBS-4 with future studies aimed and focused on elucidating the function of SCX in human stem cell differentiated tenocyte-like cells.

Heparin sulphate has previously been shown to be vital in FGF-FGFR interaction [236]. The concept of heparin/HS-FGF dimer being an essential component/step in the transduction of FGF/FGFR signalling complex still remains controversial [237]. Although, it is well established that heparin is essential for high affinity binding of FGF to FGFR when cells are unable to synthesis cell-surface HS, cells pre-treated with heparin degrading enzymes or cells exposed to sulphation inhibiting agents [238, 239]. In this study heparin was not added as a component of the differentiation media, although heparin sulphate is present in Matrigel which is used to coat culture plastic prior to seeding with hESC's. This study at disagrees with previous studies utilising heparin sulphate inclusion as part of the FGF-FGFR binding due to hMSC did not have matrigel coating of plastic prior to seeding and this may indicate that heparin sulphate supplementation is not required. Secondly, when both hESC and hMSC's showed the gene expression of TENC and the tenascin C protein may have influenced FGF-FGFR high affinity binding as tenascin C has previously been shown to be capable of binding FGF and influencing binding affinity with the FGFR [414] and this could negate the absence of heparin sulphate.

However, this study has shown in the absence of all three FGF's tendon specific gene expression is not detected post 20 days. This highlights the requirement of the combination of FGF-4, FGF-6, FGF-8, Vitamin C and a 2% O_2 environment.

After identifying a growth factor combination capable of inducing and maintaining tendon like gene markers the next logical step was to investigate the use of nanoparticle delivery of the identified growth factors.

This thesis has also highlighted the importance of controlling the parameters (Chapter 4) within the manufacturing process of PHBHHx nanoparticles with an aim to produce a controlled range of nanoparticle sizes. The control of nanoparticle size and properties will aid in the design of nanoparticle capable of delivering a precise bioactive molecule concentration over a specific time-course.

Research undertaken by Peng *et al.* [373] showed low molecular weight proteins namely insulin could be encapsulated and produce high encapsulation efficiency with a prolonged release pattern. However, this study along with numerous other studies focuses upon a single nanoparticle size [393-395].

This thesis has shown that being able to control the key process variables: Polymer concentration, sonication power and sonication cycles. A range of PHBHHx nanoparticles size can be produced (94nm – 220nm) which is significantly smaller than the particles produced in previous studies of polymer drug encapsulation [393-395].

Furthermore, this thesis has shown that altering the ratio of surfactants that a smaller nanoparticle can be produced (<75nm). The results observed in surfactant ratio alteration highlights the requirement for further multifactorial design of experiment to be undertaken utilising surfactant ratio as the fourth variable. The author of this thesis believes this undertaking will further aid in the delivery of precise nanoparticle based drug delivery. Also, the alteration of polymer concentration may well affect release

properties of the nanoparticle system in that the thickness of polymer coating acts as a release barrier. Understanding the release kinetics in both aqueous and hydrogel environments is another key area for investigation.

Further concerns in reducing nanoparticle size are: 1) physical barriers of the nanoparticle construct in that the thicker the nanoparticle polymer shell the reduced permeability for drug/bioactive molecule release. This study did not investigate the effects of reducing polymer concentration on nanoparticle coating thickness. However, future studies should employ techniques such as Atomic Force Microscopy (AFM) to quantify the polymer layer thickness with an aim of relating this physical barrier to release profile. 2) As nanoparticle size decreases a higher percentage of bioactive agent will be found on the surface of the nanoparticle which may lead to a higher level of burst release [389].

This thesis has identified that PHBHHx scaffold that contains both a stem cell and nanoparticle growth factor release system is distinctively possible with further research being focused on release kinetics of the growth factors encapsulated within a polymer nanoparticle. The identification of the growth factors capable of differentiating human stem cells towards a tenocyte-like lineage has highlighted the potential for a stem cell based alternative to current surgical techniques employed in tendon repair. Also, the use of PHBHHx-hybrid scaffold indicates a potential polymer design to be utilised in tendon repair whilst also providing a vehicle by which both a stem cell and nanoparticle loaded growth factors component can be delivered to the defect site.

Possibly the finding of most interest contained within the body of this thesis is the capability of controlling nanoparticle size and being able to predict the size of nanoparticle with a high level of accuracy. This opens the door of possibilities to the

application of polymer based nanoparticles in delivering not only growth factors but chemotherapeutical agents with a precise concentration to a desired target which may reduce systemic toxicity that is observed when administering these agents via traditional administration.

Chapter 6: Conclusion

This thesis has demonstrated that a PHBHHx based scaffold can be utilised to repair tendon defects in the rat model. Implanted hybrid PHBHHx scaffold were capable of withstanding the forces exposed to native tendon coupled with a return of function (observed in the Achilles functional index). The collagen-PHBHHx scaffold containing tenocytes showed an accelerated return of function when compared to all other experimental groups. The implanted scaffolds did not elucidate an immune response and also showed cellular alignment along the force barring fibres. The rat model also showed the PHBHHx hybrid scaffold underwent degradation of the polymer bulk which has no adverse effects on function or immune response.

This thesis has demonstrated that the growth factor combination of FGF-4, FGF-6 and FGF-8 in combination with Vitamin C and cultured at 2% O_2 as being capable of initiating cellular priming towards a tenocyte “like” differentiation with transcription of THBS-4 and TNMD being detected up to 40 days of culture. Furthermore, this thesis has indicated an element of cross-talk between FGF and BMP signalling cascades during tenogenesis. The cross-talk was identified by inhibition of the BMP induced SMAD signalling cascade. This was elucidated by the use of Dorsomorphin in FGF supplemented differentiation media, which resulted in a reduction in RNA expression for DCN and TNMD in both FGF-4 & 8 and FGF-4, 6 & 8 supplemented differentiation of human embryonic stem cells. Similar observations were made with FGF-4 and FGF-4, 6 & 8 supplemented differentiation of human mesenchymal stem cells in that TNMD transcription was not observed post 20 days stimulation.

The final chapter of this thesis has demonstrated that DOE approach can be employed to control the production of nanoparticles to fit a variety of applications within nano-

medicine. Whereby, a size prediction curve can be produced for each polymer which can then be applied to any encapsulated drug to achieve a desired nanoparticle size. These findings allow for a greater control of nanoparticle size and drug delivery in that we can manipulate the manufacturing variables to produce a nanoparticle of differing size and drug release profiles. Therefore, allowing for greater control of delivery of drug/growth factor dose to site of interest.

This thesis has utilised the combination of an *in vivo* investigations that PHBHHx can be utilised as a suitable implant material for the potential for the treatment of damaged tendon. Whilst utilising *in vitro* investigation to show the combination FGF-4, FGF-6 and FGF-8 in the presence of Vitamin C and cultured in 2% O_2 as having a potential role in the cellular priming of human mesenchymal stem cells and human embryonic stem cells to differentiate into a tenocyte “like” lineage.

The contents of this thesis, has also highlighted the importance of a controlled production of nanoparticles. By mapping the production variables and subsequent control of the variables this thesis has shown that a range of nanoparticles can be produced that have specific size and release profiles. The impact of such control mechanisms can lead to a nanoparticle based delivery system capable of delivering a precise drug/growth factor dose over a prolonged period of time.

Chapter 7: Future Perspective

The body of work of this thesis has shown that a PHBHHx scaffold was capable of withstanding the forces observed in native rat Achilles tendons, without initiating an immune response. Chapter 3 has shown that combination of FGF-4, FGF-6, FGF-8 and Vitamin C as being capable of initiating stem cell differentiation towards a tenocyte “like” lineage using both human embryonic and mesenchymal stem cells.

The ability to deliver return of function along with the capability of cellular differentiation is a logical next step in that combining the scaffold with stem cells and a drug delivery vehicle capable of controlled and sustained release of growth factors.

Therefore future investigations should employ:

1. Bioreactor investigation of growth factor release kinetics
2. Investigation of the role of HIF proteins in tenocyte differentiation
3. Atomic force microscopy of Nanoparticle shell to relate to release kinetics.
4. Investigation of FGF-4, FGF-6 and FGF-8 signalling cascade and combinational relationship.
5. Addition of Heparin Sulphate to growth factor combination to evaluate amplification of FGF signalling.
6. Design of NEW tendon bioreactor utilising hypoxic environments and the ramping of cyclic strain over time.
7. Investigate the combinational effects of FGF’s and mechanical stimulation on stem cell differentiation towards a tenocyte lineage.

References

[1] Kafienah W, Mistry S, Perry MJ, Politopoulou G, Hollander AP. Pharmacological regulation of adult stem cells: chondrogenesis can be induced using a synthetic inhibitor of the retinoic acid receptor. Int J Exp Pathol. 2007;88:A87-A.

[2] Baiguera S, Gonfiotti A, Jaus M, Comin CE, Paglierani M, Del Gaudio C, et al. Development of bioengineered human larynx. Biomaterials. 2011;32:4433-42.

[3] Kannus P. Structure of the tendon connective tissue. Scandinavian journal of medicine & science in sports. 2000;10:312-20.

[4] Mendias CL, Bakhurin KI, Faulkner JA. Tendons of myostatin-deficient mice are small, brittle, and hypocellular. Proc Natl Acad Sci U S A. 2008;105:388-93.

[5] Cheng VWT, Screen HRC. The micro-structural strain response of tendon. J Mater Sci. 2007;42:8957-65.

[6] Doral MN, Alam M, Bozkurt M, Turhan E, Atay OA, Donmez G, et al. Functional anatomy of the Achilles tendon. Knee surgery, sports traumatology, arthroscopy : official journal of the ESSKA. 2010;18:638-43.

[7] Shearn JT, Kinneberg KR, Dyment NA, Galloway MT, Kenter K, Wylie C, et al. Tendon tissue engineering: progress, challenges, and translation to the clinic. Journal of musculoskeletal & neuronal interactions. 2011;11:163-73.

[8] Yamanaka Y, Ralston A, Stephenson RO, Rossant J. Cell and molecular regulation of the mouse blastocyst. Developmental dynamics : an official publication of the American Association of Anatomists. 2006;235:2301-14.

[9] Tam PP, Khoo PL, Wong N, Tsang TE, Behringer RR. Regionalization of cell fates and cell movement in the endoderm of the mouse gastrula and the impact of loss of Lhx1(Lim1) function. Developmental biology. 2004;274:171-87.

[10] Rodda SJ, Kavanagh SJ, Rathjen J, Rathjen PD. Embryonic stem cell differentiation and the analysis of mammalian development. The International journal of developmental biology. 2002;46:449-58.

[11] Beddington RS, Robertson EJ. Axis development and early asymmetry in mammals. Cell. 1999;96:195-209.

[12] Beddington RS, Robertson EJ. Anterior patterning in mouse. Trends in genetics : TIG. 1998;14:277-84.

[13] Beddington RS, Robertson EJ. An assessment of the developmental potential of embryonic stem cells in the midgestation mouse embryo. Development. 1989;105:733-7.

[14] Edom-Vovard F, Duprez D. Signals regulating tendon formation during chick embryonic development. Developmental dynamics : an official publication of the American Association of Anatomists. 2004;229:449-57.

[15] Ros MA, Rivero FB, Hinchliffe JR, Hurle JM. Immunohistological and ultrastructural study of the developing tendons of the avian foot. Anatomy and embryology. 1995;192:483-96.

[16] Heus HC, Hing A, van Baren MJ, Joosse M, Breedveld GJ, Wang JC, et al. A physical and transcriptional map of the preaxial polydactyly locus on chromosome 7q36. Genomics. 1999;57:342-51.

[17] Zguricas J, Heus H, Morales-Peralta E, Breedveld G, Kuyt B, Mumcu EF, et al. Clinical and genetic studies on 12 preaxial polydactyly families and refinement of the localisation of the gene responsible to a 1.9 cM region on chromosome 7q36. Journal of medical genetics. 1999;36:32-40.

[18] Bouldin CM, Harfe BD. Aberrant FGF signaling, independent of ectopic hedgehog signaling, initiates preaxial polydactyly in Dorking chickens. Developmental biology. 2009;334:133-41.

[19] Bose K, Nischt R, Page A, Bader BL, Paulsson M, Smyth N. Loss of nidogen-1 and -2 results in syndactyly and changes in limb development. The Journal of biological chemistry. 2006;281:39620-9.

[20] Yu K, Ornitz DM. FGF signaling regulates mesenchymal differentiation and skeletal patterning along the limb bud proximodistal axis. Development. 2008;135:483-91.

[21] Canty EG, Kadler KE. Collagen fibril biosynthesis in tendon: a review and recent insights. Comparative biochemistry and physiology Part A, Molecular & integrative physiology. 2002;133:979-85.

[22] Richardson SH, Starborg T, Lu Y, Humphries SM, Meadows RS, Kadler KE. Tendon development requires regulation of cell condensation and cell shape via cadherin-11-mediated cell-cell junctions. Mol Cell Biol. 2007;27:6218-28.

[23] Birk DE, Trelstad RL. Extracellular compartments in tendon morphogenesis: collagen fibril, bundle, and macroaggregate formation. The Journal of cell biology. 1986;103:231-40.

[24] Shaw HM, Vazquez OT, McGonagle D, Bydder G, Santer RM, Benjamin M. Development of the human Achilles tendon enthesis organ. Journal of anatomy. 2008;213:718-24.

[25] Vogel KG, Koob TJ. Structural specialization in tendons under compression. International review of cytology. 1989;115:267-93.

[26] Gao J, Messner K, Ralphs JR, Benjamin M. An immunohistochemical study of enthesis development in the medial collateral ligament of the rat knee joint. Anatomy and embryology. 1996;194:399-406.

[27] Thomopoulos S, Kim HM, Rothermich SY, Biederstadt C, Das R, Galatz LM. Decreased muscle loading delays maturation of the tendon enthesis during postnatal development. Journal of orthopaedic research : official publication of the Orthopaedic Research Society. 2007;25:1154-63.

[28] Wood-Jones F. Structure and function as seen in the foot. 2nd ed. ed. London: Bailliere, tindall and Cox; 1949.

[29] Benjamin M, Kaiser E, Milz S. Structure-function relationships in tendons: a review. Journal of anatomy. 2008;212:211-28.

[30] Sharma P, Maffulli N. Tendon injury and tendinopathy: healing and repair. The Journal of bone and joint surgery American volume. 2005;87:187-202.

[31] Fukuta S, Oyama M, Kavalkovich K, Fu FH, Niyibizi C. Identification of types II, IX and X collagens at the insertion site of the bovine Achilles tendon. Matrix Biol. 1998;17:65-73.

[32] Ippolito E, Natali PG, Postacchini F, Accinni L, Demartino C. Morphological, Immunochemical, and Biochemical-Study of Rabbit Achilles-Tendon at Various Ages. J Bone Joint Surg Am. 1980;62:583-98.

[33] Maffulli N, Barrass V, Ewen SW. Light microscopic histology of achilles tendon ruptures. A comparison with unruptured tendons. The American journal of sports medicine. 2000;28:857-63.

[34] Mayer L. The evolution of modern tendon surgery. Annals of the Royal College of Surgeons of England. 1952;11:69-86.

[35] Ahmed IM, Lagopoulos M, McConnell P, Soames RW, Sefton GK. Blood supply of the Achilles tendon. J Orthop Res. 1998;16:591-6.

[36] Theobald P, Benjamin M, Nokes L, Pugh N. Review of the vascularisation of the human Achilles tendon. Injury. 2005;36:1267-72.

[37] Riley G. Tendinopathy - from basic science to treatment. Nat Clin Pract Rheum. 2008;4:82-9.

[38] Kvist M, Jozsa L, Jarvinen M, Kvist H. Fine-Structural Alterations in Chronic Achilles Paratendonitis in Athletes. Pathol Res Pract. 1985;180:416-23.

[39] Richardson LE, Dudhia J, Clegg PD, Smith R. Stem cells in veterinary medicine--attempts at regenerating equine tendon after injury. Trends in biotechnology. 2007;25:409-16.

[40] Jozsa L, Kannus P, Balint JB, Reffy A. Three-dimensional ultrastructure of human tendons. Acta anatomica. 1991;142:306-12.

[41] Jozsa L, Reffy A, Kannus P, Demel S, Elek E. Pathological alterations in human tendons. Archives of orthopaedic and trauma surgery. 1990;110:15-21.

[42] Paavola M, Kannus P, Jarvinen TA, Khan K, Jozsa L, Jarvinen M. Achilles tendinopathy. The Journal of bone and joint surgery American volume. 2002;84-A:2062-76.

[43] Benjamin M, Evans EJ, Copp L. The histology of tendon attachments to bone in man. Journal of anatomy. 1986;149:89-100.

[44] Aparecida de Aro A, Vidal Bde C, Pimentel ER. Biochemical and anisotropical properties of tendons. Micron. 2012;43:205-14.

[45] Jozsa L, Kannus P. Histopathological findings in spontaneous tendon ruptures. Scand J Med Sci Spor. 1997;7:113-8.

[46] Vidal BD. Evaluation of the Carbohydrate Role in the Molecular Order of Collagen Bundles - Microphotometric Measurements of Textural Birefringence. Cell Mol Biol. 1986;32:527-35.

[47] Liu SH, Yang RS, Alshaikh R, Lane JM. Collagen in Tendon, Ligament, and Bone Healing - a Current Review. Clin Orthop Relat R. 1995:265-78.

[48] O'Brien M. Structure and metabolism of tendons. Scandinavian journal of medicine & science in sports. 1997;7:55-61.

[49] Vidal BD. Image analysis of tendon helical superstructure using interference and polarized light microscopy. Micron. 2003;34:423-32.

[50] Kadler KE, Holmes DF, Trotter JA, Chapman JA. Collagen fibril formation. Biochem J. 1996;316:1-11.

[51] Kjaer M. Role of extracellular matrix in adaptation of tendon and skeletal muscle to mechanical loading. Physiological reviews. 2004;84:649-98.

[52] Benjamin M, Tyers RNS, Ralphs JR. Age-Related-Changes in Tendon Fibrocartilage. J Anat. 1991;179:127-36.

[53] Rufai A, Benjamin M, Ralphs JR. Development and ageing of phenotypically distinct fibrocartilages associated with the rat Achilles tendon. Anatomy and embryology. 1992;186:611-8.

[54] Hanson AN, Bentley JP. Quantitation of type I to type III collagen ratios in small samples of human tendon, blood vessels, and atherosclerotic plaque. Analytical biochemistry. 1983;130:32-40.

[55] Ahtikoski AM, Koskinen SO, Virtanen P, Kovanen V, Risteli J, Takala TE. Synthesis and degradation of type IV collagen in rat skeletal muscle during immobilization in shortened and lengthened positions. Acta physiologica Scandinavica. 2003;177:473-81.

[56] Ahtikoski AM, Riso EM, Koskinen SO, Risteli J, Takala TE. Regulation of type IV collagen gene expression and degradation in fast and slow muscles during dexamethasone treatment and exercise. Pflugers Archiv : European journal of physiology. 2004;448:123-30.

[57] Felisbino SL, Carvalho HF. Identification and distribution of type VI collagen in tendon fibrocartilages. Journal of submicroscopic cytology and pathology. 1999;31:187-95.

[58] Carvalho HF, Felisbino SL, Keene DR, Vogel KG. Identification, content, and distribution of type VI collagen in bovine tendons. Cell and tissue research. 2006;325:315-24.

[59] Milz S, Regner F, Putz R, Benjamin M. Expression of a wide range of extracellular matrix molecules in the tendon and trochlea of the human superior oblique muscle. Investigative ophthalmology & visual science. 2002;43:1330-4.

[60] Tsuzaki M, Yamauchi M, Banes AJ. Tendon collagens: extracellular matrix composition in shear stress and tensile components of flexor tendons. Connective tissue research. 1993;29:141-52.

[61] Vogel KG, Heinegard D. Characterization of proteoglycans from adult bovine tendon. The Journal of biological chemistry. 1985;260:9298-306.

[62] Eyre DR, Paz MA, Gallop PM. Cross-linking in collagen and elastin. Annual review of biochemistry. 1984;53:717-48.

[63] Smith-Mungo LI, Kagan HM. Lysyl oxidase: properties, regulation and multiple functions in biology. Matrix biology : journal of the International Society for Matrix Biology. 1998;16:387-98.

[64] Muller G, Michel A, Altenburg E. COMP (cartilage oligomeric matrix protein) is synthesized in ligament, tendon, meniscus, and articular cartilage. Connective tissue research. 1998;39:233-44.

[65] Brandau O, Meindl A, Fassler R, Aszodi A. A novel gene, tendin, is strongly expressed in tendons and ligaments and shows high homology with chondromodulin-I. Developmental dynamics : an official publication of the American Association of Anatomists. 2001;221:72-80.

[66] Docheva D, Hunziker EB, Fassler R, Brandau O. Tenomodulin is necessary for tenocyte proliferation and tendon maturation. Molecular and cellular biology. 2005;25:699-705.

[67] Shukunami C, Takimoto A, Oro M, Hiraki Y. Scleraxis positively regulates the expression of tenomodulin, a differentiation marker of tenocytes. Developmental biology. 2006;298:234-47.

[68] Jelinsky SA, Archambault J, Li L, Seeherman H. Tendon-selective genes identified from rat and human musculoskeletal tissues. Journal of orthopaedic research : official publication of the Orthopaedic Research Society. 2010;28:289-97.

[69] Aslan H, Kimelman-Bleich N, Pelled G, Gazit D. Molecular targets for tendon neoformation. The Journal of clinical investigation. 2008;118:439-44.

[70] Oldfield SF, Evans DJ. Tendon morphogenesis in the developing avian limb: plasticity of fetal tendon fibroblasts. Journal of anatomy. 2003;202:153-64.

[71] Newton G, Weremowicz S, Morton CC, Jenkins NA, Gilbert DJ, Copeland NG, et al. The thrombospondin-4 gene. Mammalian genome : official journal of the International Mammalian Genome Society. 1999;10:1010-6.

[72] Chung KY, Agarwal A, Uitto J, Mauviel A. An AP-1 binding sequence is essential for regulation of the human alpha2(I) collagen (COL1A2) promoter activity by transforming growth factor-beta. The Journal of biological chemistry. 1996;271:3272-8.

[73] von Pein F, Valkkila M, Schwarz R, Morcher M, Klima B, Grau A, et al. Analysis of the COL3A1 gene in patients with spontaneous cervical artery dissections. J Neurol. 2002;249:862-6.

[74] Velez-DelValle C, Marsch-Moreno M, Castro-Munozledo F, Kuri-Harcuch W. Decorin gene expression and its regulation in human keratinocytes. Biochemical and biophysical research communications. 2011;411:168-74.

[75] Yan JY, Stringer SE, Hamilton A, Charlton-Menys V, Gotting C, Muller B, et al. Decorin GAG Synthesis and TGF-beta Signaling Mediate Ox-LDL-Induced Mineralization of Human Vascular Smooth Muscle Cells. Arterioscl Throm Vas. 2011;31:608-15.

[76] Zhang GY, Robinson PS, Soslowsky LJ, Iozzo RV, Birk DE. Development of tendon structure and function in the decorin-deficient mouse: Relationship between decorin and biglycan expression. Faseb J. 2004;18:A788-A9.

[77] Vesentini S, Redaelli A, Montevecchi FM. Estimation of the binding force of the collagen molecule-decorin core protein complex in collagen fibril. J Biomech. 2005;38:433-43.

[78] Zhang GY, Ezura Y, Chervoneva I, Robinson PS, Beason DP, Carine ET, et al. Decorin regulates assembly of collagen fibrils and acquisition of biomechanical properties during tendon development. J Cell Biochem. 2006;98:1436-49.

[79] Roughley PJ, White RJ, CsSzabo G, Mort JS. Changes with age in the structure of fibromodulin in human articular cartilage. Osteoarthr Cartilage. 1996;4:153-61.

[80] Ameye L, Aria D, Jepsen K, Oldberg A, Xu TS, Young MF. Abnormal collagen fibrils in tendons of biglycan/fibromodulin-deficient mice lead to gait impairment, ectopic ossification, and osteoarthritis. Faseb J. 2002;16.

[81] Svensson L, Aszodi A, Reinholt FP, Fassler R, Heinegard D, Oldberg A. Fibromodulin-null mice have abnormal collagen fibrils, tissue organization, and altered lumican deposition in tendon. J Biol Chem. 1999;274:9636-47.

[82] Edom-Vovard F, Schuler B, Bonnin MA, Teillet MA, Duprez D. Fgf4 positively regulates scleraxis and tenascin expression in chick limb tendons. Developmental biology. 2002;247:351-66.

[83] Schweitzer R, Chyung JH, Murtaugh LC, Brent AE, Rosen V, Olson EN, et al. Analysis of the tendon cell fate using Scleraxis, a specific marker for tendons and ligaments. Development. 2001;128:3855-66.

[84] Lejard V, Brideau G, Blais F, Salingcarnboriboon R, Wagner G, Roehrl MH, et al. Scleraxis and NFATc regulate the expression of the pro-alpha1(I) collagen gene in tendon fibroblasts. The Journal of biological chemistry. 2007;282:17665-75.

[85] Murchison ND, Price BA, Conner DA, Keene DR, Olson EN, Tabin CJ, et al. Regulation of tendon differentiation by scleraxis distinguishes force-transmitting tendons from muscle-anchoring tendons. Development. 2007;134:2697-708.

[86] Kirkendall DT, Garrett WE. Function and biomechanics of tendons. Scandinavian journal of medicine & science in sports. 1997;7:62-6.

[87] Maganaris CN, Narici MV, Reeves ND. In vivo human tendon mechanical properties: effect of resistance training in old age. Journal of musculoskeletal & neuronal interactions. 2004;4:204-8.

[88] Maganaris CN, Narici MV, Almekinders LC, Maffulli N. Biomechanics and pathophysiology of overuse tendon injuries: ideas on insertional tendinopathy. Sports medicine. 2004;34:1005-17.

[89] Arampatzis A, Karamanidis K, Morey-Klapsing G, De Monte G, Stafilidis S. Mechanical properties of the triceps surae tendon and aponeurosis in relation to intensity of sport activity. Journal of biomechanics. 2007;40:1946-52.

[90] Peltonen J, Cronin NJ, Avela J, Finni T. In vivo mechanical response of human Achilles tendon to a single bout of hopping exercise. The Journal of experimental biology. 2010;213:1259-65.

[91] Couppe C, Suetta C, Kongsgaard M, Justesen L, Hvid LG, Aagaard P, et al. The effects of immobilization on the mechanical properties of the patellar tendon in younger and older men. Clinical biomechanics. 2012;27:949-54.

[92] Wang JH. Mechanobiology of tendon. Journal of biomechanics. 2006;39:1563-82.

[93] Hess GW. Achilles tendon rupture: a review of etiology, population, anatomy, risk factors, and injury prevention. Foot & ankle specialist. 2010;3:29-32.

[94] James R, Kesturu G, Balian G, Chhabra AB. Tendon: biology, biomechanics, repair, growth factors, and evolving treatment options. The Journal of hand surgery. 2008;33:102-12.

[95] Amadio P, An KN, Ejeskar A, Guimberteau JC, Harris S, Savage R, et al. IFSSH Flexor Tendon Committee report. J Hand Surg Br. 2005;30:100-16.

[96] Pioletti D.P. SO, Zambelli P.Y. Tissue Engineering of Tendon. Encyclopedia of Biomaterials and Biomedical Engineering. 2004:1672 - 6.

[97] Costa MT, Hungria Neto JS. Estudo comparativo dos métodos conservador e cirúrgico para tratamento das lesões agudas do tendão do calcâneo. Acta Ortopédica Brasileira. 2007;15:50-4.

[98] Hampson K, Forsyth, N.R., El Haj, A., & Maffuli, N. Tendon tissue engineering. In N. Ashammakhi, R. Reis & F. CHiellini (Ed). Topics in tissue engineerinf Vol 4 (Chapter 3). 2008.

[99] Miller D, Waterston S, Reaper J, Barrass V, Maffulli N. Conservative management, percutaneous or open repair of acute Achilles tendon rupture: a retrospective study. Scottish medical journal. 2005;50:160-5.

[100] Mahoney JL, Farkas LG, Lindsay WK. Quality of tendon graft healing in silastic pseudosheaths: breaking-strength studies. Surgical forum. 1976;27:572-3.

[101] Sabiston P, Frank C, Lam T, Shrive N. Allograft ligament transplantation. A morphological and biochemical evaluation of a medial collateral ligament complex in a rabbit model. The American journal of sports medicine. 1990;18:160-8.

[102] Noyes FR, Butler DL, Grood ES, Zernicke RF, Hefzy MS. Biomechanical analysis of human ligament grafts used in knee-ligament repairs and reconstructions. The Journal of bone and joint surgery American volume. 1984;66:344-52.

[103] Hasslund S, Jacobson JA, Dadali T, Basile P, Ulrich-Vinther M, Soballe K, et al. Adhesions in a murine flexor tendon graft model: autograft versus allograft reconstruction. Journal of orthopaedic research : official publication of the Orthopaedic Research Society. 2008;26:824-33.

[104] Basile P, Dadali T, Jacobson J, Hasslund S, Ulrich-Vinther M, Soballe K, et al. Freeze-dried tendon allografts as tissue-engineering scaffolds for Gdf5 gene delivery. Molecular therapy : the journal of the American Society of Gene Therapy. 2008;16:466-73.

[105] Weitzel PP, Richmond JC, Altman GH, Calabro T, Kaplan DL. Future direction of the treatment of ACL ruptures. The Orthopedic clinics of North America. 2002;33:653-61.

[106] Bagnaninchi PO, Yang Y, El Haj AJ, Maffulli N. Tissue engineering for tendon repair. British journal of sports medicine. 2007;41:e10; discussion e.

[107] Lee SJ, Goldsmith S, Nicholas SJ, McHugh M, Kremenic I, Ben-Avi S. Optimizing Achilles tendon repair: effect of epitendinous suture augmentation on the strength of achilles tendon repairs. Foot & ankle international / American Orthopaedic Foot and Ankle Society [and] Swiss Foot and Ankle Society. 2008;29:427-32.

[108] Lee DK. Achilles tendon repair with acellular tissue graft augmentation in neglected ruptures. J Foot Ankle Surg. 2007;46:451-5.

[109] Rapley JH, Crates J, Barber A. Mid-substance peroneal tendon defects augmented with an acellular dermal matrix allograft. Foot & ankle international / American Orthopaedic Foot and Ankle Society [and] Swiss Foot and Ankle Society. 2010;31:136-40.

[110] DiDomenico LA, Blasko GA, Cane L, Cross DJ. Repair of lacerated anterior tibial tendon with acellular tissue graft augmentation. J Foot Ankle Surg. 2012;51:642-4.

[111] Barber FA, Herbert MA, Coons DA. Tendon augmentation grafts: biomechanical failure loads and failure patterns. Arthroscopy. 2006;22:534-8.

[112] Barber FA, McGarry JE, Herbert MA, Anderson RB. A biomechanical study of Achilles tendon repair augmentation using GraftJacket matrix. Foot & ankle international / American Orthopaedic Foot and Ankle Society [and] Swiss Foot and Ankle Society. 2008;29:329-33.

[113] Derwin KA, Codsi MJ, Milks RA, Baker AR, McCarron JA, Iannotti JP. Rotator Cuff Repair Augmentation in a Canine Model with Use of a Woven Poly-L-Lactide Device. J Bone Joint Surg Am. 2009;91A:1159-71.

[114] Yokoya S, Mochizuki Y, Nagata Y, Deie M, Ochi M. Tendon-bone insertion repair and regeneration using polyglycolic acid sheet in the rabbit rotator cuff injury model. The American journal of sports medicine. 2008;36:1298-309.

[115] Ouyang HW, Goh JC, Thambyah A, Teoh SH, Lee EH. Knitted poly-lactide-co-glycolide scaffold loaded with bone marrow stromal cells in repair and regeneration of rabbit Achilles tendon. Tissue engineering. 2003;9:431-9.

[116] Williams SF, Martin DP, Horowitz DM, Peoples OP. PHA applications: addressing the price performance issue: I. Tissue engineering. International journal of biological macromolecules. 1999;25:111-21.

[117] Chen J, Xu J, Wang A, Zheng M. Scaffolds for tendon and ligament repair: review of the efficacy of commercial products. Expert review of medical devices. 2009;6:61-73.

[118] Khanna S, Srivastava AK. Recent advances in microbial polyhydroxyalkanoates. Process Biochemistry. 2005;40:607-19.

[119] Chen GQ, Wu Q. The application of polyhydroxyalkanoates as tissue engineering materials. Biomaterials. 2005;26:6565-78.

[120] Potter M, Steinbuchel A. Poly(3-hydroxybutyrate) granule-associated proteins: impacts on poly(3-hydroxybutyrate) synthesis and degradation. Biomacromolecules. 2005;6:552-60.

[121] Van Robertson WB, Schwartz B. Ascorbic acid and the formation of collagen. The Journal of biological chemistry. 1953;201:689-96.

[122] Robertson WV. The biochemical role of ascorbic acid in connective tissue. Annals of the New York Academy of Sciences. 1961;92:159-67.

[123] Elster SK. Effect of ascorbic acid deficiency on collagen content of guinea pig tissues. The Journal of biological chemistry. 1950;186:105-12.

[124] Sharma SR, Poddar, R., Sen, P., and Andrews J.T. Effect of Vitamin C on collagen biosynthesis and degree of birefringence in polarization sensitive optical coherence tomography (PS-OCT). African Journal of Biotechnology. 2008;7:2049-54.

[125] Murad S, Grove D, Lindberg KA, Reynolds G, Sivarajah A, Pinnell SR. Regulation of collagen synthesis by ascorbic acid. Proc Natl Acad Sci U S A. 1981;78:2879-82.

[126] Kuroyanagi M, Shimamura E, Kim M, Arakawa N, Fujiwara Y, Otsuka M. Effects of L-ascorbic acid on lysyl oxidase in the formation of collagen cross-links. Bioscience, biotechnology, and biochemistry. 2002;66:2077-82.

[127] Singh RP, Franke K, Wielockx B. Hypoxia-Mediated Regulation of Stem Cell Fate. High Alt Med Biol. 2012;13:162-8.

[128] Simon MC, Keith B. The role of oxygen availability in embryonic development and stem cell function. Nat Rev Mol Cell Bio. 2008;9:285-96.

[129] Stroka DM, Burkhardt T, Desbaillets I, Wenger RH, Neil DAH, Bauer C, et al. HIF-1 is expressed in normoxic tissue and displays an organ-specific regulation under systemic hypoxia. Faseb J. 2001;15:2445-53.

[130] Mitchell JA, Yochim JM. Intrauterine oxygen tension during the estrous cycle in the rat: its relation to uterine respiration and vascular activity. Endocrinology. 1968;83:701-5.

[131] Folkman J, Hahnfeldt P, Hlatky L. Cancer: looking outside the genome. Nat Rev Mol Cell Biol. 2000;1:76-9.

[132] Gatenby RA, Gillies RJ. Why do cancers have high aerobic glycolysis? Nat Rev Cancer. 2004;4:891-9.

[133] Takubo K, Goda N, Yamada W, Iriuchishima H, Ikeda E, Kubota Y, et al. Regulation of the HIF-1 alpha Level Is Essential for Hematopoietic Stem Cells. Cell Stem Cell. 2010;7:391-402.

[134] Mendez-Ferrer S, Michurina TV, Ferraro F, Mazloom AR, MacArthur BD, Lira SA, et al. Mesenchymal and haematopoietic stem cells form a unique bone marrow niche. Nature. 2010;466:829-U59.

[135] Mazumdar J, O'Brien WT, Johnson RS, LaManna JC, Chavez JC, Klein PS, et al. O-2 regulates stem cells through Wnt/beta-catenin signalling. Nat Cell Biol. 2010;12:1007-13.

[136] Forristal CE, Wright KL, Hanley NA, Oreffo ROC, Houghton FD. Hypoxia inducible factors regulate pluripotency and proliferation in human embryonic stem cells cultured at reduced oxygen tensions. Reproduction. 2010;139:85-97.

[137] Eliasson P, Jonsson JI. The Hematopoietic Stem Cell Niche: Low in Oxygen but a Nice Place to be. J Cell Physiol. 2010;222:17-22.

[138] Mohyeldin A, Garzon-Muvdi T, Quinones-Hinojosa A. Oxygen in Stem Cell Biology: A Critical Component of the Stem Cell Niche. Cell Stem Cell. 2010;7:150-61.

[139] Fehrer C, Brunauer R, Laschober G, Unterluggauer H, Reitinger S, Kloss F, et al. Reduced oxygen tension attenuates differentiation capacity of human mesenchymal stem cells and prolongs their lifespan. Aging Cell. 2007;6:745-57.

[140] Grayson WL, Zhao F, Bunnell B, Ma T. Hypoxia enhances proliferation and tissue formation of human mesenchymal stem cells. Biochemical and biophysical research communications. 2007;358:948-53.

[141] Ma T, Grayson WL, Fröhlich M, Vunjak-Novakovic G. Hypoxia and stem cell-based engineering of mesenchymal tissues. Biotechnology Progress. 2009;25:32-42.

[142] Forsyth NR, Musio A, Vezzoni P, Simpson A, Noble BS, McWhir J. Physiologic oxygen enhances human embryonic stem cell clonal recovery and reduces chromosomal abnormalities. Cloning and Stem Cells. 2006;8:16-23.

[143] Das B, Bayat-Mokhtari R, Tsui M, Lotfi S, Tsuchida R, Felsher DW, et al. HIF-2α Suppresses p53 to Enhance the Stemness and Regenerative Potential of Human Embryonic Stem Cells. STEM CELLS. 2012;30:1685-95.

[144] Becker AJ, Mc CE, Till JE. Cytological demonstration of the clonal nature of spleen colonies derived from transplanted mouse marrow cells. Nature. 1963;197:452-4.

[145] Martin GR. Isolation of a pluripotent cell line from early mouse embryos cultured in medium conditioned by teratocarcinoma stem cells. Proc Natl Acad Sci U S A. 1981;78:7634-8.

[146] Liu T, D'Mello V, Deng L, Hu J, Ricardo M, Pan S, et al. A multiplexed proteomics approach to differentiate neurite outgrowth patterns. Journal of neuroscience methods. 2006;158:22-9.

[147] Friel R, van der Sar S, Mee PJ. Embryonic stem cells: understanding their history, cell biology and signalling. Adv Drug Deliv Rev. 2005;57:1894-903.

[148] Friel R, Fisher D, Hook L. Embryonic stem cell technology: applications and uses in functional genomic studies. Stem cell reviews. 2006;2:31-5.

[149] Evans MJ, Kaufman MH. Establishment in culture of pluripotential cells from mouse embryos. Nature. 1981;292:154-6.

[150] Pera MF, Reubinoff B, Trounson A. Human embryonic stem cells. Journal of cell science. 2000;113 (Pt 1):5-10.

[151] Thomson JA, Kalishman J, Golos TG, Durning M, Harris CP, Becker RA, et al. Isolation of a primate embryonic stem cell line. Proc Natl Acad Sci U S A. 1995;92:7844-8.

[152] Thomson JA, Kalishman J, Golos TG, Durning M, Harris CP, Hearn JP. Pluripotent cell lines derived from common marmoset (Callithrix jacchus) blastocysts. Biology of reproduction. 1996;55:254-9.

[153] Pera MF, Trounson AO. Human embryonic stem cells: prospects for development. Development. 2004;131:5515-25.

[154] Friedenstein AJ, Latzinik NV, Gorskaya Yu F, Luria EA, Moskvina IL. Bone marrow stromal colony formation requires stimulation by haemopoietic cells. Bone and mineral. 1992;18:199-213.

[155] Bianco P, Robey PG, Simmons PJ. Mesenchymal stem cells: revisiting history, concepts, and assays. Cell Stem Cell. 2008;2:313-9.

[156] Bullough R, Finnigan T, Kay A, Maffulli N, Forsyth NR. Tendon repair through stem cell intervention: cellular and molecular approaches. Disability and rehabilitation. 2008;30:1746-51.

[157] Hoffmann A, Gross G. Tendon and ligament engineering in the adult organism: mesenchymal stem cells and gene-therapeutic approaches. International orthopaedics. 2007;31:791-7.

[158] Pallante BA, Duignan I, Okin D, Chin A, Bressan MC, Mikawa T, et al. Bone marrow Oct3/4+ cells differentiate into cardiac myocytes via age-dependent paracrine mechanisms. Circulation research. 2007;100:e1-11.

[159] Montzka K, Lassonczyk N, Tschoke B, Neuss S, Fuhrmann T, Franzen R, et al. Neural differentiation potential of human bone marrow-derived mesenchymal stromal cells: misleading marker gene expression. BMC neuroscience. 2009;10:16.

[160] Bi Y, Ehirchiou D, Kilts TM, Inkson CA, Embree MC, Sonoyama W, et al. Identification of tendon stem/progenitor cells and the role of the extracellular matrix in their niche. Nature medicine. 2007;13:1219-27.

[161] Helmreich EJM. The biochemistry of cell signalling. Oxford: Oxford University Press; 2001.

[162] Kobayashi D, Kurosaka M, Yoshiya S, Mizuno K. Effect of basic fibroblast growth factor on the healing of defects in the canine anterior cruciate ligament. Knee surgery, sports traumatology, arthroscopy : official journal of the ESSKA. 1997;5:189-94.

[163] Fukui N, Katsuragawa Y, Sakai H, Oda H, Nakamura K. Effect of local application of basic fibroblast growth factor on ligament healing in rabbits. Revue du rhumatisme. 1998;65:406-14.

[164] Chan BP, Fu S, Qin L, Lee K, Rolf CG, Chan K. Effects of basic fibroblast growth factor (bFGF) on early stages of tendon healing: a rat patellar tendon model. Acta orthopaedica Scandinavica. 2000;71:513-8.

[165] Thomopoulos S, Das R, Sakiyama-Elbert S, Silva MJ, Charlton N, Gelberman RH. bFGF and PDGF-BB for Tendon Repair: Controlled Release and Biologic Activity by Tendon Fibroblasts In Vitro. Annals of biomedical engineering. 2010;38:225-34.

[166] Henn RF, 3rd, Kuo CE, Kessler MW, Razzano P, Grande DP, Wolfe SW. Augmentation of zone II flexor tendon repair using growth differentiation factor 5 in a rabbit model. The Journal of hand surgery. 2010;35:1825-32.

[167] Forslund C, Aspenberg P. Tendon healing stimulated by injected CDMP-2. Medicine and science in sports and exercise. 2001;33:685-7.

[168] Kurtz CA, Loebig TG, Anderson DD, DeMeo PJ, Campbell PG. Insulin-like growth factor I accelerates functional recovery from Achilles tendon injury in a rat model. Am J Sport Med. 1999;27:363-9.

[169] Suwalski A, Dabboue H, Delalande A, Bensamoun SF, Canon F, Midoux P, et al. Accelerated Achilles tendon healing by PDGF gene delivery with mesoporous silica nanoparticles. Biomaterials. 2010;31:5237-45.

[170] Shen W, Chen X, Chen J, Yin Z, Heng BC, Chen W, et al. The effect of incorporation of exogenous stromal cell-derived factor-1 alpha within a knitted silk-collagen sponge scaffold on tendon regeneration. Biomaterials. 2010;31:7239-49.

[171] Wei XL, Lin L, Hou Y, Fu X, Zhang JY, Mao ZB, et al. Construction of recombinant adenovirus co-expression vector carrying the human transforming growth factor-beta1 and vascular endothelial growth factor genes and its effect on anterior cruciate ligament fibroblasts. Chinese medical journal. 2008;121:1426-32.

[172] Spindler KP, Dawson JM, Stahlman GC, Davidson JM, Nanney LB. Collagen expression and biomechanical response to human recombinant transforming growth factor beta (rhTGF-beta2) in the healing rabbit MCL. Journal of orthopaedic research : official publication of the Orthopaedic Research Society. 2002;20:318-24.

[173] Liu CF, Aschbacher-Smith L, Barthelery NJ, Dyment N, Butler D, Wylie C. What we should know before using tissue engineering techniques to repair injured tendons: a developmental biology perspective. Tissue engineering Part B, Reviews. 2011;17:165-76.

[174] Wu MY, Hill CS. Tgf-beta superfamily signaling in embryonic development and homeostasis. Developmental cell. 2009;16:329-43.

[175] Feng XH, Derynck R. Specificity and versatility in TGF-beta signaling through Smads. Annu Rev Cell Dev Bi. 2005;21:659-93.

[176] Lou J, Tu Y, Burns M, Silva MJ, Manske P. BMP-12 gene transfer augmentation of lacerated tendon repair. Journal of orthopaedic research : official publication of the Orthopaedic Research Society. 2001;19:1199-202.

[177] Williams LA, Bhargav D, Diwan AD. Unveiling the Bmp13 Enigma: Redundant Morphogen or Crucial Regulator? Int J Biol Sci. 2008;4:318-29.

[178] Wu X, Shi W, Cao X. Multiplicity of BMP signaling in skeletal development. Annals of the New York Academy of Sciences. 2007;1116:29-49.

[179] Wang QW, Chen ZL, Piao YR. Mesenchymal stem cells differentiate into tenocytes by bone morphogenetic protein (BMP) 12 gene transfer. Journal of bioscience and bioengineering. 2005;100:418-22.

[180] Lee JY, Zhou ZP, Taub PJ, Ramcharan M, Li YH, Akinbiyi T, et al. BMP-12 Treatment of Adult Mesenchymal Stem Cells In Vitro Augments Tendon-Like Tissue Formation and Defect Repair In Vivo. Plos One. 2011;6.

[181] Berasi SP, Varadarajan U, Archambault J, Cain M, Souza TA, Abouzeid A, et al. Divergent activities of osteogenic BMP2, and tenogenic BMP12 and BMP13 independent of receptor binding affinities. Growth Factors. 2011;29:128-39.

[182] Pauly S, Klatte F, Strobel C, Schmidmaier G, Greiner S, Scheibel M, et al. BMP-2 and BMP-7 affect human rotator cuff tendon cells in vitro. J Shoulder Elb Surg. 2012;21:464-73.

[183] Fu SC, Wong YP, Chan BP, Pau HM, Cheuk YC, Lee KM, et al. The roles of bone morphogenetic protein (BMP) 12 in stimulating the proliferation and matrix production of human patellar tendon fibroblasts. Life Sci. 2003;72:2965-74.

[184] Sakamoto H, Mori M, Taira M, Yoshida T, Matsukawa S, Shimizu K, et al. Transforming gene from human stomach cancers and a noncancerous portion of stomach mucosa. Proc Natl Acad Sci U S A. 1986;83:3997-4001.

[185] Ornitz DM, Itoh N. Fibroblast growth factors. Genome biology. 2001;2:REVIEWS3005.

[186] Kosaka N, Sakamoto H, Terada M, Ochiya T. Pleiotropic function of FGF-4: its role in development and stem cells. Developmental dynamics : an official publication of the American Association of Anatomists. 2009;238:265-76.

[187] Ornitz DM. FGFs, heparan sulfate and FGFRs: complex interactions essential for development. BioEssays : news and reviews in molecular, cellular and developmental biology. 2000;22:108-12.

[188] Kelley MJ, Pech M, Seuanez HN, Rubin JS, Obrien SJ, Aaronson SA. Emergence of the Keratinocyte Growth-Factor Multigene Family during the Great Ape Radiation. P Natl Acad Sci USA. 1992;89:9287-91.

[189] Wada N, Nohno T. Differential response of Shh expression between chick forelimb and hindlimb buds by FGF-4. Developmental dynamics : an official publication of the American Association of Anatomists. 2001;221:402-11.

[190] Huebner K, Ferrari AC, Bovi PD, Croce CM, Basilico C. The Fgf-Related Oncogene, K-Fgf, Maps to Human-Chromosome Region 11q13, Possibly near Int-2. Oncogene Res. 1988;3:263-70.

[191] Itoh N, Ornitz DM. Functional evolutionary history of the mouse Fgf gene family. Developmental dynamics : an official publication of the American Association of Anatomists. 2008;237:18-27.

[192] Yoshida T, Miyagawa K, Odagiri H, Sakamoto H, Little PF, Terada M, et al. Genomic sequence of hst, a transforming gene encoding a protein homologous to fibroblast growth factors and the int-2-encoded protein. Proc Natl Acad Sci U S A. 1987;84:7305-9.

[193] Taira M, Yoshida T, Miyagawa K, Sakamoto H, Terada M, Sugimura T. cDNA sequence of human transforming gene hst and identification of the coding sequence required for transforming activity. Proc Natl Acad Sci U S A. 1987;84:2980-4.

[194] Delli Bovi P, Curatola AM, Kern FG, Greco A, Ittmann M, Basilico C. An oncogene isolated by transfection of Kaposi's sarcoma DNA encodes a growth factor that is a member of the FGF family. Cell. 1987;50:729-37.

[195] Fuller-Pace F, Peters G, Dickson C. Cell transformation by kFGF requires secretion but not glycosylation. The Journal of cell biology. 1991;115:547-55.

[196] Bellosta P, Talarico D, Rogers D, Basilico C. Cleavage of K-FGF produces a truncated molecule with increased biological activity and receptor binding affinity. The Journal of cell biology. 1993;121:705-13.

[197] Niswander L, Martin GR. Fgf-4 expression during gastrulation, myogenesis, limb and tooth development in the mouse. Development. 1992;114:755-68.

[198] Rappolee DA, Basilico C, Patel Y, Werb Z. Expression and function of FGF-4 in peri-implantation development in mouse embryos. Development. 1994;120:2259-69.

[199] deLapeyriere O, Ollendorff V, Planche J, Ott MO, Pizette S, Coulier F, et al. Expression of the Fgf6 gene is restricted to developing skeletal muscle in the mouse embryo. Development. 1993;118:601-11.

[200] Zhao P, Hoffman EP. Embryonic myogenesis pathways in muscle regeneration. Developmental dynamics : an official publication of the American Association of Anatomists. 2004;229:380-92.

[201] Armand AS, Pariset C, Laziz I, Launay T, Fiore F, Della Gaspera B, et al. FGF6 regulates muscle differentiation through a calcineurin-dependent pathway in regenerating soleus of adult mice. Journal of cellular physiology. 2005;204:297-308.

[202] Armand AS, Laziz I, Chanoine C. FGF6 in myogenesis. Biochimica et biophysica acta. 2006;1763:773-8.

[203] Moon AM, Boulet AM, Capecchi MR. Normal limb development in conditional mutants of Fgf4. Development. 2000;127:989-96.

[204] Park EJ, Ogden LA, Talbot A, Evans S, Cai CL, Black BL, et al. Required, tissue-specific roles for Fgf8 in outflow tract formation and remodeling. Development. 2006;133:2419-33.

[205] Kardon G. Muscle and tendon morphogenesis in the avian hind limb. Development. 1998;125:4019-32.

[206] Eloy-Trinquet S, Wang H, Edom-Vovard F, Duprez D. Fgf signaling components are associated with muscles and tendons during limb development. Developmental dynamics : an official publication of the American Association of Anatomists. 2009;238:1195-206.

[207] Subramanian A, Wayburn B, Bunch T, Volk T. Thrombospondin-mediated adhesion is essential for the formation of the myotendinous junction in Drosophila. Development. 2007;134:1269-78.

[208] Schnorrer F, Dickson BJ. Muscle building: mechanisms of myotube guidance and attachment site selection. Dev Cell. 2004;7:9-20.

[209] Bonnin MA, Laclef C, Blaise R, Eloy-Trinquet S, Relaix F, Maire P, et al. Six1 is not involved in limb tendon development, but is expressed in limb connective tissue under Shh regulation. Mech Develop. 2005;122:573-85.

[210] Plotnikov AN, Hubbard SR, Schlessinger J, Mohammadi M. Crystal structures of two FGF-FGFR complexes reveal the determinants of ligand-receptor specificity. Cell. 2000;101:413-24.

[211] Zhu X, Komiya H, Chirino A, Faham S, Fox GM, Arakawa T, et al. Three-dimensional structures of acidic and basic fibroblast growth factors. Science. 1991;251:90-3.

[212] Eriksson AE, Cousens LS, Weaver LH, Matthews BW. Three-dimensional structure of human basic fibroblast growth factor. Proc Natl Acad Sci U S A. 1991;88:3441-5.

[213] Faham S, Hileman RE, Fromm JR, Linhardt RJ, Rees DC. Heparin structure and interactions with basic fibroblast growth factor. Science. 1996;271:1116-20.

[214] Mohammadi M, Olsen SK, Ibrahimi OA. Structural basis for fibroblast growth factor receptor activation. Cytokine & growth factor reviews. 2005;16:107-37.

[215] Huang P, Stern MJ. FGF signaling in flies and worms: more and more relevant to vertebrate biology. Cytokine & growth factor reviews. 2005;16:151-8.

[216] Johnson DE, Williams LT. Structural and Functional Diversity in the Fgf Receptor Multigene Family. Adv Cancer Res. 1993;60:1-41.

[217] Olsen SK, Garbi M, Zampieri N, Eliseenkova AV, Ornitz DM, Goldfarb M, et al. Fibroblast growth factor (FGF) homologous factors share structural but not functional homology with FGFs. J Biol Chem. 2003;278:34226-36.

[218] Olsen SK, Li JY, Bromleigh C, Eliseenkova AV, Ibrahimi OA, Lao Z, et al. Structural basis by which alternative splicing modulates the organizer activity of FGF8 in the brain. Genes & development. 2006;20:185-98.

[219] Rebscher N, Deichmann C, Sudhop S, Fritzenwanker JH, Green S, Hassel M. Conserved intron positions in FGFR genes reflect the modular structure of FGFR and reveal stepwise addition of domains to an already complex ancestral FGFR. Development genes and evolution. 2009;219:455-68.

[220] Powers CJ, McLeskey SW, Wellstein A. Fibroblast growth factors, their receptors and signaling. Endocrine-related cancer. 2000;7:165-97.

[221] Moy FJ, Safran M, Seddon AP, Kitchen D, Bohlen P, Aviezer D, et al. Properly oriented heparin-decasaccharide-induced dimers are the biologically active form of basic fibroblast growth factor. Biochemistry. 1997;36:4782-91.

[222] Ornitz DM, Xu JS, Colvin JS, McEwen DG, MacArthur CA, Coulier F, et al. Receptor specificity of the fibroblast growth factor family. J Biol Chem. 1996;271:15292-7.

[223] Koga M, Kasayama S, Matsumoto K, Sato B. Molecular mechanism of androgen-dependent growth in transformed cells. Pathway from basic science to clinical application. The Journal of steroid biochemistry and molecular biology. 1995;54:1-6.

[224] Miralles F, Czernichow P, Ozaki K, Itoh N, Scharfmann R. Signaling through fibroblast growth factor receptor 2b plays a key role in the development of the exocrine pancreas. Proc Natl Acad Sci U S A. 1999;96:6267-72.

[225] Xu J, Lawshe A, MacArthur CA, Ornitz DM. Genomic structure, mapping, activity and expression of fibroblast growth factor 17. Mechanisms of development. 1999;83:165-78.

[226] Itoh N, Ornitz DM. Evolution of the Fgf and Fgfr gene families. Trends in genetics : TIG. 2004;20:563-9.

[227] Casu B, Petitou M, Provasoli M, Sinay P. Conformational flexibility: a new concept for explaining binding and biological properties of iduronic acid-containing glycosaminoglycans. Trends in biochemical sciences. 1988;13:221-5.

[228] Wilkie AOM, Morrisskay GM, Jones EY, Heath JK. Functions of Fibroblast Growth-Factors and Their Receptors. Current Biology. 1995;5:500-7.

[229] Olwin BB, Arthur K, Hannon K, Hein P, McFall A, Riley B, et al. Role of FGFs in skeletal muscle and limb development. Molecular reproduction and development. 1994;39:90-100; discussion -1.

[230] Lucas JM, Bryans M, Lo K, Wilkie NM, Freshney M, Thornton D, et al. The FGF-4 promoter is required for transformation and is active in both embryonal and somatic cells. Oncology research. 1994;6:139-49.

[231] Herr AB, Ornitz DM, Sasisekharan R, Venkataraman G, Waksman G. Heparin-induced self-association of fibroblast growth factor-2. Evidence for two oligomerization processes. The Journal of biological chemistry. 1997;272:16382-9.

[232] Moscatelli D. High and low affinity binding sites for basic fibroblast growth factor on cultured cells: absence of a role for low affinity binding in the stimulation of plasminogen activator production by bovine capillary endothelial cells. Journal of cellular physiology. 1987;131:123-30.

[233] Flaumenhaft R, Moscatelli D, Rifkin DB. Heparin and heparan sulfate increase the radius of diffusion and action of basic fibroblast growth factor. The Journal of cell biology. 1990;111:1651-9.

[234] Basilico C, Moscatelli D. The FGF family of growth factors and oncogenes. Adv Cancer Res. 1992;59:115-65.

[235] Mach H, Volkin DB, Burke CJ, Middaugh CR, Linhardt RJ, Fromm JR, et al. Nature of the Interaction of Heparin with Acidic Fibroblast Growth-Factor. Biochemistry. 1993;32:5480-9.

[236] DiGabriele AD, Lax I, Chen DI, Svahn CM, Jaye M, Schlessinger J, et al. Structure of a heparin-linked biologically active dimer of fibroblast growth factor. Nature. 1998;393:812-7.

[237] Waksman G, Herr AB. New insights into heparin-induced FGF oligomerization. Nature structural biology. 1998;5:527-30.

[238] Rapraeger AC, Krufka A, Olwin BB. Requirement of heparan sulfate for bFGF-mediated fibroblast growth and myoblast differentiation. Science. 1991;252:1705-8.

[239] Yayon A, Klagsbrun M, Esko JD, Leder P, Ornitz DM. Cell surface, heparin-like molecules are required for binding of basic fibroblast growth factor to its high affinity receptor. Cell. 1991;64:841-8.

[240] Szebenyi G, Fallon JF. Fibroblast growth factors as multifunctional signaling factors. International review of cytology. 1999;185:45-106.

[241] Klint P, Claesson-Welsh L. Signal transduction by fibroblast growth factor receptors. Frontiers in bioscience : a journal and virtual library. 1999;4:D165-77.

[242] Vogel W, Ullrich A. Multiple in vivo phosphorylated tyrosine phosphatase SHP-2 engages binding to Grb2 via tyrosine 584. Cell Growth Differ. 1996;7:1589-97.

[243] Fang J. Role of FGF-2/FGFR signaling pathway in cancer and its signification in breast cancer. Chinese Science Bulletin. 2003;48:1539.

[244] Tsang M, Dawid IB. Promotion and attenuation of FGF signaling through the Ras-MAPK pathway. Science's STKE : signal transduction knowledge environment. 2004;2004:pe17.

[245] Tsang M, Friesel R, Kudoh T, Dawid IB. Identification of Sef, a novel modulator of FGF signalling. Nature cell biology. 2002;4:165-9.

[246] Sawada A, Shinya M, Jiang YJ, Kawakami A, Kuroiwa A, Takeda H. Fgf/MAPK signalling is a crucial positional cue in somite boundary formation. Development. 2001;128:4873-80.

[247] Smith KM, Ohkubo Y, Maragnoli ME, Rasin MR, Schwartz ML, Sestan N, et al. Midline radial glia translocation and corpus callosum formation require FGF signaling. Nature neuroscience. 2006;9:787-97.

[248] Smith TG, Karlsson M, Lunn JS, Eblaghie MC, Keenan ID, Farrell ER, et al. Negative feedback predominates over cross-regulation to control ERK MAPK activity in response to FGF signalling in embryos. FEBS letters. 2006;580:4242-5.

[249] Squarzoni P, Parveen F, Zanetti L, Ristoratore F, Spagnuolo A. FGF/MAPK/Ets signaling renders pigment cell precursors competent to respond to Wnt signal by directly controlling Ci-Tcf transcription. Development. 2011;138:1421-32.

[250] Furthauer M, Lin W, Ang SL, Thisse B, Thisse C. Sef is a feedback-induced antagonist of Ras/MAPK-mediated FGF signalling. Nature cell biology. 2002;4:170-4.

[251] Berridge MJ, Irvine RF. Inositol phosphates and cell signalling. Nature. 1989;341:197-205.

[252] Berridge MJ. Inositol Trisphosphate and Calcium Signaling. Nature. 1993;361:315-25.

[253] Klint P, Kanda S, Kloog Y, Claesson-Welsh L. Contribution of Src and Ras pathways in FGF-2 induced endothelial cell differentiation. Oncogene. 1999;18:3354-64.

[254] Albanese A, Tang PS, Chan WC. The effect of nanoparticle size, shape, and surface chemistry on biological systems. Annual review of biomedical engineering. 2012;14:1-16.

[255] Chiellini F, Piras AM, Errico C, Chiellini E. Micro/nanostructured polymeric systems for biomedical and pharmaceutical applications. Nanomedicine. 2008;3:367-93.

[256] Kim S, Kim JH, Jeon O, Kwon IC, Park K. Engineered polymers for advanced drug delivery. European journal of pharmaceutics and biopharmaceutics : official journal of Arbeitsgemeinschaft fur Pharmazeutische Verfahrenstechnik eV. 2009;71:420-30.

[257] Tian HY, Tang ZH, Zhuang XL, Chen XS, Jing XB. Biodegradable synthetic polymers: Preparation, functionalization and biomedical application. Progress in Polymer Science. 2012;37:237-80.

[258] Hoffman AS. The origins and evolution of "controlled" drug delivery systems. Journal of controlled release : official journal of the Controlled Release Society. 2008;132:153-63.

[259] Mooney DJ, Mazzoni CL, Breuer C, McNamara K, Hern D, Vacanti JP, et al. Stabilized polyglycolic acid fibre-based tubes for tissue engineering. Biomaterials. 1996;17:115-24.

[260] Holland SJ, Jolly AM, Yasin M, Tighe BJ. Polymers for biodegradable medical devices. II. Hydroxybutyrate-hydroxyvalerate copolymers: hydrolytic degradation studies. Biomaterials. 1987;8:289-95.

[261] Lee J, Cuddihy MJ, Kotov NA. Three-dimensional cell culture matrices: state of the art. Tissue engineering Part B, Reviews. 2008;14:61-86.

[262] Bikiaris DN, Papageorgiou GZ, Papadimitriou SA, Karavas E, Avgoustakis K. Novel biodegradable polyester poly(propylene succinate): synthesis and application in the preparation of solid dispersions and nanoparticles of a water-soluble drug. AAPS PharmSciTech. 2009;10:138-46.

[263] Gunatillake PA, Adhikari R. Biodegradable synthetic polymers for tissue engineering. European cells & materials. 2003;5:1-16; discussion

[264] Stoilova O, Manolova N, Gabrovska K, Marinov I, Godjevargova T, Mita DG, et al. Electrospun Polyacrylonitrile Nanofibrous Membranes Tailored for Acetylcholinesterase Immobilization. Journal of Bioactive and Compatible Polymers. 2010;25:40-57.

[265] Kellomaki M, Heller J, Tormala P. Processing and properties of two different poly (ortho esters). Journal of materials science Materials in medicine. 2000;11:345-55.

[266] Peach MS, James R, Toti US, Deng M, Morozowich NL, Allcock HR, et al. Polyphosphazene functionalized polyester fiber matrices for tendon tissue engineering: in vitro evaluation with human mesenchymal stem cells. Biomedical materials. 2012;7:045016.

[267] Friess W. Collagen--biomaterial for drug delivery. European journal of pharmaceutics and biopharmaceutics : official journal of Arbeitsgemeinschaft fur Pharmazeutische Verfahrenstechnik eV. 1998;45:113-36.

[268] DiTizio V, Karlgard C, Lilge L, Khoury AE, Mittelman MW, DiCosmo F. Localized drug delivery using crosslinked gelatin gels containing liposomes: factors influencing liposome stability and drug release. Journal of biomedical materials research. 2000;51:96-106.

[269] Elzoghby AO, Samy WM, Elgindy NA. Albumin-based nanoparticles as potential controlled release drug delivery systems. Journal of controlled release : official journal of the Controlled Release Society. 2012;157:168-82.

[270] Barbucci R, Leone G, Vecchiullo A. Novel carboxymethylcellulose-based microporous hydrogels suitable for drug delivery. Journal of biomaterials science Polymer edition. 2004;15:607-19.

[271] Tuovinen L, Ruhanen E, Kinnarinen T, Ronkko S, Pelkonen J, Urtti A, et al. Starch acetate microparticles for drug delivery into retinal pigment epithelium-in vitro study. Journal of controlled release : official journal of the Controlled Release Society. 2004;98:407-13.

[272] Wang N, Wu XS. Preparation and characterization of agarose hydrogel nanoparticles for protein and peptide drug delivery. Pharmaceutical development and technology. 1997;2:135-42.

[273] Tonnesen HH, Karlsen J. Alginate in drug delivery systems. Drug development and industrial pharmacy. 2002;28:621-30.

[274] Liu LS, Ng CK, Thompson AY, Poser JW, Spiro RC. Hyaluronate-heparin conjugate gels for the delivery of basic fibroblast growth factor (FGF-2). Journal of biomedical materials research. 2002;62:128-35.

[275] Miyazaki Y, Yakou S, Nagai T, Takayama K. Release profiles of theophylline from microspheres consisting of dextran derivatives and cellulose acetate butyrate: effect of polyion complex formation. Drug development and industrial pharmacy. 2003;29:795-804.

[276] Prabaharan M, Mano JF. Chitosan-based particles as controlled drug delivery systems. Drug delivery. 2005;12:41-57.

[277] Raffa V, Vittorio O, Riggio C, Cuschieri A. Progress in nanotechnology for healthcare. Minimally invasive therapy & allied technologies : MITAT : official journal of the Society for Minimally Invasive Therapy. 2010;19:127-35.

[278] Serda RE, Godin B, Blanco E, Chiappini C, Ferrari M. Multi-stage delivery nano-particle systems for therapeutic applications. Biochimica et biophysica acta. 2011;1810:317-29.

[279] Kost J, Langer R. Responsive polymeric delivery systems. Advanced Drug Delivery Reviews. 2012;64:327-41.

[280] Siepmann J, Siepmann F. Modeling of diffusion controlled drug delivery. Journal of controlled release : official journal of the Controlled Release Society. 2012;161:351-62.

[281] Fu Y, Kao WJ. Drug release kinetics and transport mechanisms of non-degradable and degradable polymeric delivery systems. Expert Opin Drug Del. 2010;7:429-44.

[282] Letchford K, Burt H. A review of the formation and classification of amphiphilic block copolymer nanoparticulate structures: micelles, nanospheres, nanocapsules and polymersomes. European journal of pharmaceutics and biopharmaceutics : official journal of Arbeitsgemeinschaft fur Pharmazeutische Verfahrenstechnik eV. 2007;65:259-69.

[283] Farokhzad OC. Nanotechnology for drug delivery: the perfect partnership. Expert Opin Drug Del. 2008;5:927-9.

[284] Li C, Wallace S. Polymer-drug conjugates: Recent development in clinical oncology. Advanced Drug Delivery Reviews. 2008;60:886-98.

[285] Petros RA, DeSimone JM. Strategies in the design of nanoparticles for therapeutic applications. Nature reviews Drug discovery. 2010;9:615-27.

[286] Vauthier C, Bouchemal K. Methods for the preparation and manufacture of polymeric nanoparticles. Pharmaceutical research. 2009;26:1025-58.

[287] Almeida JPM, Chen AL, Foster A, Drezek R. In vivo biodistribution of nanoparticles. Nanomedicine. 2011;6:815-35.

[288] Parveen S, Misra R, Sahoo SK. Nanoparticles: a boon to drug delivery, therapeutics, diagnostics and imaging. Nanomedicine. 2012;8:147-66.

[289] Elsabahy M, Wooley KL. Design of polymeric nanoparticles for biomedical delivery applications. Chemical Society reviews. 2012;41:2545-61.

[290] Kumari A, Yadav SK, Yadav SC. Biodegradable polymeric nanoparticles based drug delivery systems. Colloids and surfaces B, Biointerfaces. 2010;75:1-18.

[291] Makadia HK, Siegel SJ. Poly Lactic-co-Glycolic Acid (PLGA) as Biodegradable Controlled Drug Delivery Carrier. Polymers-Basel. 2011;3:1377-97.

[292] Rasiah IA. PN, Grage K., Palanisamy R., Jahns AC., Atwood JA. Biopolyester particles: preparation and applications. In: MC. F, editor. Encyclopedia of Industrial Biotechnology In: John Wiley & Sons, Inc.,; 2009.

[293] Fisher RAS, Bennett JH, Fisher RASSmfrw, Fisher RASDoe, Fisher RASSm, scientific i. Statistical methods, inference and experimental design : a re-issue of Statistical methods for Research workers, The design of experiments, and Statistical methods and scientific inference. Oxford: Oxford University Press; 1990.

[294] Webb WR, Dale TP, Lomas AJ, Zeng G, Wimpenny I, El Haj AJ, et al. The application of poly(3-hydroxybutyrate-co-3-hydroxyhexanoate) scaffolds for tendon repair in the rat model. Biomaterials. 2013;34:6683-94.

[295] Pennisi E. Tending tender tendons. Science. 2002;295:1011.

[296] Longo UG, Lamberti A, Maffulli N, Denaro V. Tendon augmentation grafts: a systematic review. British medical bulletin. 2010;94:165-88.

[297] Longo UG, Lamberti A, Petrillo S, Maffulli N, Denaro V. Scaffolds in tendon tissue engineering. Stem cells international. 2012;2012:517165.

[298] Feng Z, Tateishi Y, Nomura Y, Kitajima T, Nakamura T. Construction of fibroblast-collagen gels with orientated fibrils induced by static or dynamic stress: toward the fabrication of small tendon grafts. Journal of artificial organs : the official journal of the Japanese Society for Artificial Organs. 2006;9:220-5.

[299] Fang Q, Chen DL, Yang ZM, Li M. In vitro and in vivo research on using Antheraea pernyi silk fibroin as tissue engineering tendon scaffolds. Mat Sci Eng C-Bio S. 2009;29:1527-34.

[300] Chen GP, Sato T, Sakane M, Ohgushi H, Ushida T, Tanaka J, et al. Application of PLGA-collagen hybrid mesh for three-dimensional culture of canine anterior cruciate ligament cells. Mat Sci Eng C-Bio S. 2004;24:861-6.

[301] Kjaer M, Langberg H, Heinemeier K, Bayer ML, Hansen M, Holm L, et al. From mechanical loading to collagen synthesis, structural changes and function in human tendon. Scandinavian journal of medicine & science in sports. 2009;19:500-10.

[302] Bailey AJ, Paul RG, Knott L. Mechanisms of maturation and ageing of collagen. Mechanisms of ageing and development. 1998;106:1-56.

[303] Koob TJ. Biomimetic approaches to tendon repair. Comparative biochemistry and physiology Part A, Molecular & integrative physiology. 2002;133:1171-92.

[304] Chen GQ. A microbial polyhydroxyalkanoates (PHA) based bio- and materials industry. Chemical Society reviews. 2009;38:2434-46.

[305] Qiu YZ, Han J, Guo JJ, Chen GQ. Production of poly(3-hydroxybutyrate-co-3-hydroxyhexanoate) from gluconate and glucose by recombinant Aeromonas hydrophila and Pseudomonas putida. Biotechnology letters. 2005;27:1381-6.

[306] Chen GQ, Zhang G, Park SJ, Lee SY. Industrial scale production of poly(3-hydroxybutyrate-co-3-hydroxyhexanoate). Appl Microbiol Biotechnol. 2001;57:50-5.

[307] Wang Y-W, Wu Q, Chen G-Q. Attachment, proliferation and differentiation of osteoblasts on random biopolyester poly(3-hydroxybutyrate-co-3-hydroxyhexanoate) scaffolds. Biomaterials. 2004;25:669-75.

[308] Ye C, Hu P, Ma MX, Xiang Y, Liu RG, Shang XW. PHB/PHBHHx scaffolds and human adipose-derived stem cells for cartilage tissue engineering. Biomaterials. 2009;30:4401-6.

[309] Ji Y, Li XT, Chen GQ. Interactions between a poly(3-hydroxybutyrate-co-3-hydroxyvalerate-co-3-hydroxyhexanoate) terpolyester and human keratinocytes. Biomaterials. 2008;29:3807-14.

[310] Bian YZ, Wang Y, Aibaidoula G, Chen GQ, Wu Q. Evaluation of poly(3-hydroxybutyrate-co-3-hydroxyhexanoate) conduits for peripheral nerve regeneration. Biomaterials. 2009;30:217-25.

[311] Wang YW, Wu Q, Chen GQ. Reduced mouse fibroblast cell growth by increased hydrophilicity of microbial polyhydroxyalkanoates via hyaluronan coating. Biomaterials. 2003;24:4621-9.

[312] Lomas AJ, Chen GQ, El Haj AJ, Forsyth NR. Mechanostimulation of human mesenchymal stem cells in PHBHHx/collagen hybrid scaffolds for tendon tissue engineering applications. Journal of tissue engineering and regenerative medicine. 2012;6:46-.

[313] Lomas AJ, Webb WR, Han J, Chen GQ, Sun X, Zhang Z, et al. Poly (3-hydroxybutyrate-co-3-hydroxyhexanoate)/collagen hybrid scaffolds for tissue engineering applications. Tissue engineering Part C, Methods. 2013.

[314] Murrell GAC, Lilly EG, Davies H, Best TM, Goldner RD, Seaber AV. The Achilles Functional Index. J Orthop Res. 1992;10:398-404.

[315] Schneider CA, Rasband WS, Eliceiri KW. NIH Image to ImageJ: 25 years of image analysis. Nature methods. 2012;9:671-5.

[316] Du Clos TW. Function of C-reactive protein. Annals of medicine. 2000;32:274-8.

[317] Du Clos TW, Mold C, Bharadwaj D, Edberg JC, Kimberly RP, Stein MP. C-reactive protein binding to Fc gamma RIIa on human monocytes and neutrophils is allele-specific. Arthritis Rheum. 1999;42:S274-S.

[318] Berman S, Gewurz H, Mold C. Binding of C-Reactive Protein to Nucleated Cells Leads to Complement Activation without Cytolysis. Journal of immunology. 1986;136:1354-9.

[319] Bharadwaj D, Stein MP, Volzer M, Mold C, Du Clos TW. The major receptor for C-reactive protein on leukocytes is Fc gamma receptor II. J Exp Med. 1999;190:585-90.

[320] Bharadwaj D, Stein MP, Volzer M, Mold C, Du Clos TW. C-reactive protein (CRP) binds to Fc gamma RIIa-transfected COS cells. Faseb J. 1999;13:A281-A.

[321] Stein MP, Mold C, Bharadwaj D, Du Clos TW. C-reactive protein (CRP) binding to murine peritoneal cells requires Fc receptors (FcR). Faseb J. 1999;13:A281-A.

[322] White J, Kelly M, Dunsmuir R. C-reactive protein level after total hip and total knee replacement. J Bone Joint Surg Br. 1998;80B:909-11.

[323] Lobler M, Sass M, Kunze C, Schmitz KP, Hopt UT. Biomaterial implants induce the inflammation marker CRP at the site of implantation. Journal of biomedical materials research. 2002;61:165-7.

[324] Vrana NE, Dupret-Bories A, Bach C, Chaubaroux C, Coraux C, Vautier D, et al. Modification of macroporous titanium tracheal implants with biodegradable structures: Tracking in vivo integration for determination of optimal in situ epithelialization conditions. Biotechnol Bioeng. 2012;109:2134-46.

[325] Zhou J, Peng SW, Wang YY, Zheng SB, Wang Y, Chen GQ. The use of poly(3-hydroxybutyrate-co-3-hydroxyhexanoate) scaffolds for tarsal repair in eyelid reconstruction in the rat. Biomaterials. 2010;31:7512-8.

[326] Young RG, Butler DL, Weber W, Caplan AI, Gordon SL, Fink DJ. Use of mesenchymal stem cells in a collagen matrix for Achilles tendon repair. J Orthop Res. 1998;16:406-13.

[327] Miller-Chou BA, Koenig JL. A review of polymer dissolution. Progress in Polymer Science. 2003;28:1223-70.

[328] Cima LG, Ingber DE, Vacanti JP, Langer R. Hepatocyte Culture on Biodegradable Polymeric Substrates. Biotechnol Bioeng. 1991;38:145-58.

[329] Qu XH, Wu Q, Zhang KY, Chen GQ. In vivo studies of poly(3-hydroxybutyrate-co-3-hydroxyhexanoate) based polymers: biodegradation and tissue reactions. Biomaterials. 2006;27:3540-8.

[330] Fougerousse F, Bullen P, Herasse M, Lindsay S, Richard I, Wilson D, et al. Human-mouse differences in the embryonic expression patterns of developmental control genes and disease genes. Human molecular genetics. 2000;9:165-73.

[331] Scott A, Danielson P, Abraham T, Fong G, Sampaio AV, Underhill TM. Mechanical force modulates scleraxis expression in bioartificial tendons. Journal of musculoskeletal & neuronal interactions. 2011;11:124-32.

[332] D'Ippolito G, Diabira S, Howard GA, Menei P, Roos BA, Schiller PC. Marrow-isolated adult multilineage inducible (MIAMI) cells, a unique population of postnatal young and old human cells with extensive expansion and differentiation potential. Journal of cell science. 2004;117:2971-81.

[333] Wimpenny I, Hampson K, Yang Y, Ashammakhi N, Forsyth NR. One-step recovery of marrow stromal cells on nanofibers. Tissue engineering Part C, Methods. 2010;16:503-9.

[334] Lennon DP, Caplan AI. Isolation of rat marrow-derived mesenchymal stem cells. Experimental hematology. 2006;34:1606-7.

[335] Zhang L, Chan C. Isolation and enrichment of rat mesenchymal stem cells (MSCs) and separation of single-colony derived MSCs. Journal of visualized experiments : JoVE. 2010.

[336] Thomson JA, Itskovitz-Eldor J, Shapiro SS, Waknitz MA, Swiergiel JJ, Marshall VS, et al. Embryonic stem cell lines derived from human blastocysts. Science. 1998;282:1145-7.

[337] Peterkofsky B. Ascorbate requirement for hydroxylation and secretion of procollagen: relationship to inhibition of collagen synthesis in scurvy. The American journal of clinical nutrition. 1991;54:1135S-40S.

[338] Omeroglu S, Peker T, Turkozkan N, Omeroglu H. High-dose Vitamin C supplementation accelerates the Achilles tendon healing in healthy rats. Archives of orthopaedic and trauma surgery. 2009;129:281-6.

[339] Takahashi T, Lord B, Schulze PC, Fryer RM, Sarang SS, Gullans SR, et al. Ascorbic acid enhances differentiation of embryonic stem cells into cardiac myocytes. Circulation. 2003;107:1912-6.

[340] Heng BC, Cao T, Lee EH. Directing stem cell differentiation into the chondrogenic lineage in vitro. Stem Cells. 2004;22:1152-67.

[341] zur Nieden NI, Kempka G, Ahr HJ. In vitro differentiation of embryonic stem cells into mineralized osteoblasts. Differentiation; research in biological diversity. 2003;71:18-27.

[342] Ramirez-Bergeron DL, Simon MC. Hypoxia-inducible factor and the development of stem cells of the cardiovascular system. Stem Cells. 2001;19:279-86.

[343] Mathieu J, Zhang Z, Zhou W, Wang AJ, Heddleston JM, Pinna CM, et al. HIF induces human embryonic stem cell markers in cancer cells. Cancer research. 2011;71:4640-52.

[344] Liang M, Cornell HR, Zargar Baboldashti N, Thompson MS, Carr AJ, Hulley PA. Regulation of Hypoxia-Induced Cell Death in Human Tenocytes. Advances in Orthopedics. 2012;2012:12.

[345] Distler JH, Jungel A, Pileckyte M, Zwerina J, Michel BA, Gay RE, et al. Hypoxia-induced increase in the production of extracellular matrix proteins in systemic sclerosis. Arthritis and rheumatism. 2007;56:4203-15.

[346] Wan J, Chai H, Yu Z, Ge W, Kang N, Xia W, et al. HIF-1alpha effects on angiogenic potential in human small cell lung carcinoma. Journal of experimental & clinical cancer research : CR. 2011;30:77.

[347] Kjaer M, Langberg H, Bojsen-Moller J, Koskinen SO, Mackey A, Heinemeier K, et al. Novel methods for tendon investigations. Disability and rehabilitation. 2008;30:1514-22.

[348] Wong YP, Fu SC, Cheuk YC, Lee KM, Wong MW, Chan KM. Bone morphogenetic protein 13 stimulates cell proliferation and production of collagen in human patellar tendon fibroblasts. Acta orthopaedica. 2005;76:421-7.

[349] Hoffmann A, Pelled G, Turgeman G, Eberle P, Zilberman Y, Shinar H, et al. Neotendon formation induced by manipulation of the Smad8 signalling pathway in mesenchymal stem cells. The Journal of clinical investigation. 2006;116:940-52.

[350] Heldin CH, Miyazono K, ten Dijke P. TGF-beta signalling from cell membrane to nucleus through SMAD proteins. Nature. 1997;390:465-71.

[351] Dijke Pt, Heldin C-H. Smad signal transduction : smads in proliferation, differentiation and disease. Dordrecht: Springer; 2006.

[352] Edom-Vovard F, Bonnin M, Duprez D. Fgf8 transcripts are located in tendons during embryonic chick limb development. Mechanisms of development. 2001;108:203-6.

[353] Lanner F, Rossant J. The role of FGF/Erk signaling in pluripotent cells. Development. 2010;137:3351-60.

[354] Barsby T, Guest D. Transforming Growth Factor Beta3 Promotes Tendon Differentiation of Equine Embryo-Derived Stem Cells. Tissue engineering Part A. 2013.

[355] Barron M, Gao M, Lough J. Requirement for BMP and FGF signaling during cardiogenic induction in non-precardiac mesoderm is specific, transient, and cooperative. Developmental Dynamics. 2000;218:383-93.

[356] Lough J, Barron M, Brogley M, Sugi Y, Bolender DL, Zhu X. Combined BMP-2 and FGF-4, but neither factor alone, induces cardiogenesis in non-precardiac embryonic mesoderm. Developmental biology. 1996;178:198-202.

[357] Zhang J, Wang JH. Characterization of differential properties of rabbit tendon stem cells and tenocytes. BMC musculoskeletal disorders. 2010;11:10.

[358] Goncalves NP, Oliveira H, Pego AP, Saraiva MJ. A novel nanoparticle delivery system for in vivo targeting of the sciatic nerve: impact on regeneration. Nanomedicine. 2012;7:1167-80.

[359] Kim K, Fisher JP. Nanoparticle technology in bone tissue engineering. J Drug Target. 2007;15:241-52.

[360] Lim SM, Oh SH, Lee HH, Yuk SH, Im GI, Lee JH. Dual growth factor-releasing nanoparticle/hydrogel system for cartilage tissue engineering. J Mater Sci-Mater Med. 2010;21:2593-600.

[361] Byrne JD, Betancourt T, Brannon-Peppas L. Active targeting schemes for nanoparticle systems in cancer therapeutics. Advanced Drug Delivery Reviews. 2008;60:1615-26.

[362] Hood JD, Bednarski M, Frausto R, Guccione S, Reisfeld RA, Xiang R, et al. Tumor regression by targeted gene delivery to the neovasculature. Science. 2002;296:2404-7.

[363] Qian XM, Peng XH, Ansari DO, Yin-Goen Q, Chen GZ, Shin DM, et al. In vivo tumor targeting and spectroscopic detection with surface-enhanced Raman nanoparticle tags. Nat Biotechnol. 2008;26:83-90.

[364] Sengupta S, Eavarone D, Capila I, Zhao GL, Watson N, Kiziltepe T, et al. Temporal targeting of tumour cells and neovasculature with a nanoscale delivery system. Nature. 2005;436:568-72.

[365] Pollheimer J, Haslinger P, Fock V, Prast J, Saleh L, Biadasiewicz K, et al. Endostatin suppresses IGF-II-mediated signaling and invasion of human extravillous trophoblasts. Endocrinology. 2011;152:4431-42.

[366] De Luca G, Barakat M, Ortet P, Fochesato S, Jourlin-Castelli C, Ansaldi M, et al. The cyst-dividing bacterium Ramlibacter tataouinensis TTB310 genome reveals a well-stocked toolbox for adaptation to a desert environment. PLoS One. 2011;6:e23784.

[367] Clerici M, Cassinotti A, Onida F, Trabattoni D, Annaloro C, Della Volpe A, et al. Immunomodulatory effects of unselected haematopoietic stem cells autotransplantation in refractory Crohn's disease. Digestive and liver disease : official journal of the Italian Society of Gastroenterology and the Italian Association for the Study of the Liver. 2011;43:946-52.

[368] Liberto MC, Lamberti AG, Marascio N, Matera G, Quirino A, Barreca GS, et al. Molecular identification of Bartonella quintana infection using species-specific real-time PCR targeting transcriptional regulatory protein (bqtR) gene. Molecular and cellular probes. 2011;25:238-42.

[369] Focosi D, Boggi U. Pretransplant screening for donor-specific antibodies and graft loss. Transplantation. 2011;92:e15; author reply e-6.

[370] Siau C, Tee A, Au V, Raghuram J, Oh HM, Fock KM, et al. Influenza A H1N1 (2009): clinical spectrum of disease among adult patients admitted to a regional hospital in Singapore. Singapore medical journal. 2011;52:475-80.

[371] Peng SW, Guo XY, Shang GG, Li J, Xu XY, You ML, et al. An assessment of the risks of carcinogenicity associated with polyhydroxyalkanoates through an analysis of DNA aneuploid and telomerase activity. Biomaterials. 2011;32:2546-55.

[372] Freymann DM, Nakamura Y, Focia PJ, Sakai R, Swanson GT. Structure of a tetrameric galectin from Cinachyrella sp. (ball sponge). Acta crystallographica Section D, Biological crystallography. 2012;68:1163-74.

[373] Peng Q, Zhang ZR, Gong T, Chen GQ, Sun X. A rapid-acting, long-acting insulin formulation based on a phospholipid complex loaded PHBHHx nanoparticles. Biomaterials. 2012;33:1583-8.

[374] Lunghetti S, Palmerini E, Urselli R, Maffei S, Guarino E, Focardi M, et al. Effects of levosimendan without loading dose on systolic and diastolic function in patients with end-stage heart failure. Cardiology journal. 2011;18:532-7.

[375] Kilicay E, Demirbilek M, Turk M, Guven E, Hazer B, Denkbas EB. Preparation and characterization of poly(3-hydroxybutyrate-co-3-hydroxyhexanoate) (PHBHHX) based nanoparticles for targeted cancer therapy. European journal of pharmaceutical sciences : official journal of the European Federation for Pharmaceutical Sciences. 2011;44:310-20.

[376] Albini L, Cesana BM, Motta D, Foca E, Gotti D, Calabresi A, et al. A randomized, pilot trial to evaluate glomerular filtration rate by creatinine or cystatin C in naive HIV-infected patients after tenofovir/emtricitabine in combination with atazanavir/ritonavir or efavirenz. Journal of acquired immune deficiency syndromes. 2012;59:18-30.

[377] Wu Y, Wang WW, Chen YT, Huang KH, Shuai XT, Chen QK, et al. The investigation of polymer-siRNA nanoparticle for gene therapy of gastric cancer in vitro. Int J Nanomed. 2010;5:129-36.

[378] Yang M, Zhu S, Chen Y, Chang Z, Chen G, Gong Y, et al. Studies on bone marrow stromal cells affinity of poly (3-hydroxybutyrate-co-3-hydroxyhexanoate). Biomaterials. 2004;25:1365-73.

[379] Wohlfart S, Gelperina S, Kreuter J. Transport of drugs across the blood-brain barrier by nanoparticles. J Control Release. 2012;161:264-73.

[380] Jain TK, Morales MA, Sahoo SK, Leslie-Pelecky DL, Labhasetwar V. Iron oxide nanoparticles for sustained delivery of anticancer agents. Mol Pharm. 2005;2:194-205.

[381] Liong M, Lu J, Kovochich M, Xia T, Ruehm SG, Nel AE, et al. Multifunctional inorganic nanoparticles for imaging, targeting, and drug delivery. Acs Nano. 2008;2:889-96.

[382] Veiseh O, Gunn JW, Zhang MQ. Design and fabrication of magnetic nanoparticles for targeted drug delivery and imaging. Advanced Drug Delivery Reviews. 2010;62:284-304.

[383] Xu ZP, Zeng QH, Lu GQ, Yu AB. Inorganic nanoparticles as carriers for efficient cellular delivery. Chemical Engineering Science. 2006;61:1027-40.

[384] Zhang J, Misra RDK. Magnetic drug-targeting carrier encapsulated with thermosensitive smart polymer: Core-shell nanoparticle carrier and drug release response. Acta Biomaterialia. 2007;3:838-50.

[385] Panyam J, Labhasetwar V. Biodegradable nanoparticles for drug and gene delivery to cells and tissue. Advanced Drug Delivery Reviews. 2003;55:329-47.

[386] Konan YN, Gurny R, Allemann E. Preparation and characterization of sterile and freeze-dried sub-200 nm nanoparticles. International journal of pharmaceutics. 2002;233:239-52.

[387] Della Torre C, Zaja R, Loncar J, Smital T, Focardi S, Corsi I. Interaction of ABC transport proteins with toxic metals at the level of gene and transport activity in the PLHC-1 fish cell line. Chemico-biological interactions. 2012;198:9-17.

[388] Park JH, von Maltzahn G, Zhang L, Schwartz MP, Ruoslahti E, Bhatia SN, et al. Magnetic Iron Oxide Nanoworms for Tumor Targeting and Imaging. Adv Mater. 2008;20:1630-5.

[389] Faraji AH, Wipf P. Nanoparticles in cellular drug delivery. Bioorganic & medicinal chemistry. 2009;17:2950-62.

[390] Focken T, Steinemann D, Skawran B, Hofmann W, Ahrens P, Arnold N, et al. Human BRCA1-associated breast cancer: no increase in numerical chromosomal instability compared to sporadic tumors. Cytogenetic and genome research. 2011;135:84-92.

[391] Montgomery DC. THE USE OF STATISTICAL PROCESS-CONTROL AND DESIGN OF EXPERIMENTS IN PRODUCT AND PROCESS IMPROVEMENT. IIE Trans. 1992;24:4-17.

[392] Williams DJ, Thomas RJ, Hourd PC, Chandra A, Ratcliffe E, Liu Y, et al. Precision manufacturing for clinical-quality regenerative medicines. Philosophical transactions Series A, Mathematical, physical, and engineering sciences. 2012;370:3924-49.

[393] Lamprecht A, Ubrich N, Perez MH, Lehr CM, Hoffman M, Maincent P. Biodegradable monodispersed nanoparticles prepared by pressure homogenization-emulsification. Int J Pharm. 1999;184:97-105.

[394] Lamprecht A, Ubrich N, Perez MH, Lehr CM, Hoffman M, Maincent P. Influences of process parameters on nanoparticle preparation performed by a double emulsion pressure homogenization technique. Int J Pharm. 2000;196:177-82.

[395] Gutierro I, Hernandez RM, Igartua M, Gascon AR, Pedraz JL. Size dependent immune response after subcutaneous, oral and intranasal administration of BSA loaded nanospheres. Vaccine. 2002;21:67-77.

[396] Gryparis EC, Mattheolabakis G, Bikiaris D, Avgoustakis K. Effect of conditions of preparation on the size and encapsulation properties of PLGA-mPEG nanoparticles of cisplatin. Drug Deliv. 2007;14:371-80.

[397] Almeida JP, Chen AL, Foster A, Drezek R. In vivo biodistribution of nanoparticles. Nanomedicine (Lond). 2011;6:815-35.

[398] Feczko T, Toth J, Dosa G, Gyenis J. Influence of process conditions on the mean size of PLGA nanoparticles. Chem Eng Process. 2011;50:846-53.

[399] Thummala AS, Leach JK, O'Rear EA. Factors affecting the particle size and in vitro release of bovine serum albumin from polyethylene glycol microparticles. Biomed Sci Instrum. 2003;39:318-23.

[400] Liao W-Y, Li H-J, Chang M-Y, Tang ACL, Hoffman AS, Hsieh PCH. Comprehensive characterizations of nanoparticle biodistribution following systemic injection in mice. Nanoscale. 2013;5:11079-86.

[401] Dartsch PC, Hammerle H. Orientation response of arterial smooth muscle cells to mechanical stimulation. European journal of cell biology. 1986;41:339-46.

[402] Dartsch PC, Hammerle H, Betz E. Orientation of cultured arterial smooth muscle cells growing on cyclically stretched substrates. Acta anatomica. 1986;125:108-13.

[403] Chen B, Kemkemer R, Deibler M, Spatz J, Gao H. Cyclic stretch induces cell reorientation on substrates by destabilizing catch bonds in focal adhesions. PLoS One. 2012;7:e48346.

[404] Williams DF, Biological Engineering Society London., Institute of Physics (Great Britain). Materials and Testing Group., Hospital Physicists Association. Biocompatibility of implant materials. LondonTunbridge Wells: Sector ;Distributed by Pitman Medical; 1976.

[405] Maquirriain J. Achilles tendon rupture: avoiding tendon lengthening during surgical repair and rehabilitation. The Yale journal of biology and medicine. 2011;84:289-300.

[406] Zhang X, Ibrahimi OA, Olsen SK, Umemori H, Mohammadi M, Ornitz DM. Receptor specificity of the fibroblast growth factor family. The complete mammalian FGF family. The Journal of biological chemistry. 2006;281:15694-700.

[407] Boswell BA, Overbeek PA, Musil LS. Essential role of BMPs in FGF-induced secondary lens fiber differentiation. Developmental biology. 2008;324:202-12.

[408] Boswell BA, Lein PJ, Musil LS. Cross-talk between fibroblast growth factor and bone morphogenetic proteins regulates gap junction-mediated intercellular communication in lens cells. Molecular biology of the cell. 2008;19:2631-41.

[409] Chen X, Yin Z, Chen J-l, Shen W-l, Liu H-h, Tang Q-m, et al. Force and scleraxis synergistically promote the commitment of human ES cells derived MSCs to tenocytes. Sci Rep. 2012;2.

[410] Abraham T, Fong G, Scott A. Second harmonic generation analysis of early Achilles tendinosis in response to in vivo mechanical loading. BMC musculoskeletal disorders. 2011;12:26.

[411] Pryce BA, Watson SS, Murchison ND, Staverosky JA, Dunker N, Schweitzer R. Recruitment and maintenance of tendon progenitors by TGFbeta signaling are essential for tendon formation. Development. 2009;136:1351-61.

[412] Pryce BA, Brent AE, Murchison ND, Tabin CJ, Schweitzer R. Generation of transgenic tendon reporters, ScxGFP and ScxAP, using regulatory elements of the scleraxis gene. Developmental dynamics : an official publication of the American Association of Anatomists. 2007;236:1677-82.

[413] Shen H, Gelberman RH, Silva MJ, Sakiyama-Elbert SE, Thomopoulos S. BMP12 induces tenogenic differentiation of adipose-derived stromal cells. PLoS ONE. 2013;8:e77613.

[414] De Laporte L, Rice JJ, Tortelli F, Hubbell JA. Tenascin C promiscuously binds growth factors via its fifth fibronectin type III-like domain. PLoS One. 2013;8:e62076.

Appendix

Standard Curve for Methods

CRP standard curve

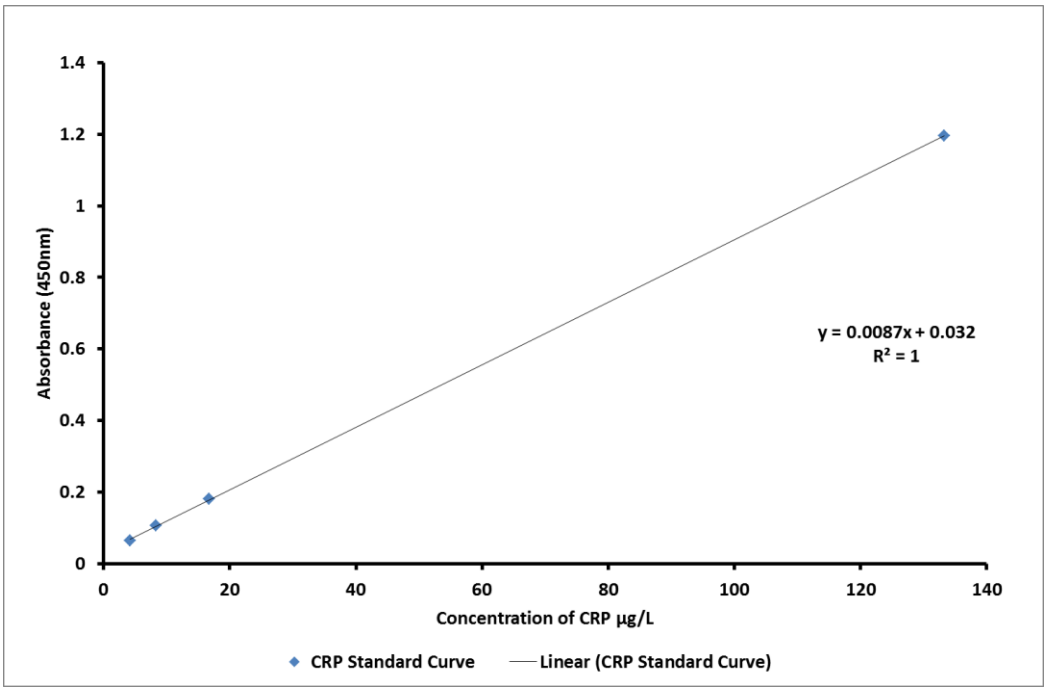

Standard Curve 1 CRP Elisa standard curve

Albumin HPLC standard curve

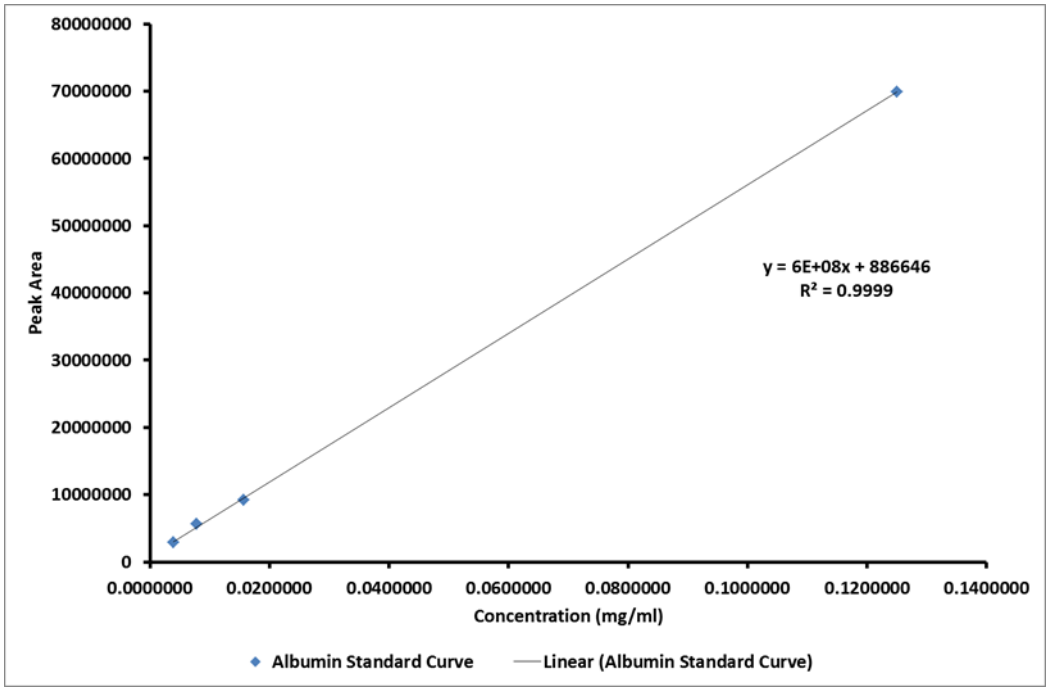

Standard Curve 2 Albumin HPLC standard curve

Haperzine A GCMS standard curve

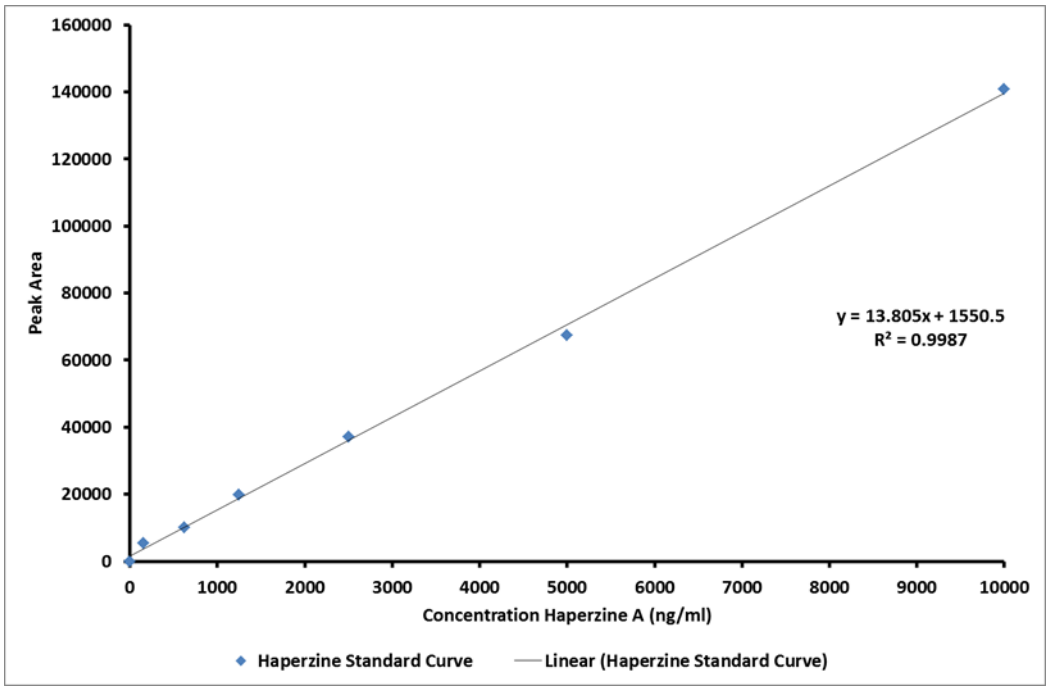

Standard Curve 3 Haperzine A standard curve

Paclitaxel standard curve

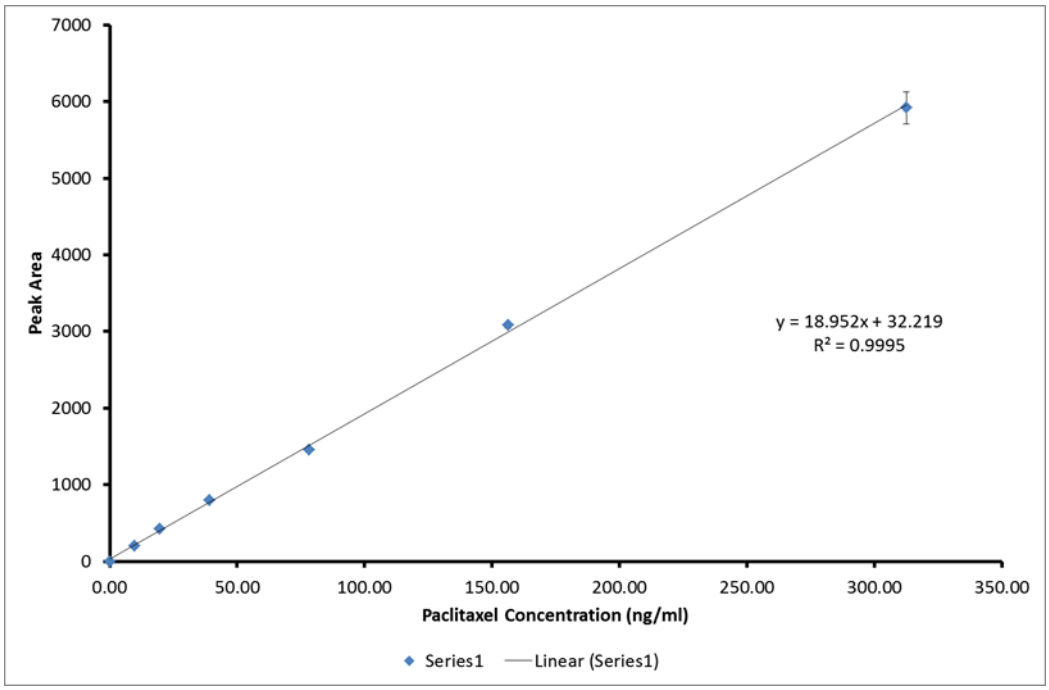

Standard Curve 4 Paclitaxel standard curve